



**Versatile Hybrid Nanomaterials:  
Periodic Mesoporous Organosilicas as adsorbent and catalyst**

Dissertation submitted in fulfillment of the requirements for  
the degree of Doctor of Science: Chemistry

by

Els De Canck

Promotor: Prof. dr. Pascal Van Der Voort

Department of Inorganic and Physical Chemistry

Faculty of Sciences

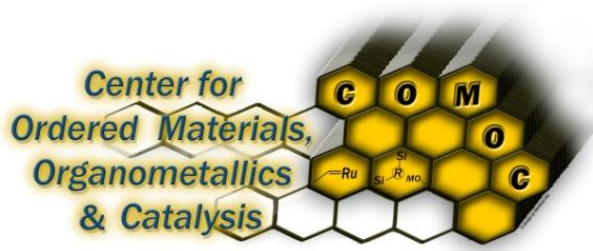
Ghent University

2013

© 2013 Ghent University, Department of Inorganic and Physical Chemistry, COMOC - *Center for Ordered Materials, Organometallics & Catalysis*, Krijgslaan 281-S3, 9000 Ghent, Belgium.

Alle rechten voorbehouden. Niets uit deze uitgave mag worden vermenigvuldigd en/of openbaar gemaakt worden door middel van druk, fotokopie, microfilm, elektronisch of op welke andere wijze ook zonder voorafgaandelijk schriftelijke toestemming van de uitgever.

All rights reserved. No part of the publication may be reproduced in any form by print, photo print, microfilm, electronic or any other means without written permission from the publisher.



## ***Members of the dissertation jury***

Prof. dr. Pascal Van Der Voort	Universiteit Gent
Prof. dr. Isabel Van Driessche	Universiteit Gent
Prof. dr. Francisco J. Romero-Salguero	Universidad de Córdoba
Prof. dr. Pegie Cool	Universiteit Antwerpen
dr. Maria Dolores Esquivel Merino	Universiteit Gent
Prof. dr. Kristof Van Hecke	Universiteit Gent
Prof. dr. Willy Baeyens	Vrije Universiteit Brussel

# ***Table of contents***

Table of contents.....	iv
Scientific publications.....	viii
Acknowledgements .....	xv
Preface.....	xviii
Outline.....	xx
Abbreviations.....	xxii
1 A new class of hybrid nanomaterials: Periodic Mesoporous Organosilicas ....	1.1
1.1 Introduction.....	1.2
1.2 PMOs with simple organic bridges.....	1.10
1.2.1 The ethane-PMO .....	1.10
1.2.2 The methane-PMO .....	1.11
1.2.3 The benzene-PMO .....	1.11
1.2.4 The ethene-PMO .....	1.13
1.3 Properties of PMOs.....	1.19
1.4 Post-modification of the PMO material .....	1.22
1.5 Concluding remarks.....	1.27
1.6 References .....	1.28
2 Applications of Periodic Mesoporous Organosilicas .....	2.1
2.1 Introduction.....	2.2
2.2 Ultra stable PMOs as chromatographic packing and super insulating low- <i>k</i> film.....	2.2
2.3 Functional PMOs as adsorbents and catalysts .....	2.7
2.4 PMOs as adsorbents.....	2.7
2.5 PMOs as heterogeneous catalyst.....	2.16
2.6 Emerging applications in biomedical sciences and drug release .....	2.33
2.7 Aim of this dissertation .....	2.37
2.8 References .....	2.38
3 The ethenylene-bridged Periodic Mesoporous Organosilica .....	3.1
3.1 Introduction.....	3.2
3.2 Synthesis of <i>trans</i> 1,2-bis(triethoxysilyl)ethenylene .....	3.2
3.3 Synthesis of the ethenylene-bridged PMO material .....	3.3
3.4 Conclusion .....	3.6

3.5	Experimental section.....	3.6
3.6	References .....	3.7
4	The development of Periodic Mesoporous Organosilicas as mercury(II) adsorbents .....	4.1
4.1	Introduction.....	4.2
4.2	Synthesis of benchmark adsorbents: thiol containing silica based materials	4.2
4.2.1	The grafting of MPTES on SBA-15 materials.....	4.3
4.2.2	Preparation of SBA-15 type materials via an one-pot-synthesis.....	4.8
4.2.3	Determination of the reachability of the thiol groups .....	4.9
4.2.4	Summary of properties concerning the selected thiol containing adsorbents.....	4.10
4.3	Development of thiol-containing Periodic Mesoporous Organosilica .....	4.12
4.3.1	The theory behind the Grignard reagent preparation .....	4.13
4.3.2	The formation of the Grignard reagent and subsequent substitution reaction .....	4.14
4.3.3	Optimization of thiol amount.....	4.15
4.3.4	Characterization of the ethenylene-bridged PMO material and the subsequent modified materials with bromine and propylthiol .....	4.19
4.4	Mercury(II) adsorption experiments .....	4.20
4.5	Conclusion .....	4.27
4.6	Experimental section.....	4.28
4.7	References .....	4.32
5	The use of the thiol containing PMO in DGT probes for determining dissolved mercury concentrations.....	5.1
5.1	Introduction to <i>Diffusive Gradients in Thin (DGT) films</i> .....	5.2
5.1.1	The DGT probe .....	5.3
5.1.2	Advantages of the DGT method .....	5.5
5.1.3	Parameters affecting the DGT measurement.....	5.5
5.2	Synthesis and characteristics of the resins used in the DGT probe .....	5.5
5.3	Mercury DGT experiments with the resins.....	5.9
5.3.1	Mercury concentrations in the bulk solution .....	5.9
5.3.2	Mercury accumulation on the Chelex-100 resin gel in a DGT .....	5.9
5.3.3	Mercury accumulation on SH-PMO, SH-SBA, SQR and SH-KG resin gels in a DGT .....	5.12

5.3.4	Field work results .....	5.12
5.4	Conclusions .....	5.13
5.5	Experimental section.....	5.14
5.6	References .....	5.17
6	The development of nitrogen containing PMO as adsorbent for CO <sub>2</sub> .....	6.1
6.1	Introduction.....	6.2
6.2	Modification of the PMO materials with amine functionality .....	6.2
6.3	Materials characterization .....	6.6
6.4	CO <sub>2</sub> adsorption experiments .....	6.10
6.5	Conclusions.....	6.15
6.6	Experimental section.....	6.15
6.7	References .....	6.17
7	The modification of an ethenylene-bridged PMO material towards sulfonic acid groups .....	7.1
7.1	PART 1: Sulfonation of the double bond of the ethenylene-bridged PMO material.....	7.3
7.1.1	Introduction.....	7.3
7.1.2	Sulfonation of the double bond.....	7.3
7.1.3	Characterization of the sulfonated solids.....	7.5
7.2	Catalysis: the esterification of acetic acid with 1-propanol .....	7.8
7.2.1	Catalytic experiments with sulfonated PMO materials .....	7.9
7.2.2	Reusability of the sulfonated PMO materials.....	7.11
7.3	PART 2: The modification of the thiol containing PMO material towards a sulfonic acid group.....	7.16
7.3.1	Synthesis of the PMO based acid catalyst.....	7.16
7.3.2	Characterization of the solids .....	7.17
7.4	Catalytic experiments and recyclability.....	7.22
7.5	Conclusions.....	7.25
7.6	Experimental section.....	7.26
7.7	References .....	7.29

8	Anchoring a manganese complex on PMOs for oxidation catalysis.....	8.1
8.1	Introduction.....	8.2
8.2	Synthesis of a multi-organic bridged PMO material.....	8.4
8.3	Anchoring of manganese (acac) <sub>2</sub> on the allyl ring-PMO .....	8.5
8.4	Characterization of the different modified allyl ring-PMOs.....	8.6
8.5	Oxidation Catalysis .....	8.10
8.6	Conclusions .....	8.16
8.7	Experimental section.....	8.17
8.8	References .....	8.21
9	Concluding remarks.....	9.1
10	Nederlandse samenvatting.....	10.1
10.1	Periodieke Mesoporeuze Organosilica's .....	10.1
10.2	Thiol gefunctionaliseerde PMOs als kwik adsorbent .....	10.2
10.3	Amine gefunctionaliseerde PMOs als CO <sub>2</sub> adsorbent .....	10.5
10.4	PMOs gemodificeerd met sulfonzure groepen als katalysator voor esterificatie reacties .....	10.7
10.5	PMOs gemodificeerd met een mangaan complex als katalysator voor epoxidatie reacties .....	10.9
10.6	Conclusies .....	10.11

# *Scientific publications*

## *A1 publications*

Indenylidene complexes of ruthenium bearing NHC ligands - Structure elucidation and performance as catalysts for olefin metathesis.

Stijn Monsaert, Els De Canck, Renata Drozdak, Pascal Van Der Voort, Francis Verpoort, José C. Martins and Pieter M.S. Hendrickx, *European Journal of Organic Chemistry*, 2009, 5, 655-665.

New ultrastable mesoporous adsorbent for the removal of mercury ions.

Els De Canck, Linsey Lapeire, Jeriffa De Clercq, Francis Verpoort and Pascal Van Der Voort, *Langmuir*, 2010, 26, 12, 10076-10083.

Verwijdering van kwik uit waterige oplossingen: vergelijking van een nieuw ultrastabiel mesoporeus adsorbens met een commercieel ionenwisselaarshars.

Jeriffa De Clercq, Els De Canck and Pascal Van Der Voort, *WT – Afvalwater*, 2010, 10, 5, 119-126.

Formation and functionalization of surface Diels–Alder adducts on ethenylene-bridged periodic mesoporous organosilica.

Dolores Esquivel, Els De Canck, César Jiménez-Sanchidrián, Pascal Van Der Voort and Francisco J. Romero-Salguero, *Journal of Materials Chemistry*, 2011, 21, 29, 10990-10998.

Synthesized mercaptopropyl nanoporous resins in DGT probes for determining dissolved mercury concentrations.

Yue Gao, Els De Canck, Martine Leermakers, Willy Baeyens and Pascal Van Der Voort, *Talanta*, 2011, 87, 262-267.



Calcium phosphate cements modified with pore expanded SBA-15 materials.

Natasja Van den Vreken, [Els De Canck](#), Matthias Ide, Kevin Lamote, Pascal Van Der Voort and Ronald Verbeeck, *Journal of Materials Chemistry*, 2012, 22, 29, 14502-14509.

Quantification of silanol sites for the most common mesoporous ordered silicas and organosilicas: total versus accessible silanols.

Matthias Ide, Mohamad El-Roz, [Els De Canck](#), Aurélie Vincente, Tom Planckaert, Thomas Bogaerts, Isabel Van Driessche, Frederic Lynen, Veronique Van Speybroeck, Frédéric Thybault-Starzyk and Pascal Van Der Voort, *Physical Chemistry Chemical Physics*, 2013, 15, 2, 642-650.

Periodic mesoporous organosilicas: from simple to complex bridges: a comprehensive overview of functions, morphologies and applications.

Pascal Van Der Voort, Dolores Esquivel, [Els De Canck](#), Frederik Goethals, Isabel Van Driessche, Francisco J. Romero-Salguero, *Chemical Society Reviews*, 2013, 42, 9, 3913-3955.

Periodic mesoporous organosilicas functionalized with a wide variety of amines for CO<sub>2</sub> adsorption.

[Els De Canck](#), Isabelle Ascoop, Abdelhamid Sayari, Pascal Van Der Voort, *Physical Chemistry Chemical Physics*, 2013, 15, 24, 9792-9799.

Pore narrowing of mesoporous silica materials.

Frederik Goethals, Elisabeth Levrau, [Els De Canck](#), Mikhail R. Baklanov, Christophe Detavernier, Isabel Van Driessche and Pascal Van Der Voort, *Materials*, 2013, 6, 2, 570-579.

Periodic mesoporous organosilica functionalized with sulfonic acid groups as acid catalyst for glycerol acetylation.

[Els De Canck](#), Inmaculada Dosuna-Rodríguez, Eric M. Gaigneaux and Pascal Van Der Voort, *Materials*, 2013, 6, 3556-3570.

Silanol assisted aldol condensation on aminated silica: understanding the arrangement of functional groups.

Jeroen Lauwaert, Els De Canck, Dolores Esquivel, Joris W. Thybaut, Pascal Van Der Voort and Guy B. Marin, ChemCatChem, 2013, accepted.

Manganese containing periodic mesoporous organosilica for epoxidation reactions.

Els De Canck *et al.*, 2013, in preparation.

### ***Book chapters***

Ruthenium–indenylidene complexes bearing saturated N-heterocyclic carbenes: synthesis and application in ring-closing metathesis reactions.

Stijn Monsaert, Els De Canck, Renata Drozdak, Pascal Van Der Voort, Pieter M.S. Hendrickx, José C. Martins and Francis Verpoort, 2010. NATO Science for Peace and Security, series A: chemistry and biology, in Green metathesis chemistry: great challenges in synthesis, catalysis and nanotechnology, ed. V. Dragutan, A. Demonceau, I. Dragutan, and E.S. Finkelshtein, 31-38, Dordrecht, The Netherlands: Springer.

A new sulphonic acid functionalized periodic mesoporous organosilica as a suitable catalyst.

Els De Canck, Carl Vercaemst, Francis Verpoort, and Pascal Van Der Voort. 2010. Studies in Surface Science and Catalysis, ed. E.M. Gaigneaux, M. Devillers, S. Hermans, P.A. Jacobs, J.A. Martens, and P. Ruiz, 175, 365-368, Amsterdam, The Netherlands: Elsevier.

Periodic mesoporous organosilicas: hybrid porous materials with exciting applications.

Els De Canck, Dolores Esquivel, Francisco J. Romero-Salguero and Pascal Van Der Voort. 2013. Comprehensive guide for mesoporous material, Nova-Science Publishers, submitted.

### ***National and international oral presentations***

New mesoporous ultrastable adsorbent for the removal of mercury ions in water.

Els De Canck, International workshop on Advanced Inorganic Materials (INANOMAT), 18 March 2010, Namen, Belgium.

Ultrastable adsorbent for the removal of mercury(II) ions.

Els De Canck, Freya Van den Broeck and Pascal Van Der Voort, 1st International workshop of the European Nanoporous Materials Institute of Excellence: nanostructured materials for sorption, separation and catalysis (ENMIX), 04-05 October 2010, Antwerp, Belgium.

Mesoporous phenolic resins as acid catalyst for esterification reactions.

Ilke Muylaert, Els De Canck, Jeremy Spileers, An Verberckmoes and Pascal Van Der Voort, Nanoporous Materials VI, 21-24 August 2011, Banff, Canada.

Different functionalization routes to fine-tune periodic mesoporous organosilicas.

Els De Canck, Dolores Esquivel and Pascal Van Der Voort, Netherlands' Catalysis and Chemistry Conference (NCCC XIV), 11-13 March 2013, Noordwijkerhout, The Netherlands.

### ***National and international poster presentations***

Dynamic properties and conformational analysis of a series of rutheniumindenyliene complexes by NMR.

Pieter M.S. Hendrickx, Els De Canck, Renata Drozdak, Stijn Monsaert, José C. Martins and Francis Verpoort, Euromar Magnetic Resonance Conference, 01-06 July 2007, Tarragona, Spain.

Removal of heavy metals from aqueous solutions using hybrid nanoporous materials.

Els De Canck and Pascal Van Der Voort, Innovation for Sustainable Production (i-SUP2008), 22-25 April 2008, Bruges, Belgium.

Hybride nanoporeuze materialen voor de verwijdering van zware metalen uit waterige oplossingen.

Els De Canck and Pascal Van Der Voort, 9de Vlaams Jongeren Congres van de Chemie (Jong KVCV), 04 April 2008, Antwerp, Belgium.

Comparative study of mesoporous sulfur functionalized adsorbents.

Els De Canck, Linsey Lapeire and Pascal Van Der Voort, Doctoraatssymposium UGent Faculteit Wetenschappen, 29 April 2009, Ghent, Belgium.

Heterogeneous acid catalysts for esterification reactions.

Els De Canck, Freya Van den Broeck and Pascal Van Der Voort, 11<sup>th</sup> Netherlands Catalysis and Chemistry Conference (NCCC XI), 01-03 March 2010, Noordwijkerhout, The Netherlands.

Sulphur containing periodic mesoporous organosilica: from adsorbent to acid catalyst.

Els De Canck, Freya Van den Broeck and Pascal Van Der Voort, Methusalem Advisory Board meeting, 28 June 2010, Ghent, Belgium.

Sulphur containing periodic mesoporous organosilica: from adsorbent to acid catalyst.

Els De Canck, Freya Van den Broeck and Pascal Van Der Voort, Scientific Bases for the Preparation of Heterogeneous Catalysts, 10<sup>th</sup> International symposium (PREPA 10), 11-15 July 2010, Louvain-la-Neuve, Belgium.

Use of newly synthesized mercaptopropyl resins in DGT probes for determining dissolved mercury concentrations.

Yue Gao, Els De Canck, Pascal Van Der Voort and Willy Baeyens, Geochemical Speciation and Bioavailability of Trace Elements, 07-08 September 2010, Lancaster, United Kingdom.

Ultrastable adsorbent for the removal of mercury(II) ions.

Els De Canck, Freya Van den Broeck and Pascal Van Der Voort, 1st International workshop of the European Nanoporous Materials Institute of Excellence: nanostructured materials for sorption, separation and catalysis (ENMIX), 04-05 October 2010, Antwerp, Belgium.

The development of mesoporous phenolic resins as new solid acid catalyst.

Ilke Muylaert, Els De Canck, Jeremy Spileers, An Verberckmoes and Pascal Van Der Voort, Netherlands Catalysis and Chemistry Conference (NCCC XII), 28 February - 02 March 2011, Noordwijkerhout, The Netherlands.

The sulfonation of mesoporous phenolic resins and their catalytic activity as acid solid catalyst in esterification reactions.

Ilke Muylaert, Els De Canck, Jeremy Spileers, An Verberckmoes and Pascal Van Der Voort, 5<sup>th</sup> International FEZA conference, 03-07 July 2011, Valencia, Spain.

Sulfur containing ethene bridged PMOs as adsorbent and catalyst.

Els De Canck and Pascal Van Der Voort, 5<sup>th</sup> International FEZA conference, 03-07 July 2011, Valencia, Spain.

Formation of surface Diels-Alder adducts on ethenylene-bridged periodic mesoporous organosilicas.

Dolores Esquivel, Els De Canck, César Jiménez-Sanchidrián, Pascal Van Der Voort and Francisco J. Romero-Salguero, 5<sup>th</sup> International FEZA conference, 03-07 July 2011, Valencia, Spain.

Modification of an (E)-ethenylene-bridged PMO through Diels-Alder reactions.

Dolores Esquivel, Els De Canck, César Jiménez-Sanchidrián, Francisco J. Romero-Salguero and Pascal Van Der Voort, 13<sup>th</sup> Netherlands' Catalysis and Chemistry Conference (NCCC XII), 05-07 March 2012, Noordwijkerhout, The Netherlands.

Incorporating of new functionalities on (E)-ethenylene-bridged PMO through Diels-Alder reactions.

Dolores Esquivel, Els De Canck, César Jiménez-Sanchidrián, Francisco J. Romero-Salguero and Pascal Van Der Voort, Multifunctional, Hybrid and Nanomaterials, 3<sup>rd</sup> International conference, 03-07 March 2013, Sorrento, Italy.

Advanced periodic mesoporous organosilicas functionalized *via* different strategies for catalytic applications.

Els De Canck, Dolores Esquivel and Pascal Van Der Voort, International Conference on Advanced Complex Inorganic Nanomaterials (ACIN 2013), 15-19 July 2013, Namur, Belgium.

### ***Awards***

Best poster presentation award rewarded by the journal “Energy and Environmental Science” (EES, RSC Publishing) at the 2<sup>nd</sup> International Symposium on Advanced Complex Inorganic Nanomaterials (ACIN 2013), 15-19 July 2013, Namur, Belgium.

## ***Acknowledgements***

Een doctoraat bestaat uit meer dan enkel “proefjes” uitvoeren in het laboratorium. Het omvat zelfstandig onderzoek uitvoeren, maar ook samenwerken met collega’s; studenten begeleiden; leren organiseren en plannen; omgaan met hoogtes en laagtes, met tegenslagen en successen. Maar bovenal is het uitvoeren van een doctoraat een verrijking en een continu leerproces. Eentje dat ik gelukkig niet alleen heb moeten doorlopen...

In de eerste plaats wil ik Prof. dr. Pascal Van Der Voort danken. Hij verwelkomde me in de pas startende onderzoeksgroep *COMOC* en introduceerde de fascinerende wereld van de PMO materialen. Een uitdagend thema waarin Prof. Van Der Voort me niet enkel de kans gaf om mezelf te ontplooien als onderzoekster naar de bereiding en modificatie van PMO-materialen, maar hij liet me ook kennis maken met een waaier aan karakterisatiemogelijkheden en toepassingen. Als promotor stimuleerde Prof. Van Der Voort deze veelzijdigheid. Daarnaast, gaf hij me het vertrouwen en de verantwoordelijkheid in het lesgeven en begeleiden van studenten.

Uiteraard kwam dit uitgebreid werk niet tot stand zonder de samenwerking met andere onderzoekers en onderzoeksgroepen die natuurlijk ook een woordje van dank verdienen. Daarom dank ik graag Prof. dr. Willy Baeyens en dr. Yue Gao (VUB), dr. Jeriffa De Clercq (Hogeschool Gent) en Prof. dr. Abdelhamid Sayari (Ottawa University, Canada) voor de vruchtbare samenwerkingsverbanden betreffende adsorptie. Aangaande het gebied van katalyse, vermeld ik graag Prof. dr. Eric M. Gaigneaux en dr. Inmaculada Dosuna-Rodríguez (*UCL*).

Ik dank ook van harte de leden van de lees- en examencommissie voor het grondig nalezen van dit werk en voor het zetelen in mijn jury.

Daarnaast hebben ook vele andere onderzoekers en professoren mijn pad gekruist tijdens dit doctoraat die ik zeker wil danken voor hun inbreng, soms klein of groot, maar van grote waarde.

Mijn onderzoek en dit boekje zouden niet tot stand gekomen zijn zonder de onverminderde steun van onze onderzoeksgroep. De aangename atmosfeer en het geweldige groepsgevoel zijn absoluut de sterkste punten van *COMOC* en ik ben blij dat ik hiervan deel mag uitmaken. Daarom een welgemeende dankjewel aan mijn allerliefste collega's, ook aan hen die ons al verlaten hebben: Babs, Frederik, Elien, Ilke, Karen, Liesje en Matthias. Bij hen kon ik altijd terecht voor wetenschappelijk en niet-wetenschappelijk advies. *And of course, I cannot forget my foreign colleagues. Ying-Ya, thank you very much for your support. You are a great colleague but definitely also a fantastic friend. I always enjoyed our talks very much and I wish you all the best in China. Dolores, me gustaría darle las gracias por su ayuda durante mi tesis y por las muchas discusiones sobre los PMOs, así como sobre la cocina española y la hermosa España. ¡Su paella es fantástica!*

Vervolgens dank ik ook zeker de “jongere” generatie doctoraatsstudenten die ik bovendien ontzettend veel succes toewens in hun onderzoek: Hannes, Jeroen D.D., Jeroen L., Jonas B., Kevin, Mieke, Sander, Wannas en in het bijzonder Isabelle en Thomas. Isabelle, het was een plezier je te zien groeien van “mijn” thesisstudente naar een volwaardige onderzoekster. Bedankt voor de leuke babbels en steun. Thomas, ik wil jou van harte bedanken voor je immer positieve ingesteldheid, onuitputbare behulpzaamheid en de hilarische momenten in de bureau, het labo en de practicumzaal.

De vele bachelor- en masterstudenten die ik onder mijn hoede heb gehad, dank ik ook voor hun inzet, enthousiasme en leergierigheid. In het bijzonder: Linsey, Freya V.d.B., Isabelle en Jonathan. Het was een plezier samen onderzoek uit te voeren.

Het personeel en de andere onderzoeksgroepen van het departement Anorganische en Fysische Chemie dank ik van harte. In het bijzonder Tom en Danny voor hun hulp bij metingen en experimenten, mijn medeassistenten en de praktijkassistenten. An, Claudine, Els B. en Ilse zet ik graag in de bloemetjes voor de aangename gesprekken en steun tijdens dit doctoraat.



Graag wil ook een aantal personen vermelden die me buiten het wetenschappelijke wereldje hebben gesteund en voor de soms broodnodige afleiding hebben gezorgd. Sigelinde en Sylvia voor de gezellige etentjes en babbels. Cindy voor de leuke logeerweekendjes. Mijn percussievrienden voor gezellige repetities, spannende optredens en gewoon veel plezier en muziek: Barbara, Chris, Ineke, Joëlle, Kevin, Lut, en Wim. Mijn kooklesvrienden voor lekkere gerechten en veel hilariteit tijdens de les: An, Araksya, Edwinne, Geert, Imgard, Marianne en Pieter.

Heel in het bijzonder dank ik Freya D. voor de vriendschap en steun, niet enkel tijdens dit doctoraat, maar zeker ook daarbuiten.

Tot slot, dank ik zeker ook mijn ouders voor de altijd aanwezige steun tijdens dit doctoraatsonderzoek en de schrijfperiode. En als laatste, maar eigenlijk de belangrijkste van allemaal, dank ik mijn zus Evelien voor haar eerlijke advies, steun en het kritisch nalezen van dit doctoraat.

*Els De Canck*  
*Gent, September 2013*

## ***Preface***

Periodic Mesoporous Organosilicas are a very interesting class of hybrid nanomaterials that combine the framework and the rigidity of inorganic silicas with organic bridges. The latter is of great importance as it determines the properties of the materials such as hydrophobicity and stability. On top of this, the organic bridge can be chemically modified to introduce functional groups. This fine-tunes the PMO material for very specific *high-end* applications.

PMO materials are prepared by the hydrolysis and subsequent polycondensation of a polysilsesquioxane, most often a bis-silane, around a template. This template or surfactant forms micelles in acidic, basic or neutral aqueous environment. After formation of the organosilica network, the template is removed and a mesoporous hybrid material is obtained. The properties can be easily changed by altering the synthesis conditions, *e.g.*, surfactant, additives, swellers, pH, temperature, reaction time and stirring but the bridge of the silane is also a key factor. Many different organic bridges are reported: very simple units such as methane, ethane, ethene, benzene, *etc.* and more advanced organic moieties, *e.g.*, bridges containing chiral catalytic metal species. The organic function between the two silicon atoms will determine for which kind of applications it can be employed. PMO materials can be utilized in various fields such as heterogeneous catalysis by the inclusion of acid, base or metal functions, metal scavenging, gas sequestration, thin films for micro-electronics, stationary phases for HPLC columns,...

In this dissertation, it is attempted to show the versatility of PMO materials by developing and post-modifying PMOs for different applications. Post-modification is a very useful tool to incorporate the desired functionality as the initial structural properties of the PMO material are unaffected. Stable materials can be obtained as covalent anchoring occurs *via* the organic moiety and not *via* the grafting of silanes on silanols. The latter will lead to materials which are highly sensitive for leaching of the functionalities.

In this dissertation, the ethenylene-bridged PMO material is used as support for further modification procedures to obtain a mercury and CO<sub>2</sub> adsorbent but also to develop an acid containing catalyst. To achieve these goals, thiols, amines and sulfonic acid groups are incorporated, respectively. After thorough characterisation, the resulting sorbents or catalysts are evaluated for their specific application. Moreover, the heterogenization of a manganese complex for oxidation catalysis is performed on PMOs. A different type of PMO, containing multi-organic bridges, is used for this purpose and after Manganese attachment, the performance of the obtained catalyst in an epoxidation reaction is studied.

Many challenges still remain in this field, but I am confident that a bright future exists for PMO materials. Hopefully with this work, I will show you the existing diversity and extreme versatility of PMOs with its numerous advantages. But most of all, I sincerely hope you will enjoy reading this dissertation on this very fascinating class of hybrid nanomaterials.

*Els De Canck*

*Ghent, September 2013*

## Outline

This work consists of 10 chapters where Chapter 1 and 2 provide a *state of the art* overview concerning the synthesis and application of PMO materials, respectively. Chapters 3 to 8 present experimental work and describe the development of mercury adsorbents (Chapter 4 and 5), CO<sub>2</sub> adsorbents (Chapter 6), acid catalysts (Chapter 7) and oxidation catalysts (Chapter 8). At the end, Chapter 9 provides a brief summary and the overall conclusion of this work and Chapter 10 comprises of a Dutch summary.

**Chapter 1** introduces a class of hybrid nanomaterials, namely Periodic Mesoporous Organosilicas and describes in the first place the general synthesis. It also discusses the preparation of several PMOs with simple organic bridges and the influence of synthesis conditions on morphology and structural properties. Emphasis is mostly placed upon the PMO with ethenylene bridges. At the end of this chapter, a summary concerning post-modifications on PMOs is presented.

**Chapter 2** provides a *state of the art* overview on PMOs applied in different fields. Applications such as chromatography and low-*k* films for micro-electronics are described where especially simple organic bridges are essential. Also more advanced and complex PMO materials and their use in adsorption and catalysis are highlighted. Furthermore, the employment of these hybrid nanomaterials in biomedical orientated applications is included. Finally, the aim of this dissertation is summarized.

**Chapter 3** presents details concerning the synthesis of the precursor *trans* 1,2-bis(triethoxysilyl)ethenylene and the subsequent preparation of the ethenylene-bridged PMO material. The characterisation of the solids is discussed.

**Chapter 4** focuses on the development of a mercury adsorbent by the incorporation of thiol functionalities on the ethene-PMO. First the preparation of several benchmark materials is given. Afterwards, the different post-modification steps performed on the PMO are presented in detail. Finally, mercury sorption experiments are performed to evaluate the adsorbent. The regeneration abilities of this thiol containing PMO is researched.

**Chapter 5** expands the applicability of the thiol containing ethene-PMO by incorporating this sorbent in *Diffusive Gradients in Thin* (DGT) films. Mercury sorption experiments are performed and the PMO adsorbent is compared with two commercially available resins and two thiol functionalised silica materials.

**Chapter 6** describes the modification of ethenylene-bridged PMO materials with different amine functionalities. The resulting amine PMOs are thoroughly characterised and their CO<sub>2</sub> sorption ability is investigated. A comparison is made with an amine containing SBA-15 material.

**Chapter 7** explores the introduction of sulfonic acid functionalities on ethene-PMOs to use them as solid acid catalysts. First, the direct sulfonation is probed and the resulting materials are evaluated for the esterification of acetic acid and 1-propanol. Afterwards the oxidation of the thiol containing PMO towards a sulfonic acid group is discussed. The catalytic activity of the sulfonic acid PMO is determined and compared with the commercial catalyst Amberlyst-15. Moreover, the regeneration ability of this PMO material is examined.

**Chapter 8** comprises of the heterogenization of a Mn(acac)<sub>2</sub> complex on a multi-organic bridged PMO that consists of interconnected [Si(CH<sub>2</sub>)]<sub>3</sub> rings. The different post-modification steps are described in detail and characterisation is provided. The resulting Manganese catalyst is evaluated in the epoxidation of cyclohexene and its regeneration ability is studied.

**Chapter 9** gives a short summary and some general conclusions of this work and provides some future perspectives.

**Chapter 10** consists of a Dutch summary of this dissertation.

# Abbreviations

## A

Å	Ångström
AAS	Atomic Absorbance Spectroscopy
acac	Acetylacetonate
AFS	Atomic Fluorescence Spectroscopy
APTES	(3-aminopropyl)triethoxysilane
APTMS	(3-aminopropyl)trimethoxysilane
ATDSCH	allyl-(1,3,5[tris(diethoxy)sila]cyclohexane)

## B

BET	Brunauer Emmett Teller
BHT	2,6-bis(1,1-dimethylethyl)-4-methylphenol
BINAP	(2,2'-bis(diphenylphosphino)-1,1'-binaphthyl)
BINOL	(1,1'-binaphthalene)-2,2'-diol
BJH	Barret Joyner Halenda
Boc	Di- <i>tert</i> -butyl dicarbonate
BTX	Benzene, toluene, <i>o</i> - and <i>p</i> -xylene

## C

$c_{mc}$	Critical micelle concentration
CP	Cross polarization
cod	Cyclooctadiene
conv	Conversion
CV	Cold vapor
Cp	Cyclopentadienyl
Cy	Cyclohexyl

## D

DACH	<i>trans</i> -(1 <i>R</i> ,2 <i>R</i> )-diaminocyclohexane
DAB	Diaminobutane
DADD	Diaminododecane
DAG	Glycerol diacetate
DAH	Diaminohexane
DCM	Dichloromethane
DDT	Dichlorodiphenyltrichloroethane
DETA	Diethylenetriamine
DMF	<i>N,N</i> -dimethylformamide
DGT	Diffusive Gradients in Thin film
DIPEA	<i>N,N</i> -diisopropyl-ethylamine
dist.	Distilled
DRIFT	Diffuse Reflectance Infrared Fourier Transform

## E

ee	Enantiomeric excess
EISA	Evaporation Induced Self Assembly

<b>F</b>	
FID	Flame Ionization Detector
<b>G</b>	
GC	Gas Chromatography
<b>H</b>	
HMDS	1,1,1,3,3,3-hexamethyldisilazane
HPLC	High Performance Liquid Chromatography
HSAB	Hard Soft Acids and Bases
<b>I</b>	
IR	Infrared Spectroscopy
<b>K</b>	
KG	Kiesel gel
<b>L</b>	
LC	Liquid Chromatography
<b>M</b>	
MAG	Glycerol monoacetate
MAS	Magic Angle Spinning
mCBPA	3-chloroperoxybenzoic acid
MCM	Mobil Composition of Matter
MOF	Metal Organic Framework
MOM-Cl	Methyl chloro methyl ether
MPTES	(3-mercaptopropyl)triethoxysilane
MPTMS	(3-mercaptopropyl)trimethoxysilane
<b>N</b>	
NMR	Nuclear Magnetic Resonance
<b>P</b>	
p.a.	Pro analysi
PEG	Poly(ethyleneglycol)
PEO	Polyethylene oxide
Ph	Phenyl
PMO	Periodic Mesoporous Organosilica
POSS	Polyhedral oligomeric silsesquioxane
ppm	Parts per million
PPO	Polypropylene oxide
ppt	Parts per trillion
<b>R</b>	
rt	Room temperature
RC	Resistor-Capacitor

## S

$S_{\text{BET}}$	Specific surface area calculated <i>via</i> the BET theory
sel	Selectivity
SBA	Santa Barbara Amorphous material
SDA	Structure directing agent
SEM	Scanning electron microscopy
SQR	Sumichelate Q10R

## T

TAG	Glycerol triacetate
TBHP	<i>tert</i> -butylhydroperoxide
TDSCH	1,3,5[tris(diethoxy)sila]cyclohexane
TEOS	Tetraethoxyorthosilicate
TEM	Transmission electron microscopy
TEMED	<i>N,N,N,N</i> -tetraethylenediamine
TEPA	Tetraethylenepentamine
TGA	Thermogravimetric analysis
THF	Tetrahydrofuran
TMB	1,3,5-trimethylbenzene
TMOS	Tetramethoxyorthosilicate
TMS	Tetramethylsilane
TMSCN	Trimethylsilyl cyanide
TOF	Turnover Frequency
TON	Turnover Number
TPB	1,3,5-triisopropylbenzene

## U

UV	Ultra violet
----	--------------

## V

VOC	Volatile organic compound
$V_p$	Pore volume
VTES	Vinyltriethoxysilane

## X

XPS	X-ray photoelectron spectroscopy
XRD	X-ray diffraction spectroscopy
XRF	X-ray fluorescence spectroscopy

## Y

YAG	Yttrium aluminium garnet
-----	--------------------------

## Z

ZSM	Zeolite Socony Mobil
-----	----------------------



# **1 A new class of hybrid nanomaterials:**

## ***Periodic Mesoporous Organosilicas***

This chapter introduces the class of *Periodic Mesoporous Organosilicas* or *PMOs* and describes the general synthesis procedure of these nanomaterials. It will also provide the main differences with mesoporous templated silicas. Next, a brief literature overview of the different types of PMO materials is presented with simple organic functions. Emphasis is mostly placed upon the ethenylene function which will be the main subject of this dissertation. Furthermore, several interesting properties of this material are briefly discussed, such as the hydrophobicity and stability of PMOs. A final section will summarize the *state of the art* concerning the post-modification of these nanomaterials.

Parts of this chapter were published as

Pascal Van Der Voort, Dolores Esquivel, Els De Canck, Frederik Goethals, Isabel Van Driessche and Francisco J. Romero-Salguero, *Chemical Society Reviews*, **2013**, 42, 9, 3913-3955.

## 1.1 Introduction

The research field of nanoporous materials is an interesting and exciting topic with countless researchers involved worldwide. Two types of hybrid solids, combining organic and inorganic properties in one material, were developed during the latest decade and are considered as important subjects in this field. The first class includes *Metal Organic Frameworks* or *MOFs* and they consist of metal ions or metal clusters connected with organic linkers. Probably the most famous MOF material is MOF-5, first reported by Yaghi *et al.*<sup>1</sup> These hybrid materials are employed in a very broad area of applications and excellent reviews have recently appeared concerning this hybrid nanomaterial.<sup>2-7</sup>

The second class of hybrid nanomaterial is the *Periodic Mesoporous Organosilica* or abbreviated as *PMO*. The first reports appeared in 1999, published by three independent research groups, namely Stein *et al.*,<sup>8</sup> Inagaki *et al.*,<sup>9</sup> and Ozin *et al.*<sup>10</sup> This development occurred very shortly after the first account on the now well-known SBA-type materials<sup>11, 12</sup> and also a few years after the development of the famous ordered mesoporous silicas (MCM materials) by the Mobil Oil company.<sup>13</sup> Both materials, SBA and MCM, are considered to be the “ancestors” of PMOs as similarities can be found between the syntheses.

PMOs are prepared by the hydrolysis of a bis-silane and subsequent polycondensation around a template (Figure 1.1). The bis-silane is represented by  $(OR')_3\text{-Si-R-Si-(OR')}_3$  with R the organic functionality and OR' a hydrolysable alkoxy moiety, mostly methoxy or ethoxy groups. The template or surfactant will aggregate in the aqueous environment and form micelles around which the bis-silane will polycondense. A variety of silanes and surfactants exists and acid, basic or neutral conditions can be employed to alter the final properties. Naturally, this opens up many opportunities for the preparation of very different materials. After aging, surfactant removal is performed by extraction or calcination under inert atmosphere to open up the porous structure of the PMO material. Figure 1.1 presents a schematic overview of a general synthesis procedure with the template Pluronic P123 ( $\text{PEO}_{20}\text{PPO}_{70}\text{PEO}_{20}$ ) and a generic bis-silane.

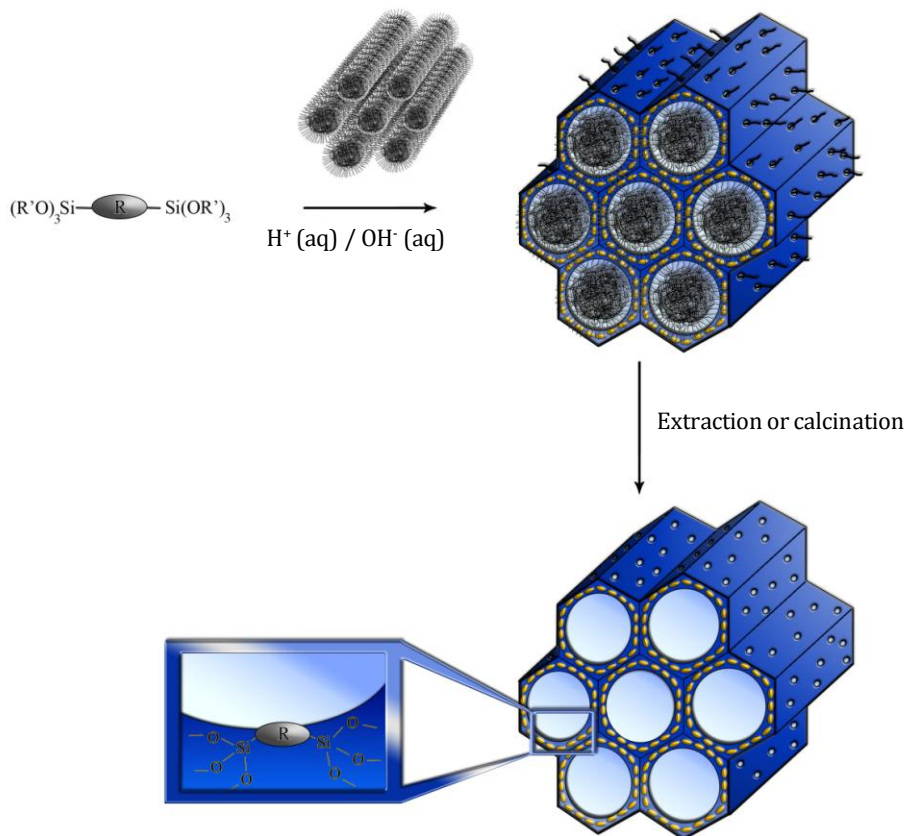


**Figure 1.1:** Schematic representation of the synthesis of a Periodic Mesoporous Organosilica: the bis-silane with the organic functionality R and the alkoxy groups OR' hydrolyzes and polycondenses around the micelles of the surfactant. After extraction or calcination, a porous material is obtained.<sup>14</sup>

The synthesis can occur hydrothermally, via the *Evaporation Induced Self Assembly* (EISA) process,<sup>15</sup> or even with the use of microwaves.<sup>16</sup> The EISA method, described by Brinker *et al.*,<sup>17</sup> is a procedure that can be used to prepare thin films (Figure 1.2). It consists of the addition of a large excess of volatile solvent, *e.g.* ethanol, next to the common ingredients such water, surfactant and catalyst (*e.g.* HCl). In this state, the initial concentration of the surfactant ( $c_0$ ) is below the critical micelle concentration or  $c_{mc}$ . Only when the solvent evaporates, an enrichment of the surfactant will occur and  $c_{mc}$  will be exceeded. This will lead to micelle formation and the silane will hydrolyze and condensate around the micelles.<sup>15</sup>

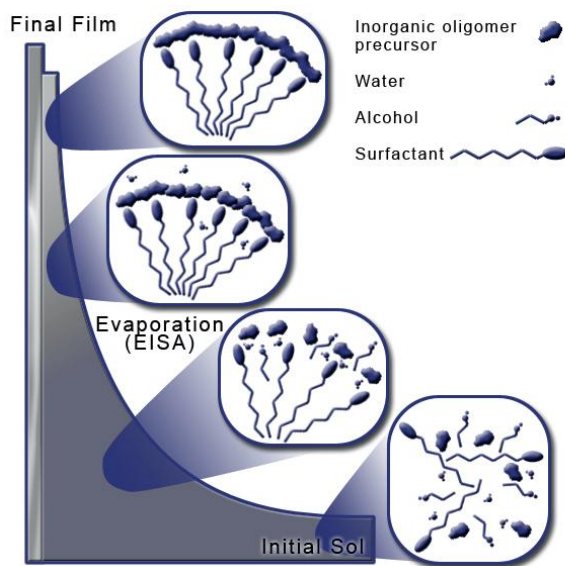


**Figure 1.2: Schematic representation of the Evaporation Induced Self Assembly process for the preparation of thin films.<sup>18</sup>**

The described hydrothermal procedure is relatively similar to the synthesis of SBA-15.<sup>11, 12</sup> Nevertheless a few major and important differences exist. The functional groups of a PMO are homogeneously distributed, not only on the surface of the material, but also inside the pore walls (Figure 1.1). The functions inside the walls are not accessible and thus not available for any chemical modification. However, these organic groups are beneficial for the overall structural properties of the PMO material due to the addition of rigidity or flexibility. In contrast, the organic bridges on the surface of the PMO material are reachable and can be chemically modified.

These bridges can be very short and uncomplicated such as a methane, ethane, ethene and benzene function. On the other hand, also very complex bridges exist that contain hetero-atoms or chiral structures, metal complexes or nanoparticles. A brief overview of the most commonly used bis-silanes and their abbreviations is given in Table 1.1. Furthermore, Table 1.2 presents an overview of the most common templates and their abbreviations.

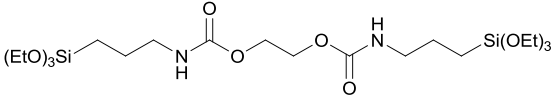
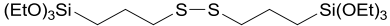
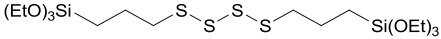
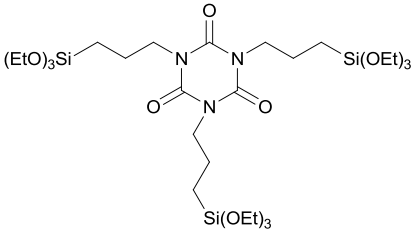
Table 1.1 only shows a small amount of the numerous bis-silanes that exist. More complex and advanced structures are reported including multi-organic bridged

precursors. This variation in silanes provides materials for all different kinds of applications including chromatography, sensing, catalysis, adsorption, micro-electronics and biomedical applications. Several reviews have appeared on the subject of Periodic Mesoporous Organosilicas,<sup>19-29</sup> including the very recent publication of a comprehensive review in *Chemical Society Reviews* by our group.<sup>30</sup>

**Table 1.1: Limited overview of the most common silanes used in PMO synthesis.**

Abbreviation	Full name	Structural formula
BTME	1,2-Bis(trimethoxysilyl)ethane	
BTEE	1,2-Bis(triethoxysilyl)ethane	
BTEENE	1,2-Bis(triethoxysilyl)ethylene	
BTEM	1,2-Bis(triethoxysilyl)methylene	
BTEB	1,4-Bis(triethoxysilyl)benzene	
BTEEB	1,4-Bis(triethoxysilylethyl)benzene	
BTEVB	1,4-Bis((E)-2-(triethoxysilyl)vinyl)benzene	
BTEVS	1,4-Bis((E)-2-(triethoxysilyl)vinyl)stilbene	
BTET	2,5-Bis-(triethoxysilyl)thiophene	

Table 1.1 – Continued.

BTEPUE	Bis[3-(triethoxysilyl)propyl urethane] ethane	
BTEPDS	Bis[3-(triethoxysilyl)propyl] disulfide	
BTEPTS	1,4-Bis(triethoxysilyl)propane tetrasulfide	
ICS	Tris [3-(trimethoxysilyl)propyl]isocyanurate	

**Table 1.2: Limited overview of the most common templates used in PMO synthesis.**

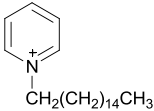
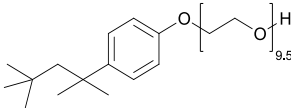
Abbreviation	Full name	Structural formula
CTAC/CTAB	cetyltrimethylammonium chloride/bromide	$\begin{array}{c} \text{CH}_3 \\   \\ \text{H}_3\text{C}-\text{N}^+(\text{CH}_2)_{15}\text{CH}_3 \\   \\ \text{CH}_3 \end{array} \quad \text{Cl}^- / \text{Br}^-$
OTAC	octadecyltrimethylammonium chloride	$\begin{array}{c} \text{CH}_3 \\   \\ \text{H}_3\text{C}-\text{N}^+(\text{CH}_2)_{17}\text{CH}_3 \\   \\ \text{CH}_3 \end{array} \quad \text{Cl}^-$
C <sub>n</sub> TMACl/Br	alkyltrimethylammonium chloride/bromide	$\begin{array}{c} \text{CH}_3 \\   \\ \text{H}_3\text{C}-\text{N}^+(\text{CH}_2)_{n-1}\text{CH}_3 \\   \\ \text{CH}_3 \end{array} \quad \begin{array}{l} \text{Cl}^- / \text{Br}^- \\ (n = 8, 10, 12, 14, 16, 18) \end{array}$
CPCl	cetylpyridinium chloride	
FC4	fluorocarbon surfactant	$\text{C}_3\text{F}_7\text{O}(\text{CF}_2\text{CF}_2\text{O})_2\text{CF}_2\text{CF}_2\text{CONH}(\text{CH}_2)_3-\text{N}^+(\text{C}_2\text{H}_5)_2 \quad \text{I}^-$
Brij-30	polyoxyethylene (4) lauryl ether	$\text{HO} \left[ \text{CH}_2\text{CH}_2\text{O} \right]_4 \text{CH}_2(\text{CH}_2)_{10}\text{CH}_3$
Brij-56	polyoxyethylene (10) cetyl ether	$\text{HO} \left[ \text{CH}_2\text{CH}_2\text{O} \right]_{10} \text{CH}_2(\text{CH}_2)_{14}\text{CH}_3$



Table 1.2 – Continued.

Brij-76	polyoxyethylene (10) stearyl ether	$\text{HO} \left[ \text{CH}_2\text{CH}_2\text{O} \right]_{10} \text{CH}_2(\text{CH}_2)_{16}\text{CH}_3$
Triton-X100	polyoxyethylene (10) octylphenyl ether	
P123	Pluronic® P123 poly(ethylene glycol)-poly(propylene glycol)-poly(ethylene glycol)	$\text{HO} \left[ \text{CH}_2\text{CH}_2\text{O} \right]_{20} \left[ \text{CH}_2\text{CH}(\text{CH}_3)\text{O} \right]_{70} \left[ \text{CH}_2\text{CH}_2\text{O} \right]_{20} \text{H}$
F127	Pluronic® F127 poly(ethylene glycol)-poly(propylene glycol)-poly(ethylene glycol)	$\text{HO} \left[ \text{CH}_2\text{CH}_2\text{O} \right]_{100} \left[ \text{CH}_2\text{CH}(\text{CH}_3)\text{O} \right]_{65} \left[ \text{CH}_2\text{CH}_2\text{O} \right]_{100} \text{H}$
B50-6600	poly(ethylene oxide)–poly(butylene oxide)–poly(ethylene oxide)	$\text{HO} \left[ \text{CH}_2\text{CH}_2\text{O} \right]_{39} \left[ \text{CH}_2\text{CH}_2\text{CH}_2\text{CH}_2\text{O} \right]_{47} \left[ \text{CH}_2\text{CH}_2\text{O} \right]_{39} \text{H}$
PEO-GLGA-PEO	poly(ethylene oxide)–poly(lactic acid-co-glycolic acid)–poly(ethylene oxide)	$\text{HO} \left[ \text{CH}_2\text{CH}_2\text{O} \right]_x \left[ \text{O} \left( \text{C}(=\text{O})\text{CH}(\text{CH}_3) \right)_y \left( \text{C}(=\text{O})\text{CH}_2 \right)_z \right]_y \left[ \text{CH}_2\text{CH}_2\text{O} \right]_x \text{H}$
C <sub>n-s-m</sub>	Divalent and <i>gemini</i> surfactants	$\text{C}_n\text{H}_{2n+1} \left[ \text{N}^+(\text{CH}_3)_2 \right] (\text{CH}_2)_s \left[ \text{N}^+(\text{CH}_3)_2 \right] \text{C}_m\text{H}_{2m+1} 2 \text{Br}^-$

## 1.2 PMOs with simple organic bridges

A number of synthetic parameters will influence the formation of the Periodic Mesoporous Organosilicas. The type of precursor and organic bridge, template, catalyst, additives, swelling agents, synthetic compositions and conditions and the post-treatments such as extraction or calcination are all important elements during the synthesis. In this section, focus is placed upon PMO materials with relatively small and simple organic bridges and a short discussion on the properties or peculiarities concerning ethylene-bridged (-CH<sub>2</sub>CH<sub>2</sub>-), methylene-bridged (-CH<sub>2</sub>-) and phenylene-bridged (-C<sub>6</sub>H<sub>4</sub>-) PMOs is given below. A more extensive part with regard to the ethenylene-bridged (-CH=CH-) PMO materials is presented as this PMO is the main subject of this dissertation.

### 1.2.1 The ethane-PMO

The ethylene-bridged PMO or more easily the ethane-PMO is in general well-described in literature as it is the most commonly used PMO material. The precursor BTME or BTEE is solely employed in the synthesis or it is polycondensed with other organosilanes. Different types of surfactants (cationic and non-ionic) are employed and will influence the ordering of the mesophase and can also have an effect on the external morphology of the particles.

**Cationic Surfactants.** The first reports on PMOs in 1999 by Stein *et al.* and Inagaki *et al.* described the synthesis of ethylene-bridged PMOs with the cationic surfactants CTAB<sup>8</sup> and OTAC<sup>9</sup>, respectively. Only the latter exhibited long-range ordering as 2D-hexagonal (*P6mm*) and 3D-hexagonal (*P6<sub>3</sub>/mmc*) symmetries were observed depending on the synthetic composition. Whereas normally the surfactants C<sub>n</sub>TMACl provide materials with 2D-hexagonal ordering, CTAC can also yield materials with a cubic arrangement.<sup>31</sup> Another cubic symmetry is witnessed when PMOs are prepared with C<sub>16</sub>TEABr in acidic environment. The co-condensation of tetraethyl orthosilicate (TEOS) and BTEE delivers materials that exhibit a *Pm3n* space group.<sup>32</sup> Besides, the use of *gemini* surfactants for the synthesis of PMOs is also probed.<sup>33,34</sup> By using cationic surfactants, different external morphologies can be synthesized. The

materials with a 2D-hexagonal arrangement normally exhibit rope- and gyroid-shaped particles<sup>9, 35, 36</sup> whereas the cubic arrangements preferably offer spherical,<sup>35</sup> decaoctahedral<sup>37,38</sup> and dodecahedral<sup>39</sup> shapes.

**Non-ionic surfactants.** In contrast to cationic surfactants, the employment of neutral templates can significantly increase the pore size of the resulting PMO material. Two types of surfactants are used: the block-copolymers such as P123,<sup>40-43</sup> F127,<sup>44,45</sup> PEO-PLGA-PEO<sup>46,47</sup> and B50-6600;<sup>48</sup> and the poly(alkylene)oxides such as Triton-X100<sup>49</sup> and Brij-56. The latter surfactant tends to provide good quality PMO materials with a 2D-hexagonal symmetry, not only for the ethylene bridges but also for other silanes (ethenylene, methylene and phenylene).<sup>50-52</sup>

The external morphology is of major importance for some applications such as chromatography, but also for the adsorption of drugs and immobilization of enzymes or proteins. Especially hollow spheres<sup>53-56</sup> and nanotubes<sup>57,58</sup> are of great interest. A more extensive overview of different methods to prepare ethylene-bridged PMOs, properties and references can be found in reference 30.

### **1.2.2 *The methane-PMO***

Only a few reports can be found on these methylene-bridged PMO materials. It was the group of Ozin who initially reported them and the materials were prepared with BTEM and CTAB in basic environment.<sup>59</sup> However, only materials with small pores were obtained. PMOs with larger pores were synthesized by the use of P123 in acidic aqueous medium with the addition of NaCl.<sup>60,61</sup>

### **1.2.3 *The benzene-PMO***

Extensive investigation on the phenylene-bridged PMOs by various research groups occurred and is still on-going since the moment that the group of Ozin reported a type of PMO material with an aromatic bridge.<sup>62</sup> With mild acidic conditions, an ionic surfactant CPCI and BTEB, they were able to produce PMO materials with a high specific surface area of 1365 m<sup>2</sup> g<sup>-1</sup> and pore sizes of 2 nm. Similar to the methylene- and ethylene-bridged materials, large pore materials were

accomplished by the use of P123 for a 2D-hexagonal and F127 for 3D-cubic systems with pores of 6.0-7.4 nm<sup>63</sup> and 8 nm,<sup>64</sup> respectively. One publication already briefly mentioned the occurrence of  $\pi$ --- $\pi$  stacking between the phenylene moieties and describes some degree of ordering in the pore walls.<sup>65</sup> One year later, Inagaki *et al.* reported the first 2D-hexagonal phenylene-bridged PMO material with crystal-like pore walls with the aid of OTAC under basic conditions.<sup>66</sup> The material with a  $S_{\text{BET}}$  of 818 m<sup>2</sup> g<sup>-1</sup> and pore size of 3.8 nm, displayed a structural periodicity of 7.6 Å along the direct channels caused by the alternation of silica and benzene moieties. This alternation created hydrophobic and hydrophilic layers within the same material. It is said that the molecular-scale periodicity exists due to hydrophobic and hydrophilic or  $\pi$ --- $\pi$  interactions of the BTEB which helps the self assembly during synthesis. Although one study confirmed this,<sup>67</sup> another study provides evidence that is not in agreement with the  $\pi$ --- $\pi$  stacking. An advanced NMR investigation exposes the rotational mobility of biphenylene bridges in a PMO material with crystal-like framework.<sup>68</sup> More space was eventually available than in a face-to-face close-packed system which allowed rotation.

As the example was set with the phenylene-bridged PMO, the research was extended by the preparation of PMO materials with different aromatic bis-silanes. Precursors such as 1,4-bis(triallylsilyl)benzene,<sup>69</sup> 1,3-bis(triethoxysilyl)benzene,<sup>70</sup> 1,4-bis(diallylethoxysilyl)benzene and 1,4-bis-(triallylsilyl)benzene<sup>71</sup> gave rise to PMOs, with and without molecular-scale periodicity. The presence of the benzene moiety raises interesting functionalisation opportunities.

### 1.2.4 The ethene-PMO

In contrast to the large amount of research performed on the ethylene-bridged PMO material, less investigation is executed on the unsaturated variant. Even though the ethenylene-bridged PMO offers more chemical modification possibilities due to the presence of the interesting C=C bond.

It was again the group of Ozin who published one of the earliest reports in *Nature* on the synthesis of ethenylene-bridged PMO materials.<sup>72</sup> The surfactant CTAB in basic medium (NH<sub>4</sub>OH) was used as template and BTEENE as bis-silane. These materials with a hexagonal symmetry showed a specific surface area of 637 m<sup>2</sup> g<sup>-1</sup>, a pore volume of 0.60 mL g<sup>-1</sup> and a pore diameter of almost 4 nm. At the same moment Stein *et al.*<sup>8</sup> also synthesized ethenylene-bridged materials. Although these authors used CTAB as well, the BTEENE was hydrolyzed in an acidic medium (H<sub>2</sub>SO<sub>4</sub>) before the precipitation was induced by raising the pH with NaOH. This method resulted in less-ordered materials with wormlike structures in comparison with Ozin's ethenylene-bridged PMOs. However the specific surface was significantly higher, namely 1210 m<sup>2</sup> g<sup>-1</sup>, but smaller pores of 2.4 nm were observed.

Furthermore, the group of Mokaya *et al.* also published on the synthesis of ethenylene-bridged PMO materials. They prepared PMOs using BTEENE and different alkyltrimethylammonium bromide surfactants (C<sub>n</sub>TMABr, n = 14, 16, 18).<sup>73</sup> Materials with different morphologies (Figure 1.3) were obtained such as monodisperse spheres (n = 12), rod- or cage-like particles (n = 14) and rope-like particles (n = 16 or 18). The same group also observed molecular-scale periodicity similar to the ordering observed in phenylene-bridged PMO materials.<sup>74,75</sup> Next to the expected intense (100) and two other well-resolved signals in the range of 3-10°, an extra reflection at 2θ = 16.5° appeared (Figure 1.4). The authors assigned this as the lamellar ordering of the ethene groups with a basal spacing of 5.6 Å.

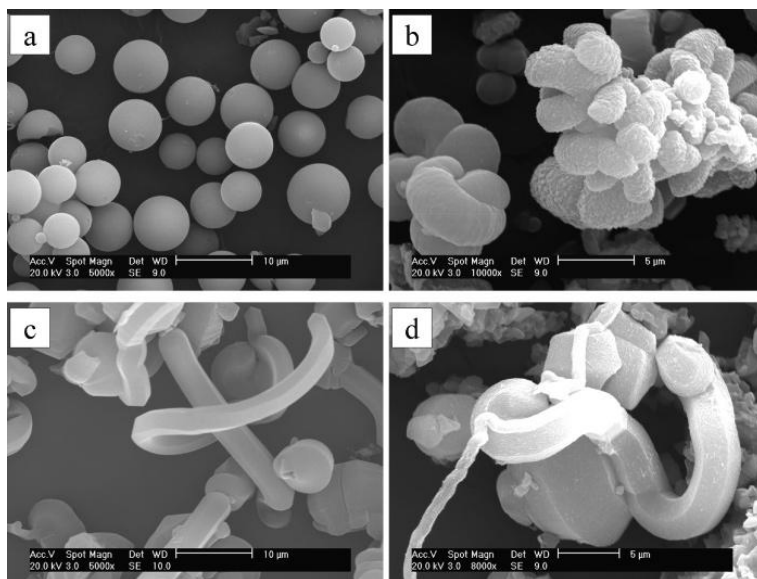


**Figure 1.3:** SEM images of ethynylene-bridged PMO materials prepared with different surfactants: (a)  $C_{12}$ TMABr, (b)  $C_{14}$ TMABr, (c)  $C_{16}$ TMABr, and (d)  $C_{18}$ TMABr.<sup>73</sup>

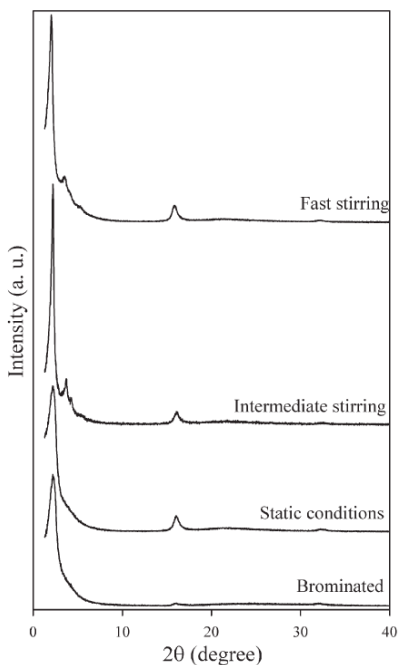


**Figure 1.4:** X-ray diffraction patterns for ethynylene-bridged PMO materials prepared under different synthesis conditions and after bromination of the double bond.<sup>74</sup>

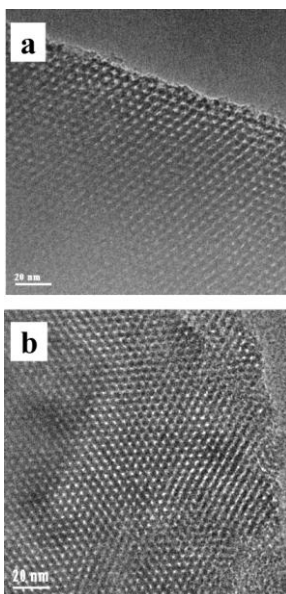


**Figure 1.5:** TEM images for an ethenylene-bridged PMO material prepared with the surfactants Brij-76 (a) and Brij-56 (b). (Both projected along the [001] zone axes)<sup>76</sup>

In an attempt to synthesize ethenylene-bridged PMO materials with larger pores, the same type of surfactant is used as for the ethylene-, methylene- and phenylene-bridged PMOs, namely non-ionic block copolymers<sup>76,77</sup> and poly(alkylene oxides)<sup>76</sup> as templates. A series of PMOs was synthesized by using the surfactants Brij-56, -58, -76 and -78 under acidic conditions.<sup>76</sup> Specific surface areas of 847-981 m<sup>2</sup> g<sup>-1</sup> and pore sizes up to 5.1 nm were noted. The PMO materials prepared with Brij-56 and especially Brij-76 exhibited a well-ordered structure with a hexagonal symmetry (Figure 1.5). The use of the Pluronic P123 led to the increase of the pores up to 8.6 nm and also a large pore volume of 0.91 mL g<sup>-1</sup>. The authors also showed that the addition of 1-butanol during the synthesis significantly narrowed the pore size distribution in comparison to the material prepared without additives and thus improves the overall quality of the PMO.

The research concerning this type of PMO materials has significantly expanded with the work of Van Der Voort *et al.*<sup>78-85</sup> The authors were the first to synthesize diastereoisomerically pure BTEENE with 100% *trans* configuration by using an olefin metathesis reaction with the first generation Grubbs' catalyst. At the same moment

they reported the synthesis of a *trans* ethylene-bridged PMO material.<sup>78</sup> Moreover, they were able to considerably reduce the synthesis time and still retain excellent structural properties of the PMO material with a specific surface area of  $>1000 \text{ m}^2 \text{ g}^{-1}$ . Next to materials with the pure *trans* isomer, it was also possible to vary the ratio of *cis* and *trans* configuration.<sup>84</sup> Distinct differences between the resulting PMOs were detected by examining the porosity and ordering of the mesostructure. In particular, an increase of the *cis* isomer diminished the hydrothermal stability of the PMO (Figure 1.6) and differences on molecular level were discovered with solid state NMR. Further investigation was performed on the influence of different synthetic parameters such as the pH, use of additives and extraction procedure.<sup>82</sup> And also a system with partial pore blocking was developed analogous to the work on silica materials.<sup>81, 82</sup>

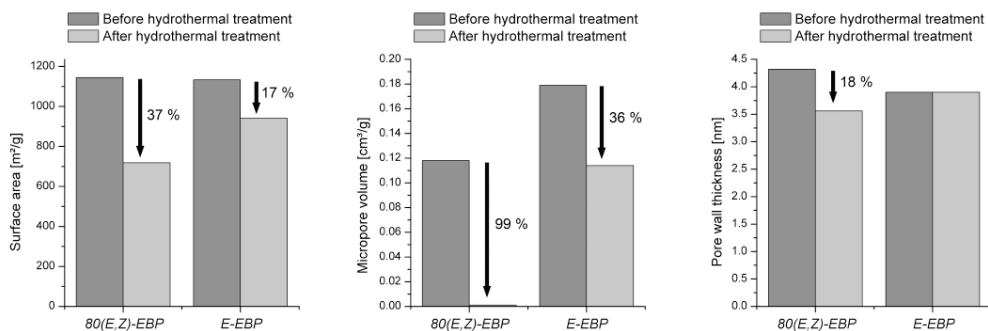


**Figure 1.6: Influence of the isomeric configuration on the hydrothermal stability of the ethylene-bridged PMO material: comparison between a PMO prepared with 80% *trans* and 20% *cis* (80(E,Z)-EBP) and 100% *trans* (E-EBP) ethene bonds.<sup>84</sup>**

A few studies have emphasized controlling the morphology of the ethylene-bridged PMO material. For example, spherical particles with molecular-scale periodicity were obtained by employing  $\text{C}_{12}\text{TMABr}$  in highly basic conditions.<sup>86</sup> However, decreasing the basicity did not lead to any periodicity and ethanol had to be added in order to obtain spherical particles.<sup>87</sup> Furthermore, it was possible to achieve other morphologies.<sup>74, 88</sup>

A literature overview is presented in Table 1.3 concerning the synthesis of ethylene-bridged PMO materials. It comprises of a list with a summary of the used synthetic conditions, the structural properties and the references.



**Table 1.3: Representative syntheses of ethenylene-bridged PMOs.**

	Surfactant	Gelling agent	Additive	Structure / Symmetry	S <sub>BET</sub> m <sup>2</sup> g <sup>-1</sup>	d <sub>p</sub> nm	Year	Ref.
cationic	CTAB	H <sub>2</sub> SO <sub>4</sub> /NaOH	-	Wormlike	1210	2.4	1999	8
		NH <sub>4</sub> OH	-	Hexagonal	637	3.9	1999	72
		NaOH	-	2D-hexagonal/ <i>P6mm</i> (crystal-like pore walls)	1296	3.9	2005	75
	C <sub>n</sub> TMABr	NaOH		Hexagonal/ <i>P6mm</i> with <i>n</i> =12, 14, 16 (crystal-like pore walls)	952 - 1205	2.4 - 4.1	2006	73
Block-copolymers	P123	HCl	-	2D-hexagonal/ <i>P6mm</i>	676	8.6	2004	76
			BuOH		624	8.0		
		HCl	-	2D-hexagonal/ <i>P6mm</i>	705	6.3	2005	77
		HCl	BuOH	2D-hexagonal/ <i>P6mm</i>	1018	5.9	2007	82, 89

Table 1.3 - Continued.

	Surfactant	Gelling agent	Additive	Structure / Symmetry	$S_{\text{BET}}$ $\text{m}^2 \text{g}^{-1}$	$d_p$ nm	Year	Ref.
Poly(alkylene oxide)	Brij-56/-76	HCl	-	2D-hexagonal/ <i>P6mm</i>	868 - 894	4.0 - 5.1	2004	76
	Brij-58/-78	HCl	-	Low order	847 - 981	3.1 - 3.5	2004	76
	$\text{C}_{12}\text{TMABr}^{\text{a}}$	NaOH	-	2D-hexagonal/ <i>P6mm</i> (spherical particles)	940 - 1006	2.0 - 2.3	2006	86
	CTAB <sup>a</sup>	$\text{NH}_4\text{OH}$	EtOH	Hexagonal (spherical particles)	1000 - 1884	2.2 - 2.6	2005	87
		NaOH	-	Cage- and rope-like	1222 - 1315	3.3 - 3.7	2006	74
	FC-4911 <sup>b</sup> + CTAB <sup>a</sup>	NaOH	-	2D-hexagonal/ <i>(P6mm)</i> (twisted rod-like)	965	2.7	2007	88

<sup>a</sup> Focus is placed upon the external morphology of the particles.

<sup>b</sup> FC-4911 is an achiral cationic fluorinated surfactant:  $\text{CF}_3(\text{CF}_2)_3\text{SO}_2\text{NH}(\text{CH}_2)_3\text{N}^+(\text{CH}_3)_3\text{I}^-$ .

### 1.3 Properties of PMOs

An important aspect of tailoring a PMO material is the ability to enlarge the pore size. This is also called *pore size engineering*. Especially for applications such as the immobilization or adsorption of proteins, enzymes or drugs, this is of major importance. The employment of block-copolymers and poly(alkylene oxides) already resulted in larger pores, however values above 10 nm could not be achieved. The addition of swelling agents to the reaction mixture can provide an answer for this issue. These additives are typically hydrophobic compounds and will interact with the surfactant by settling in the hydrophobic part of the polymer. An expansion of the core of the surfactant will occur and this results in larger pores. Typical swelling agents are 1,3,5-trimethylbenzene (TMB), 1,3,5-triisopropylbenzene (TPB), cyclohexane but also xylene, toluene and benzene are reported.

This method is applied for ethenylene-bridged PMO materials with TMB as swelling agent.<sup>80</sup> Several PMOs were prepared by the addition of TMB just after completely dissolving P123. The amount of swelling agent was varied and a pore expansion up to 28.3 nm was accomplished. The effect of TMB can be noticed in the nitrogen sorption isotherms (Figure 1.7). Not only an enlargement of the pores occurred, also the pore volume reached an extremely high value, namely 2.25 mL g<sup>-1</sup>. Still using TMB, but with slightly altered reaction conditions, the authors also succeeded developing PMO materials with a bimodal pore size distribution (Figure 1.8). The resulting PMO exhibited pore sizes of 8.1 and 21.3 nm.

The group of Kruk on the other hand, utilized cyclohexane in combination with P123 to acquire large pore ethenylene-bridged PMO materials.<sup>90</sup> The authors noticed that a decrease of the initial temperature during the synthesis, expanded the pores significantly. Therefore, with initial temperatures of 10 to 15°C, a pore expansion of 11.9 up to 22.0 nm was achieved. They extended this method to methylene-, ethylene- and phenylene-bridged PMOs with the use of cyclohexane but also with TPB. In addition it was observed that the type of bridge drastically affected the formation of the framework and the unit-cell size.

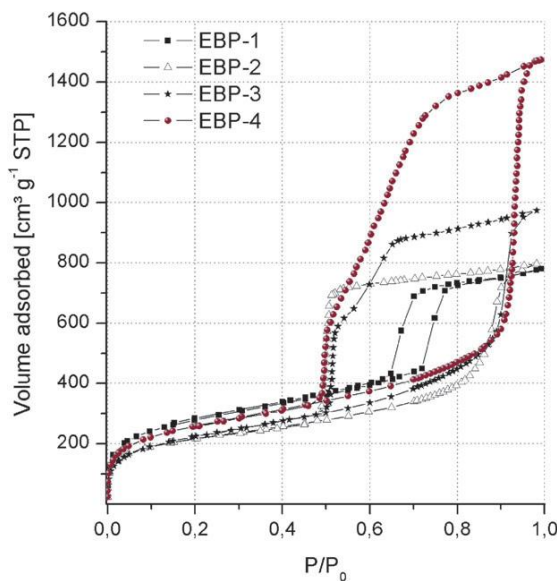


**Figure 1.7:** Nitrogen adsorption-desorption isotherms of the ethylene-PMOs EBP-1, EBP-2, EBP-3 and EBP-4 prepared with the addition of 0, 1.73, 2.59 and 7.76 mmol TMB, respectively.<sup>80</sup>

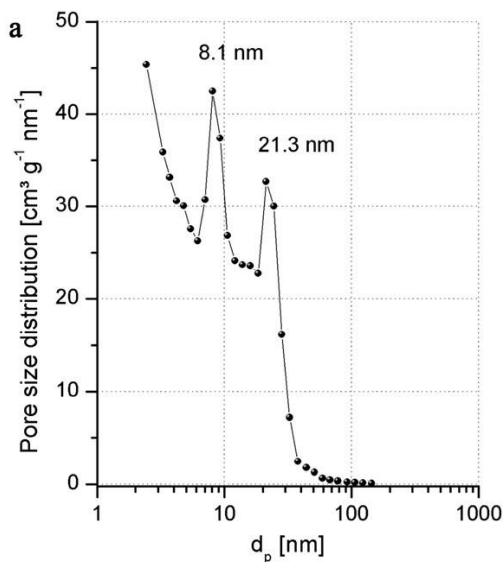


**Figure 1.8:** Pore size distribution of a bimodal PMO material (calculated from the adsorption branch of the isotherm with the BJH method).<sup>80</sup>

The type of PMO bridge also determines the thermal stability of the entire material. The organic bridges can decompose when a heat treatment is applied.

Besides the organic moiety, the stability also depends on the atmosphere used during calcination (air or inert). Generally phenylene-bridged PMO materials are the most thermally stable and they can withstand temperatures up to 500-570°C in air.<sup>66, 70, 91</sup> The thermal stability of ethenylene-bridged PMO materials is only limited to 200-300°C in air.<sup>77, 92</sup> An overview of the upper temperature limits reported for several PMOs with simple organic bridges is presented in Table 1.4.

**Table 1.4: Upper temperature limit of stability for PMOs with different bridges.**

Bridge	T <sub>air</sub> (°C)	T <sub>nitrogen</sub> (°C)	Ref.
Ethane	200-300	400-540	38, 39, 92, 93
Ethene	200-300	-	75, 77, 92
Methane	400	-	59
Benzene	500-570	500	47, 66, 70, 91

An important aspect of PMO materials is the hydrophobicity as this will strongly influence the hydrothermal and mechanical stability. This relationship originates from the structural degradation by hydrolysis. A more hydrophobic material prevents this and exhibits a higher mechanical stability. Furthermore, the hydrophobicity combined with thicker pore walls further improves the stability in comparison with silica materials. This has been observed by several authors where the hydrothermal stability of PMOs was higher.<sup>8, 66, 94</sup> This did not only imply the retainment of the mesoporous ordering but also involved the molecular-scale periodicity of the material. It was observed that the periodicity in ethenylene- and phenylene-bridged PMO materials was retained after severe hydrothermal treatments.<sup>75, 94</sup>

The effect of the organic bridge on the hydrophobicity of the overall material was clearly shown by water adsorption experiments.<sup>32</sup> Materials prepared with different ratios of TEOS and BTEE, demonstrated that an increasing amount of ethylene bridges resulted in a decreasing amount of adsorbed water. The hydrophobic nature of the ethylene-bridged PMO material was also confirmed by Markowitz *et al.*<sup>94</sup> They described the hydrophilic character of certain PMO materials in comparison with silica. The following sequence was obtained: ethylene < phenylene < methylene < 1.21

silica. The mechanical stability was better for the more hydrophobic materials, thus emphasising the relationship between structural degradation and hydrolysis by water.

The hydrothermal and mechanical stability of ethenylene-bridged PMO materials was compared with the stability of the ethylene variant.<sup>85</sup> A steam treatment of 3 days at 105°C was applied for both materials. The ethylene-bridged PMO turned out to possess a higher stability as the ethenylene-bridged PMO showed a significant decrease in specific surface area, pore volume and micropore volume. The same trend was observed for the mechanical stability. Hydrophobization with HMDS greatly improved the stability of the ethenylene-bridged PMO and no great differences were observed anymore between the materials. This clearly proved that the hydrophobicity is of paramount importance.

## **1.4 *Post-modification of the PMO material***

The inclusion of hetero-atoms or functionalities in Periodic Mesoporous Organosilicas is very straightforward by the use of the appropriate precursor. Although already many precursors are commercially available or can be synthesized, sometimes it is more useful to post-functionalise a PMO material. Many precursors that include hetero-atoms are too large and flexible in order to assemble a rigid PMO framework. One way to circumvent this is the addition of a small bis-silane (*e.g.* BTEE), TEOS or TMOS to increase the rigidity of the walls. Alternatively, post-functionalisation is a useful method that allows maintaining the high ordering of the materials while introducing the appropriate function.

A PMO material can be post-functionalised in two ways: the organic bridges of the PMO material itself can be functionalised by different methods or the silanol groups present on the surface of the PMO can be used as an anchoring site. The latter is comparable to the functionalisation of MCM- or SBA-type materials and ideal to create bifunctional materials.<sup>19, 95</sup> Herein, only the post-modification of the organic bridge will be discussed.

### 1.4.1 Post-functionalisation of the unsaturated bridges

The most common unsaturated carbon bridge of PMO materials is the ethenylene bridge. Less common is the butenylene bridge.<sup>96</sup> A whole array of organic reactions can be performed to convert the double bond on the surface to a more appropriate functionality.

#### 1.4.1.1 Bromination of the double bond – Nucleophilic substitution

One of the most familiar reactions is the bromination of the C=C. The addition of bromine is already elaborately described by different research groups such as Stein *et al.*,<sup>8</sup> Ozin *et al.*,<sup>72</sup> Sayari *et al.*,<sup>76</sup> Mokaya *et al.*,<sup>74, 86, 87</sup> Yoshitake *et al.*<sup>97</sup> and Van Der Voort *et al.*<sup>84</sup> The reaction is very straightforward and relatively easy to perform with gaseous bromine or bromine dissolved in a chlorinated solvent (Table 1.5). The bromination of the ethenylene groups of the PMO material can have different purposes. For example, it can probe the chemical accessibility of the ethenylene bonds of the material. In addition Table 1.5 summarizes the accessibility of the C=C bridge. Values between 10 to 50% are reported depending on the bromination method but also on the preparation of the PMO material itself.

In general, bromination with gaseous bromine instead of dissolved bromine in dichloromethane results in a higher yield. Furthermore, bromination on materials synthesized with the triblock copolymer P123 resulted in lower accessibility values (30%) than materials prepared with Brij surfactants (51%). The most important advantage of this bromination procedure is the creation of an excellent leaving group which can be very useful in nucleophilic substitution reactions (*vide infra*).

Brominating the ethenylene bond of the PMO material did not have a large effect on the mesostructure of the material. This has been confirmed *via* a whole array of characterisation techniques such as Raman and infrared spectroscopy, X-ray diffraction, TEM, Solid State NMR spectroscopy, especially <sup>29</sup>Si and <sup>13</sup>C NMR, and nitrogen sorption. In general, the specific surface area, pore volume and pore diameter decrease because of the modification. The general ordering and mesopore structure is maintained in all cases. However, a large reduction of the molecular scale

periodicity is observed.<sup>66, 74, 78, 86</sup> An in-depth study of the bromination process and characterisation of the ethylene-bridged PMO is provided by Yoshitake *et al.*<sup>97</sup>

**Table 1.5: Summary of several bromination procedures on the ethylene-bridged PMO material reported in literature.**

Bromination procedure	Accessibility %	Ref.
closed beaker set-up with gaseous bromine 18 h, rt washed with CH <sub>2</sub> Cl <sub>2</sub> , H <sub>2</sub> O <sup>a</sup>	29	8
refluxing treatment in Br <sub>2</sub> /CH <sub>2</sub> Cl <sub>2</sub> 8 d, 40°C washed with CH <sub>2</sub> Cl <sub>2</sub> <sup>a</sup>	10	72
vacuum treatment with gaseous bromine 24 h, rt washed with CH <sub>2</sub> Cl <sub>2</sub>	30 <sup>b</sup> 51 <sup>c</sup>	76
closed beaker set-up with gaseous bromine 24 h, rt washed with CH <sub>2</sub> Cl <sub>2</sub> , H <sub>2</sub> O, EtOH <sup>a</sup>	<sup>d</sup>	74, 86, 87
closed sample tube set-up with gaseous bromine 12 h, rt thermal treatment for 12 h, 100°C <sup>a</sup>	45	97
vacuum treatment with gaseous bromine 6 h, 35°C thermal treatment at 90°C <sup>a</sup>	25-30	84

<sup>a</sup> After treatment to remove physisorbed Br<sub>2</sub>. <sup>b</sup> PMO prepared with P123. <sup>c</sup> PMO prepared with Brij-56 and Brij-76. <sup>d</sup> Not reported.

The bromine atom is an excellent leaving group and can be substituted by more useful functionalities. One method proposed in literature is the substitution of the bromine with a diamine. Yoshitake *et al.*<sup>97</sup> used ethylenediamine as nucleophile in order to obtain a nitrogen-containing material. A total amount of 0.87 mmol of amine groups per gram is achieved and is used as arsenate adsorbent.

### 1.4.1.2 Epoxidation

Inagaki *et al.*<sup>98, 99</sup> optimized the epoxidation reaction to functionalise the C=C bond of a PMO material (Figure 1.9). After investigating several oxidation procedures (temperature, pH and oxidants) the authors concluded that the epoxidation is best performed under mild basic conditions with anhydrous *tert*-butylhydroperoxide as oxidant.



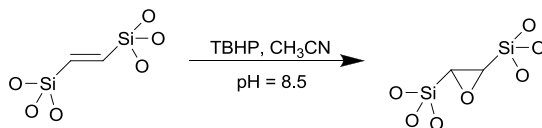


**Figure 1.9: Epoxidation reaction of the ethylene-bridged PMO material with *tert*-butylhydroperoxide as oxidant.**

The resulting oxirane was further modified through a ring-opening reaction with the introduction of an amine and alcohol function. Together with the grafting of silanol groups with functionalised trialkoxysilanes, this method can result in materials with different functional groups on the same PMO. This epoxidation procedure of Inagaki *et al.* and subsequent modification can attach basic and acidic groups in a straightforward manner without any protection and deprotection procedures. Approximately 1.29 mmol g<sup>-1</sup> and 1.14 mmol g<sup>-1</sup> of -NH<sub>2</sub> and -SO<sub>3</sub>H groups were observed, respectively. This method allowed the authors to obtain a bifunctional material which is unsurprisingly a promising catalyst for combined acid–base catalytic reactions.

### 1.4.1.3 Ozonolysis

Ozonolysis can be performed on double bonds to perform a cleavage of the bridge and obtain carboxylic acid functionalities (Figure 1.10). However, a partial breakdown of organic moieties on the surface occurs. This implies the creation of small indentations inside the pore walls thus really embedding the functionalities instead of adding them on top of the surface. This procedure with ozone, applied by Polarz *et al.* on a butenylene-bridged PMO material, has been recently reported.<sup>96</sup> Carboxylic acid functionalities were observed in <sup>13</sup>C and <sup>29</sup>Si MAS NMR and therefore confirm the cleavage of the double bond and formation of acetic acid groups.

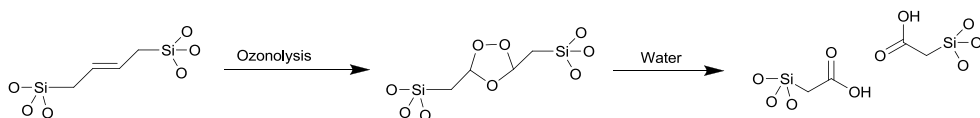


**Figure 1.10: Ozonolysis of the double bond of the butenylene-bridged PMO.**

The described procedure cannot be applied on the ethenylene-bridged PMO material. It was reported by Polarz *et al.* that attempts to ozonolyse the C=C resulted in the complete removal of the organic bridge. The PMO was converted in a material that retains its hexagonal ordering, but a complete removal of all the organic compounds was observed which leads to a general shrinkage of the material. It was concluded that the ozone treatment on the ethenylene-bridge PMO was impossible due to the  $\alpha$ -position of the siloxane moieties in position to the double bond.

#### 1.4.1.4 Diels-Alder reaction

An interesting modification of ethenylene-bridged PMO materials was first reported by Kondo *et al.*<sup>100,101</sup> By means of a Diels-Alder reaction between the ethene bridge and benzocyclobutene, a new functionality was successfully incorporated in the PMO material. The resulting aromatic ring was subsequently sulfonated with concentrated sulfuric acid giving rise to materials with an acidity of 1.44 mmol g<sup>-1</sup>. Inspired by these results Romero-Salguero *et al.* significantly extended this method with other dienes, *e.g.*, anthracene and cyclopentadiene.<sup>102</sup>

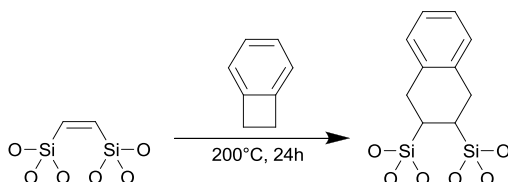


**Figure 1.11: Diels-Alder reaction with benzocyclobutene and the ethenylene-bridged PMO material.**

#### 1.4.1.5 Friedel-Crafts reaction

Another post-modification method performed on the ethenylene-bridge was developed by Dubé *et al.* and involved a Friedel-Crafts reaction.<sup>103</sup> The ethene bond was arylated with benzene and AlCl<sub>3</sub> as a catalyst. This material was subsequently sulfonated to produce an acid catalyst.

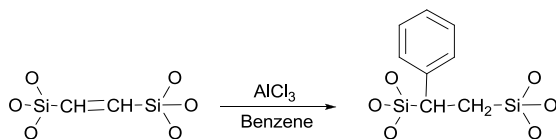


**Figure 1.12: Friedel-Crafts reaction with benzene and the ethenylene-bridged PMO material.**

### 1.4.1.6 Post-modification of other PMOs

The post-functionalisation methods, described above, all concern the modification of an ethene bond. However, also aromatic bridges have been functionalised based upon electrophilic aromatic substitutions. For example, the phenylene-bridged PMO material was sulfonated to obtain sulfonic acid groups.<sup>66,104</sup> Moreover, amines were introduced by two subsequent functionalisations, *i.e.*, a nitration of the benzene moiety followed by a reduction towards an amine.<sup>105</sup> Furthermore, bromination of the phenylene ring was also attempted.<sup>106</sup>

## 1.5 Concluding remarks

Periodic Mesoporous Organosilicas are attractive nanomaterials with interesting structural properties such as high specific surface areas, large pore volumes and pores in the meso-range. By carefully choosing the surfactant or by using additives, the characteristics of the materials can be altered, *e.g.*, the morphology or symmetry. A proper selection of the organic bridge introduces tailor-made functionalities and modifies the physical properties of the materials, such as stability, hydrophobicity, *etc.* This makes PMOs highly tuneable for a specific application.

On top of this, the possibility to post-modify a PMO material is very useful. This functionalisation method introduces new interesting functional groups while maintaining the ordering and structural properties of the PMO.

## 1.6 References

1. H. Li, M. Eddaoudi, M. O'Keeffe and O. M. Yaghi, *Nature*, 1999, **402**, 276-279.
2. J. R. Li, J. Sculley and H. C. Zhou, *Chemical Reviews*, 2012, **112**, 869-932.
3. P. Horcajada, R. Gref, T. Baati, P. K. Allan, G. Maurin, P. Couvreur, G. Ferey, R. E. Morris and C. Serre, *Chemical Reviews*, 2012, **112**, 1232-1268.
4. U. Schubert, *Chemical Society Reviews*, 2011, **40**, 575-582.
5. G. Ferey, C. Serre, T. Devic, G. Maurin, H. Jobic, P. L. Llewellyn, G. De Weireld, A. Vimont, M. Daturi and J. S. Chang, *Chemical Society Reviews*, 2011, **40**, 550-562.
6. J. R. Li, R. J. Kuppler and H. C. Zhou, *Chemical Society Reviews*, 2009, **38**, 1477-1504.
7. J. Lee, O. K. Farha, J. Roberts, K. A. Scheidt, S. T. Nguyen and J. T. Hupp, *Chemical Society Reviews*, 2009, **38**, 1450-1459.
8. B. J. Melde, B. T. Holland, C. F. Blanford and A. Stein, *Chemistry of Materials*, 1999, **11**, 3302-3308.
9. S. Inagaki, S. Guan, Y. Fukushima, T. Ohsuna and O. Terasaki, *Journal of the American Chemical Society*, 1999, **121**, 9611-9614.
10. T. Asefa, M. J. MacLachan, N. Coombs and G. A. Ozin, *Nature*, 1999, **402**, 867-871.
11. D. Y. Zhao, J. L. Feng, Q. S. Huo, N. Melosh, G. H. Fredrickson, B. F. Chmelka and G. D. Stucky, *Science*, 1998, **279**, 548-552.
12. D. Y. Zhao, Q. S. Huo, J. L. Feng, B. F. Chmelka and G. D. Stucky, *Journal of the American Chemical Society*, 1998, **120**, 6024-6036.
13. J. S. Beck, J. C. Vartuli, W. J. Roth, M. E. Leonowicz, C. T. Kresge, K. D. Schmitt, C. T. W. Chu, D. H. Olson, E. W. Sheppard and et al., *Journal of the American Chemical Society*, 1992, **114**, 10834-10843.
14. P. Van Der Voort, C. Vercaemst, D. Schaubroeck and F. Verpoort, *Physical Chemistry Chemical Physics*, 2008, **10**, 347-360.
15. C. J. Brinker, *Mrs Bulletin*, 2004, **29**, 631-640.
16. G. Smeulders, V. Meynen, G. Van Baelen, M. Mertens, O. I. Lebedev, G. Van Tendeloo, B. U. W. Maes and P. Cool, *Journal of Materials Chemistry*, 2009, **19**, 3042-3048.
17. Y. F. Lu, R. Ganguli, C. A. Drewien, M. T. Anderson, C. J. Brinker, W. L. Gong, Y. X. Guo, H. Soye, B. Dunn, M. H. Huang and J. I. Zink, *Nature*, 1997, **389**, 364-368.
18. M. Ide, Ghent University, Ph.D. thesis, 2012.
19. F. Hoffmann, M. Cornelius, J. Morell and M. Froba, *Angewandte Chemie-International Edition*, 2006, **45**, 3216-3251.
20. F. Hoffmann, M. Cornelius, J. Morell and M. Froba, *Journal of Nanoscience and Nanotechnology*, 2006, **6**, 265-288.
21. F. Hoffmann and M. Froba, *Chemical Society Reviews*, 2011, **40**, 608-620.
22. F. Hoffmann and M. Fröba, *The Supramolecular Chemistry of Organic-Inorganic Hybrid Materials*, 2010, 39-102.
23. D. M. Ford, E. E. Simanek and D. F. Shantz, *Nanotechnology*, 2005, **16**, S458-S475.
24. B. Hatton, K. Landskron, W. Whitnall, D. Perovic and G. A. Ozin, *Accounts of Chemical Research*, 2005, **38**, 305-312.

25. W. J. Hunks and G. A. Ozin, *Journal of Materials Chemistry*, 2005, **15**, 3716-3724.
26. M. Jaroniec, *Nature*, 2006, **442**, 638-640.
27. M. P. Kapoor and S. Inagaki, *Bulletin of the Chemical Society of Japan*, 2006, **79**, 1463-1475.
28. N. Mizoshita, T. Tani and S. Inagaki, *Chemical Society Reviews*, 2011, **40**, 789-800.
29. H. S. Xia, C. H. Zhou, D. S. Tong and C. X. Lin, *Journal of Porous Materials*, 2010, **17**, 225-252.
30. P. Van Der Voort, D. Esquivel, E. De Canck, F. Goethals, I. Van Driessche and F. J. Romero-Salguero, *Chemical Society Reviews*, 2013, **42**, 3913-3955.
31. S. Hamoudi, Y. Yang, I. L. Moudrakovski, S. Lang and A. Sayari, *Journal of Physical Chemistry B*, 2001, **105**, 9118-9123.
32. Y. C. Pan, H. Y. Wu, G. L. Jheng, H. H. G. Tsai and H. M. Kao, *Journal of Physical Chemistry C*, 2009, **113**, 2690-2698.
33. B. Lee, H. J. Im, H. M. Luo, E. W. Hagaman and S. Dai, *Langmuir*, 2005, **21**, 5372-5376.
34. H. I. Lee, C. Pak, S. H. Yi, J. K. Shon, S. S. Kim, B. G. So, H. Chang, J. E. Yie, Y. U. Kwon and J. M. Kim, *Journal of Materials Chemistry*, 2005, **15**, 4711-4717.
35. A. Sayari, S. Hamoudi, Y. Yang, I. L. Moudrakovski and J. R. Ripmeester, *Chemistry of Materials*, 2000, **12**, 3857-3863.
36. C. H. Lee, S. S. Park, S. J. Choe and D. H. Park, *Microporous and Mesoporous Materials*, 2001, **46**, 257-264.
37. S. Guan, S. Inagaki, T. Ohsuna and O. Terasaki, *Journal of the American Chemical Society*, 2000, **122**, 5660-5661.
38. S. Y. Guan, S. Inagaki, T. Ohsuna and O. Terasaki, *Microporous and Mesoporous Materials*, 2001, **44**, 165-172.
39. M. P. Kapoor and S. Inagaki, *Chemistry of Materials*, 2002, **14**, 3509-3514.
40. S. Z. Qiao, C. Z. Yu, Q. H. Hu, Y. G. Jin, X. F. Zhou, X. S. Zhao and G. Q. Lu, *Microporous and Mesoporous Materials*, 2006, **91**, 59-69.
41. H. G. Zhu, D. J. Jones, J. Zajac, J. Roziere and R. Dutartre, *Chemical Communications*, 2001, 2568-2569.
42. O. Muth, C. Schellbach and M. Fröba, *Chemical Communications*, 2001, 2032-2033.
43. X. Y. Bao, X. S. Zhao, X. Li and J. Li, *Applied Surface Science*, 2004, **237**, 380-386.
44. L. Zhao, G. S. Zhu, D. L. Zhang, Y. Di, Y. Chen, O. Terasaki and S. L. Qiu, *Journal of Physical Chemistry B*, 2005, **109**, 764-768.
45. W. P. Guo, I. Kim and C. S. Ha, *Chemical Communications*, 2003, 2692-2693.
46. E. B. Cho, K. W. Kwon and K. Char, *Chemistry of Materials*, 2001, **13**, 3837-3839.
47. E. B. Cho and K. Char, *Chemistry of Materials*, 2004, **16**, 270-275.
48. J. R. Matos, M. Kruk, L. P. Mercuri, M. Jaroniec, T. Asefa, N. Coombs, G. A. Ozin, T. Kamiyama and O. Terasaki, *Chemistry of Materials*, 2002, **14**, 1903-1905.
49. M. D. McNall, J. Scott, L. Mercier and P. J. Kooyman, *Chemical Communications*, 2001, 2282-2283.
50. A. Sayari and Y. Yang, *Chemical Communications*, 2002, 2582-2583.
51. M. C. Burleigh, S. Jayasundera, C. W. Thomas, M. S. Spector, M. A. Markowitz and B. P. Gaber, *Colloid and Polymer Science*, 2004, **282**, 728-733.

52. M. C. Burleigh, S. Jayasundera, M. S. Spector, C. W. Thomas, M. A. Markowitz and B. P. Gaber, *Chemistry of Materials*, 2004, **16**, 3-5.
53. N. Li, J. G. Wang, H. J. Zhou, P. C. Sun and T. H. Chen, *Chemistry of Materials*, 2011, **23**, 4241-4249.
54. N. Hao, H. T. Wang, P. A. Webley and D. Y. Zhao, *Microporous and Mesoporous Materials*, 2010, **132**, 543-551.
55. J. Liu, S. Y. Bai, H. Zhong, C. Li and Q. H. Yang, *Journal of Physical Chemistry C*, 2010, **114**, 953-961.
56. M. Mandal and M. Kruk, *Chemistry of Materials*, 2012, **24**, 123-132.
57. M. Mandal and M. Kruk, *Chemistry of Materials*, 2012, **24**, 149-154.
58. X. Liu, X. B. Li, Z. H. Guan, J. Liu, J. Zhao, Y. Yang and Q. H. Yang, *Chemical Communications*, 2011, **47**, 8073-8075.
59. T. Asefa, M. J. MacLachlan, H. Grondy, N. Coombs and G. A. Ozin, *Angewandte Chemie-International Edition*, 2000, **39**, 1808-1811.
60. W. H. Zhang, B. Daly, J. O'Callaghan, L. Zhang, J. L. Shi, C. Li, M. A. Morris and J. D. Holmes, *Chemistry of Materials*, 2005, **17**, 6407-6415.
61. X. Y. Bao, X. Li and X. S. Zhao, *Journal of Physical Chemistry B*, 2006, **110**, 2656-2661.
62. C. Yoshina-Ishii, T. Asefa, N. Coombs, M. J. MacLachlan and G. A. Ozin, *Chemical Communications*, 1999, 2539-2540.
63. E. B. Cho and D. Kim, *Microporous and Mesoporous Materials*, 2008, **113**, 530-537.
64. E. B. Cho, D. Kim, J. Gorka and M. Jaroniec, *Journal of Materials Chemistry*, 2009, **19**, 2076-2081.
65. G. Temtsin, T. Asefa, S. Bittner and G. A. Ozin, *Journal of Materials Chemistry*, 2001, **11**, 3202-3206.
66. S. Inagaki, S. Guan, T. Ohsuna and O. Terasaki, *Nature*, 2002, **416**, 304-307.
67. K. Okamoto, Y. Goto and S. Inagaki, *Journal of Materials Chemistry*, 2005, **15**, 4136-4140.
68. S. Bracco, A. Comotti, P. Valsesia, B. F. Chmelka and P. Sozzani, *Chemical Communications*, 2008, 4798-4800.
69. M. P. Kapoor, M. Yanagi, Y. Kasama, T. Yokoyama, S. Inagaki, T. Shimada, H. Nanbu and L. R. Juneja, *Journal of Materials Chemistry*, 2006, **16**, 3305-3311.
70. M. P. Kapoor, Q. H. Yang and S. Inagaki, *Chemistry of Materials*, 2004, **16**, 1209-1213.
71. M. P. Kapoor, S. Inagaki, S. Ikeda, K. Kakiuchi, M. Suda and T. Shimada, *Journal of the American Chemical Society*, 2005, **127**, 8174-8178.
72. T. Asefa, M. J. MacLachlan, N. Coombs and G. A. Ozin, *Nature*, 1999, **402**, 867-871.
73. Y. D. Xia and R. Mokaya, *Journal of Physical Chemistry B*, 2006, **110**, 3889-3894.
74. Y. D. Xia and R. Mokaya, *Journal of Materials Chemistry*, 2006, **16**, 395-400.
75. Y. D. Xia, W. X. Wang and R. Mokaya, *Journal of the American Chemical Society*, 2005, **127**, 790-798.
76. W. H. Wang, S. H. Xie, W. Z. Zhou and A. Sayari, *Chemistry of Materials*, 2004, **16**, 1756-1762.
77. K. Nakajima, I. Tomita, M. Hara, S. Hayashi, K. Domen and J. N. Kondo, *Journal of Materials Chemistry*, 2005, **15**, 2362-2368.

78. C. Vercaemst, M. Ide, B. Allaert, N. Ledoux, F. Verpoort and P. Van Der Voort, *Chemical Communications*, 2007, 2261-2263.
79. C. Vercaemst, J. T. A. Jones, Y. Z. Khimyak, J. C. Martins, F. Verpoort and P. Van Der Voort, *Physical Chemistry Chemical Physics*, 2008, **10**, 5349-5352.
80. C. Vercaemst, P. E. de Jongh, J. D. Meeldijk, B. Goderis, F. Verpoort and P. Van Der Voort, *Chemical Communications*, 2009, 4052-4054.
81. C. Vercaemst, H. Friedrich, P. E. de Jongh, A. V. Neimark, B. Goderis, F. Verpoort and P. Van Der Voort, *Journal of Physical Chemistry C*, 2009, **113**, 5556-5562.
82. C. Vercaemst, M. Ide, H. Friedrich, K. P. de Jong, F. Verpoort and P. Van Der Voort, *Journal of Materials Chemistry*, 2009, **19**, 8839-8845.
83. C. Vercaemst, Ghent University, Ph.D. thesis, 2009.
84. C. Vercaemst, M. Ide, P. V. Wiper, J. T. A. Jones, Y. Z. Khimyak, F. Verpoort and P. Van Der Voort, *Chemistry of Materials*, 2009, **21**, 5792-5800.
85. F. Goethals, C. Vercaemst, V. Cloet, S. Hoste, P. Van Der Voort and I. Van Driessche, *Microporous and Mesoporous Materials*, 2010, **131**, 68-74.
86. Y. D. Xia, Z. X. Yang and R. Mokaya, *Chemistry of Materials*, 2006, **18**, 1141-1148.
87. Y. D. Xia and R. Mokaya, *Microporous and Mesoporous Materials*, 2005, **86**, 231-242.
88. X. J. Meng, T. Yokoi, D. L. Lu and T. Tatsumi, *Angewandte Chemie-International Edition*, 2007, **46**, 7796-7798.
89. C. Vercaemst, M. Ide, B. Allaert, N. Ledoux, F. Verpoort and P. Van Der Voort, *Chem Commun*, 2007, 2261-2263.
90. M. Mandal and M. Kruk, *Journal of Materials Chemistry*, 2010, **20**, 7506-7516.
91. Y. Goto and S. Inagaki, *Chemical Communications*, 2002, 2410-2411.
92. D. Esquivel, C. Jiménez-Sanchidrián and F. J. Romero-Salguero, *Mater Lett*, 2011, **65**, 1460-1462.
93. M. Kruk, M. Jaroniec, S. Y. Guan and S. Inagaki, *Journal of Physical Chemistry B*, 2001, **105**, 681-689.
94. M. C. Burleigh, M. A. Markowitz, S. Jayasundera, M. S. Spector, C. W. Thomas and B. P. Gaber, *Journal of Physical Chemistry B*, 2003, **107**, 12628-12634.
95. P. Van Der Voort and E. F. Vansant, *Journal of Liquid Chromatography & Related Technologies*, 1996, **19**, 2723-2752.
96. S. Polarz, F. Jeremias and U. Haunz, *Advanced Functional Materials*, 2011, **21**, 2953-2959.
97. K. Nakai, Y. Oumi, H. Horie, T. Sano and H. Yoshitake, *Microporous and Mesoporous Materials*, 2007, **100**, 328-339.
98. M. Sasidharan, S. Fujita, M. Ohashi, Y. Goto, K. Nakashima and S. Inagaki, *Chemical Communications*, 2011, **47**, 10422-10424.
99. M. Sasidharan and A. Bhaumik, *Acs Applied Materials & Interfaces*, 2013, **5**, 2618-2625.
100. K. Nakajima, I. Tomita, M. Hara, S. Hayashi, K. Domen and J. N. Kondo, *Advanced Materials*, 2005, **17**, 1839-1842.
101. K. Nakajima, I. Tomita, M. Hara, S. Hayashi, K. Domen and J. N. Kondo, *Catal Today*, 2006, **116**, 151-156.
102. D. Esquivel, E. De Canck, C. Jiménez-Sanchidrián, P. Van Der Voort and F. J. Romero-Salguero, *Journal of Materials Chemistry*, 2011, **21**, 10990-10998.

103. D. Dubé, M. Rat, F. Beland and S. Kaliaguine, *Microporous and Mesoporous Materials*, 2008, **111**, 596-603.
104. D. Esquivel, C. Jiménez-Sanchidrián and F. J. Romero-Salguero, *Journal of Materials Chemistry*, 2011, **21**, 724-733.
105. M. Ohashi, M. P. Kapoor and S. Inagaki, *Chemical Communications*, 2008, 841-843.
106. G. Smeulders, V. Meynen, K. Houthoofd, S. Mullens, J. A. Martens, B. U. W. Maes and P. Cool, *Microporous and Mesoporous Materials*, 2012, **164**, 49-55.



## **2 Applications of Periodic Mesoporous Organosilicas**

Periodic Mesoporous Organosilicas can be used in a wide range of applications. In this chapter, a literature overview is presented concerning the application of PMOs as insulating low-*k* film, chromatographic packing, adsorbent, catalyst and for biomedical applications. At the end of this chapter, the aim of this dissertation is given.

Parts of this chapter were published as

Pascal Van Der Voort, Dolores Esquivel, Els De Canck, Frederik Goethals, Isabel Van Driessche and Francisco J. Romero-Salguero, *Chemical Society Reviews*, **2013**, 42, 9, 3913-3955.

## **2.1 Introduction**

Periodic Mesoporous Organosilicas are applied in many different fields due to their versatility as their structural and chemical properties can be easily altered. A large amount of research is performed to broaden their usability. PMOs are utilized as heterogeneous catalyst (acid, base, redox, chiral); adsorbent (metals, gasses, organic pollutants); low-*k* film; stationary chromatographic phase; light-harvesting device; drug delivery system; and biomedical support for proteins and enzymes.<sup>1</sup> A large amount of publications is available on this variety of topics and an overview is presented below. The use as light-harvesting device is well-described in reference 2.

## **2.2 Ultra stable PMOs as chromatographic packing and super insulating low-*k* film**

PMO materials with simple organic bridges such as methane, ethane and benzene possess an intrinsic quality which is of great importance in some applications, *i.e.*, the hydrophobicity induced by the organic moieties. This property is especially useful in chromatography or electronic devices when the PMO is applied as normal or reversed phase or as low-*k* film, respectively.

For chromatographic applications, it is necessary to prepare spherical particles and this is performed for silica materials by using the well-known Stöber method<sup>3</sup> which was further adapted to obtain porous spherical particles.<sup>4</sup> A large amount of literature is available on the synthesis and applicability of highly porous silica spheres in chromatography. The amount of work performed on introducing PMOs as chromatographic phase is rather limited although they counter a few essential disadvantages when applying porous spherical silica particles in HPLC columns. As the latter deteriorate quickly by hydrolysis and loss of functionality.

Inagaki *et al.*<sup>5</sup> and Fröba *et al.*<sup>6</sup> reported in the same year the first phenylene-bridged PMO with spherical morphology. Based upon the Stöber method, they prepared uniform spheres under basic conditions with cationic surfactants and an alcohol as co-solvent. Particles with an average size between 0.4 and 0.5  $\mu\text{m}$  were obtained.<sup>6</sup> Larger benzene-PMO spheres were acquired with particle diameters

between 3 and 15  $\mu\text{m}$  by using a combination of the surfactants CTAB and P123 in acidic environment (Figure 2.1).<sup>7</sup> The PMO material also exhibited a high specific surface area ( $1180\text{ m}^2\text{ g}^{-1}$ ) and narrow pore size distribution.

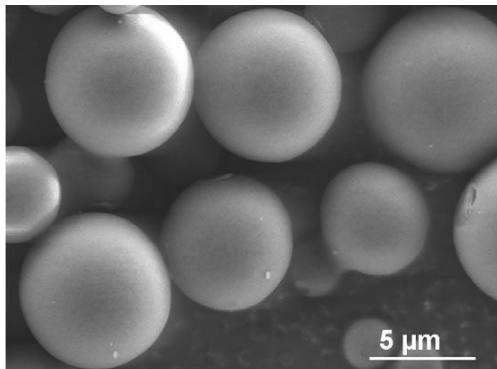


**Figure 2.1: SEM image of a spherical phenylene-bridged PMO material (sph-PMO).<sup>7</sup>**

Chromatographic tests were performed to evaluate the spherical benzene-PMO and comparison was made with the commercial Nucleosil 50-10. Different test mixtures were selected and the PMO material was able to separate the three mixtures in contrast to the Nucleosil material. Even higher retention was observed for the benzene-PMO when a mixture of (poly)aromatic compounds was separated (Figure 2.2). The combination of hydrophilic silanols and hydrophobic benzene moieties combines the properties for normal and reversed chromatographic phase in one material and this material shows potential as chromatographic packing. Besides PMOs synthesized with the precursor BTEB, PMO materials with other organic bridges are probed as normal or reversed phase for chromatography. Instead of BTEB with *para* orientation of the ethoxy silyl moieties, 1,3-bis(triethoxysilyl)-benzene was condensed with TEOS and this resulted in a *meta* orientated benzene PMO where highly monodisperse spherical particles were observed.<sup>8</sup> The *meta* variant showed higher retention than the *para* benzene-PMO due to the position of the aromatic rings in the pore walls. The functional groups partially stick out from the walls and this resulted in  $\pi$ --- $\pi$  interactions between the analytes and surface of the packing. This work was continued by the synthesis of large pore phenylene-bridged PMO spheres.<sup>9</sup> They reported the best plate height of 10  $\mu\text{m}$ .

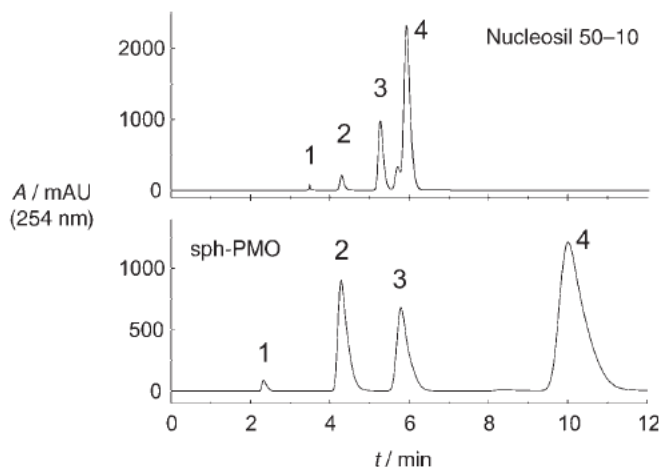


**Figure 2.2: Chromatograms of mixture 1 (benzene (1), naphthalene (2), biphenyl (3), and phenanthrene (4)) separated with n-hexane at a flow rate of 1 mL min<sup>-1</sup> on the Nucleosil 50-10 column or a flow rate of 2 mL min<sup>-1</sup> on the sph-PMO column.<sup>7</sup>**

More complex PMOs with advanced organic bridges are employed as a chiral phase for HPLC applications. A PMO material containing ethane bridges in combination with the chiral *trans*-(1*R*, 2*R*)-diaminocyclohexane (DACH) functionality was probed for the separation of racemic amino acids.<sup>10</sup> The particles, with an average size of 5-7  $\mu\text{m}$ , showed better separation than silica materials merely grafted with DACH. Other functionalised PMO materials are prepared *via* the condensation of BTTE or TEOS and a silane that contains *trans*-(1*R*, 2*R*)-bis-(ureido)-cyclohexane,<sup>11, 12</sup> amines<sup>13</sup> or a camphorsulfonamide<sup>14</sup> functionality.

PMO materials are not only potential chromatographic packing materials, they can also be applied as insulating interlayer or low-*k* material. A low-*k* material possesses a low dielectric constant (*k*) and reduces the RC-delay that is induced between wires that are in close proximity. The *k*-value is preferably below 2 to act as an insulating interlayer. The intrinsic properties of PMOs make them very useful in micro-electronic devices. Their high porosity or plainly stated, *cavities filled with air*, reduces the *k*-value significantly as  $k_{\text{air}} \approx 1$ . Furthermore the organic bridges (methane and ethane) are less polarisable than silicon dioxide ( $k = 3.9$ ), which diminishes the *k*-value even more.<sup>15</sup>

In order to function as an interlayer, PMO thin films must be prepared. This can be achieved by two methods: (1) the deposition on a substrate using the well-known Evaporation Induced Self Assembly or EISA method<sup>16</sup> in combination with spin- or dip-coating or (2) the preparation by hydrothermal synthesis.<sup>17</sup> The latter procedure is not frequently used, but can result in the growth of a free standing PMO film at the liquid-reaction poly-ethylene bottle interface.

Lu *et al.* reported the first PMO thin films for this application,<sup>18</sup> although the majority of the work was performed by the research groups of Ozin and Van Der Voort. An overview of the reported materials is presented in Table 2.3 together with the porosity and observed *k*-value.

**Table 2.1: Overview of different types of PMO films and their dielectric constants.**

PMO	Surfactant	Porosity %	<i>k</i> -value	Ref.
Methane-PMO	CTAC	n.a.	1.8	19
	CTAC	53	1.6	20
Ethane-PMO	Brij-56	56	1.98	18
	CTAC	n.a.	1.9	19
	CTAC	45	1.67	20
	Brij-76	39.5	2.15	21
	CTAC	47	1.7	22
Ethene-PMO	CTAC	44	1.7	20
Ring-PMO <sup>a</sup>	CTAC	n.a.	2.0	23
	CTAC	50	1.63	20
	Brij-76	55	1.8	24
POSS-PMO <sup>b</sup>	CTAC	39	1.7	25

<sup>a</sup> Prepared with the precursor 1,1,3,3,5,5-hexaethoxy-1,3,5-trisilacyclohexane. <sup>b</sup> Prepared with a polyhedral oligomeric silane.

Ozin *et al.* elaborately described the preparation of thin films consisting of methane-, ethane-, ethene- or ring-PMOs, the latter being a multi-organic bridged organosilica made out of interconnected  $[\text{Si}(\text{CH}_2)]_3$  rings. The group thoroughly investigated their dielectric, mechanical and hydrophobic properties.<sup>19, 20, 22, 23</sup> Especially the hydrophobicity of the ring-PMO is a key factor as less silanol groups are

present and the adsorption of water is reduced. The presence of water can significantly increase the dielectric constant as  $k_{\text{water}} \approx 80$ .

The group of Van Der Voort extended the applicability of the ring-PMO as low- $k$  film (Figure 2.3).<sup>24</sup> By employing Brij-76 instead of the surfactant CTAB, they improved the chemical stability of the thin films. This was explained by the presence of thicker pore walls in combination with the  $-\text{CH}_2-$  moieties. The ring-PMO thin films sustained a treatment with 1 M NaOH. Moreover, they recently developed a method to modify the top surface of a low- $k$  film in order to seal the pores.<sup>21, 26</sup> By applying this procedure, the  $k$ -value was lowered and the mechanical and chemical stability was improved. But most importantly, it also lowers the leak current.<sup>26</sup>

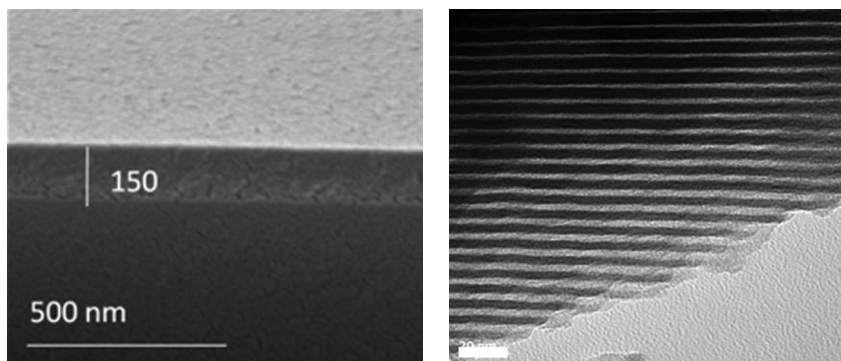


**Figure 2.3: SEM and TEM image of a ring-PMO thin film, prepared *via* spin-coating with Brij-76 and ethanol in acidic medium. The length of the scale bar on the TEM image represents 20 nm.<sup>24</sup>**

Another type of interesting PMO material for low- $k$  applications is presented by Ozin *et al.*<sup>25</sup> A thin film was spin-coated by using a polyhedral oligomeric silsesquioxane or POSS precursor. The resulting PMO possesses air pockets in the pore walls which is beneficial for the dielectric constant. A  $k$ -value of 1.7 was achieved.

This overview presented above clearly indicates that PMOs can be applied as chromatographic packing materials or as low- $k$  materials in microelectronic devices. Although more extended research is definitely necessary to improve their performance, very recent patents of the group of Van Der Voort already show evidence of their potential.<sup>27, 28</sup>

## **2.3 Functional PMOs as adsorbents and catalysts**

For applications such as adsorption and heterogeneous catalysis, more advanced and often complex functional groups are needed in comparison with the sometimes simple organic bridges utilized in chromatography and microelectronic devices.

## **2.4 PMOs as adsorbents**

A huge number of studies has been carried out on the environmental applications of non-ordered and ordered mesoporous silicas, particularly addressing the adsorption of heavy metals (*e.g.*, cations, oxyanions and radionuclides), toxic organic species and even gasses (*e.g.*, volatile organic compounds). Excellent reviews on this matter have been published.<sup>29,30</sup> Since the discovery of PMOs, the possibility of using them as adsorbents for all kinds of pollutants has also been explored and the main challenge is to develop PMO materials that can outperform the classical functionalised silica materials as well as commercial adsorbents such as activated carbon.

### **2.4.1 Metal ion adsorption**

The adsorption of metal ions is one of the most investigated research areas because of its importance in waste water treatment and purification processes. Although other techniques, such as ion-exchange, precipitation and electro-coagulation can be used for the removal of toxic metals, metal adsorption is often employed.<sup>31</sup> This method is relatively easy, straightforward and trustworthy. Furthermore, the total cost price is relatively low as no large equipment with high maintenance is needed. Activated carbon is often utilized because it is cheap, stable and it possesses a high specific surface area. However, this material lacks selectivity for certain metals and this poses a huge disadvantage. Therefore, an adsorbent that contains functional groups which induce the selectivity, with a high specific surface area and good hydrothermal stability can be a solution. Moreover, it would be beneficial if this adsorbent can be regenerated multiple times and if the adsorbed metals can be recuperated.

Various PMO materials have been used as adsorbents. Some of them are reviewed by Walcarius *et al.*<sup>29</sup> in 2010, including ordered mesoporous silicas. A concise literature overview of PMO adsorbents for metals is presented in Table 2.2. Three different strategies are used to develop an adsorbent.

The first method consists of the introduction of one type of functionality, *e.g.*, urea, disulfide or pyridine containing bis-silanes for the adsorption of iron(III),<sup>32</sup> mercury(II)<sup>33</sup> and copper(II),<sup>34</sup> respectively. As these silanes are sometimes too flexible to obtain rigid PMO structures, a co-condensation with TEOS is performed. Secondly, it is also very interesting to incorporate multiple functionalities in one PMO material. This is achieved by combining several silsesquioxanes and organotrialkoxysilanes during the synthesis. An example of this is presented in Figure 2.4 where mercury adsorbents are prepared through the combination of a large organic group such as isocyanurate (ICS) and a simple functionality such as tetrasulfide.<sup>35</sup>

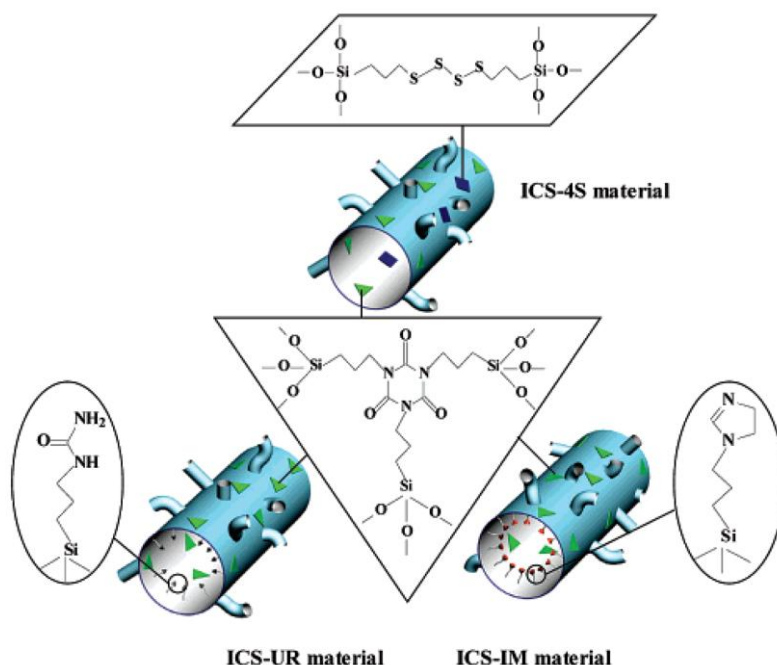


**Figure 2.4:** PMO materials synthesized *via* the combination of different precursors, *i.e.*, BTEPTS (top; 4S), ICS (middle), ureidopropyltrimethoxysilane (left; UR) and N-(3-triethoxysilylpropyl)4,5-dihydroimidazole (right; IM).<sup>35</sup>



It was clear from the study that the incorporation of a secondary group can negatively affect the structural ordering of the material but this strongly depends on the type of functionality. Incorporation of the tetrasulfide unit leads to a decrease in pore size while the decrease for the ureido and imidazole functionality was less noticeable. The combination of an isocyanurate and tetrasulfide moiety resulted in a high amount of Hg(II) adsorbed on the PMO (1.37 mmol g<sup>-1</sup>).

A third very remarkable approach to produce adsorbents has been reported by Burleigh *et al.*<sup>36</sup> and is known as *molecular imprinting*. The authors used the metal salts of nickel, copper or zinc during the synthesis of the PMO together with BTEE, N-[3-(trimethoxysilyl)propyl]ethylenediamine and CTAC as surfactant. The metal ion forms a complex with the amines during the synthesis and after preparation of the materials, the Ni(II), Cu(II) or Zn(II) is removed with HNO<sub>3</sub>. This results in a material possessing cavities shaped as the metal with identical chemical environment. When using this material in an adsorption process, the metal ions of the same type which were used during synthesis, will selectively bind to the cavity, especially with solutions containing high concentrations in the range of 10<sup>-3</sup> mol L<sup>-1</sup>. Furthermore the materials prepared *via* the imprinting technique exhibited a higher metal binding capacity than the non-imprinted material.

**Table 2.2: Overview of PMO materials investigated for metal (cation) adsorption.**

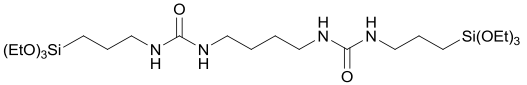
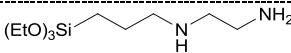
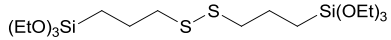
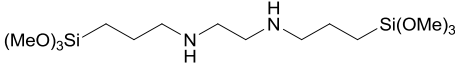
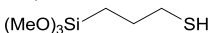
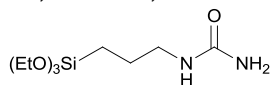
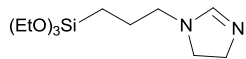
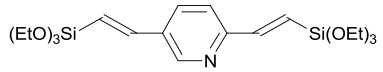
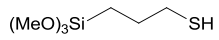
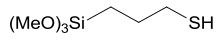
Precursor	Surface functionality	Metal	Metal capacity mmol g <sup>-1</sup>	Ref.
 TEOS	-NH-C=O-NH-	Fe(III)	0.19	32
 BTEE	-NH <sub>2</sub> , -NH- -CH <sub>2</sub> CH <sub>2</sub> -	Cu(II) Ni(II) Zn(II)	-	36
 TEOS	-S-S-	Hg(II)	3.57	33
 TEOS	-NH-	Cu(II) Ni(II) Zn(II)	0.020 - 0.034 2.3·10 <sup>-3</sup> - 1.5·10 <sup>-3</sup> 1.1·10 <sup>-3</sup> - 0.9·10 <sup>-3</sup>	37
BTEPTS, <sup>a</sup> TMOS	-S-S-S-S-	Hg(II)	0.92 - 7.48	38
ICS, <sup>a</sup> TEOS	-N-C=O-N-	Hg(II)	9.7	39
 ICS, <sup>a</sup> TEOS	-N-C=O-N- -SH	Hg(II)	4.23 - 5.64	40

Table 2.2 – Continued.

ICS, <sup>a</sup> BTEPTS, <sup>a</sup>  	-N-C=O-N- -S-S-S-S- -NH-C=O-NH <sub>2</sub> -N-C <sub>3</sub> H <sub>5</sub> -N	Hg(II)	0.40 - 1.37	35
	-NC <sub>5</sub> H <sub>3</sub> -	Cu(II)	2.4	34
BTEE, TMOS 	-CH <sub>2</sub> CH <sub>2</sub> - -SH	Hg(II)	1.42 - 2.31	41
BTEE 	-CH <sub>2</sub> CH <sub>2</sub> - -SH	Hg(II) Zn(II) Cu(II) Cr(II) Cd(II)	0.76 - 1.75 0.37 0.98 - 1.29 2.04 - 3.27 1.14 - 1.62	42
BTEPTS, <sup>a</sup> TEOS	-S-S-S-S-	Hg(II)	3.13 - 13.51	43

<sup>a</sup> See Table 1.1.

Only a few reports have appeared on the very challenging topic of the adsorption of anionic metal species, *i.e.*, the adsorption of oxyanions such as  $\text{ReO}_4^-$  molecules<sup>44, 45</sup> and the adsorption of  $\text{AsO}_4^{3-}$ .<sup>46</sup>

A key element in the investigation of PMOs as adsorbents should be the stability of the materials during the adsorption process, but also the reusability is of major importance, which is not discussed in many papers. A PMO material can only compete with and outperform functionalised silica materials and commercial materials if it is reusable.

## 2.4.2 Gas Adsorption

Although less reports have been published on the adsorption of gases and volatile organic compounds (VOCs) on PMOs, some promising and interesting results have already been obtained. An overview is presented in Table 2.3.

**Table 2.3: Overview of PMO materials investigated for gas adsorption.**

Bis-silylated precursor	Surface functionality	Gas/VOC	Ref.
1,4-bis(triallylsilyl)phenylene	-C <sub>6</sub> H <sub>4</sub> - -C <sub>6</sub> H <sub>3</sub> (SO <sub>3</sub> H)-	acetaldehyde	47
1,4-bis(triethoxysilyl)benzene	-C <sub>6</sub> H <sub>4</sub> -	benzene, hexafluorobenzene, cyclohexane, ethanol, xenon, methane, carbon dioxide	48
1,4-bis(triethoxysilyl)benzene	-C <sub>6</sub> H <sub>4</sub> -	benzene, toluene, hexane	49
4,4'-bis(triethoxysilyl)-1,1'-biphenyl	-C <sub>6</sub> H <sub>3</sub> -C <sub>6</sub> H <sub>3</sub> -		
1,4-bis(trimethoxysilylethyl)benzene	-C <sub>2</sub> H <sub>4</sub> -C <sub>6</sub> H <sub>4</sub> -C <sub>2</sub> H <sub>4</sub> - porphyrin		
3-aminopropyltrimethoxysilane,	-CH <sub>2</sub> CH <sub>2</sub> -	sulfur dioxide,	50
3-isocyanatopropyl-triethoxysilane,	-(CH <sub>2</sub> ) <sub>3</sub> NH <sub>2</sub>	cyanogen chloride,	
1,2-bis(trimethoxysilyl)ethane	-(CH <sub>2</sub> ) <sub>3</sub> NCO	ammonia, octane	
1,2-bis(triethoxysilyl)ethane	-CH <sub>2</sub> CH <sub>2</sub> -	hydrogen	51
1,2-bis(triethoxysilyl)ethylene	-CH=CH-		
1,4-bis(triethoxysilyl)benzene	-C <sub>6</sub> H <sub>4</sub> -		
4,4'-bis(triethoxysilyl)-1,1'-biphenyl	-C <sub>6</sub> H <sub>3</sub> -C <sub>6</sub> H <sub>3</sub> -		
1,4-bis(triethoxysilyl)benzene	-C <sub>6</sub> H <sub>4</sub> -	CO, CO <sub>2</sub> , CH <sub>4</sub>	52
Bis[3-(trimethoxysilyl)propyl]amine	-(CH <sub>2</sub> ) <sub>3</sub> -NH-(CH <sub>2</sub> ) <sub>3</sub> -	CO <sub>2</sub>	53
Bis[3-(triethoxysilyl)propyl]-ethylene	-(CH <sub>2</sub> ) <sub>3</sub> -NH-(CH <sub>2</sub> ) <sub>2</sub> -	CO <sub>2</sub>	52
diamine	NH-(CH <sub>2</sub> ) <sub>3</sub> -		53

The adsorption of VOCs, such as acetaldehyde, was firstly studied in 2006 when a comparison was made between benzene-PMOs with 2D-hexagonal and 3D-cubic symmetries as well as the corresponding sulfonated materials.<sup>47</sup> It was reported that the 3D-structured materials outperformed the 2D-structured and that the attachment of sulfonic acid groups even improved the adsorption. The same conclusion was obtained comparing PMOs with polyamidoamine dendritic species inside their pores and the non-functionalised material.<sup>54</sup> This confirms the importance of the pore structure but also the presence of functionalities.

The interaction of different VOCs, *i.e.*, benzene, hexafluorobenzene, cyclohexane and ethanol, and gases, such as xenon, methane and carbon dioxide is more examined in detail by Sozanni *et al.*<sup>48</sup> using a phenylene-bridged PMO material. They concluded that those interactions occurred *via* CH--- $\pi$  bonds and not *via*  $\pi$ --- $\pi$  bonds as one would initially expect. Also, the phenylene-bridged PMO appeared to be a good adsorbent for CO<sub>2</sub> storage with an adsorption of 90 w% without further functionalisation. A few years later, a theoretical study appeared on the adsorption of CO, CO<sub>2</sub> and CH<sub>4</sub> on benzene PMOs.<sup>52</sup> Additionally, the adsorption of benzene, toluene and hexane was studied on PMOs with different aromatic bridges.<sup>49</sup>

The CO<sub>2</sub> adsorption ability of PMOs can be improved by the introduction of nitrogen functionalities. This has been shown very recently for PMO materials by the use of the amine containing precursors bis[3-(triethoxysilyl)propyl]-ethylene diamine<sup>55,56</sup> and bis[3-(trimethoxysilyl)propyl]amine<sup>53</sup>. To obtain a rigid and highly porous structure, these precursors were co-condensed with TEOS<sup>55</sup> or BTME<sup>53</sup>, respectively. Promising results were already obtained with these hybrid materials.

Recently, Melde *et al.*<sup>50</sup> reported the adsorption of other gasses such as sulfur dioxide, cyanogen chloride, ammonia and octane on an ethane-PMO as well as the effect of humidity on its adsorption behaviour and the influence of post-functionalisation with an aminopropyl and isocyanatopropyl functionality.

The adsorption of hydrogen gas and its interaction with the pore walls of ethenylene-, ethylene-, phenylene- and biphenylene-bridged PMOs has recently been

compared.<sup>51</sup> PMOs containing  $\pi$ -electrons adsorbed more hydrogen than the ethane-PMO. But also the stacking of the aromatic rings in the phenylene-bridged materials had an influence on the interaction. Out of the tested materials, the ethene-PMO showed the highest amount of hydrogen stored, namely 2.23 molecules  $\text{nm}^{-2}$  or 0.62 w%. This value is relatively low compared to the hydrogen uptake of other types of materials such as Metal Organic Frameworks. Values up to 4.5 w% for a MOF-5 material are reported.<sup>57</sup>

When developing gas adsorbents, one should consider the importance of the structural properties (*e.g.* 2D versus 3D pore structures) and the interactions with the functionalities present on the organic bridges.

### **2.4.3 Adsorption of organic compounds**

Only a few studies have appeared on the use of PMOs as adsorbents for organic compounds in liquid phase. Herein, we present a brief overview of some representative studies on the adsorption of organics on PMOs in Table 2.4. Especially materials containing aromatic bridges have been used and investigated. The presence of benzene moieties is particularly beneficial when the adsorption of aromatic pollutants is concerned due to the  $\pi$ --- $\pi$  interactions between adsorbate and adsorbent.

This interaction was clearly observed when researchers synthesized a phenylene derived PMO material based on BTEEB and compared it with an ethylene-bridged PMO material.<sup>58</sup> Although the phenylene derived material was disordered and less porous than the ethylene-bridged PMO, it showed a high uptake of 4-nitrophenol, 4-chlorophenol and 4-methylphenol. When a comparison was made between the phenylene derived material and activated carbon, both showed a similar adsorption. However, a large difference in regeneration could be observed. The PMO material was regenerated with absolute ethanol and thus almost 98% of the phenolic compounds were removed from the material. Only 1-2% could be removed from the activated carbon after washing with EtOH. More investigation was performed on the adsorption of aromatic compounds *via* an in-depth kinetic study with benzene, toluene, *o*-, and *p*-xylene (BTX) on phenylene-bridged PMOs.<sup>59</sup> The material was used in batch

2.14

experiments but also in a column set-up. The adsorption capacity of BTX decreased in the following sequence: benzene > *o*-xylene > *p*-xylene > toluene.

The removal of other organic compounds from aqueous solutions with nitro functionalities or a more complex structure is also explored. A recent publication focused on the use of PMOs prepared with BTEB and BTEEB for the preconcentration of trinitrotoluene and the importance of imprinting similar to the method used for metal adsorption.<sup>60</sup> Furthermore, two papers appeared on the adsorption of more complicated organic compounds with where the adsorption of polycyclic aromatic hydrocarbons and nicotine was described.<sup>61, 62</sup>

The limited amount of reports published on the adsorption of organics in liquid phase clearly emphasizes the need for further investigation in this area. Issues such as the influence of introducing functionalities on the materials, batch and column set-ups and especially the adsorption of larger complex molecules is only very vaguely explored for PMO materials. The investigation of the adsorption of dyes or pesticides and insecticides (*e.g.* DDT) would be especially interesting, not only for sequestration but also for more advanced applications such as sensing.

**Table 2.4: Overview of PMO adsorbents used for organic compounds.**

Bis-silylated precursor	Organic compound	Ref.
BTEB, BTEE	4-chlorophenol	63
BTEE, BTMEB <sup>a</sup>	4-nitrophenol, 4-chlorophenol, 4-methylphenol	58
BTEB, BTEMB	trinitrotoluene	60
BTEB	benzene, toluene, <i>o</i> -xylene, and <i>p</i> -xylene	59
BTEB, 1-phenyltriethoxysilane	acenaphtene, fluoranthene, fluorene, naphthalene, pyrene	61
BTEB, BTES-biphenyl <sup>b</sup> , BTMS-amine <sup>c</sup>	nicotine	62

<sup>a</sup> 1,4-bis(trimethoxysilylethyl) benzene. <sup>b</sup> 4,4'-bis(triethoxysilyl)biphenyl.

<sup>c</sup> bis[3-(trimethoxysilyl)propyl]amine.

## 2.5 PMOs as heterogeneous catalyst

The field of catalysis is considered as the major application of PMOs and this resulted in a numerous amount of published reports. Several catalytic species can be incorporated in the PMO such as acid or base functions but also metals and metal complexes. Furthermore, also advanced catalytic reactions are researched where bifunctional catalysts or chiral bridges play an important role. A summary is presented below, each section focussing on a specific catalytic function.

### 2.5.1 Acid catalysis

Concerning acid catalysis, the most incorporated functionality is the sulfonic acid ( $-\text{SO}_3\text{H}$ ) group. This Brønsted acid site was introduced *via* different routes and resulted in a variety of acid PMO materials. A summary is shown in Figure 2.5. The materials are obtained *via* direct sulfonation (**a**, **b**); co-condensation with an organosilane (**c-i**); post-modification of the organic bridges (**j-m**) and grafting without (**n**) or with post-modification (**o-r**). These PMOs are employed as acid catalyst and Table 2.5 summarizes the reactions catalyzed by these solids and the corresponding references.

Although high acidities are reported for sulfonated PMOs, this acidity does not relate very obviously with the observed catalytic activity.<sup>64-66</sup> The latter is influenced by structural properties of the PMO material but also by the accessibility and acid strength of the catalytic site. Furthermore, the hydrophobicity of the material is also of great importance.

The group of Melero demonstrated the hydrophobic and hydrophilic effect with PMOs obtained *via* the co-condensation of BTEE with propyl and arene sulfonic acid functionalised silanes.<sup>67</sup> These materials showed a higher catalytic activity in the etherification of vanillyl alcohol with 1-hexanol in comparison with SBA-15 type materials prepared with the same organosilanes. In contrast to the  $-\text{SO}_3\text{H}$  containing silicas, the acid sites of the PMOs were not deactivated by water, a by-product of the catalytic reaction, due to their local hydrophobic environment around the sulfonic acid site. This higher resistance against deactivation emphasises that hydrophobicity



is an essential factor for the overall stability. The sulfonated PMO (Figure 2.5, type **c**) was employed in a flow reactor during several runs for the alkylation of phenol with 2-propanol.<sup>68</sup>

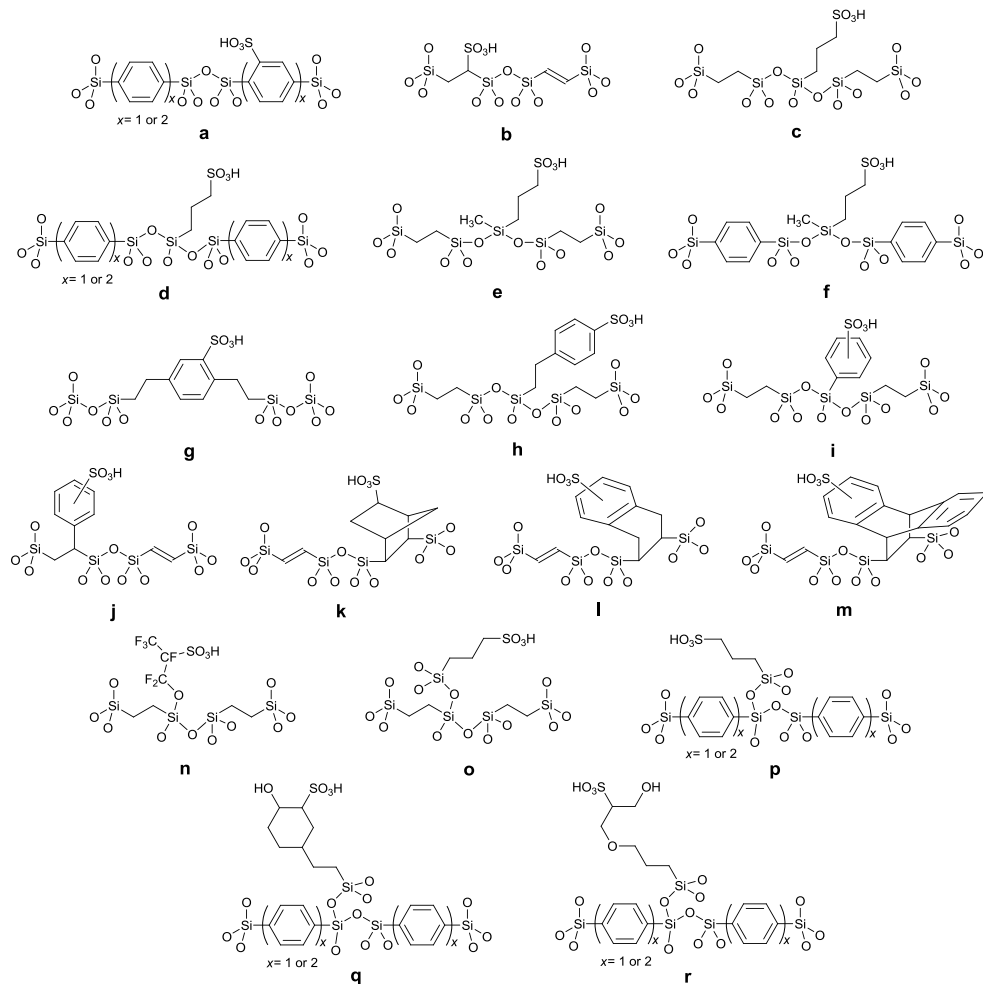


**Figure 2.5:** Types of acid PMOs functionalised with a sulfonic acid group.

**Table 2.5: Overview of reactions catalyzed by sulfonated PMOs (presented in Figure 2.5).**

Reaction type	Structure
Acetalization of heptanal by 1-butanol	c <sup>69</sup> , h <sup>69</sup> , n <sup>70</sup>
Alkylation of isobutane with 1-butene	n <sup>71</sup>
Claisen-Schmidt condensation between benzaldehyde and acetophenone	c <sup>72</sup> , i <sup>66</sup>
Self-condensation of heptanal to crotonaldehyde	j <sup>73</sup> , n <sup>70</sup>
Dehydration of 1-butanol to butyl ether	c <sup>74</sup> , h <sup>75</sup>
Dimerization of 2-phenylpropene	a <sup>65</sup> , d <sup>65</sup>
Esterification	a <sup>76</sup> , b <sup>77</sup> , c <sup>78</sup> , d <sup>79,80</sup> , g <sup>81</sup> , k <sup>82</sup> , l <sup>82,83</sup> , m <sup>82</sup> , p <sup>79,80</sup> , q <sup>80</sup> , r <sup>80</sup>
Transesterification (biodiesel production)	e <sup>84</sup> , f <sup>84</sup>
Etherification	a <sup>85</sup> , c <sup>67</sup> , h <sup>67</sup>
Friedel-Crafts reactions	
Alkylation	a <sup>65</sup> , c <sup>68</sup> , d <sup>65</sup>
Acylation and Fries rearrangement	a <sup>65,86</sup> , d <sup>65</sup>
Hydroxyalkylation	a <sup>85</sup> , c <sup>87</sup> , d <sup>87</sup> , i <sup>66</sup> , o <sup>87</sup> , p <sup>80,87</sup> , q <sup>80</sup> , r <sup>80</sup>
Hydration of propylene oxide to propylene glycol	c <sup>74</sup>
Hydrolysis	
of cyclohexylacetate	c <sup>78</sup>
of sugars	c <sup>64</sup> , o <sup>64</sup> , p <sup>64</sup>
Rearrangement	
Beckmann rearrangement	l <sup>88</sup>
Pinacol-pinacolone rearrangement	l <sup>88</sup>
Rearrangement-aromatization of ketoisophorone	a <sup>65</sup> , d <sup>65</sup>

By examining the overview of the reported catalytic reactions, it is clear that more attention is paid to organic reactions that involve the expulsion of water which is

often a by-product.<sup>89</sup> The hydrophobicity of the material is in that case beneficial as it will assist in the diffusion of the organic reactants into the pores and the water out of the pores.<sup>69, 81</sup> When the PMOs are compared with silicas containing similar functional groups, or zeolites and commercially available resins, a higher catalytic activity per acid site is observed.<sup>69, 72, 83, 88</sup>

It is reported by a number of authors that sulfonated PMOs are stable during several subsequent catalytic runs without a decrease of catalytic activity.<sup>64, 74, 83</sup> However, the method of introducing sulfonic acid groups plays a key role in the stability of the resulting PMO material. The difference in stability between a sulfonated PMO material obtained by co-condensation (Figure 2.5, type **d**) or by a grafting method (Figure 2.5, type **p**) was observed when the materials were employed in the esterification of acetic acid and ethanol.<sup>79</sup>

### 2.5.2 *Base catalysis*

A large amount of research is performed on the preparation and catalytic evaluation of acid PMO catalysts. In contrast, less reports are published on the development of base PMO catalysts. Kapoor *et al.* described the employment of amino functionalised PMOs as base catalysts.<sup>54</sup> *Via* a post-synthetic modification of a phenylene-bridged PMO and silica, they obtained polyamidoamine dendrimers inside the pores. These materials were compared with PMOs and silicas functionalised with APTES. The dendritic nanomaterials possessed a higher catalytic activity in the Knoevenagel condensation between benzaldehyde and malononitrile.

Aminated phenylene-bridged PMO materials were applied for the same catalytic reaction.<sup>90</sup> First a nitration of a crystal-like benzene-PMO was performed, followed by a reduction to obtain amine functionalities. The materials showed approximately 80% of conversion after two hours and no loss of catalytic activity was observed during the first recycle. Also tertiary amines were probed for this type of reaction by employing PMOs prepared with tris(3-(trimethoxysilyl)propyl)amine.<sup>91</sup> Interesting results were obtained, also for the Henry reaction of benzaldehyde and nitroethane and the ring opening reaction of glycidol and lauric acid.

Furthermore, base catalysts were obtained *via* co-condensation processes of BTME and APTMS for the aldol condensation of benzaldehyde with nitromethane<sup>92</sup> or by the condensation of tris-silylated melamine and a silica source for the coupling of propylene oxide with CO<sub>2</sub>.<sup>93</sup> On the other hand, a grafting procedure with a thiazolium precursor on phenylene- and ethylene-bridged PMOs resulted in base catalysts for the benzoin condensation of benzaldehyde and for the cross-coupling of aldehydes and acyl imines to amido ketones.<sup>94</sup> Higher catalytic activity and stability were obtained for the PMO with benzene moieties.

### 2.5.3 Catalysis by metal sites

Metal sites are mostly incorporated in PMOs to execute redox processes. As can be seen from Figure 2.6, the metals Ti, Sn, V and Nb, introduced as tetrahedral sites in the framework of the PMO were employed in different types of catalytic reactions such as oxidations, ammoximations, alkylations, *etc.*

The selective epoxidation of  $\alpha$ -pinene<sup>95</sup> and 1-octene<sup>96</sup> was catalyzed by Ti-PMO and used H<sub>2</sub>O<sub>2</sub> and TBHP as oxidant, respectively. The same oxidants were used when Sn-PMOs were probed in the epoxidation of norbornene and *cis*-cyclooctene<sup>97</sup> and V-PMOs were reported to catalyze the epoxidation of styrene.<sup>98</sup> The metal Nb was also incorporated in PMOs with an ethane and octane bridge.<sup>99</sup> These materials were employed in the oxidation of stearic acid and epoxidation of methyl oleate with hydrogen peroxide as mild oxidant. Cr-PMOs oxidized cyclohexane into cyclohexanol and cyclohexanone.<sup>100</sup>

Furthermore Ti-PMO catalyzed ammoximation reactions of cyclic ketones (cyclohexanone and cyclododecanone)<sup>101</sup> and Al-PMO were utilized as acid catalysts for the alkylation of 2,4-di-*tert*-butylphenol with cinnamyl alcohol.<sup>102</sup> The latter was prepared *via* an one-pot condensation of BTME and Al(*i*PrO)<sub>3</sub>. The hydrophobicity introduced by the organic bridges generally resulted in a higher activity per metal center. It was observed that the metal containing PMO materials are mostly more active and selective in comparison with silica materials that contained the same metal site. Although the PMOs were more stable, metal leaching was sometimes unavoidable, especially for V- and Cr-PMOs.

Besides the metal mentioned above, also Zr and Pd are incorporated PMOs. The Zr-PMOs catalyzed the methanolysis of crude palm oil and are interesting catalysts for biodiesel production.<sup>103</sup> Furthermore, phenylene- and ethylene-bridged PMOs were used as support for palladium nanoparticles.<sup>104</sup> They were active in the Suzuki cross-coupling reaction between bromobenzene and phenylboronic acid.

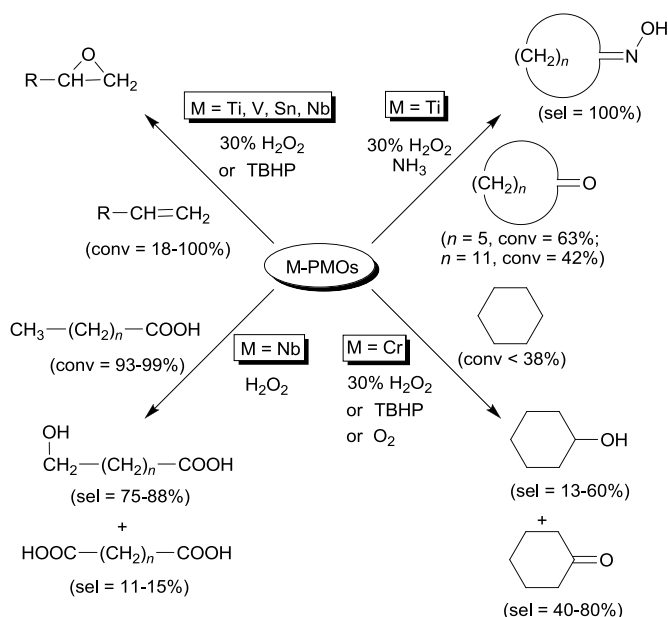


**Figure 2.6:** Redox processes catalyzed by metal sites (Ti, V, Sn, Nb and Cr) that are incorporated in PMO materials.

### 2.5.4 Catalysis by metal complexes

A variety of metal complexes is incorporated in PMO materials in an effort to heterogenize organometallic catalysts. This can be achieved by the proper choice of precursor where the metal can either be attached to the organic bridge prior to the PMO synthesis, or the metal can be coordinated to the PMO in a post-modification step. Corriu *et al.*<sup>105, 106</sup> reported that the two reaction pathways are distinctively different. When a cyclam precursor was used, a mesoporous material with high specific surface area (*ca.* 800 m<sup>2</sup> g<sup>-1</sup>) was obtained. The metal, *e.g.*, Cu<sup>2+</sup>, was then included *via* the reaction of the solid material with the metal chloride. However, when

the metal is first coordinated to the cyclam precursor, less ordered and less porous materials were obtained.

Several different metal complexes, used as a catalyst, are presented in Table 2.6. As can be seen, metals such as Pd, Mo, Ni, V, Cr, Fe and Ru are heterogenized. Well-performing and stable organometallic catalysts were developed when bis(8-quinolinolato)dioxomolybdenum(VI) complexes,<sup>107</sup> metalloporphyrins (Fe, Cu, Sn),<sup>108</sup> and  $\alpha$ -diimine complexes with Ni<sup>109</sup> were used as PMO bridge. These catalysts were more active than their homogenous counterparts. The incorporation of a V Schiff base complex even resulted in a catalyst that showed no leaching.<sup>110</sup>

A numerous amount of PMOs with organophosphine complexes with Pd(II), Rh(I), Ru(II) and Au(I) were developed by the co-condensation with the bis- or tris-silylated phosphine complex with TEOS, BTEB or 4,4'-bis(triethoxysilyl)biphenyl. These catalysts were evaluated for various organic reactions such as the Barbier reaction between substituted benzaldehyde and allyl halide, the Suzuki cross-coupling reaction of arylboronic acid and aryl halide, *etc.*<sup>111-114</sup>

Table 2.6: Overview of catalytic processes in PMOs with metal complexes as bridges.

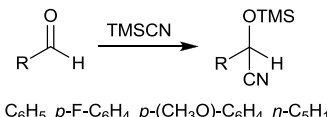
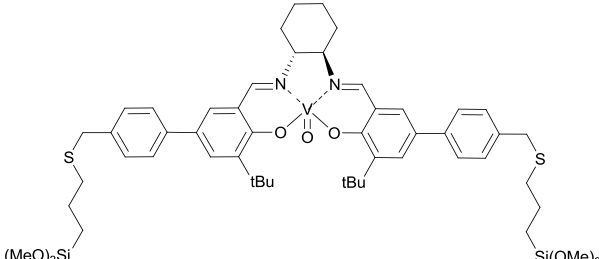
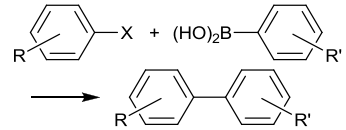
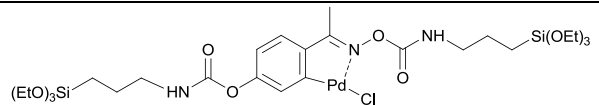
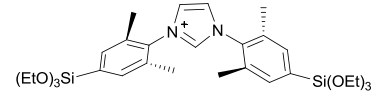
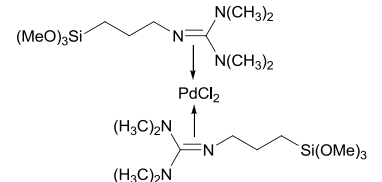
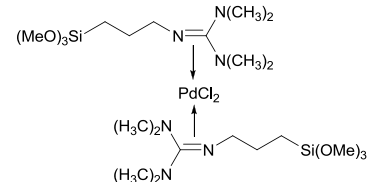
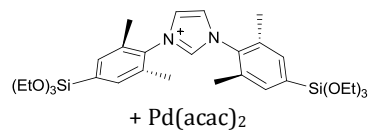
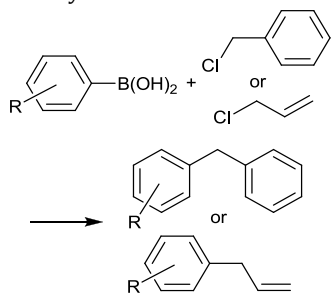
Reaction	Precursor	Catalytic Perf.	Ref.
Cyanosilylation of aldehydes  $R = \text{C}_6\text{H}_5, p\text{-F-C}_6\text{H}_4, p\text{-(CH}_3\text{O)-C}_6\text{H}_4, n\text{-C}_5\text{H}_{11}$		Conv = 71-86%, Sel > 98%	110
Suzuki-Miyaura coupling  $X = \text{Cl, Br}$	  + Pd(acac) <sub>2</sub>	$Y > 99\%$ (X= Br) $Y = 5\text{-}12\%$ (X= Cl)	115
		$Y = 81\text{-}93$ (X= Br) $Y = 50\text{-}100\%$ (X= Cl)	116- 118
		Y = 76-99% (X= Br)	119

Table 2.6 – Continued.

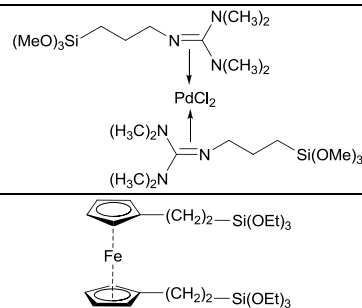
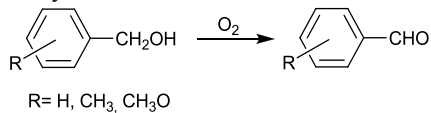
Coupling of benzylic/allylic chlorides and arylboronic acids



Y = 61-95%

116,  
117

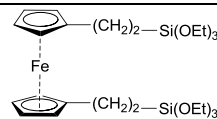
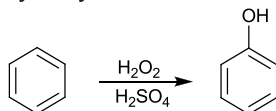
Aerobic oxidation of benzylic alcohols



Y ≈ 98%

119

Hydroxylation of benzene

Y ~ 20%,  
Sel ~ 65%

120

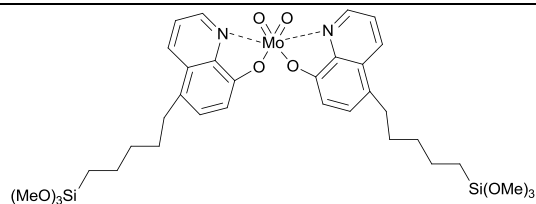
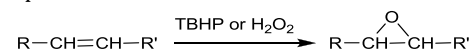


Table 2.6 – Continued.

<p>Aerobic Baeyer-Villiger oxidation</p> $\text{R}-\overset{\text{O}}{\parallel}{\text{C}}-\text{R}' \xrightarrow{\text{O}_2} \text{R}-\overset{\text{O}}{\parallel}{\text{C}}-\text{O}-\text{R}'$		<p>Y = 50-100%      108</p>
<p>Hydrosilylation of 1-hexyne</p> $\text{CH}_3-(\text{CH}_2)_3-\text{C}\equiv\text{CH} + (\text{CH}_3\text{CH}_2)_3\text{SiH} \longrightarrow \begin{array}{l} \text{CH}_3-(\text{CH}_2)_3 \\   \\ (\text{CH}_3\text{CH}_2)_3\text{Si}-\text{C}=\text{CH}_2 \end{array}$	<p>BTEB + <math>[(\text{CH}_3\text{CN})_3\text{RuCp}]\text{PF}_6</math></p>	<p>Conv <math>\approx</math> 28%      121</p>

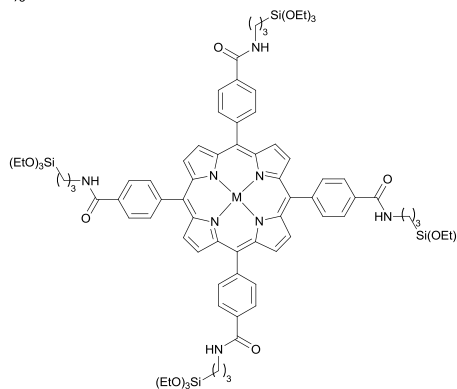
Table 2.6 – Continued.

## Epoxidation of alkenes



Y ~ 49%

122

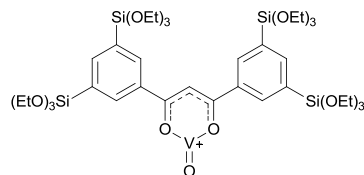
M = Fe  
Conv = 41%

123

BTEB + M(CO)<sub>6</sub>M = Mo, Cr  
Conv = 37-100%

124,

125

Sel = 100%  
Conv = 55%

126

With Conv = conversion; Sel = selectivity; Y = yield. TMSCN = trimethylsilyl cyanide. Cp = cyclopentadienyl.

### 2.5.5 Catalysis by bifunctional PMOs

The examples of bifunctional PMOs used as catalyst are rather limited. These PMOs possess two different catalytic functions and this concept was first introduced by Mehdi *et al.*, although they did not perform any catalytic experiments.<sup>127</sup> They prepared PMOs with sulfonic acid groups by the oxidation of BTEPDS and dangling amine functions originating from Boc protected APTMS.

Another approach is the use of crystal-like phenylene-bridged PMOs, synthesized by the co-condensation of BTEB and APTMS, where the benzene moieties are sulfonated.<sup>128</sup> This resulted in a material with sulfonic acid groups on the hydrophobic layer and amine functions on the hydrophilic silica layer. The catalytic activity of this PMO was evaluated in a tandem reaction, *i.e.*, the one-pot deacetalization and nitroaldol condensation reaction catalyzed by the acid and basic function, respectively. A yield of 97.5% was obtained for the end-product *trans*- $\beta$ -nitrostyrene.

Similar methods were employed to create bifunctional PMOs. Inagaki and Sasidharan<sup>129, 130</sup> modified ethenylene-bridged PMOs with sulfonic acid and amine groups and Polarz *et al.*<sup>131</sup> converted phenylene-bridged PMOs in bifunctional materials by introducing amine and carboxylic acid functionalities. This -COOH group was subsequently used to anchor [VO]<sup>2+</sup>.

Furthermore, Li *et al.* described a PMO prepared by the co-condensation of BTEE and MPTMS that was impregnated with H<sub>2</sub>AuCl<sub>4</sub>.<sup>132</sup> A partial oxidation of the thiol groups was performed and Au nanoparticles were coordinated to the remaining -SH functions. A cooperative effect of the nanoparticles and sulfonic acid groups was observed for the hydration of alkynes. This catalyst showed a higher activity than the homogeneous catalyst Au(PPh<sub>3</sub>)Cl.

### 2.5.6 Enantioselective catalysis by PMOs

Enantioselective catalysts are most important for pharmaceutical industry when chiral compounds are produced. An overview of chiral PMOs is presented in Table 2.7. Large chiral vanadyl Schiff base complexes were incorporated as organic bridge in

PMO materials by the group of Corma.<sup>110, 133</sup> The V containing PMO was probed for the cyanosilylation of benzaldehyde but a lower enantiomeric excess was observed in comparison with homogenous complexes under certain conditions.

Garcia *et al.* prepared chiral PMOs with bis-silylated *trans*-(1*R*,2*R*)-cyclohexadiamine moieties by a co-condensation process with TEOS.<sup>134</sup> This PMO was used as a nanoreactor for the photochemical di- $\pi$ -methane rearrangement of dibenzobarrelene. [Rh(cod)Cl]<sub>2</sub> complexes were coordinated to similar chiral cyclohexadiamine units and their catalytic performance in the asymmetric transfer hydrogenation of a variety of aromatic ketones was evaluated.<sup>135, 136</sup> The materials however could not be reused due to the leaching of the Rh metal or decomposition of the active center.<sup>135</sup>

Tartrate derivatives can coordinate titanium and therefore bis-silylated chiral tartramide precursors together with TEOS were employed for the preparation of PMOs.<sup>137</sup> A sulfoxide yield of 70% (30% ee) was observed for the asymmetric sulfoxidation of methyl phenyl sulfide. The PMOs were reusable for a second catalytic experiment. However, a decrease of the yield and enantiomeric excess was observed. The same group also reported the *in-situ* synthesis of this chiral bridge by a transamidation reaction.<sup>138</sup> Herein, a co-condensation with BTEE was used and the resulting materials exhibited tartramide loadings from 0.59 up to 1.62 mmol g<sup>-1</sup>. The catalytic results were similar to those previously reported.<sup>137</sup> Li *et al.* evaluated the tartramide PMO in combination with Ti(*i*PrO)<sub>4</sub> for the epoxidation of allyl alcohols.<sup>139</sup>

Several BINOL based bis-silanes were developed by the group of Yang.<sup>140, 141</sup> They synthesized a variety of chiral bis-silylated R-(+)-BINOL precursors that are co-condensed with TMOS or BTME. When Ti is coordinated to the BINOL unit, the asymmetric addition of diethylzinc to benzaldehyde was catalyzed. The use of the ethane bridge not only improved the catalyst significantly as it was more active with a conversion of 99% and enantioselectivity of ~40%, it was also more stable. Furthermore, the synthesis of nanospheres with this BINOL precursor is reported where TEOS was used in the co-condensation process.<sup>142</sup> By changing the synthetic environment, nanospheres with different mesostructural ordering was obtained. This

PMO, with titanium coordinated to the BINOL unit, was more enantioselective than the homogeneous counterpart. A high ee-value of 94% was observed at 99% conversion. García *et al.* also incorporated this BINOL unit by the co-condensation of a bis-silylated BINOL precursor with TEOS and utilized this PMO for the asymmetric oxidation of methyl phenyl sulfide.<sup>143</sup> High enantioselectivity (99%) was also observed in the asymmetric hydrogenation of  $\beta$ -keto-esters when  $[\text{RuCl}_2\text{-(benzene)}]_2$  was coordinated at BINAP containing PMOs.<sup>144</sup> These chiral materials were prepared via co-condensation with TMOS.

Furthermore, other chiral bridges in PMO hollow nanospheres were reported such as L-prolinamide<sup>145</sup> or the incorporation of N,N-dipropyl cyclohexanediamine<sup>146</sup> via acid-base interactions between the amine and sulfonic acid groups present on the PMO. In both cases BTME was used in the co-condensation process and the resulting materials were probed as catalysts in the asymmetric aldol condensation of aldehydes with cyclohexanone. Also BTEB was employed to prepare hollow spheres. This time, a hard templating route with hematite nanoparticles was used, together with 3-azidopropyltrimethoxysilane.<sup>147</sup> The latter was post-modified by click chemistry. The resulting materials were tested in the Diels-Alder reaction between 1,3-cyclopentadiene and *trans*-cinnamaldehyde.

Polarz *et al.* reported the modification of chiral bridges with  $\text{AlMe}_2\text{Cl}$ .<sup>148</sup> The resulting Al containing PMO materials were used in the carbonyl ene reaction of  $\alpha$ -methylstyrene and trichloroacetaldehyde. Higher ee-values were reported for the chiral PMOs (72%) at  $-55^\circ\text{C}$  than for the homogeneous catalyst (17%).

**Table 2.7: Overview of catalytic processes in PMOs with chiral bridges.**

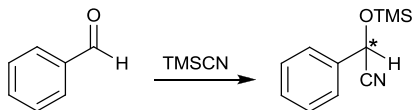
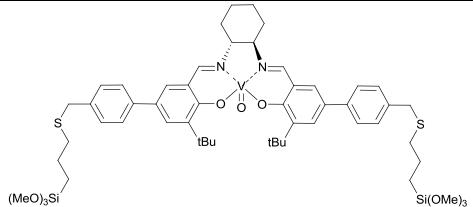
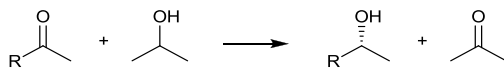
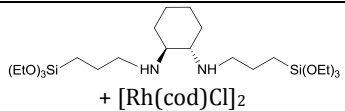
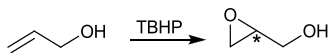
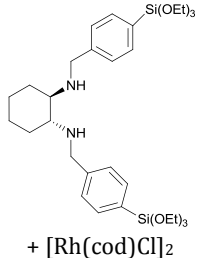
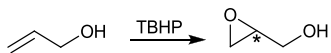
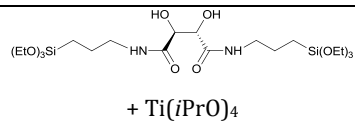
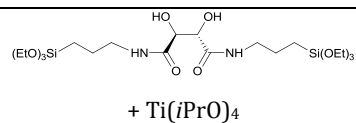
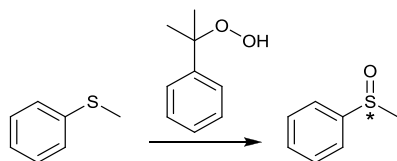
Reaction	Bridge	Catalytic performance	Ref.
<p>Cyanosilylation of benzaldehyde</p> 		Conv = 80%; ee = 30%	110, 133
<p>Transfer hydrogenation of aromatic ketones</p> 	 <p>+ [Rh(cod)Cl]<sub>2</sub></p>	Conv = 16-36%, ee = 8%	136
<p>Epoxidation of allyl alcohol</p> 	 <p>+ [Rh(cod)Cl]<sub>2</sub></p>	Conv = 39-98%, ee = 22-41%	135, 136
<p>Epoxidation of allyl alcohol</p> 	 <p>+ Ti(<i>i</i>PrO)<sub>4</sub></p>	Conv = 46%, ee = 20%	139

Table 2.7 – Continued.

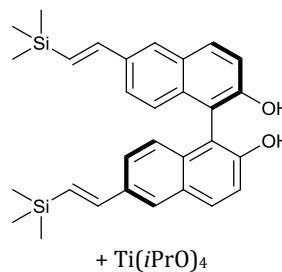
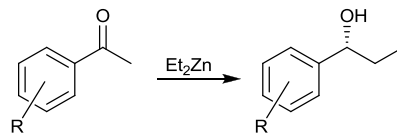
Sulfoxidation of methyl phenyl sulfide



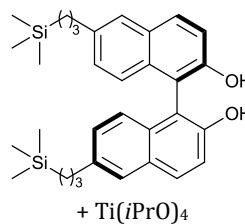
Conv = 70%, ee = 30%

137

Addition of diethylzinc to aldehydes

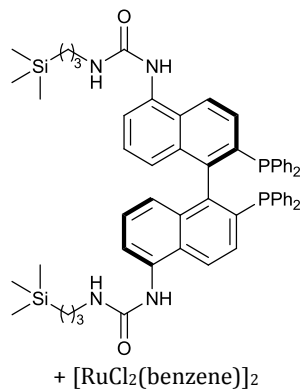
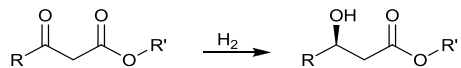
Conv = 98% (R=H), ee =  
40%

140

Conv = 40-99%, ee = 68-  
93%

141

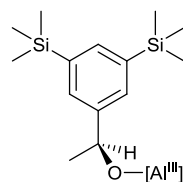
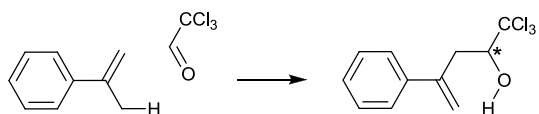
Table 2.7 – Continued.

Hydrogenation of  $\beta$ -keto esters

Conv = 40-99%, ee = 92-99%

149

## Carbonyl ene reaction



Y = 60-80%, ee = 0-80%

148



## ***2.6 Emerging applications in biomedical sciences and drug release***

The adsorption or immobilization of proteins, enzymes, amino acids and drugs is of great interest in the field of biomedical applications. An overview of immobilized or adsorbed biomolecules on PMOs is presented in Table 2.8.

One of the first reports presented the adsorption of a protein *via* electrostatic interactions.<sup>150</sup> Cytochrome *c* (*Bovine heart*) was adsorbed on large pore ethylene-bridged PMO materials. The adsorption capacity reached a maximum at the isoelectric point of the protein, however it did not exceed the values obtained for SBA-15 materials. This research on the adsorption of proteins was expanded by using benzene- and biphenyl-PMOs for Cytochrome *c* (*Horse heart*)<sup>151</sup> and ethane based PMO materials for the adsorption of serum albumin<sup>152-154</sup> and hemoglobin<sup>154</sup>. The ethane PMO does not only act as a support, it can assist in protein refolding (Figure 2.7).<sup>155</sup> Hen egg white lysozyme was entrapped in the pores of the PMO *via* hydrophilic and hydrophobic interactions and aggregation of the biomolecules was prevented. Continuous elution of the lysozyme triggered by poly(ethyleneglycol) (PEG) resulted in refolding of the protein.

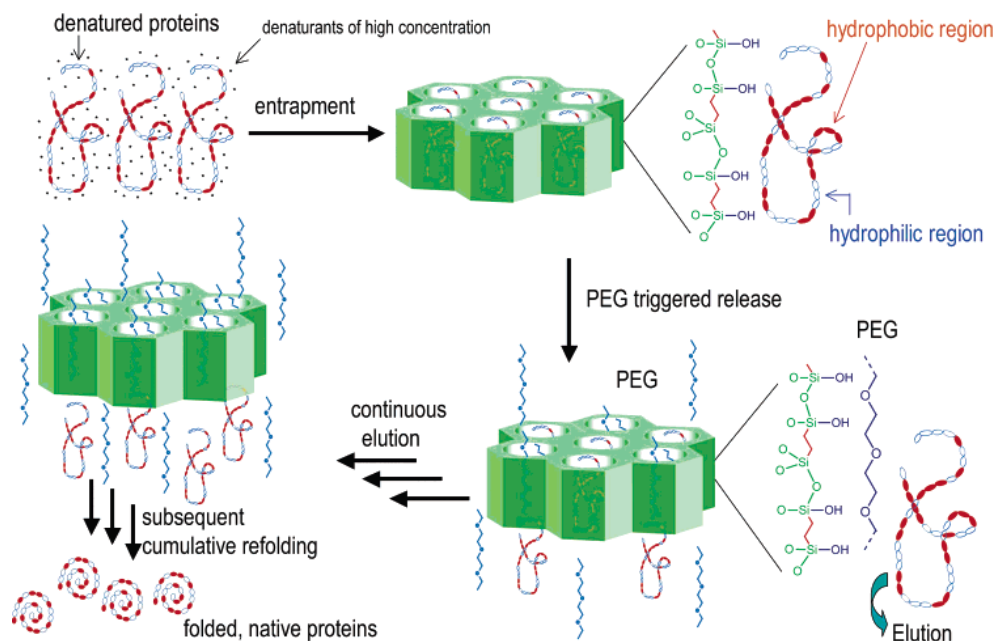


**Figure 2.7: Refolding of hen egg white lysozyme assisted by an ethylene-bridged PMO material.<sup>155</sup>**

Besides enzymes, also amino acids<sup>156</sup> and drugs were immobilized. The latter is of great importance in controlled drug delivery systems. The use of PMO for this purpose was reported for the first time in 2009.<sup>157</sup> Ethylene-bridged PMO materials were prepared as hollow spheres and solid spheres and their use as drug carrier for the hydrophobic antibiotic tetracycline was compared with MCM-41 type materials. The hollow spheres of PMO showed a higher loading capacity and the drug was released with a slower rate due to the empty core and hydrophobic interactions, respectively. This example was followed by research on the adsorption of *cisplatin*, an anticancer drug, on ethane PMOs.<sup>158</sup> More complex bridges were incorporated to adsorb drugs such as *captopril*,<sup>159, 160</sup> and *5-fluorouracil*<sup>159-161</sup>. *Ibuprofen* was adsorbed on PMO materials containing amidoxime moieties.<sup>161</sup>

**Table 2.8: Bio-molecules and drugs immobilized onto PMOs.**

Type	Adsorbed molecule	Support or carrier (surface functionality)	Structure/Morphology	Ref.	
Protein	Cytochrome c <i>bovine heart</i> <i>horse heart</i>	-CH <sub>2</sub> -CH <sub>2</sub> -	2D-hexagonal/rod-like	150	
		-C <sub>6</sub> H <sub>4</sub> - / -(C <sub>6</sub> H <sub>4</sub> ) <sub>2</sub> -	disordered/ hollow spherical particles	151	
	Serum albumin <i>bovine</i>	-CH <sub>2</sub> -CH <sub>2</sub> -	cubic/hollow particles	152	
			hollow spheres	153	
	Hemoglobin		-CH <sub>2</sub> -CH <sub>2</sub> - functionalised with -NH <sub>2</sub> or -COOH	2D-hexagonal/rod-like	154
			-CH <sub>2</sub> -CH <sub>2</sub> - functionalised with -NH <sub>2</sub> or -COOH	2D-hexagonal/rod-like	154
Enzyme	Lysozyme <i>hen egg white</i>	-CH <sub>2</sub> -CH <sub>2</sub> -	2D-hexagonal/rod-like	162	
		-(CH <sub>2</sub> ) <sub>3</sub> -NH-(CH <sub>2</sub> ) <sub>3</sub> - / -C <sub>6</sub> H <sub>4</sub> - / -(C <sub>6</sub> H <sub>4</sub> ) <sub>2</sub> -	hollow spherical particles	163	
		-CH <sub>2</sub> -CH <sub>2</sub> -	cubic/hollow particles	152	
	Lipase <i>Rhizopus oryzae</i> <i>Candida antarctica</i> <i>fraction B</i> <i>Thermomyces</i> <i>lanuginosus</i>	-CH <sub>2</sub> -CH <sub>2</sub> -	n.a.	164	
		-CH <sub>2</sub> -CH <sub>2</sub> -	2D-hexagonal/rod-like	165	
		-CH <sub>2</sub> -CH <sub>2</sub> - / -CH=CH- / -C <sub>6</sub> H <sub>4</sub> -	-/mesocellular cage-like	166	
	Papain	-CH <sub>2</sub> -CH <sub>2</sub> - functionalised with -(CH <sub>2</sub> ) <sub>3</sub> -O-CH <sub>2</sub> -(CH) <sub>2</sub> O	2D-hexagonal	167	
	Chloroperoxidase	-(CH <sub>2</sub> ) <sub>3</sub> -NH-(CH <sub>2</sub> ) <sub>3</sub> -	Disordered	168	
			2D-hexagonal	169	
	Horseradish	-(CH <sub>2</sub> ) <sub>3</sub> -NH-CO-NH-(CH <sub>2</sub> ) <sub>3</sub> - / -(CH <sub>2</sub> ) <sub>3</sub> -NH-CO-S-(CH <sub>2</sub> ) <sub>3</sub> -			

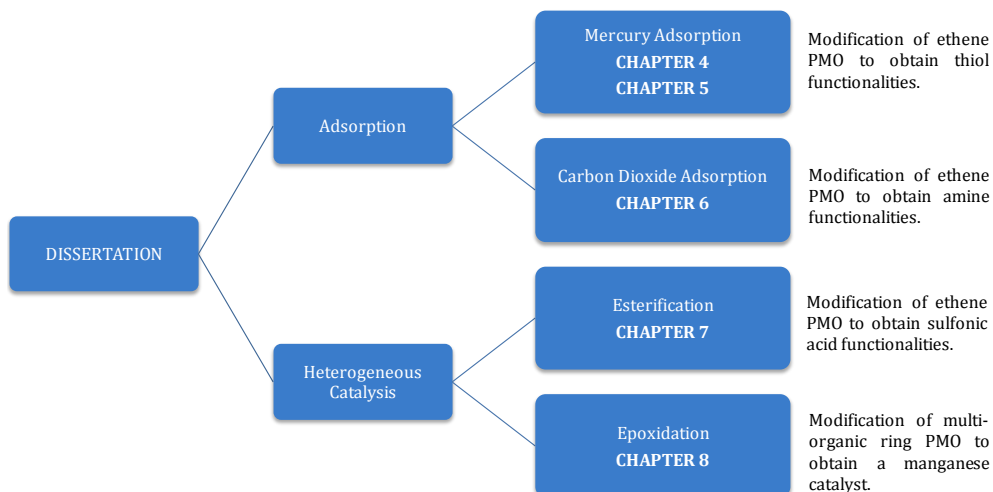
Chapter 2 – Applications of PMOs

	Peroxidase	$-(\text{CH}_2)_3\text{-S-CH}_2\text{-CHOH-CH}_2\text{-O-}(\text{CH}_2)_3\text{-}$	2D-hexagonal	170
Amino-acids	Glycine, L-Lysine, Isoleucine	$-\text{C}_6\text{H}_4\text{-}$	disordered/ hollow spherical	156
		$-(\text{C}_6\text{H}_4)_2\text{-} / \text{-}(\text{CH}_2)_3\text{-NH-}(\text{CH}_2)_3\text{-}$	worm-like/hollow spherical	156
Drug	Tetracycline	$-\text{CH}_2\text{-CH}_2\text{-}$	2D-hexagonal/spherical particles	157
	Cisplatin	$-\text{CH}_2\text{-CH}_2\text{-}$	2D-hexagonal	158
	Captopril	$-(\text{CH}_2)_3\text{-NH-CO-NH-C}_6\text{H}_4\text{-SO}_2\text{-NH-CO-NH-}(\text{CH}_2)_3\text{-}$	2D-hexagonal/rod-like	159
		$-(\text{CH}_2)_3\text{-NH-CO-N}((\text{CH}_2)_2)_2\text{N-CO-NH-}(\text{CH}_2)_3\text{-}$	2D-hexagonal/ polyhedral bipyramidal crystals	160
	5-Fluorouracil	$-(\text{CH}_2)_3\text{-NH-CO-NH-C}_6\text{H}_4\text{-SO}_2\text{-NH-CO-NH-}(\text{CH}_2)_3\text{-}$	2D-hexagonal/rod-like	159
		$-(\text{CH}_2)_3\text{-NH-CO-N}((\text{CH}_2)_2)_2\text{N-CO-NH-}(\text{CH}_2)_3\text{-}$	2D-hexagonal/ polyhedral bipyramidal crystals	160
		$-(\text{CH}_2)_3\text{-NH-CO-NH-CCN=CCN-NH-CO-NH-}(\text{CH}_2)_3\text{-}$	2D-hexagonal/shaped tubular-twisted columns-micro-elongated particles	161
Ibuprofen	$-(\text{CH}_2)_3\text{-NH-CO-NH-CCN=CCN-NH-CO-NH-}(\text{CH}_2)_3\text{-}$	2D-hexagonal/shaped tubular-twisted columns-micro-elongated particles	161	

## 2.7 Aim of this dissertation

From the literature overview given above, it is clear that PMOs can be developed for a wide range of applications in very different fields. In this dissertation, it is attempted to develop new functionalised PMO materials that can be applied in *high-end* applications while making use of their chemical and structural stability. Focus is placed upon adsorption and catalysis, showing the versatility of these hybrid materials.

In the first place, the ethenylene-bridged PMO material was chosen as PMO framework. This PMO possesses ethene bonds which can be functionalised with a variety of organic reactions. Different functionalisation routes were followed, and several modified PMO materials were obtained which can be employed as mercury and CO<sub>2</sub> adsorbent and solid acid catalyst. In the second place, a multi-organic bridged PMO material with terminal ethene bonds was selected to be further modified. The resulting materials were utilized to heterogenize a manganese(II) complex for oxidation catalysis. A general representation of this dissertation with the different specific applications is presented below.



## 2.8 References

1. P. Van Der Voort, D. Esquivel, E. De Canck, F. Goethals, I. Van Driessche and F. J. Romero-Salguero, *Chemical Society Reviews*, 2013, **42**, 3913-3955.
2. N. Mizoshita, T. Tani and S. Inagaki, *Chemical Society Reviews*, 2011, **40**, 789-800.
3. W. Stober, A. Fink and E. Bohn, *Journal of Colloid and Interface Science*, 1968, **26**, 62-69.
4. M. Grun, I. Lauer and K. K. Unger, *Advanced Materials*, 1997, **9**, 254-257.
5. M. P. Kapoor and S. Inagaki, *Chem Lett*, 2004, **33**, 88-89.
6. V. Rebbin, M. Jakubowski, S. Potz and M. Froba, *Microporous and Mesoporous Materials*, 2004, **72**, 99-104.
7. V. Rebbin, R. Schmidt and M. Froba, *Angewandte Chemie-International Edition*, 2006, **45**, 5210-5214.
8. Y. P. Zhang, Y. Jin, P. Dai, H. Yu, D. H. Yu, Y. X. Ke and X. M. Liang, *Anal Methods-Uk*, 2009, **1**, 123-127.
9. Y. P. Zhang, Y. Jin, H. Yu, P. C. Dai, Y. X. Ke and X. M. Liang, *Talanta*, 2010, **81**, 824-830.
10. G. R. Zhu, D. M. Jiang, Q. H. Yang, J. Yang and C. Li, *Journal of Chromatography A*, 2007, **1149**, 219-227.
11. G. R. Zhu, H. Zhong, Q. H. Yang and C. Li, *Microporous and Mesoporous Materials*, 2008, **116**, 36-43.
12. X. Wu, L. You, B. Di, W. Hao, M. Su, Y. Gu and L. Shen, *Journal of Chromatography A*, 2013, **1299**, 78-84.
13. C. Li, B. Di, W. Q. Hao, F. Yan and M. X. Su, *Journal of Chromatography A*, 2011, **1218**, 408-415.
14. J. Lu, L. L. Huang, B. Di, F. Feng and M. X. Su, *Chromatographia*, 2011, **74**, 515-521.
15. F. Hoffmann, M. Cornelius, J. Morell and M. Froba, *Angewandte Chemie-International Edition*, 2006, **45**, 3216-3251.
16. M. A. Wahab and C. B. He, *Langmuir*, 2009, **25**, 832-838.
17. S. S. Park, D. H. Park and C. S. Ha, *Chemistry of Materials*, 2007, **19**, 2709-2711.
18. Y. F. Lu, H. Y. Fan, N. Doke, D. A. Loy, R. A. Assink, D. A. LaVan and C. J. Brinker, *Journal of the American Chemical Society*, 2000, **122**, 5258-5261.
19. B. D. Hatton, K. Landskron, W. Whitnall, D. D. Perovic and G. A. Ozin, *Advanced Functional Materials*, 2005, **15**, 823-829.
20. W. D. Wang, D. Grozea, S. Kohli, D. D. Perovic and G. A. Ozin, *Acs Nano*, 2011, **5**, 1267-1275.
21. F. Goethals, M. R. Baklanov, I. Ciofi, C. Detavernier, P. Van Der Voort and I. Van Driessche, *Chemical Communications*, 2012, **48**, 2797-2799.
22. W. D. Wang, D. Grozea, A. Kim, D. D. Perovic and G. A. Ozin, *Advanced Materials*, 2010, **22**, 99-102.
23. K. Landskron, B. D. Hatton, D. D. Perovic and G. A. Ozin, *Science*, 2003, **302**, 266-269.
24. F. Goethals, I. Ciofi, O. Madia, K. Vanstreels, M. R. Baklanov, C. Detavernier, P. Van der Voort and I. Van Driessche, *Journal of Materials Chemistry*, 2012, **22**, 8281-8286.

25. M. Seino, W. D. Wang, J. E. Lofgreen, D. P. Puzzo, T. Manabe and G. A. Ozin, *Journal of the American Chemical Society*, 2011, **133**, 18082-18085.
26. F. Goethals, E. Levrau, G. Pollefeyt, M. R. Baklanov, I. Ciofi, K. Vanstreels, C. Detavernier, I. Van Driessche and P. Van der Voort, *Journal of Materials Chemistry C*, 2013, **1**, 3961-3966.
27. Matthias Ide, Pascal Van Der Voort, Frédéric Lynen, Patrick Sandra, 23/12/2011, "Novel Organosilica compounds" EPO, EP 11195603.3; International: PCT/EP2012/076685; WO 2013/093022 (27/06/2013)
28. Frederik Goethals, Pascal Van Der Voort, Mihail Baklanov, Isabel Van Driessche, 23/09/2011, "Method for pore sealing of a porous material and the sealed porous material thereof", US 61/538,431. (Provisional), UGent ref: P2011/056 - IMEC - CARBON-BRIDGED SILICAS AND EP 12185247.9; 20/09/2012; US2013/0075876 A1, publication date: 28/03/2013
29. A. Walcarius and L. Mercier, *Journal of Materials Chemistry*, 2010, **20**, 4478-4511.
30. P. K. Jal, S. Patel and B. Mishra, *Talanta*, 2004, **62**, 1005-1028.
31. A. Derden, B. Kenniscentrum, E. van den Broeck, P. Vergauwen, D. Vancolen and R. Dijkmans, *Gids waterzuiveringstechnieken*, Academia Press, 2001.
32. M. Benitez, D. Das, R. Ferreira, U. Pischel and H. Garcia, *Chemistry of Materials*, 2006, **18**, 5597-5603.
33. N. Hao, L. Han, Y. X. Yang, H. T. Wang, P. A. Webley and D. Y. Zhao, *Applied Surface Science*, 2010, **256**, 5334-5342.
34. M. Waki, N. Mizoshita, T. Ohsuna, T. Tani and S. Inagaki, *Chemical Communications*, 2010, **46**, 8163-8165.
35. O. Olkhovyk and M. Jaroniec, *Industrial & Engineering Chemistry Research*, 2007, **46**, 1745-1751.
36. M. C. Burleigh, S. Dai, E. W. Hagaman and J. S. Lin, *Chemistry of Materials*, 2001, **13**, 2537-2546.
37. K. Z. Hossain and L. Mercier, *Advanced Materials*, 2002, **14**, 1053-1056.
38. J. Liu, J. Yang, Q. H. Yang, G. Wang and Y. Li, *Advanced Functional Materials*, 2005, **15**, 1297-1302.
39. O. Olkhovyk and M. Jaroniec, *Journal of the American Chemical Society*, 2005, **127**, 60-61.
40. O. Olkhovyk, S. Pikus and M. Jaroniec, *Journal of Materials Chemistry*, 2005, **15**, 1517-1519.
41. H. Y. Wu, C. H. Liao, Y. C. Pan, C. L. Yeh and H. M. Kao, *Microporous and Mesoporous Materials*, 2009, **119**, 109-116.
42. L. M. Yang, Y. J. Wang, G. S. Luo and Y. Y. Dai, *Microporous and Mesoporous Materials*, 2005, **84**, 275-282.
43. L. X. Zhang, W. H. Zhang, J. L. Shi, Z. Hua, Y. S. Li and J. Yan, *Chemical Communications*, 2003, 210-211.
44. B. Lee, L. L. Bao, H. J. Im, S. Dai, E. W. Hagaman and J. S. Lin, *Langmuir*, 2003, **19**, 4246-4252.
45. B. Lee, H. J. Im, H. M. Luo, E. W. Hagaman and S. Dai, *Langmuir*, 2005, **21**, 5372-5376.
46. K. Nakai, Y. Oumi, H. Horie, T. Sano and H. Yoshitake, *Microporous and Mesoporous Materials*, 2007, **100**, 328-339.

47. M. P. Kapoor, M. Yanagi, Y. Kasama, T. Yokoyama, S. Inagaki, T. Shimada, H. Nanbu and L. R. Juneja, *Journal of Materials Chemistry*, 2006, **16**, 3305-3311.
48. A. Comotti, S. Bracco, P. Valsesia, L. Ferretti and P. Sozzani, *Journal of the American Chemical Society*, 2007, **129**, 8566-8576.
49. B. J. Johnson, N. E. Anderson, P. T. Charles, A. P. Malanoski, B. J. Melde, M. Nasir and J. R. Deschamps, *Sensors*, 2011, **11**, 886-904.
50. B. J. Johnson, B. J. Melde, G. W. Peterson, B. J. Schindler and P. Jones, *Chem Eng Sci*, 2012, **68**, 376-382.
51. M. Kubo, K. Ishiyama, A. Shimojima and T. Okubo, *Microporous and Mesoporous Materials*, 2012, **147**, 194-199.
52. U. Martinez and G. Pacchioni, *Microporous and Mesoporous Materials*, 2010, **129**, 62-67.
53. S. Y. Bai, J. Liu, J. S. Gao, Q. H. Yang and C. Li, *Microporous and Mesoporous Materials*, 2012, **151**, 474-480.
54. M. P. Kapoor, Y. Kasama, T. Yokoyama, M. Yanagi, S. Inagaki, N. Hironobu and L. R. Juneja, *Journal of Materials Chemistry*, 2006, **16**, 4714-4722.
55. Y. D. Tang and K. Landskron, *Journal of Physical Chemistry C*, 2010, **114**, 2494-2498.
56. G. Qi, L. Fu, X. Duan, B. H. Choi, M. Abraham and E. P. Giannelis, *Greenhouse Gases: Science and Technology*, 2011, **1**, 278-284.
57. M. P. Suh, H. J. Park, T. K. Prasad and D. W. Lim, *Chemical Reviews*, 2012, **112**, 782-835.
58. M. C. Burleigh, M. A. Markowitz, M. S. Spector and B. P. Gaber, *Environmental Science & Technology*, 2002, **36**, 2515-2518.
59. C. P. Moura, C. B. Vidal, A. L. Barros, L. S. Costa, L. C. G. Vasconcellos, F. S. Dias and R. F. Nascimento, *Journal of Colloid and Interface Science*, 2011, **363**, 626-634.
60. S. A. Trammell, M. Zeinali, B. J. Melde, P. T. Charles, F. L. Velez, M. A. Dinderman, A. Kusterbeck and M. A. Markowitz, *Analytical Chemistry*, 2008, **80**, 4627-4633.
61. C. B. Vidal, A. L. Barros, C. P. Moura, A. C. A. de Lima, F. S. Dias, L. C. G. Vasconcellos, P. B. A. Fechine and R. F. Nascimento, *Journal of Colloid and Interface Science*, 2011, **357**, 466-473.
62. J. H. Shin, S. S. Park and C. S. Ha, *Colloids and Surfaces B-Biointerfaces*, 2011, **84**, 579-584.
63. M. C. Burleigh, S. Jayasundera, M. S. Spector, C. W. Thomas, M. A. Markowitz and B. P. Gaber, *Chemistry of Materials*, 2004, **16**, 3-5.
64. P. L. Dhepe, M. Ohashi, S. Inagaki, M. Ichikawa and A. Fukuoka, *Catal Lett*, 2005, **102**, 163-169.
65. B. Rac, P. Hegyes, P. Forgo and A. Molnar, *Applied Catalysis a-General*, 2006, **299**, 193-201.
66. J. Yang, Q. H. Yang, G. Wang, Z. C. Feng and J. Liu, *Journal of Molecular Catalysis a-Chemical*, 2006, **256**, 122-129.
67. G. Morales, G. Athens, B. F. Chmelka, R. van Grieken and J. A. Melero, *Journal of Catalysis*, 2008, **254**, 205-217.
68. X. D. Yuan, H. I. Lee, J. W. Kim, J. E. Yie and J. M. Kim, *Chem Lett*, 2003, **32**, 650-651.



69. M. Rat, M. H. Zahedi-Niaki, S. Kaliaguine and T. O. Do, *Microporous and Mesoporous Materials*, 2008, **112**, 26-31.
70. D. Dubé, M. Rat, W. Shen, F. Beland and S. Kaliaguine, *J Mater Sci*, 2009, **44**, 6683-6692.
71. W. Shen, D. Dube and S. Kaliaguine, *Catalysis Communications*, 2008, **10**, 291-294.
72. S. Shylesh, P. P. Samuel, C. Srilakshmi, R. Parischa and A. P. Singh, *Journal of Molecular Catalysis a-Chemical*, 2007, **274**, 153-158.
73. D. Dubé, M. Rat, F. Beland and S. Kaliaguine, *Microporous and Mesoporous Materials*, 2008, **111**, 596-603.
74. J. Liu, J. Yang, C. M. Li and Q. H. Yang, *Journal of Porous Materials*, 2009, **16**, 273-281.
75. B. Sow, S. Hamoudi, M. H. Zahedi-Niaki and S. Kaliaguine, *Microporous and Mesoporous Materials*, 2005, **79**, 129-136.
76. D. Esquivel, C. Jiménez-Sanchidrián and F. J. Romero-Salguero, *Journal of Materials Chemistry*, 2011, **21**, 724-733.
77. E. De Canck, C. Vercaemst, F. Verpoort and P. Van Der Voort, in *Scientific Bases for the Preparation of Heterogeneous Catalysts: Proceedings of the 10th International Symposium*, eds. E. M. Gaigneaux, M. Devillers, S. Hermans, P. A. Jacobs, J. A. Martens and P. Ruiz, Elsevier Science Bv, Amsterdam, 2010, pp. 365-368.
78. Q. H. Yang, M. P. Kapoor, N. Shirokura, M. Ohashi, S. Inagaki, J. N. Kondo and K. Domen, *Journal of Materials Chemistry*, 2005, **15**, 666-673.
79. Q. H. Yang, M. P. Kapoor, S. Inagaki, N. Shirokura, J. N. Kondo and K. Domen, *Journal of Molecular Catalysis a-Chemical*, 2005, **230**, 85-89.
80. M. P. Kapoor, W. Fujii, Y. Kasama, M. Yanagi, H. Nanbu and L. R. Juneja, *Journal of Materials Chemistry*, 2008, **18**, 4683-4691.
81. C. M. Li, H. Yang, X. Shi, R. Liu and Q. H. Yang, *Microporous and Mesoporous Materials*, 2007, **98**, 220-226.
82. D. Esquivel, E. De Canck, C. Jiménez-Sanchidrián, P. Van Der Voort and F. J. Romero-Salguero, *Journal of Materials Chemistry*, 2011, **21**, 10990-10998.
83. K. Nakajima, I. Tomita, M. Hara, S. Hayashi, K. Domen and J. N. Kondo, *Advanced Materials*, 2005, **17**, 1839-1842.
84. B. Karimi, H. M. Mirzaei and A. Mobaraki, *Catalysis Science & Technology*, 2012, **2**, 828-834.
85. A. Karam, J. C. Alonso, T. I. Gerganova, P. Ferreira, N. Bion, J. Barrault and F. Jerome, *Chemical Communications*, 2009, 7000-7002.
86. M. P. Kapoor, Y. Kasama, M. Yanagi, T. Yokoyama, S. Inagaki, T. Shimada, H. Nanbu and L. R. Juneja, *Microporous and Mesoporous Materials*, 2007, **101**, 231-239.
87. Q. H. Yang, J. Liu, J. Yang, M. P. Kapoor, S. Inagaki and C. Li, *Journal of Catalysis*, 2004, **228**, 265-272.
88. K. Nakajima, I. Tomita, M. Hara, S. Hayashi, K. Domen and J. N. Kondo, *Catal Today*, 2006, **116**, 151-156.
89. C. M. Kang, J. L. Huang, W. H. He and F. Zhang, *Journal of Organometallic Chemistry*, 2010, **695**, 120-127.
90. M. Ohashi, M. P. Kapoor and S. Inagaki, *Chemical Communications*, 2008, 841-843.

91. S. El Hankari, B. Motos-Perez, P. Hesemann, A. Bouhaouss and J. J. E. Moreau, *Journal of Materials Chemistry*, 2011, **21**, 6948-6955.
92. L. Zhang, J. Liu, J. Yang, Q. Yang and C. Li, *Microporous and Mesoporous Materials*, 2008, **109**, 172-183.
93. E. A. Prasetyanto, M. B. Ansari, B. H. Min and S. E. Park, *Catal Today*, 2010, **158**, 252-257.
94. S. Shylesh, Z. Zhou, Q. G. Meng, A. Wagener, A. Seifert, S. Ernst and W. R. Thiel, *Journal of Molecular Catalysis a-Chemical*, 2010, **332**, 65-69.
95. M. P. Kapoor, A. Bhaumik, S. Inagaki, K. Kuraoka and T. Yazawa, *Journal of Materials Chemistry*, 2002, **12**, 3078-3083.
96. J. A. Melero, J. Iglesias, J. M. Arsuaga, J. Sainz-Pardo, P. de Frutos and S. Blazquez, *Journal of Materials Chemistry*, 2007, **17**, 377-385.
97. S. Sisodiya, S. Shylesh and A. P. Singh, *Catalysis Communications*, 2011, **12**, 629-633.
98. S. Shylesh and A. P. Singh, *Microporous and Mesoporous Materials*, 2006, **94**, 127-138.
99. A. Feliczak, K. Walczak, A. Wawrzynczak and I. Nowak, *Catal Today*, 2009, **140**, 23-29.
100. S. Shylesh, C. Srilakshmi, A. P. Singh and B. G. Anderson, *Microporous and Mesoporous Materials*, 2007, **99**, 334-344.
101. A. Bhaumik, M. P. Kapoor and S. Inagaki, *Chemical Communications*, 2003, 470-471.
102. Q. H. Yang, Y. Li, L. Zhang, J. Yang, J. Liu and C. Li, *Journal of Physical Chemistry B*, 2004, **108**, 7934-7937.
103. R. Sanchez-Vazquez, C. Pirez, J. Iglesias, K. Wilson, A. F. Lee and J. A. Melero, *Chemcatcher*, 2013, **5**, 994-1001.
104. J. A. Corral, M. I. Lopez, D. Esquivel, M. Mora, C. Jimenez-Sanchidrian and F. J. Romero-Salguero, *Materials*, 2013, **6**, 1554-1565.
105. G. Dubois, R. J. P. Corriu, C. Reye, S. Brandes, F. Denat and R. Guilard, *Chemical Communications*, 1999, 2283-2284.
106. G. Dubois, C. Reye, R. J. P. Corriu, S. Brandes, F. Denat and R. Guilard, *Angewandte Chemie-International Edition*, 2001, **40**, 1087-1090.
107. Y. Yang, Y. Zhang, S. Hao and Q. Kan, *Journal of Colloid and Interface Science*, 2011, **362**, 157-163.
108. E. Y. Jeong, M. B. Ansari and S. E. Park, *Acs Catalysis*, 2011, **1**, 855-863.
109. B. K. Bahuleyan, B. R. Jermy, I. Y. Ahn, H. Suh, D. W. Park, C. S. Ha and I. Kim, *Catalysis Communications*, 2009, **11**, 252-256.
110. C. Baleizao, B. Gigante, D. Das, M. Alvaro, H. Garcia and A. Corma, *Journal of Catalysis*, 2004, **223**, 106-113.
111. F. Zhang, C. Kang, Y. Wei and H. Li, *Advanced Functional Materials*, 2011, **21**, 3189-3197.
112. J. L. Huang, F. X. Zhu, W. H. He, F. Zhang, W. Wang and H. X. Li, *Journal of the American Chemical Society*, 2010, **132**, 1492-1493.
113. V. Dufaud, F. Beauchesne and L. Bonneviot, *Angewandte Chemie-International Edition*, 2005, **44**, 3475-3477.
114. X. S. Yang, F. X. Zhu, J. L. Huang, F. Zhang and H. X. Li, *Chemistry of Materials*, 2009, **21**, 4925-4933.

115. A. Corma, D. Das, H. Garcia and A. Leyva, *Journal of Catalysis*, 2005, **229**, 322-331.
116. H. Q. Yang, G. A. Li, Z. C. Ma, J. B. Chao and Z. Q. Guo, *Journal of Catalysis*, 2010, **276**, 123-133.
117. H. Q. Yang, X. J. Han, G. A. Li, Z. C. Ma and Y. J. Hao, *Journal of Physical Chemistry C*, 2010, **114**, 22221-22229.
118. G. Li, H. Q. Yang, W. Li and G. L. Zhang, *Green Chemistry*, 2011, **13**, 2939-2947.
119. H. Q. Yang, Z. C. Ma, Y. Qing, G. Y. Xie, J. Gao, L. Zhang, J. H. Gao and L. Du, *Applied Catalysis a-General*, 2010, **382**, 312-321.
120. T. M. Zhang, C. G. Gao, H. Q. Yang and Y. X. Zhao, *J Porous Mat*, 2010, **17**, 643-649.
121. T. Kamegawa, M. Saito, T. Watanabe, K. Uchihara, M. Kondo, M. Matsuoka and M. Anpo, *Journal of Materials Chemistry*, 2011, **21**, 12228-12231.
122. Y. Yang, Y. Zhang, S. J. Hao and Q. B. Kan, *J Colloid Interf Sci*, 2011, **362**, 157-163.
123. E. Y. Jeong, A. Burri, S. Y. Lee and S. E. Park, *Journal of Materials Chemistry*, 2010, **20**, 10869-10875.
124. A. C. Coelho, S. S. Balula, S. M. Bruno, J. C. Alonso, N. Bion, P. Ferreira, M. Pillinger, A. A. Valente, J. Rocha and I. S. Goncalves, *Advanced Synthesis & Catalysis*, 2010, **352**, 1759-1769.
125. A. C. Coelho, S. S. Balula, M. M. Antunes, T. I. Gerganova, N. Bion, P. Ferreira, M. Pillinger, A. A. Valente, J. Rocha and I. S. Goncalves, *Journal of Molecular Catalysis a-Chemical*, 2010, **332**, 13-18.
126. A. Kuschel, M. Luka, M. Wessig, M. Drescher, M. Fonin, G. Kiliani and S. Polarz, *Advanced Functional Materials*, 2010, **20**, 1133-1143.
127. J. Alauzun, A. Mehdi, C. Reye and R. J. P. Corriu, *Journal of the American Chemical Society*, 2006, **128**, 8718-8719.
128. S. Shylesh, A. Wagener, A. Seifert, S. Ernst and W. R. Thiel, *Angewandte Chemie-International Edition*, 2010, **49**, 184-187.
129. M. Sasidharan, S. Fujita, M. Ohashi, Y. Goto, K. Nakashima and S. Inagaki, *Chemical Communications*, 2011, **47**, 10422-10424.
130. M. Sasidharan and A. Bhaumik, *Acs Applied Materials & Interfaces*, 2013, **5**, 2618-2625.
131. A. Kuschel, M. Drescher, T. Kuschel and S. Polarz, *Chemistry of Materials*, 2010, **22**, 1472-1482.
132. F.-X. Zhu, W. Wang and H.-X. Li, *Journal of the American Chemical Society*, 2011, **133**, 11632-11640.
133. C. Baleizao, B. Gigante, D. Das, M. Alvaro, H. Garcia and A. Corma, *Chemical Communications*, 2003, 1860-1861.
134. M. Benitez, G. Bringmann, M. Dreyer, H. Garcia, H. Ihmels, M. Waidelich and K. Wissel, *Journal of Organic Chemistry*, 2005, **70**, 2315-2321.
135. D. M. Jiang, J. S. Gao, J. Li, Q. H. Yang and C. Li, *Microporous and Mesoporous Materials*, 2008, **113**, 385-392.
136. D. M. Jiang, Q. H. Yang, H. Wang, G. R. Zhu, J. Yang and C. Li, *Journal of Catalysis*, 2006, **239**, 65-73.
137. R. A. Garcia, R. van Grieken, J. Iglesias, V. Morales and D. Gordillo, *Chemistry of Materials*, 2008, **20**, 2964-2971.

138. R. A. Garcia, R. van Grieken, J. Iglesias, V. Morales and N. Villajos, *Journal of Catalysis*, 2010, **274**, 221-227.
139. L. Zhang, J. Liu, J. Yang, Q. Yang and C. Li, *Chemistry-an Asian Journal*, 2008, **3**, 1842-1849.
140. P. Y. Wang, J. Yang, J. Liu, L. Zhang and Q. H. Yang, *Microporous and Mesoporous Materials*, 2009, **117**, 91-97.
141. X. Liu, P. Y. Wang, Y. Yang, P. Wang and Q. H. Yang, *Chemistry-an Asian Journal*, 2010, **5**, 1232-1239.
142. X. A. Liu, P. Y. Wang, L. Zhang, J. Yang, C. Li and Q. H. Yang, *Chemistry-a European Journal*, 2010, **16**, 12727-12735.
143. V. Morales, J. A. Villajos and R. A. Garcia, *J Mater Sci*, 2013, **48**, 5990-6000.
144. P. Wang, X. Liu, J. Yang, Y. Yang, L. Zhang, Q. Yang and C. Li, *Journal of Materials Chemistry*, 2009, **19**, 8009-8014.
145. J. S. Gao, J. Liu, J. T. Tang, D. M. Jiang, B. Li and Q. H. Yang, *Chemistry-a European Journal*, 2010, **16**, 7852-7858.
146. J. S. Gao, J. Liu, S. Y. Bai, P. Y. Wang, H. Zhong, Q. H. Yang and C. Li, *Journal of Materials Chemistry*, 2009, **19**, 8580-8588.
147. J. Y. Shi, C. A. Wang, Z. J. Li, Q. Wang, Y. Zhang and W. Wang, *Chemistry-a European Journal*, 2011, **17**, 6206-6213.
148. A. Kuschel and S. Polarz, *Journal of the American Chemical Society*, 2010, **132**, 6558-6565.
149. P. Y. Wang, X. Liu, J. Yang, Y. Yang, L. Zhang, Q. H. Yang and C. Li, *Journal of Materials Chemistry*, 2009, **19**, 8009-8014.
150. S. Z. Qiao, C. Z. Yu, W. Xing, Q. H. Hu, H. Djojoputro and G. Q. Lu, *Chemistry of Materials*, 2005, **17**, 6172-6176.
151. M. Park, S. S. Park, M. Selvaraj, I. Kim and C. S. Ha, *Journal of Porous Materials*, 2011, **18**, 217-223.
152. N. Li, J. G. Wang, H. J. Zhou, P. C. Sun and T. H. Chen, *Chemistry of Materials*, 2011, **23**, 4241-4249.
153. N. Hao, H. T. Wang, P. A. Webley and D. Y. Zhao, *Microporous and Mesoporous Materials*, 2010, **132**, 543-551.
154. L. Zhu, X. Liu, T. Chen, Z. Xu, W. Yan and H. Zhang, *Appl Surf Sci*, 2012, **258**, 7126-7134.
155. X. Q. Wang, D. N. Lu, R. Austin, A. Agarwal, L. J. Mueller, Z. Liu, J. Z. Wu and P. Y. Feng, *Langmuir*, 2007, **23**, 5735-5739.
156. J. H. Shin, S. S. Park, M. Selvaraj and C. S. Ha, *Journal of Porous Materials*, 2012, **19**, 29-35.
157. C. X. Lin, S. Z. Qiao, C. Z. Yu, S. Ismadiji and G. Q. Lu, *Microporous and Mesoporous Materials*, 2009, **117**, 213-219.
158. R. Vathyam, E. Wondimu, S. Das, C. Zhang, S. Hayes, Z. M. Tao and T. Asefa, *Journal of Physical Chemistry C*, 2011, **115**, 13135-13150.
159. S. Parambadath, V. K. Rana, S. Moorthy, S. W. Chu, S. K. Park, D. Lee, G. Sung and C. S. Ha, *J Solid State Chem*, 2011, **184**, 1208-1215.
160. S. Parambadath, V. K. Rana, D. Y. Zhao and C. S. Ha, *Microporous and Mesoporous Materials*, 2011, **141**, 94-101.
161. M. S. Moorthy, S. S. Park, D. Fuping, S. H. Hong, M. Selvaraj and C. S. Ha, *Journal of Materials Chemistry*, 2012, **22**, 9100-9108.

162. S. Z. Qiao, H. Djojoputro, Q. H. Hu and G. Q. Lu, *Progress in Solid State Chemistry*, 2006, **34**, 249-256.
163. M. Park, S. S. Park, M. Selvaraj, D. Y. Zhao and C. S. Ha, *Microporous and Mesoporous Materials*, 2009, **124**, 76-83.
164. M. Shakeri and K. Kawakami, *Catalysis Communications*, 2008, **10**, 165-168.
165. E. Serra, E. Diez, I. Diaz and R. M. Blanco, *Microporous and Mesoporous Materials*, 2010, **132**, 487-493.
166. Z. Zhou, R. N. K. Taylor, S. Kullmann, H. X. Bao and M. Hartmann, *Adv Mater*, 2011, **23**, 2627-2632.
167. W. Na, Q. Wei, J. N. Lan, Z. R. Nie, H. Sun and Q. Y. Li, *Microporous and Mesoporous Materials*, 2010, **134**, 72-78.
168. S. Hudson, J. Cooney, B. K. Hodnett and E. Magner, *Chemistry of Materials*, 2007, **19**, 2049-2055.
169. N. Lin, L. Gao, Z. Chen and J. H. Zhu, *New Journal of Chemistry*, 2011, **35**, 1867-1875.
170. M. M. Wan, L. Gao, Z. Chen, Y. K. Wang, Y. Wang and J. H. Zhu, *Microporous and Mesoporous Materials*, 2012, **155**, 24-33.



### **3 *The ethenylene-bridged Periodic Mesoporous Organosilica***

This chapter describes the synthesis and characterisation of the ethenylene-bridged Periodic Mesoporous Organosilica as this material will be mainly used throughout this dissertation as starting material. The presence of the ethene bridge in this PMO is of key importance due to the chemical modification possibilities of the C=C bond. This can fine-tune the material for a very specific application.

However, prior to the preparation of the solid itself, the precursor *trans* 1,2-bis(triethoxysilyl)ethenylene must be synthesized by using a cross-metathesis reaction and a Ruthenium catalyst.

### 3.1 Introduction

The synthesis of a PMO with ethene bridges incorporated in the entire material requires the use of an appropriate bis-silane. The precursor 1,2-bis(triethoxysilyl)ethenylene is commercially available and it cannot be purchased in its pure form. The commercial product consists of a mixture with 80% *trans* and 20% *cis* isomer. A previous study in our research group showed that the use of a 100% *trans* precursor significantly improves the structural properties and hydrothermal stability of the resulting material.<sup>1,2</sup> The use of the mixture on the other hand leads to a less stable PMO. It was noticed in the X-ray diffraction patterns that the ordering of the *trans* ethenylene-bridged PMO was superior to the ordering of the materials prepared with the pure *cis* precursor or a mixture of *cis* and *trans*. Moreover the nitrogen sorption experiments showed that an increase of *cis* isomer in the material results in a decrease of the pore size and a broadening of the pore size distribution. Investigation of the hydrothermal stability illustrated that materials containing more *cis* ethene bridges are less stable due to the poor stacking of the ethene bridges and lower condensation degree inside the pores walls.

Thus, to obtain a stable ethenylene-bridged PMO material, the precursor *trans* 1,2-bis(triethoxysilyl)ethenylene must be synthesized first.

### 3.2 Synthesis of *trans* 1,2-bis(triethoxysilyl)ethenylene

The procedure is based upon the recipe of Marciniak *et al.* that describes the cross-metathesis reaction of vinyltriethoxysilane (VTES) with the addition of a ruthenium catalyst, (PPh)<sub>3</sub>RuCl<sub>2</sub>.<sup>3</sup> A mixture between the *trans* and *cis* isomer is obtained. Changing the [Ru]-catalyst into the Grubbs' first generation catalyst but still using a cross-metathesis reaction, results in only the *trans* isomer.<sup>1, 4</sup> The overall reaction is presented in Figure 3.1.

After the olefin metathesis reaction and subsequent purification steps, a clear liquid *E*-1,2-bis(triethoxysilyl)ethenylene is obtained. The product is characterised with NMR measurements. <sup>1</sup>H NMR (CDCl<sub>3</sub>): δ = 6.66 (s, 2 H), δ = 3.84 (q, 12 H), δ = 1.23 ppm (t, 18 H).



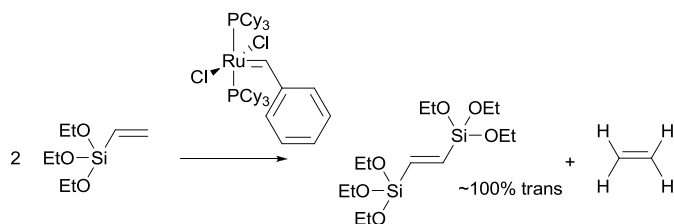


**Figure 3.1:** Cross-metathesis reaction of VTES catalyzed by the Grubbs' first generation catalyst:  $\sim 100\%$  *trans* 1,2-bis(triethoxysilyl)ethenylene is obtained with ethene gas as by-product. Cy = cyclohexyl.

### 3.3 Synthesis of the ethenylene-bridged PMO material

The precursor *trans* 1,2-bis(triethoxysilyl)ethenylene is subsequently employed in the synthesis of *trans* ethenylene-bridged PMO materials. The recipe uses the Pluronic<sup>®</sup> P123 as surfactant, HCl and 1-butanol in aqueous environment. The synthetic procedure is based upon an ultra-fast recipe described by our research group which uses a short stirring and aging step to prepare the solids.<sup>1,4</sup>

The template P123 cannot be removed by the procedure normally used for ordered templated silicas, *i.e.*, a calcination step. This method would lead to the decomposition of the surfactant but also the destruction of the organic bridges of the PMO. Thus, a softer method should be used. Normally, the template is removed by an extraction with acidified ethanol. Nevertheless, herein a Soxhlet extraction with acetone is performed to remove the surfactant. It is reported that this method exhibits a higher extraction efficiency for P123 and the procedure is significantly shorter.<sup>4</sup>

A representation of the synthesis method is provided in Figure 3.2. A typical nitrogen adsorption-desorption isotherm and X-ray diffraction pattern for this type of material can be found in Figure 3.3. A typical synthesis normally yields ethenylene-bridged PMO materials with specific surface areas in the range of 700-1100 m<sup>2</sup> g<sup>-1</sup>, pore volumes of 0.7-1.0 mL g<sup>-1</sup>, and pore diameters between 5 and 7 nm. The isotherm of type IV possesses a type H1 hysteresis indicative for a mesoporous material with cylindrical pores. A steep slope of the capillary condensation step is observed, which stands for a narrow pore size distribution and thus uniform pores. The XRD pattern clearly reveals three signals. A sharp signal originating from the (100) reflection and

two second-order reflections of (110) and (200) are clearly visible. This indicates a well-ordered PMO material with a 2D-hexagonal space group ( $P6mm$ ).

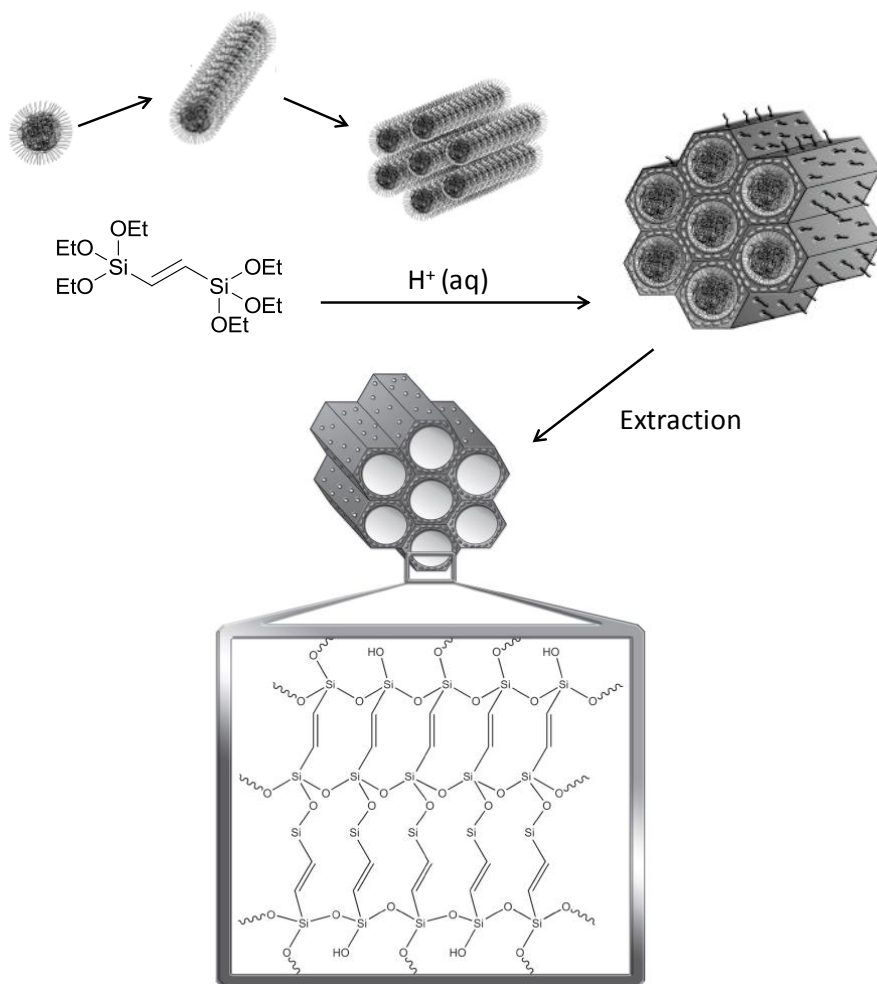


**Figure 3.2:** Schematic representation of the synthesis of a *trans* ethenylene-bridged PMO material with P123 as surfactant, HCl and 1-butanol. An extraction removes the surfactant and this results in a mesoporous organosilica material.

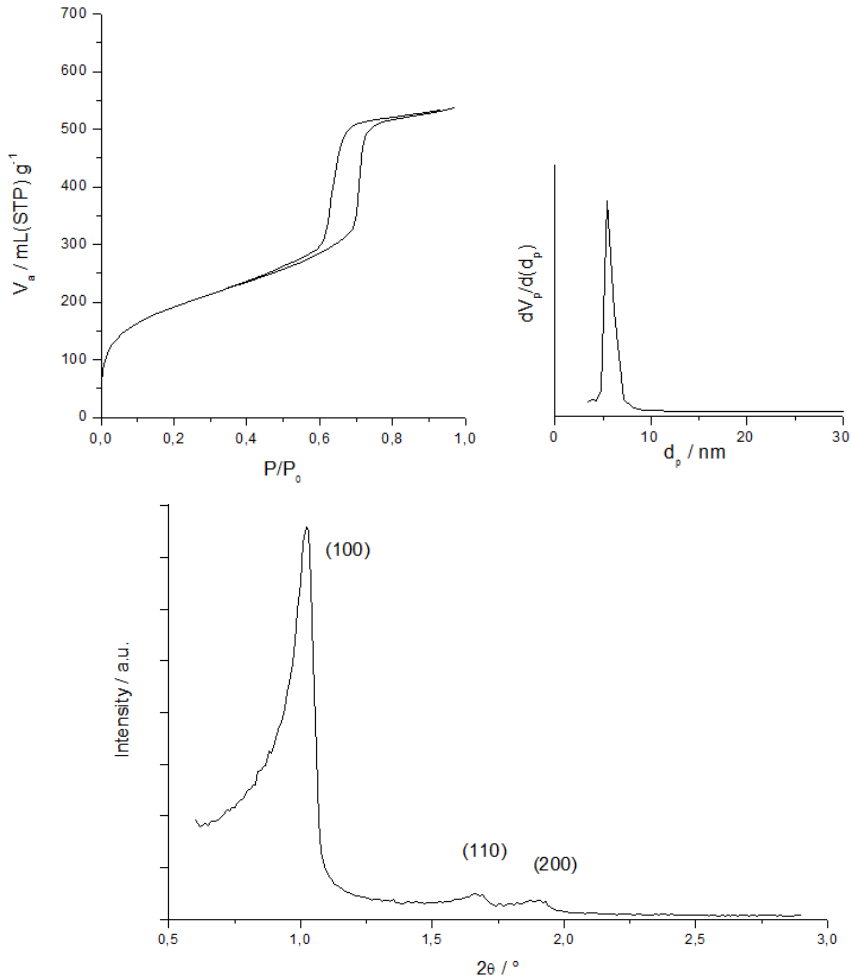


**Figure 3.3: Typical nitrogen sorption isotherm, pore size distribution (calculated from the desorption branch) and X-ray diffraction pattern of a *trans* ethenylene-bridged PMO material. ( $S_{BET} = 704 \text{ m}^2 \text{ g}^{-1}$ ,  $V_p = 0.83 \text{ mL g}^{-1}$  and  $d_p = 5.47 \text{ nm}$ )**

The ethene bond of this PMO material can be modified by chemical organic reactions so that more appealing functionalities can be obtained. This makes the PMO more interesting for applications such as adsorption and catalysis.

### 3.4 Conclusion

The synthesis of a pure *trans* precursor, 1,2-bis(triethoxysilyl)ethenylene, is successfully performed. This silane is subsequently used for the synthesis of a stable ethenylene-bridged PMO material with high specific surface area, large pore volume and pore diameter. This well-ordered material exhibits cylindrical pores and a 2D-hexagonal ordering.

The procedure to synthesize the precursor and the ethenylene-bridged PMO material both described in the chapter will be used throughout this dissertation, unless stated otherwise.

### 3.5 Experimental section

**Chemicals.** Vinyltriethoxysilane (VTES; 97%) was purchased from ABCR. The pluronic<sup>®</sup> PEO<sub>20</sub>PPO<sub>70</sub>PEO<sub>20</sub> (P123), Grubbs' first generation catalyst, hydrochloric acid (37%; p.a.), acetone (>99,5%) and 1-butanol were acquired from Sigma-Aldrich.

**Synthesis of *trans* 1,2-bis(triethoxysilyl)ethenylene.** The 100% *trans* 1,2-bis(triethoxysilyl)ethenylene was synthesized as follows:<sup>1,5</sup> 0.0535 g of Grubbs' first generation catalyst (PCy<sub>3</sub>)<sub>2</sub>Cl<sub>2</sub>Ru=CH-Ph was added to a Schlenk flask under argon atmosphere which contains 42.95 mL of vinyltriethoxysilane. The mixture was stirred for 1 h at room temperature and refluxed for 3 h. Subsequently, the mixture was distilled to remove the remaining VTES. At the end, a vacuum distillation separated the Grubbs' catalyst from the *trans* 1,2-bis(triethoxysilyl)ethenylene.

**Synthesis of *trans* ethenylene-bridged PMO material.** The *trans* ethenylene-bridged PMO material was synthesized using the recipe published by our group.<sup>6</sup> An amount of 1 g of P123 was dissolved in 47.8 mL of water, 3.42 mL of concentrated hydrochloric acid, and 2.45 mL of 1-butanol. The mixture was vigorously stirred for 1.5 h. Then 1.86 mL of homemade 100% *trans* 1,2-bis(triethoxysilyl)ethenylene<sup>1</sup> was added, and the temperature was raised to 45°C. A white precipitation was formed. After 4 h of stirring, the mixture was heated to 90°C under static conditions for 16 h. After cooling down of the mixture, the solids were filtered and washed with water and

acetone. To remove the template, a Soxhlet extraction was performed with acetone for 5 h.<sup>4</sup> Afterward, the PMO was dried at 120°C under vacuum.

**Characterisation.** The nitrogen sorption isotherms were recorded on Belsorp Mini II equipment at -196°C. The samples were pretreated at 120°C while degassing. X-ray diffraction was performed with an ARL X'tra X-ray diffractometer of Thermo Scientific equipped with a Cu K $\alpha$ 1 tube and a Peltier cooled lithium drifted silicon solid stage detector.

### 3.6 References

1. C. Vercaemst, M. Ide, P. V. Wiper, J. T. A. Jones, Y. Z. Khimyak, F. Verpoort and P. Van Der Voort, *Chemistry of Materials*, 2009, **21**, 5792-5800.
2. C. Vercaemst, Ghent University, Ph.D. thesis, 2009.
3. B. Marciniec, H. Maciejewski, J. Gulinski and L. Rzejak, *Journal of Organometallic Chemistry*, 1989, **362**, 273-279.
4. C. Vercaemst, M. Ide, B. Allaert, N. Ledoux, F. Verpoort and P. Van Der Voort, *Chemical Communications*, 2007, 2261-2263.
5. P. Schwab, R. H. Grubbs and J. W. Ziller, *Journal of the American Chemical Society*, 1996, **118**, 100-110.
6. C. Vercaemst, M. Ide, H. Friedrich, K. P. de Jong, F. Verpoort and P. Van Der Voort, *Journal of Materials Chemistry*, 2009, **19**, 8839-8845.



## **4 The development of Periodic Mesoporous Organosilicas as mercury(II) adsorbents**

This chapter of the dissertation describes the development of a new mesoporous adsorbent for the removal of mercury(II) ions which is stable and can be reused. This new adsorbent is based upon a pure *trans* ethenylene-bridged Periodic Mesoporous Organosilica which is subsequently modified *via* two synthetic steps to obtain a suitable adsorbent.

The outcome is a new thiol-containing ethenylene-bridged PMO material which combines the adsorption affinity of the thiol group towards the heavy metal mercury with the well-known stability of ethenylene-bridged PMO materials. During the adsorption process, this material not only retains its mesoporous structure and ordering, it also completely preserves the amount of organic functionalities, allowing recycling and reuse of the adsorbent. Thus the PMO based adsorbent possesses a high structural and chemical stability. Next to the adsorption kinetics and isotherm, special emphasis is placed upon the long-term stability and recyclability in acidic medium of this PMO adsorbent.

The thiol functionalised PMO material is able to reduce the Hg(II) amount in aqueous solutions below  $0.5 \mu\text{g L}^{-1}$ , and the adsorbent exhibits a maximal adsorption capacity of  $64 \text{ mg g}^{-1}$  which means an apparent 1:1 ratio mercury(II) ion to thiol.

Adsorption experiments in this chapter were partially performed by dr. Jeriffa De Clercq at Hogeschool Gent.

The results presented in this chapter are published as  
Els De Canck, Linsey Lapeire, Jeriffa De Clercq, Francis Verpoort and Pascal Van Der Voort, *Langmuir*, **2010**, 26, 12, 10076-10083.

## 4.1 Introduction

The development of a well-performing adsorbent for mercury requires the presence of the right functionalities. The *Hard and Soft Acids and Bases* (HSAB) theory, first introduced by R.G. Pearson, states that the soft acid mercury exhibits a high affinity for soft bases such as the thiol functionality.<sup>1</sup> Furthermore, an adsorbent should be stable during the adsorption process but also during the regeneration of the adsorbent and the recuperation of the mercury. The required stability can be found in Periodic Mesoporous Organosilicas as it is established that PMOs possess a higher hydrothermal stability than ordered templated silica materials.<sup>2</sup>

It is attempted to combine the affinity of mercury for thiols with the known hydrothermal stability of PMO materials. This is accomplished by the development of a new PMO based adsorbent with the *trans* ethenylene-bridged PMO as starting material. By employing several post-modification steps, a thiol containing adsorbent is obtained.

This chapter describes the modification of the ethenylene-bridged PMO material and the characterisation of the adsorbent. Next, its mercury(II) adsorption behaviour is tested and the chemical and structural stability of the material is examined. However first, the preparation of several reference materials is described which will be used as benchmark materials during the mercury(II) adsorption experiments.

## 4.2 Synthesis of benchmark adsorbents: thiol-containing silica based materials

Several thiol-containing silica materials are synthesized to compare their mercury(II) adsorption possibilities with a newly developed thiol-containing Periodic Mesoporous Organosilica material, *i.e.*, a standard SBA-15 material grafted *via* two different methods with (3-mercaptopropyl)triethoxysilane or MPTES and a SBA-15-like material prepared by the co-condensation of (3-mercaptopropyl)trimethoxysilane or MPTMS and TEOS.



## 4.2.1 The grafting of MPTES on SBA-15 materials

### 4.2.1.1 The theory behind grafting

The grafting or anchoring of an organosilane onto the surface of a silica material (silica gel or MCM and SBA type materials) is elaborately described in literature by use of reagents such as alkoxy silanes, chlorosilanes, disilazanes,...<sup>3-7</sup> When using organoalkoxy silanes, *e.g.*, with an amine or thiol functionality, the grafting procedure sometimes consist of refluxing the support in toluene in the presence of the chosen alkoxy silane for a certain period of time.<sup>8-12</sup> Some of the reports even use dry toluene<sup>13, 14</sup>, as the presence of water can induce the selfcondensation of the hydrolyzed silanes<sup>15</sup> as shown in Figure 4.1.b. Instead of forming a monolayer of silanes on the silica surface, a three-dimensional network can be created due to uncontrollable polymerization of silanes. Eventually, multiple thiol functionalities will be present per initial silanol group.

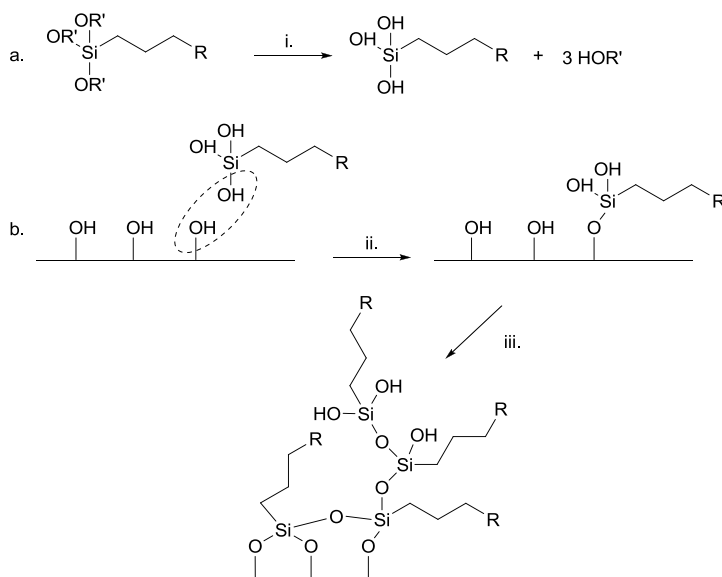


**Figure 4.1:** a. Hydrolysis of a general organoalkoxy silane; b.i. Anchoring of the hydrolyzed silane on a silica surface and b.iii. Selfcondensation of the silane on the silica surface. R and R' represent an organic functionality and methyl or ethyl group, respectively. Figure adapted from reference 15.

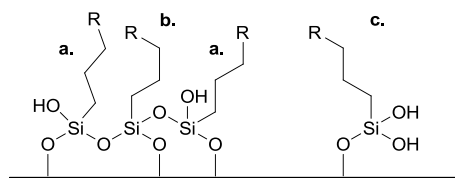


**Figure 4.2: Existing species on the silica surface after a selfcondensation process with a. End-standing; b. Cross-linked and c. Isolated organic functionalities. Figure adapted from reference 16.**

This selfcondensation process thus creates organic functionalities that are cross-linked, end-standing or isolated (Figure 4.2). This heterogeneity of grafted species was observed in  $^{13}\text{C}$  and  $^{29}\text{Si}$  solid state NMR experiments performed by Feng *et al.*<sup>16</sup>

To avoid this uncontrollable process, one must operate in a controlled environment with dry solvents, *e.g.*, dry toluene, with just the right amount of water available on the surface to induce siloxane hydrolysis.<sup>16</sup> However, by choosing a different grafting procedure, yet less common, the reaction time can be drastically reduced and at the same time, the selfcondensation process can be avoided. The addition of an amine as activator in the grafting process is an option which is not frequently used in literature although the method possesses some important advantages.<sup>17</sup> The silylation rate increases significantly and the process occurs more under control. The selfcondensation reaction is limited by using room temperature or lower temperatures<sup>18</sup> than the generally accepted reflux processes in toluene or another solvent. Several amines can be used as activator, such as ammonia, ethylamine, diethylamine, triethylamine and pyridine. First, the amine is added to the dry silica material with an anhydrous solvent, commonly toluene. This step is also known as the *preactivation step*. The weaker bases will physically interact *via* hydrogen bonding with the silanols, while the stronger bases will induce a proton transfer and are chemically adsorbed to the silica. This interaction, physically or chemically, will assist during the silylation process. However, before addition of the silane, the large excess of amine must be removed from the reaction mixture without removing the necessary adsorbed amines. This is best achieved with the activator triethylamine.<sup>19</sup> Figure 4.3 presents an overview of the anchoring procedure with triethylamine as example.

From the figure, it is clear that the tertiary amine will interact with the silanol group *via* hydrogen bonding, which significantly weakens the oxygen-hydrogen bond of the silanol, followed by a nucleophilic substitution reaction which eventually results in a successful anchoring of the organosilane. Nonetheless, if the grafting reaction with amine activation does not occur in a water free environment, caused by the use of wet solvent or moist silica support, the selfcondensation process will be drastically increased by the amines. This can lead to a three dimensional siloxane network prior to any grafting on the surface of the silica material.<sup>18</sup>

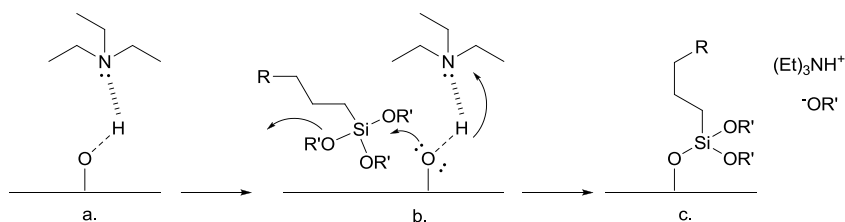


**Figure 4.3: Grafting procedure of an organoalkoxysilane in anhydrous medium using the amine preactivation method: a. Activation with triethylamine; b. Nucleophilic attack of the silanol and c. Successful anchoring of the silane. Adapted from reference 17.**

By using an alkoxyorganosilane such as (3-mercaptopropyl)trimethoxysilane or (3-mercaptopropyl)triethoxysilane, a thiol functionality can be introduced on a silica material and thus a mercury adsorbent can be created. It is interesting to know if the used grafting procedure has any influence on the mercury(II) adsorption and most important, the stability of the adsorbent. Therefore, several grafting procedures are performed on SBA-15 materials to investigate the anchoring procedure and in the final stage, the influence on Hg(II) adsorption.

#### 4.2.1.2 The anchoring of MPTES

The SBA-15 material is first synthesized based upon a procedure described by Zhao *et al.*<sup>20, 21</sup> Next, a grafting procedure is used, varying the activator, reaction time but also the temperature during the grafting. An overview of the materials is presented in Table 4.1, together with the specific surface area, pore volume, pore diameter. The resulting silica materials are denoted as SBA-*x-y-z-T* where *x* represents the activator with an indication of the concentration, *y* the amount of water in ppm

units present in HCl,  $z$  the reaction time in hours and  $T$  the temperature in °C. For the syntheses with  $\text{NEt}_3$ ,  $z$  and  $T$  concern the second step of the grafting, not the preactivation. The table also gives an indication whether full coverage of the surface is accomplished by the grafting procedure, *i.e.*, if the signal of the silanol in infrared measurements (DRIFT) is still present or not.

As can be seen from Table 4.1, in order to completely remove the silanol signal and thus obtain a full grafting, the reaction temperature of the silane anchoring step should be raised to 65°C for a short period of time, *i.e.*, 2 hours of reaction time, when using triethylamine as activator. Furthermore, it is also clear that the addition of a larger excess of MPTES results in a full coverage of the silanol groups. Hydrochloric acid can also be used, however a significant decrease in specific surface area is observed after grafting which can only be explained by the selfcondensation of the silane on the surface of the material.

Two materials are selected from the synthesized materials which are described in Table 4.1 for the mercury(II) adsorption experiments. First, a thiol containing SBA-15 material that is prepared *via* the optimized amine activated process, *i.e.*, SBA- $\text{NEt}_3(10x)$ -/-2h-65°C is chosen. This material possesses a surface grafted with MPTES and without any remaining silanols but also without any selfcondensation. Secondly, a material is selected which clearly shows selfcondensation (SBA-5%HCl-90-96h-50°C).

**Table 4.1: Overview of thiol functionalised SBA-15 materials with a semi-quantitative interpretation of the silanol vibrations.**

	$S_{\text{BET}}^{\text{a}}$	$V_{\text{p}}^{\text{b}}$	$d_{\text{p}}^{\text{c}}$	$\nu$ (Si-OH)
	$\text{m}^2 \text{g}^{-1}$	$\text{mL g}^{-1}$	nm	
SBA-15	865	0.84	5.47	Present
SBA-NEt <sub>3</sub> (5x)-/-2h-RT <sup>d</sup>	685	0.75	4.82	Present
SBA-NEt <sub>3</sub> (5x)-/-6h-RT <sup>d</sup>	609	0.70	4.82	Present
SBA-NEt <sub>3</sub> (5x)-/-6h-50°C <sup>d,e</sup>	637	0.69	4.82	Present
<b>SBA-NEt<sub>3</sub>(10x)-/-2h-65°C<sup>d,e,f</sup></b>	587	0.61	4.82	Absent
SBA-5%HCl-90-2h-RT	788	0.75	4.82	Present
SBA-5%HCl-90-6h-RT	785	0.76	4.82	Present
SBA-5%HCl-90-6h-50°C	480	0.53	4.82	Present
<b>SBA-5%HCl-90-96h-50°C</b>	286	0.29	4.25	Absent

<sup>a</sup> The specific surface area calculated *via* the BET equation. <sup>b</sup> Total pore volume at  $P/P_0 = 0.98$ . <sup>c</sup> Pore diameter calculated from the desorption isotherm with the BJH method. <sup>d</sup> An excess of triethylamine and MP TES is used in the synthesis (5:1; ratio NEt<sub>3</sub> or MP TES to silanol). <sup>e</sup> The temperature is raised for the second step of the grafting procedure. The preactivation still occurs at room temperature. <sup>f</sup> In the synthesis, a larger excess of triethylamine and silane is used, namely a ratio of 10:1 for MP TES: silanol, with the same molar amount of NEt<sub>3</sub> as MP TES.

### **4.2.2 Preparation of SBA-15 type materials via an one-pot-synthesis**

SBA-15 type materials that contain thiol functionalities can also be prepared *via* an one-pot-synthesis instead of the grafting procedure. This so-called co-condensation process is widely used for a variety of organosilanes by several authors and makes use of the organosilane in combination with a silica source such as TEOS or TMOS. A recipe based on Aguado *et al.*<sup>22</sup> and Mercier *et al.*<sup>23</sup> is chosen. This uses the Pluronic P123 as surfactant in an acidic aqueous environment with TEOS as silica source next to MPTMS. First TEOS is dissolved in the mixture of P123, water and HCl and stirred for a certain amount of time during the *prehydrolysis*. Afterwards, MPTMS is added. Different ratios of TEOS to MPTMS are selected and the materials are denoted as co-cond-*x* where *x* represents the molar percentage of MPTMS. Relatively low amounts of MPTMS (10-20%) are incorporated to obtain a good mesostructure (*vide infra*).

Table 4.2 presents a summary of the materials prepared *via* this method and their physical properties. As can be seen from the table, materials with a high amount of organic functionality (20%) exhibit a lower specific surface area in comparison with materials with a lower amount (10%). This is also generally observed in literature.<sup>22, 24, 25</sup> When a high amount of organosilane is co-condensed with TEOS or TMOS, the mesostructure of the materials is (partially) lost. Furthermore, the incorporation of too much mercaptopropyl functionalities does not necessarily lead to higher adsorption capacities as the high concentration of thiols results in many unreachable functions.<sup>22</sup>

One material co-cond-10, prepared by the described co-condensation process, is selected for the mercury(II) adsorption experiments.

**Table 4.2: Overview of materials prepared *via* the co-condensation procedure, together with the physical properties determined *via* nitrogen sorption measurements.**

	$S_{\text{BET}}^{\text{a}}$	$V_{\text{p}}^{\text{b}}$	$d_{\text{p}}^{\text{c}}$
	$\text{m}^2 \text{g}^{-1}$	$\text{mL g}^{-1}$	nm
co-cond-20	502	0.38	3.32
co-cond-15	684	0.66	3.75
co-cond-10	704	0.78	4.82

<sup>a</sup> The specific surface area calculated *via* the BET equation. <sup>b</sup> Total pore volume at  $P/P_0 = 0.98$ . <sup>c</sup> Pore diameter calculated from the desorption isotherm with the BJH method.

### 4.2.3 Determination of the reachability of the thiol groups

Next to the structural characterisation of the synthesized materials, one parameter of major importance is not mentioned yet: the amount of reachable thiol functionalities. It is essential to know this parameter as only these thiol functionalities will participate in the mercury(II) adsorption process. Therefore a procedure is established based upon the Volgard titration.<sup>26, 27</sup>

In general, the procedure consists of two steps: (1) a reaction between the reachable thiol functionalities and a large excess of silver(I) ions will occur, followed by (2) the titration of the silver(I) ions remaining in solution with potassium thiocyanate as reagent in the presence of  $\text{Fe}(\text{NH}_4)(\text{SO}_4)_2 \cdot 12\text{H}_2\text{O}$ . A silver thiocyanate precipitation is formed during the reaction. The latter will react with the iron compound which is a very sensitive indicator that forms red iron cyanate complexes in a slightly acidic environment.

The amount of reachable thiol functionalities is calculated from the titration results and an overview of the values for the materials described above, is presented in Table 4.3. The materials prepared with HCl as activator and at higher temperature exhibit a remarkable high amount of thiol functionalities, which can only be explained by the selfcondensation of the silane on the surface of the material.<sup>16</sup>

**Table 4.3: Amount of reachable thiol functionalities expressed in mmol per g and groups per nm<sup>2</sup> for the materials prepared via the grafting or co-condensation processes.**

	mmol SH g <sup>-1</sup>	# SH nm <sup>-2</sup>
SBA-15	0.018	-
SBA-NEt <sub>3</sub> (5x)-/-2h-RT	0.39	0.27
SBA-NEt <sub>3</sub> (5x)-/-6h-RT	0.32	0.23
SBA-NEt <sub>3</sub> (5x)-/-6h-50°C	0.58	0.40
SBA-NEt <sub>3</sub> (10x)-/-2h-65°C	1.60	1.10
SBA-5%HCl-90-2h-RT	0.54	0.37
SBA-5%HCl-90-6h-RT	0.58	0.40
SBA-5%HCl-90-6h-50°C	5.10	3.57
SBA-5%HCl-90-96h-50°C	10.00	7.02
co-cond-20	2.30	1.62
co-cond-15	1.40	0.99
co-cond-10	1.10	0.75

#### ***4.2.4 Summary of properties concerning the selected thiol-containing adsorbents***

Table 4.4 summarizes the selected thiol containing silica adsorbents that are tested for mercury(II) adsorption. Furthermore an overview of their structural characteristics is presented in the table, together with the thiol content for clarity. The difference between the three materials is unmistakably visible. This is also observable from the DRIFT measurements presented in Figure 4.4. A broadening of the signals originating from the propyl moiety is observed when selfcondensation occurs (spectrum C) whereas sharp peaks are noticed in spectrum B of the material with only one monolayer of grafted silane.



**Table 4.4: Summary of the selected adsorbents with structural and chemical characteristics.**

	$S_{\text{BET}}^{\text{a}}$	$V_{\text{p}}^{\text{b}}$	$d_{\text{p}}^{\text{c}}$	mmol SH $\text{g}^{-1}$ $^{\text{d}}$	# SH $\text{nm}^{-2}$
	$\text{m}^2 \text{g}^{-1}$	$\text{mL g}^{-1}$	nm		
SBA-NEt <sub>3</sub> (10x)-/-2h-65°C	587	0.61	4.82	1.60	1.10
SBA-5%HCl-90-96h-50°C	286	0.29	4.25	10.00	7.02
co-cond-10	704	0.78	4.82	1.10	0.75

<sup>a</sup> The specific surface area calculated *via* the BET equation. <sup>b</sup> Total pore volume at  $P/P_0 = 0.98$ . <sup>c</sup> Pore diameter calculated from the desorption isotherm with the BJH method. <sup>d</sup> Determined *via* thiol titration.

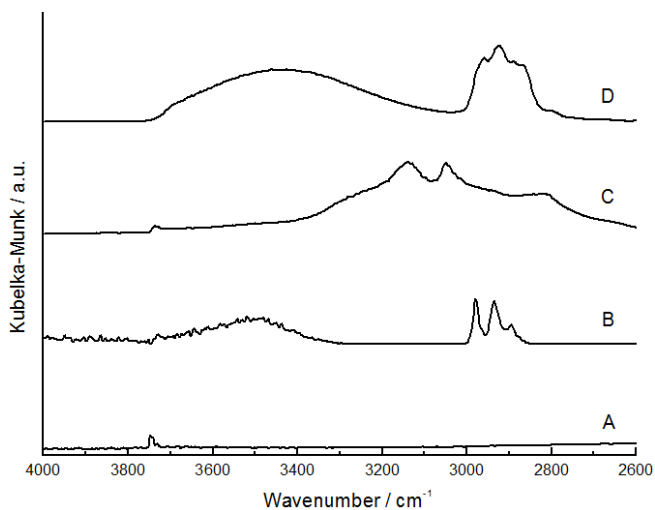


**Figure 4.4: DRIFT spectra of (A) SBA-15; (B) SBA-NEt<sub>3</sub>(10x)-/-2h-65°C; (C) SBA-5%HCl-90-96h-50° and (D) co-cond-10.**

### 4.3 Development of thiol-containing Periodic Mesoporous Organosilica

The ethene bond of the ethenylene-bridged PMO material can be used as an anchoring point for more interesting functionalities such as the thiol group, necessary for mercury adsorption. However, before anchoring the -SH group, an intermediate step must be carried out (Figure 4.5).

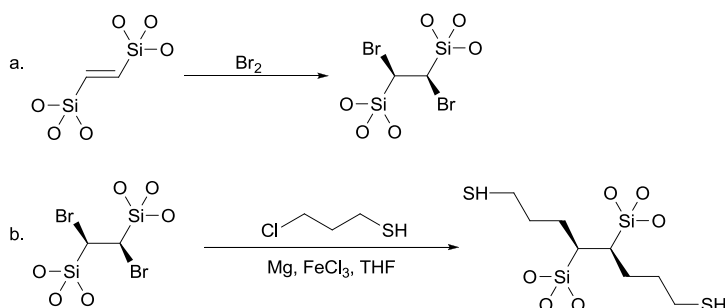


**Figure 4.5: Modification of the ethenylene bond of the PMO material: a. Bromination of double bond and b. Substitution of the bromine atom with the Grignard reagent of 3-chloro-1-propanethiol.**

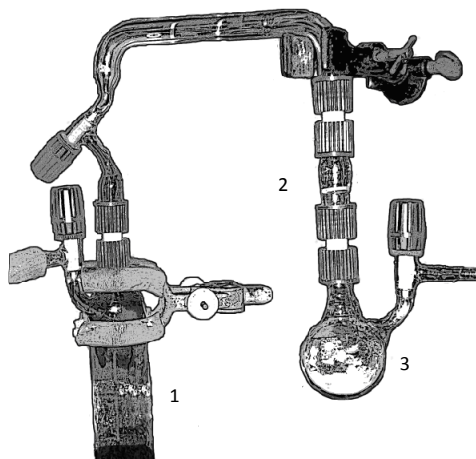
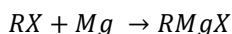


**Figure 4.6: Experimental set-up for the bromination of an ethenylene-bridged PMO material: Flask with bromine (1) connected with Schlenk glassware and filter (2) to the dried PMO material (3).**

A bromination of the double bond, resulting in the addition of two bromine atoms, is performed to create a leaving group on the PMO material.<sup>28, 29</sup> This reaction is executed by letting the solid material come into contact with bromine gas *via* a specially designed Schlenk glassware system (Figure 4.6). The amount of bromine attached to the surface is determined gravimetrically. After bromination, a substitution reaction is carried out for the introduction of a thiol functionality. The chosen pathway consists first of the *in-situ* generation of a Grignard reagent of 3-chloro-1-propanethiol.

### 4.3.1 *The theory behind the Grignard reagent preparation*

This chemical reaction is discovered by Victor Grignard in 1900 and is now a reaction of paramount importance and used worldwide. His discovery even resulted in winning the Nobel Prize in Chemistry in 1912.<sup>30</sup> It consists of the reaction between an organic halide (RX) and metallic magnesium with the formation of an organometallic reagent. It is generally described in the most simple form as



where X represents a chloride, bromide or iodide. However, prior to the formation of the Grignard reagent, the magnesium turnings utilized in the synthesis reaction must be activated with iron(III)chloride. This preactivation step, further referred to as *Reaction 1*, is executed for two reasons. First, it is performed to remove the thin “oxide” layer with a thickness of approximately 1.6 nm.<sup>31</sup> This layer mainly consists of Mg(OH)<sub>2</sub> and a small amount of Mg(HCO<sub>3</sub>)<sub>2</sub> and covers the entire surface of the magnesium. To use the magnesium in the formation of a Grignard reagent, this layer must be removed. Secondly, the iron(III)chloride also creates initiation sites on the surface when Fe(III) is reduced to Fe(0).<sup>32</sup> The iron crystals which are microcrystalline impurities on the magnesium surface will drastically increase the reaction rate of the overall reaction. Without this activation step, the formation of the Grignard reagent would be significantly slower. Tetrahydrofuran (THF) is a solvent commonly used for this type of reactions due to its ability to coordinate to several organomagnesium compounds that are formed *in-situ*. In the first place, it stabilizes the Mg structures but also dissolves by-products such as magnesium halides.<sup>31</sup>

### 4.3.2 The formation of the Grignard reagent and subsequent substitution reaction

For the preactivation of magnesium, *i.e.*, *Reaction 1*, an optimized recipe of Brondani *et al.*<sup>33</sup> is used which involves dissolving 2% FeCl<sub>3</sub> in tetrahydrofuran prior to adding the magnesium turnings. After this activation step, which results in a bright yellow solution, 3-chloro-1-propanethiol is added to the mixture and stirred to create the *in-situ* Grignard reagent (*Reaction 2*). The formation can be followed visually as the solution changes into a very viscous black mixture. Although extensive research has been performed by various authors on the unravelling of the mechanism of the Grignard reactions, a lot of discussion still exists with even contradictory theories.<sup>31</sup> Hence, only a simplified reaction scheme is presented (Figure 4.7).

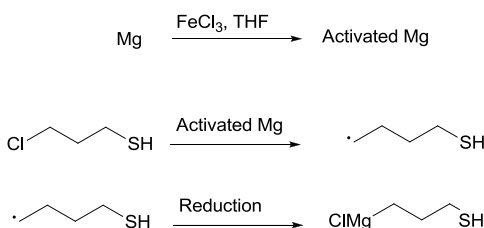


**Figure 4.7: *In-situ* formation of the Grignard reagent of 3-chloro-1-propane thiol (*Reaction 1* and *Reaction 2*).**

Afterwards the brominated ethylene-bridged PMO material, suspended in tetrahydrofuran, is added and stirred at elevated temperature for a certain amount of time. During this reaction step (*Reaction 3*), the Grignard reagent will react as a strong nucleophile and a substitution reaction is performed (Figure 4.8).

The modification of the brominated ethylene-bridged PMO material with the Grignard reagent is in-depth investigated by varying several parameters in order to maximize the thiol amount anchored to the material.

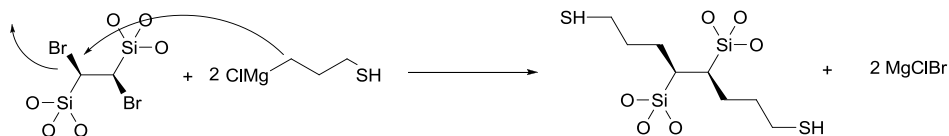


**Figure 4.8: Nucleophilic reaction between the Grignard reagent and the brominated ethylene-bridged PMO material (*Reaction 3*).**

### 4.3.3 Optimization of thiol amount

Grignard reactions normally do not exhibit high yields due to the occurrence of many side reactions and the formation of by-products.<sup>31</sup> Nevertheless, an attempt is made to optimize the two reactions described above and maximize the final thiol content. For *Reaction 1*, the same procedure (50°C; 30 minutes) is used for all the experiments.<sup>33</sup>

The temperature and reaction time are the first parameters that are altered for *Reaction 2* and *Reaction 3* and an overview is presented in Table 4.5. The reaction temperature is increased for *Reaction 2* while the synthetic conditions for the other two reactions are kept constant. In the experiments denoted by entry 1 to 3, one can see that an increase of this temperature does not result in a higher amount of thiols. Furthermore, the elongation of the reaction time results in an increase of mmol SH per gram material. When comparing entry 1 and 4, an amount of 0.40 mmol SH g<sup>-1</sup> is observed when the reaction time is doubled. However, a further increase to 18 hours (entry 5) results in a decrease again.

Entries 1, 6 and 7 provide the thiol amount when investigating the increase in reaction temperature of *Reaction 3*. As can be seen, a higher temperature results also in a decrease of the thiol content. Moreover, an increase in reaction time (entry 8) results also in a decrease of the thiol content.

From these experiments, it can be concluded that the optimal reaction conditions are described in entry 4 of Table 4.5. This procedure results in 0.40 mmol SH g<sup>-1</sup>. Further increase in reaction time and reaction temperature provides lower quantities of thiols and this can possibly be explained by the presence of side reactions. The

experiment described in entry 4 is repeated several times and provided the same amount of thiol functionalities.

**Table 4.5: Overview of the parameters altered in Reaction 2 and Reaction 3 of the thiol functionalisation process.**

Entry	Reaction 2		Reaction 3		mmol SH g <sup>-1</sup> <sup>a</sup>
1	RT	2 h	40°C	24 h	0.20
2	50°C	2 h	40°C	24 h	0.15
3	75°C	2 h	40°C	24 h	0.20
<b>4</b>	<b>RT</b>	<b>4 h</b>	<b>40°C</b>	<b>24 h</b>	<b>0.40</b>
5	RT	18 h	40°C	24 h	0.15
6	RT	2 h	60°C	24 h	0.05
7	RT	2 h	80°C	24 h	0.10
8	RT	2 h	40°C	48 h	0.10

<sup>a</sup> Determined *via* thiol titration.

To increase the thiol content even more, the possibility to avoid side reactions is explored. It is possible that the thiol functionality of 3-chloro-1-propanethiol reacts with the formed Grignard reagent instead of the brominated ethenylene-bridged PMO material. Hence, a protection of the thiol groups is performed before adding the 3-chloro-1-propanethiol to the activated magnesium.

The thiol functionality is protected with a methyl chloromethyl ether reagent or MOM-Cl. This protection group is well-known for the protection of alcohol. Because of the comparable reactivity of alcohol and thiol groups, a similar protection step will be used as described for alcohols in literature.<sup>34</sup> First, N,N-diisopropylethylamine or DIPEA is added to MOM-Cl to deprotonate the thiol (Figure 4.9). Secondly, the deprotonated 3-chloro-1-propanethiol is mixed with the MOM-Cl in order to protect the thiol functionality.

To evaluate the success of this protection procedure, one must deprotect the thiol functionalities before the thiol determination *via* titration. In literature, the removal of the MOM protection group is executed by a reaction with an acidic solution. The

filtration step that is normally performed in a procedure without protection, already uses a washing procedure with 2 M hydrochloric acid. Therefore, an experiment with no special deprotection step is performed and the filtration with 2 M HCl is carried out as normal. However, it is clear from Table 4.6 that this procedure is too mild to remove the MOM functionality. It also confirms that the protection reaction actually took place as no thiol functionalities could be titrated.

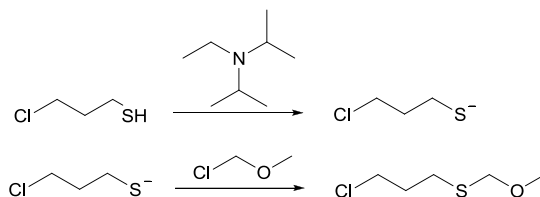


**Figure 4.9: Protection of 3-chloro-1-propanethiol with MOM-Cl.**

Other deprotection procedures have been attempted and the procedures can be found in Table 4.6. The amounts of thiol functionalities are compared to the amount obtained after a procedure without any protection of the SH functionality.

**Table 4.6: Different methods for the deprotection of the thiol functionalities together with the thiol amounts**

Procedure	mmol SH g <sup>-1</sup> <sup>a</sup>
No protection <sup>b</sup>	<b>0.20</b>
No deprotection <sup>c</sup>	0.00
2 M HCl, 45 min, RT	0.10
2 M <i>p</i> -toluenesulfonic acid, 1 h, RT	0.17
6 M HCl, 6 h, RT	0.15

<sup>a</sup> Determined *via* thiol titration. <sup>b</sup> No protection or deprotection step took place. <sup>c</sup> A normal filtration procedure is performed including a washing step with 2 M hydrochloric acid.

Only the procedure that uses *p*-toluenesulfonic acid approximates the value obtained with the procedure without an extra protection step (Table 4.5, entry 1). From these results it is clear that the protection and deprotection of the thiol functionality did not provide the desired increase of the thiol group content on the modified ethenylene-bridged PMO material. This can imply that the protection strategy has no effect on the overall yield and that other side reactions still occur or

that the deprotection step did not sufficiently remove the MOM moiety. It must be noted that Grignard reactions possess typically low yields due to several other undesired reactions that can occur.

Table 4.7 provides the optimized recipe for the substitution reaction with the brominated ethenylene-bridged PMO material. Results varying from 0.39 to 0.44 mmol SH g<sup>-1</sup> are obtained.

**Table 4.7: Overview of the optimized recipe for the substitution reaction with the brominated ethenylene-bridged PMO material and the Grignard reagent of 3-chloro-1-propanethiol.**

Reaction 1		Reaction 2		Reaction 3		mmol SH g <sup>-1</sup> <sup>a</sup>
50°C	30 min	RT	4 h	40°C	24 h	0.40

<sup>a</sup> Determined *via* thiol titration.

The thiol containing PMO material with the highest amount of -SH groups (0.44 mmol SH g<sup>-1</sup>) is used in the mercury(II) adsorption experiments.



### 4.3.4 Characterisation of the ethenylene-bridged PMO material and the subsequent modified materials with bromine and propylthiol

The physical-chemical characteristics of the -SH containing ethenylene-bridged PMO materials are presented in Table 4.8, together with the properties of the pristine PMO material and the brominated variant.

**Table 4.8: Characteristics of the Periodic Mesoporous Organosilicas: the pristine, brominated and thiol functionalised PMO materials are presented.**

	$S_{\text{BET}}^{\text{a}}$ $\text{m}^2 \text{g}^{-1}$	$V_{\text{p}}^{\text{b}}$ $\text{cm}^3 \text{g}^{-1}$	$d_{\text{p}}^{\text{c}}$ nm	mmol SH $\text{g}^{-1}$ <sup>d</sup>	number SH $\text{nm}^{-2}$
ePMO	1182	1.08	6.23	-	-
Br-ePMO	558	0.55	5.47	-	-
SH-ePMO	636	0.55	6.23	0.44	0.22

<sup>a</sup> The specific surface area calculated *via* the BET equation. <sup>b</sup> Total pore volume at  $P/P_0 = 0.98$ . <sup>c</sup> Pore diameter calculated from the desorption isotherm with the BJH method. <sup>d</sup> Determined *via* thiol titration.

The nitrogen sorption isotherms and pore size distributions are presented in Figure 4.10 and show the rather limited influence of the different modification steps. A decrease in  $S_{\text{BET}}$  and  $V_{\text{p}}$  is noticeable as the large bromine atoms and propylthiol functions are attached to the pore walls.

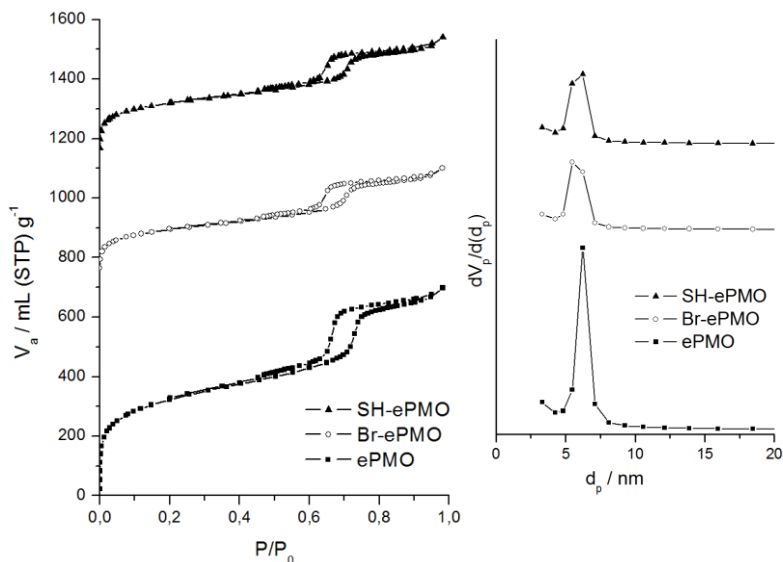


**Figure 4.10:** Nitrogen sorption isotherms and pore size distributions (determined *via* the desorption branch) of ePMO; Br-ePMO and SH-ePMO.

#### 4.4 Mercury(II) adsorption experiments

In total, four thiol containing adsorbents are selected for the mercury(II) adsorption experiments. An overview of the prepared adsorbents is presented in Table 4.9 accompanied by the most important differences between the materials and the amount of reachable thiol functionalities.

**Table 4.9:** Summary of the selected adsorbents for the mercury(II) experiments.

	Highlight	mmol SH g <sup>-1</sup> <sup>a</sup>	#SH nm <sup>-2</sup>
SBA-NEt <sub>3</sub> (10x)-/-2u-65°C	Post-synthesis Monolayer of thiols	1.6	1.1
SBA-5%HCl-90-96u-50°C	Post-synthesis Multilayer of thiols	10.0	7.0
co-cond-10	One-pot-synthesis	1.1	1.6
SH-ePMO	Post-synthesis Monolayer of thiols	0.44	0.22

<sup>a</sup> Determined *via* thiol titration.

The materials SBA-NEt<sub>3</sub>(10x)-/-2h-65°C and SBA-5%HCl-90-96h-50°C will be further referred to as SBA-SH-NEt<sub>3</sub> and SBA-SH-HCl, respectively.

For the development of a good quality adsorbent, the regeneration ability is of course a key feature. Only materials which show a high chemical and structural stability, are considered good candidates. Therefore the stability of the adsorbent after a mercury(II) ion adsorption/desorption cycle needs to be studied. In addition to the preservation of the structure, the materials should keep their functionalities during the adsorption of mercury(II) ions and the regeneration process. Hence, the number of functional groups is evaluated before and after the regeneration.

Preliminary mercury ion adsorption experiments are performed with the four adsorbents to determine the time necessary for each material to reach equilibrium in an experiment with a low mercury(II) ion concentration. Therefore the materials are stirred for a certain amount of time in a mercury(II) solution. After removal of the solids, the concentration of the mercury(II) was determined with CV-AFS. When using a typical concentration of 10 µg L<sup>-1</sup>, complete equilibrium is observed before 15 minutes for all materials.

The recyclability of these materials is of key importance in the total evaluation of an adsorbent. In the recycling experiments, a low concentration Hg(II) solution (10 µg L<sup>-1</sup>) is added to the adsorbent and stirred for a period of 15 minutes. After separation of the solids, the solids are thoroughly washed several times with a 2 M hydrochloric acid solution to recover the mercury(II) ion. These adsorption cycles with the low mercury(II) ion solution of 10 µg L<sup>-1</sup> are repeated three times, and every mesoporous material could remove >99.99% of the mercury(II) ions. Thus, their adsorption capacity is comparable after three cycles at 10 µg L<sup>-1</sup> mercury(II) ion concentration. However, remarkable differences can be noticed when their stability is examined. The structural stability and the chemical stability of the materials will be discussed separately.

The overall mesoporous structure of the material is examined with nitrogen sorption and X-ray diffraction measurements before and after adsorption of the heavy

metal. Significant differences can be observed. Starting with the nitrogen sorption measurement of SBA-SH-HCl (Figure 4.11; A), the isotherm shows a change in structure of the material, where the specific surface area has increased with approximately  $220 \text{ m}^2 \text{ g}^{-1}$ . This demonstrates the unblocking of the pores by removal of the functionalities. The SBA-SH- $\text{NEt}_3$  material displays a similar behavior (Figure 4.11; B).

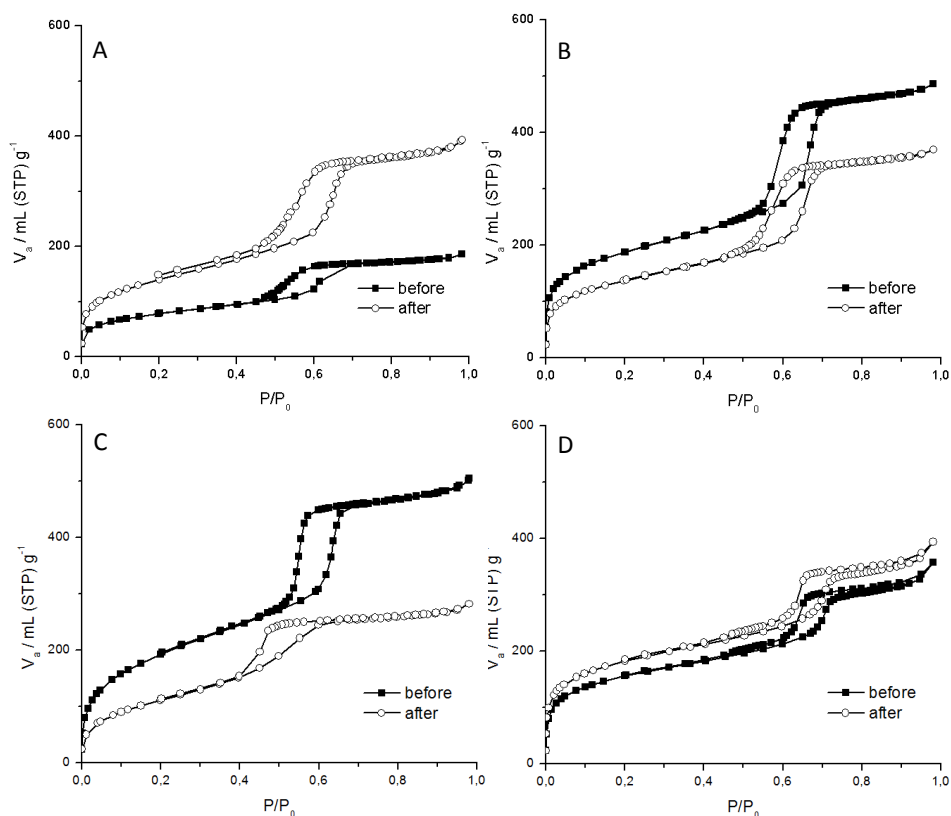


**Figure 4.11:**  $\text{N}_2$  sorption isotherms of the adsorbents, before (■) and after three (○) mercury(II) ion adsorption cycles. (A) SBA-SH-HCl, (B) SBA-SH- $\text{NEt}_3$ , (C) co-cond-10, and (D) SH-ePMO.

The specific surface area also increases, yet not as much as the SBA-SH-HCl. The isotherm retains its typical type IV hysteresis, and thus, the material still exhibits its ordered structure. When examining the isotherm of sample co-cond-10 (Figure 4.11; C), a structural collapse can be observed. Whereas the material shows a good ordering before the adsorption experiments, it loses its structure upon adsorption and

regeneration. For the thiol modified PMO material (Figure 4.11; D), the shape of the isotherm is similar, albeit slightly shifted to higher volumes of adsorbed nitrogen gas. Consequently, the specific surface area increases only  $30 \text{ m}^2 \text{ g}^{-1}$ . This slight increase might be caused by the opening of blocked micropores by using the hydrochloric acid treatment during the rinsing step of the adsorption experiment. It is known that some micropores can be blocked with the surfactant P123 since the surfactant extraction only removes about 95% of the surfactant.<sup>35</sup>

The XRD patterns of the adsorbents before and after three regeneration cycles are displayed in Figure 4.12. The (100), (110), and (200) reflections, characteristic for a *P6mm* space group, can be observed in the XRD patterns of SBA-SH- $\text{NEt}_3$  and SBA-SH-HCl. Co-cond-10 possesses a sharp (100) reflection and less pronounced (110) and (200) reflections. ePMO and SH-ePMO both possess these characteristic reflections even after performing the bromination and substitution with 3-chloro-1-propanethiol. The patterns of all the adsorbents slightly broadens when mercury(II) ion adsorption and regeneration of the materials are performed. The (110) and (200) reflections of SBA-SH- $\text{NEt}_3$  and SBA-SH-HCl become smaller and especially the (110) reflection is less pronounced in the XRD pattern after the three regeneration cycles. This is consistent with the nitrogen sorption measurement. The material made by the one-pot-synthesis (co-cond-10) does not completely retain its ordered structure. The (100) reflection broadens after regeneration, and the (110) and (200) reflections disappear completely. The SH-ePMO adsorbent on the other hand preserves its ordered hexagonal structure; only a slight broadening of the pattern can be observed.

To examine the stability of the PMO adsorbent in strong acidic solution, the material is stirred for 96 hours in 2M hydrochloric acid. After filtering, washing, and drying the adsorbent, the material is characterised again to evaluate the stability of its structure. Figure 4.13 shows the nitrogen adsorption/desorption isotherms. Only a small difference can be seen in the isotherms, the result of further unblocking of the micropores. This effect is heavily pronounced in the isotherm as the removal of surfactant also makes the sample lighter, and these isotherms are always expressed in millilitres of  $\text{N}_2$  adsorbed per gram of sample. This proves that the materials can resist acidic media without loss of structure.

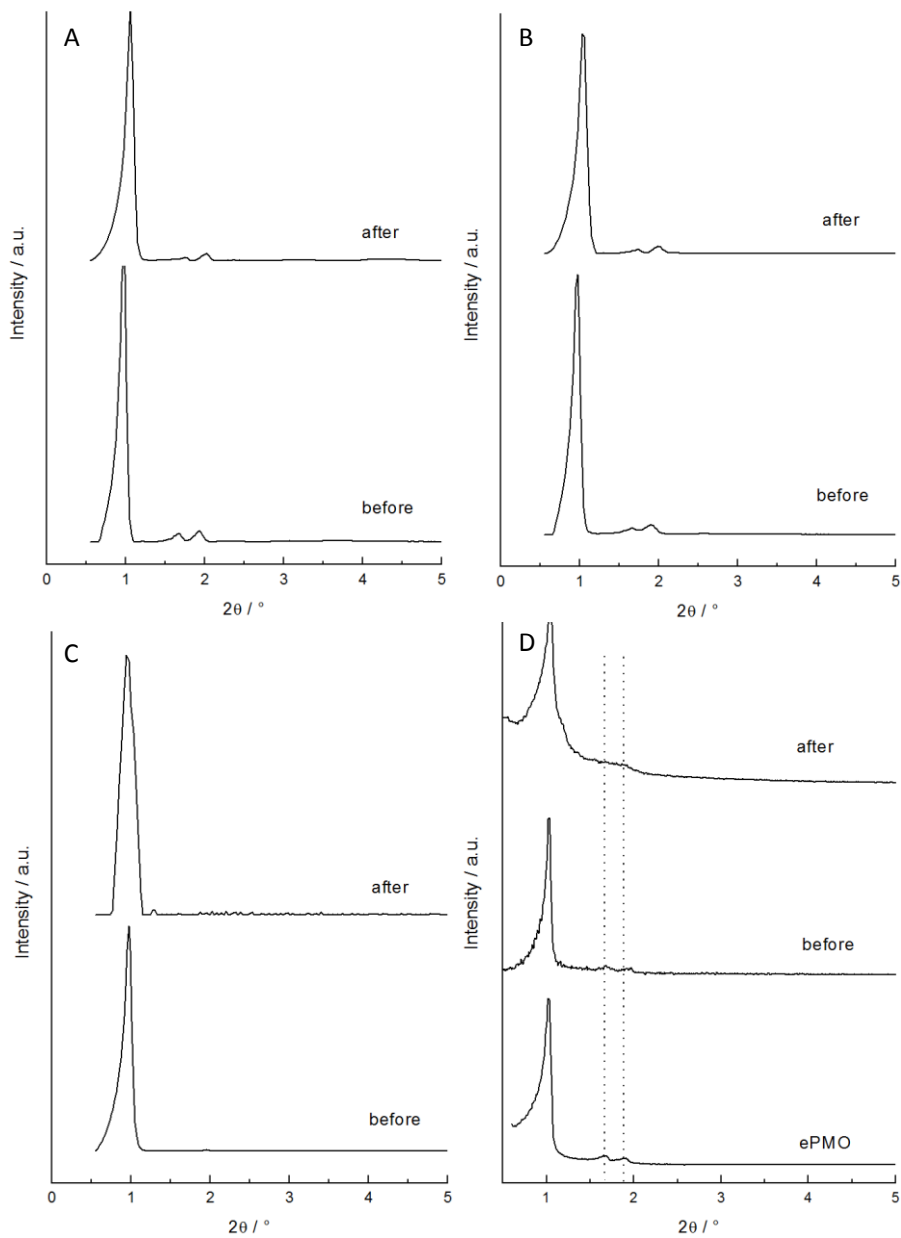


**Figure 4.12: Powder X-ray diffraction patterns of (A) SBA-SH-NEt<sub>3</sub>; (B) SBA-SH-HCl; (C) co-cond-10; (D) SH-ePMO before and after three regeneration cycles. The XRD pattern of ePMO is also displayed.**

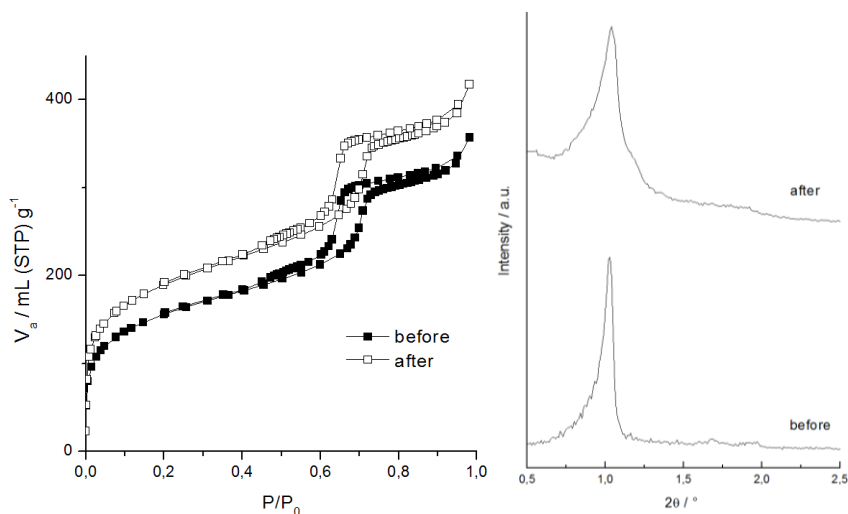


**Figure 4.13: Nitrogen sorption isotherm of SH-ePMO before and after 96 hours of stirring in 2 M HCl. (left) Powder x-ray diffraction patterns of SH-ePMO before and after 96 hours of stirring in 2 M HCl. (right)**

The results of the thiol titration are presented in Table 4.10. When a comparison is made between the SBA-materials, the co-condensation and the PMO, the differences in the stabilities of the functional groups are remarkable.

**Table 4.10: Characteristics of the adsorbents after the adsorption of mercury(II) ions.<sup>a</sup>**

	$S_{\text{BET}}^{\text{b}}$ $\text{m}^2 \text{g}^{-1}$	$V_{\text{p}}^{\text{c}}$ $\text{mL g}^{-1}$	$d_{\text{p}}^{\text{d}}$ $\text{nm}$	$\text{mmol SH g}^{-1 \text{e}}$	Leaching %
SBA-SH-HCl	510	0.61	4.82	1.00	90
SBA-SH-NEt <sub>3</sub>	614	0.57	4.82	0.76	53
Co-cond-10	416	0.44	3.75	0.85	23
SH-ePMO	666	0.61	5.47	0.44	0

<sup>a</sup> Every time, three cycles are performed before examining the material by nitrogen sorption measurements and thiol titration. <sup>b</sup> Specific surface area calculated *via* the BET equation. <sup>c</sup> Total pore volume at  $P/P_0 = 0.98$ . <sup>d</sup> Pore diameter calculated from the desorption branch *via* the BJH method. <sup>e</sup> Determined *via* thiol titration.

Whereas the Periodic Mesoporous Organosilica material retains 100% of the thiol groups, the materials prepared *via* the post-synthetic route and the one-pot synthesis both show significant loss of their functionalities. As shown in Table 4.10, sample SBA-SH-HCl even leaches 90% of its thiol groups. This can be explained by the sensitivity of

the siloxane bridges that are responsible for the attachment of the functionalities. During the grafting procedure, these bridges are very sensitive to hydrolysis, especially when the material is treated with the acidified solution used for regeneration. Samples SBA-SH-NEt<sub>3</sub> and co-cond-10 also suffer from functionality loss, although the loss is smaller. In the PMO, the propylthiol group is attached to the surface by means of a C-C group. The strength of this bond results in a material which does not leach any functionalities.

The XRD, nitrogen sorption measurements and thiol determination results clearly show the sustainability of the thiol functionalised PMO in comparison with the silica materials where the functionality is anchored *via* Si-O-Si bonds. The stability of PMOs in general is also described by Burleigh *et al.* and recently by our research group.<sup>2,36</sup> Furthermore, additional mercury(II) ion adsorption experiments are performed to provide a better insight into the adsorption behavior of the ultrastable SH-ePMO.

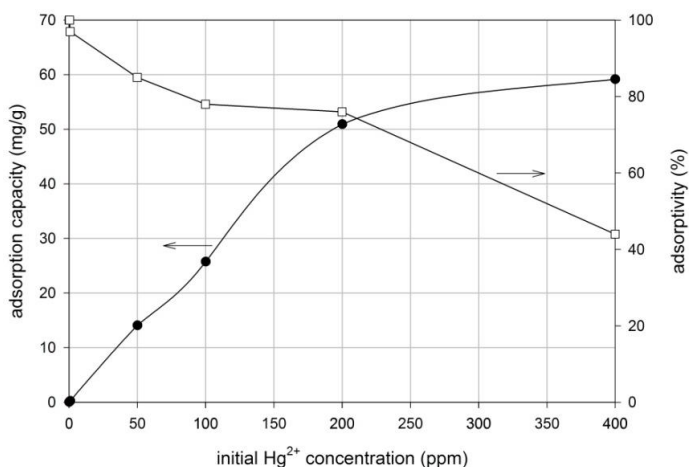


**Figure 4.14: Effect of the initial Hg(II) concentration on the equilibrium Hg(II) adsorption on SH-ePMO (150 mg) in Hg(NO<sub>3</sub>)<sub>2</sub> solution (50 mL) at 20°C.**

The effects of the initial mercury(II) ion concentration on the adsorption and adsorptivity (% of the Hg(II) adsorbed) are shown in Figure 4.14. The adsorptivity decreases with increasing Hg(II) concentrations, whereas the adsorption capacity increases. The maximal adsorption capacity of the mesoporous adsorbent was approximately 64 mg g<sup>-1</sup>. This implies a 1:1 stoichiometry of the mercury(II) ion



towards the thiol group of the mesoporous material and is consistent with previously reported literature (Figure 4.15).<sup>10, 13, 37</sup> After adsorption, the pH of the solution decreased; that is protons were released during the adsorption, confirming the adsorption mechanism earlier suggested in literature. The adsorption capacity as a function of time is shown in Figure 4.16. The kinetics of the adsorption of mercury(II) ion are best described by a pseudo-second-order rate.

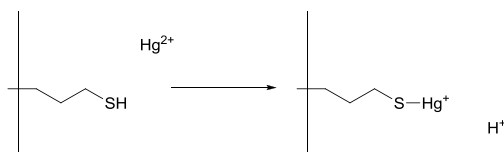


**Figure 4.15: Proposed adsorption mechanism of mercury(II) ion on the mesoporous SH-ePMO adsorbent.**

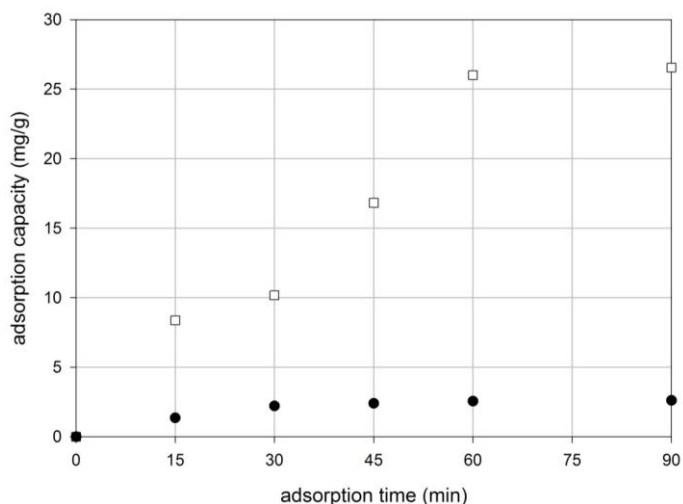


**Figure 4.16: Effect of adsorption time on Hg(II) adsorption onto SH-ePMO at initial Hg(II) concentration of 10 (●) and 100 (□) ppm.**

## 4.5 Conclusion

The continuing search for new metal adsorbents has resulted in the development of a new functionalised Periodic Mesoporous Organosilica. The PMO material was compared with adsorbents prepared *via* a post-synthetic route starting from SBA-15 and *via* one-pot synthesis. The outcome of modifying an ethenylene-bridged PMO with propylthiol is an ultrastable adsorbent for the adsorption of mercury(II) ion. The

material keeps its structure after multiple regeneration cycles and maintains its amount of thiol functionalities. The hydrochloric acid solution, necessary for the regeneration, does not affect the material on any level. The material was compared with the three other mesoporous silica materials synthesized in this study and was proven to be by far the most stable material. Even when treated for a longer period in hydrochloric acid, the material sustains its mesoporous structure. All other materials (functionalised SBA-15, co-condensed materials) quickly lose their structure and/or functionalities during adsorption or regeneration. The thiol functionalised PMO showed a maximal adsorption capacity of 64 mg g<sup>-1</sup> and a 1:1 ratio of Hg<sup>2+</sup> : SH.

## 4.6 Experimental section

**Chemicals.** Vinyltriethoxysilane (VTES; 97%), (3-mercaptopropyl)triethoxysilane (MPTES; 98%) and (3-mercaptopropyl)trimethoxysilane (MPTMS; 98%) were purchased from ABCR. Tetraethoxyorthosilicate (TEOS; 98%), the pluronic® PEO<sub>20</sub>PPO<sub>70</sub>PEO<sub>20</sub> (P123), Grubbs' first generation catalyst, 3-chloro-1-propanethiol (98%), triethylamine (>99%), magnesium, iron(III) chloride (98%; anhydrous), hydrochloric acid (37%; p.a.), acetonitrile (99,5%; p.a.), acetone (>99,5%), ethanol (96%), 1-butanol, *N,N*-diisopropyl-ethylamine (DIPEA), methyl chloromethyl ether (MOM-Cl) and tetrahydrofuran (p.a.) were acquired from Sigma-Aldrich. Hg(NO<sub>3</sub>)<sub>2</sub> in HNO<sub>3</sub> (2 M) was purchased from VWR. Triethylamine, acetonitrile, and tetrahydrofuran were dried and degassed before use.

**Synthesis of SBA-15 material.** The mesoporous material was synthesized according to the procedure published by Zhao *et al.*<sup>20,21</sup> An amount of 4 g of P123 was dissolved into 120 mL of 2M hydrochloric acid and 30 mL of distilled water. The mixture was stirred at room temperature until the surfactant completely dissolves. An amount of 9 mL of TEOS was added, and the temperature was increased to 45°C for 5 h under stirring. A white precipitation was formed. Subsequently, the temperature was raised to 90°C for 16 h under static conditions. The solids were filtered and subsequently washed with water and acetone. Finally, the material (denoted as SBA-15) was calcined at 550°C for 6 h.

**Functionalisation of SBA-15 material.**

**A) With triethylamine.** A total amount of 0.7 g of SBA-15 was mounted into a Schlenk flask under an inert atmosphere. Then 10 mL of acetonitrile and 2.7 mL of triethylamine, behaving as an activator,<sup>17</sup> were added. The reaction mixture was stirred for 2 h at room temperature, and subsequently the mixture of triethylamine and acetonitrile was removed under inert atmosphere. Volumes of 10 mL acetonitrile and 5.0 mL MPTES were added to the material. The mixture was allowed to react for 2 h at 65°C before the solids were filtered and washed with acetonitrile and acetone. The material (SBA-SH-NEt<sub>3</sub>) was dried at 90°C under vacuum for 16 h.

**B) With hydrochloric acid.** A total amount of 0.3 g of SBA-15 material was put in a flask. Then 10 mL of acetonitrile, 0.89 mL of hydrochloric acid (2 M), and 0.44 mL of MPTES were added. The reaction mixture was stirred for 96 h at 50°C before the solids were filtered and washed with acetonitrile and acetone. The material (SBA-SH-HCl) was dried at 90°C under vacuum for 16 h.

**One-step synthesis of a thiol functionalised SBA-15-like material.** The synthesis was based on the recipes published by Aguado *et al.*<sup>22</sup> and Mercier *et al.*<sup>23</sup> A total amount of 1 g of P123 was allowed to dissolve in 30 mL of 2M hydrochloric acid for 45 min at room temperature. Following that, 2.10 mL of TEOS was added and stirred for 45 min at 40°C. Then 0.20 mL of MPTMS was added and stirred for 20 h. A white precipitation was formed and allowed to age at 100°C for 24 h. After filtering and washing with water and acetone, the surfactant P123 was extracted with a mixture of ethanol/hydrochloric acid. The sample, listed as co-cond-10, was dried at 90°C under vacuum for 16 h.

**Preparation of SH-ePMO.**

**Synthesis of *trans* 1,2-bis(triethoxysilyl)ethenylene and the *trans* ethenylene-bridged PMO material.** The procedure to synthesize *trans* 1,2-bis(triethoxysilyl)ethenylene and the *trans* ethenylene-bridged PMO were elaborately described in Chapter 3.

**Bromination of the *trans* ethenylene-bridged PMO material.** A certain amount of *trans* ethenylene-bridged PMO was charged in to a Schlenk flask of 100 mL and

attached to the set-up shown in Figure 4.6. After three hours of contact with bromine fumes, the PMO material (Br-ePMO) was dried at 120°C under vacuum overnight. The amount of bromine chemically bonded to the PMO material was gravimetrically determined. The flask containing the dry material was weighed before the reaction. After bromination and removal of the physisorbed bromine by the drying step, the flask and material is weighed again. The difference represents the added mass of the bromine atoms.

**Modification of the brominated ethenylene-bridged PMO.** A mixture of magnesium (0.74 g), iron(III)chloride (0.54 g), and tetrahydrofuran (30 mL) was prepared under an inert atmosphere. This viscous solution was allowed to stir for 30 min at a temperature of 50°C to activate the magnesium. 3-Chloro-1-propanethiol (0.22 mL) was added, and the mixture was stirred for 2 h at room temperature. Immediately following, the mixture was added to a Schlenk flask containing Br-ePMO. After stirring for 5 h at 40°C, filtration was executed and the material was washed with THF, 2 M HCl, water, and acetone. Finally, the solids (SH-ePMO) were collected and dried at 90°C for 16 h.

**Protection of 3-chloro-1-propanethiol.** An amount of 0.18 mL 3-chloro-1-propanethiol (1 eq), 0.31 mL *N,N*-diisopropyl-ethylamine (0.8 eq; DIPEA) and 0.13 mL methyl chloromethyl ether (0.8 eq; MOM-Cl) were added to 25 mL of tetrahydrofuran. This mixture was stirred for 1 hour at room temperature and was subsequently added to the activated magnesium mixture. The bromine substitution was executed as described above.

**Determination of reachable thiol functionalities.** The amount of reachable thiol functionalities on the synthesized mesoporous materials was determined by silver titration.<sup>26, 27</sup> The thiol groups on the materials reacted with a known concentration of silver nitrate, and the excess of silver was titrated with potassium thiocyanate, using an iron indicator ( $\text{FeNH}_4(\text{SO}_4)_2 \cdot 12\text{H}_2\text{O}$  in 0.3 M  $\text{HNO}_3$ ). The number of thiol groups were subsequently calculated.

**Mercury(II) ion adsorption experiments.**

**In the low concentration range.** A 150 mg amount of the material was measured out, and 50 mL of  $10 \mu\text{g L}^{-1}$  mercury(II) solution was added. The mixture was stirred at room temperature for 15 min and filtered, and then the amount of mercury(II) ion in the filtrate was quantified with cold vapor atomic fluorescence spectroscopy (CV-AFS). The regeneration of the material was performed as follows. A sample of the Hg(II)-loaded material was washed three times with 10 mL of 2M HCl and three times with 10 mL of water. The amount of Hg(II) leached out of the adsorbent was measured by CV-AFS. The materials were dried in an oven at  $90^\circ\text{C}$  for 1 h before reuse. Three regeneration cycles were performed on each sample. The structures of the adsorbents were evaluated afterwards. Nitrogen sorption measurements were performed each time, and the amount of thiol groups was specified.

**In the high concentration range.** Adsorbent equilibrium experiments were performed with 150 mg of mesoporous adsorbent (SH-ePMO) and 50 mL of Hg(II) solution with different concentrations between  $100 \mu\text{g L}^{-1}$  and  $400 \text{mg L}^{-1}$ . The mixture was stirred at room temperature for 90 min and filtered, and the amount of mercury(II) ion in the filtrate was quantified with cold vapor atomic absorption spectroscopy (CV-AAS). The adsorption experiments were performed at the pH that resulted from the Hg(II) solution without further adjustment. The initial and final pH of these Hg(II) solutions were measured. For the mercury(II) ion adsorption kinetic experiments, 300 mg of mesoporous adsorbent (SH-ePMO) was contacted with 100 mL of Hg(II) solution with Hg(II) concentrations of 10 and  $100 \text{mg L}^{-1}$ . At predetermined intervals of time, samples of the mixture were withdrawn, filtered, and analyzed by CV-AAS.

**Characterisation.** The nitrogen sorption isotherms were recorded on Belsorp Mini II equipment at  $-196^\circ\text{C}$ . The samples were pretreated at  $120^\circ\text{C}$  while degassing. CHNS elemental analysis was executed by the *Centre National de la Recherche Scientifique* (CNRS, France). Diffuse reflectance infrared Fourier transform (DRIFT) spectroscopy was performed on a hybrid IR-RAMAN spectrophotometer, Equinox 55S (FRA 106; Bruker) with a MCT-detector, using a Graseby Specac diffuse reflectance cell, operating under vacuum and at  $120^\circ\text{C}$ . X-ray diffraction was performed with an

ARL X'tra X-ray diffractometer of Thermo Scientific equipped with a Cu K $\alpha$ 1 tube and a Peltier cooled lithium drifted silicon solid stage detector. Cold vapor atomic fluorescence spectroscopy (CV-AFS) was performed on a Mercur spectrophotometer (Analytik Jena) with a UV source of 253.7 nm. Experimental data were processed with WinAAS version 4.2.0. Cold vapor atomic absorption spectroscopy (CV-AAS) was performed on a GBC-933 instrument combined with GBCHG3000 (GBC Scientific Equipment).

## 4.7 References

1. R. G. Pearson, *Journal of the American Chemical Society*, 1963, **85**, 3533-3539.
2. M. C. Burleigh, M. A. Markowitz, S. Jayasundera, M. S. Spector, C. W. Thomas and B. P. Gaber, *Journal of Physical Chemistry B*, 2003, **107**, 12628-12634.
3. A. Vinu, K. Z. Hossain and K. Ariga, *Journal of Nanoscience and Nanotechnology*, 2005, **5**, 347-371.
4. D. Bruhwiler, *Nanoscale*, 2010, **2**, 887-892.
5. G. E. Fryxell, S. V. Mattigod, Y. H. Lin, H. Wu, S. Fiskum, K. Parker, F. Zheng, W. Yantasee, T. S. Zemanian, R. S. Addleman, J. Liu, K. Kemner, S. Kelly and X. D. Feng, *Journal of Materials Chemistry*, 2007, **17**, 2863-2874.
6. P. K. Jal, S. Patel and B. Mishra, *Talanta*, 2004, **62**, 1005-1028.
7. A. Stein, B. J. Melde and R. C. Schroden, *Advanced Materials*, 2000, **12**, 1403-1419.
8. L. Mercier and T. J. Pinnavaia, *Advanced Materials*, 1997, **9**, 500-503.
9. S. A. Idris, S. R. Harvey and L. T. Gibson, *Journal of Hazardous Materials*, 2011, **193**, 171-176.
10. L. Mercier and T. J. Pinnavaia, *Environmental Science & Technology*, 1998, **32**, 2749-2754.
11. A. Walcarius, M. Etienne and C. Delacote, *Analytica Chimica Acta*, 2004, **508**, 87-98.
12. A. Walcarius and C. Delacote, *Analytica Chimica Acta*, 2005, **547**, 3-13.
13. A. Walcarius, M. Etienne and J. Bessiere, *Chemistry of Materials*, 2002, **14**, 2757-2766.
14. L. X. Zhang, C. C. Yu, W. R. Zhao, Z. L. Hua, H. R. Chen, L. Li and J. L. Shi, *Journal of Non-Crystalline Solids*, 2007, **353**, 4055-4061.
15. B. Arkles, *Chemtech*, 1977, **7**, 766-778.
16. X. Feng, G. E. Fryxell, L. Q. Wang, A. Y. Kim, J. Liu and K. M. Kemner, *Science*, 1997, **276**, 923-926.
17. J. P. Blitz, R. S. S. Murthy and D. E. Leyden, *Journal of Colloid and Interface Science*, 1988, **126**, 387-392.
18. M. C. B. Salon, P. A. Bayle, M. Abdelmouleh, S. Boufi and M. N. Belgacem, *Colloids and Surfaces a-Physicochemical and Engineering Aspects*, 2008, **312**, 83-91.
19. L. D. White and C. P. Tripp, *Journal of Colloid and Interface Science*, 2000, **227**, 237-243.
20. D. Y. Zhao, Q. S. Huo, J. L. Feng, B. F. Chmelka and G. D. Stucky, *Journal of the American Chemical Society*, 1998, **120**, 6024-6036.
21. D. Y. Zhao, J. L. Feng, Q. S. Huo, N. Melosh, G. H. Fredrickson, B. F. Chmelka and G. D. Stucky, *Science*, 1998, **279**, 548-552.
22. J. Aguado, J. M. Arsuaga and A. Arencibia, *Microporous and Mesoporous Materials*, 2008, **109**, 513-524.
23. J. Brown, R. Richer and L. Mercier, *Microporous and Mesoporous Materials*, 2000, **37**, 41-48.
24. A. S. M. Chong, X. S. Zhao, A. T. Kustedjo and S. Z. Qiao, *Microporous and Mesoporous Materials*, 2004, **72**, 33-42.
25. J. Aguado, J. M. Arsuaga and A. Arencibia, *Industrial & Engineering Chemistry Research*, 2005, **44**, 3665-3671.

26. A. I. Vogel, *A text-book of quantitative inorganic analysis including elementary instrumental analysis*, Harlow : Longman, London, 1961.
27. E. B. Sandell and I. M. Kolthoff, *Textbook of quantitative inorganic analysis*, Macmillan Company, New York, 1952.
28. K. Nakai, Y. Oumi, H. Horie, T. Sano and H. Yoshitake, *Microporous and Mesoporous Materials*, 2007, **100**, 328-339.
29. C. Vercaemst, M. Ide, P. V. Wiper, J. T. A. Jones, Y. Z. Khimyak, F. Verpoort and P. Van Der Voort, *Chemistry of Materials*, 2009, **21**, 5792-5800.
30. D. Seyferth, *Organometallics*, 2009, **28**, 1598-1605.
31. J. E. Garst and M. R. Soriaga, *Coordination Chemistry Reviews*, 2004, **248**, 623-652.
32. C. E. Teerlinck and W. J. Bowyer, *Journal of Organic Chemistry*, 1996, **61**, 1059-1064.
33. D. J. Brondani, R. J. P. Corriu, S. Elayoubi, J. J. E. Moreau and M. W. C. Man, *Tetrahedron Letters*, 1993, **34**, 2111-2114.
34. G. Zweifel and M. Nantz, *Modern Organic Synthesis*, W. H. Freeman, 2007.
35. C. Vercaemst, M. Ide, B. Allaert, N. Ledoux, F. Verpoort and P. Van Der Voort, *Chemical Communications*, 2007, 2261-2263.
36. F. Goethals, C. Vercaemst, V. Cloet, S. Hoste, P. Van Der Voort and I. Van Driessche, *Microporous and Mesoporous Materials*, 2010, **131**, 68-74.
37. H.-Y. Wu, C.-H. Liao, Y.-C. Pan, C.-L. Yeh and H.-M. Kao, *Microporous and Mesoporous Materials*, 2009, **119**, 109-116.



## ***5 The use of the thiol containing PMO in DGT probes for determining dissolved mercury concentrations***

Taking into account the promising results of the batch laboratory experiments described in Chapter 4, the possibility of applying the thiol functionalised ethylene-bridged PMO material as a mercury(II) adsorbent in a more realistic aqueous environment is investigated. Therefore the employment of this SH-PMO material in the *Diffusive Gradients in Thin* (DGT) film technique is explored. This technique allows *in-situ* speciation of heavy metals such as mercury(II) in waste water or fresh water such as ponds, lakes or rivers.

Furthermore a comparison with two commercially available resins (Chelex-100 and Sumichelate Q10R) and two thiol functionalised silica materials was conducted. According to our results, the Chelex-100 resin presents a much lower affinity for mercury than the thiol based resins. The non-linear accumulation profile of mercury with time for the Chelex-100 resin makes it in fact impossible to use Fick's law for estimating the diffusion coefficient of Hg. The 4 other resins all show a linear accumulation profile of mercury with time. Although the highest accumulation rate is observed for SH-PMO followed by Sumichelate Q10R and the silica based sorbents, these values do not differ very much.

Adsorption experiments were performed by dr. Yue Gao under the guidance of Prof. dr. Willy Baeyens of the Laboratory of Analytical and Environmental Chemistry (ANCH) of the Vrije Universiteit Brussel (VUB).

The results in this chapter were published as  
Yue Gao, Els De Canck, Martine Leermakers, Willy Baeyens and Pascal Van Der Voort, *Talanta*, **2011**, 87, 262– 267.

## 5.1 *Introduction to Diffusive Gradients in Thin (DGT) films*<sup>1, 2</sup>

Mercury is one of the most hazardous metals and the removal of mercury from waste water or the purification of natural waters is an issue that still concerns many research groups. Not only the total amount or the abundance of the mercury present in the aqueous environment, but also the physical and chemical form plays a key role in the toxicity of metals. Only those metals that are bio-available pose a threat for aquatic and terrestrial environments. Therefore it is of great importance to determine the forms of the mercury present in a specific stream or pond. Knowledge of the speciation of mercury and the fluctuation of water flows is crucial for predicting impacts on aquatic biota and allows us, if necessary, to interfere properly.

In order to monitor the metal concentration and to perform speciation, water samples have to be taken which are completely representative of the natural environment.<sup>1</sup> This also includes natural fluctuations of the concentrations. This has of course an impact on the procedures of sample taking. The easiest ways of sampling are grab sampling and composite sampling.<sup>1</sup> The biggest issue with these two sampling methods is the preservation of the sample. The constitution of the sample has to remain the same from the moment it has been taken to the analysis in the lab so that the sample is still representative. During the collection, transportation, storage and handling, physical changes can occur and can cause a change in the physico-chemical parameters, resulting in a possible change of the chemical form of the metal and resulting in a different species distribution.<sup>1, 2</sup>

To prevent these problems, the *Diffusive Gradients in Thin (DGT) films* technique can be used. This unique system has been developed by Davison and Zhang in 1994<sup>3</sup> and is now a valuable technique used frequently worldwide in the field of speciation and monitoring. In the DGT probe (*vide infra*), an adsorbent or resin is present which captures the metals. After collection of the probes, the speciation of mercury is unaffected by any change of physical parameters during transport or storage. An additional advantage of this technique, is that DGT only measures labile metals. This includes free metal ions and labile or weak metal complexes. Thus the DGT

5.2

concentration obtained is an approximation of the bioavailability of mercury and therefore represents the metals that are in fact hazardous for the environment.

### 5.1.1 The DGT probe<sup>4</sup>

The DGT sampler or probe contains an assembly of two gels that are being held together by a piston-like plastic casing (Figure 5.1). The plastic casing consists of a base and a cap that are clicked together and hold several gel components.

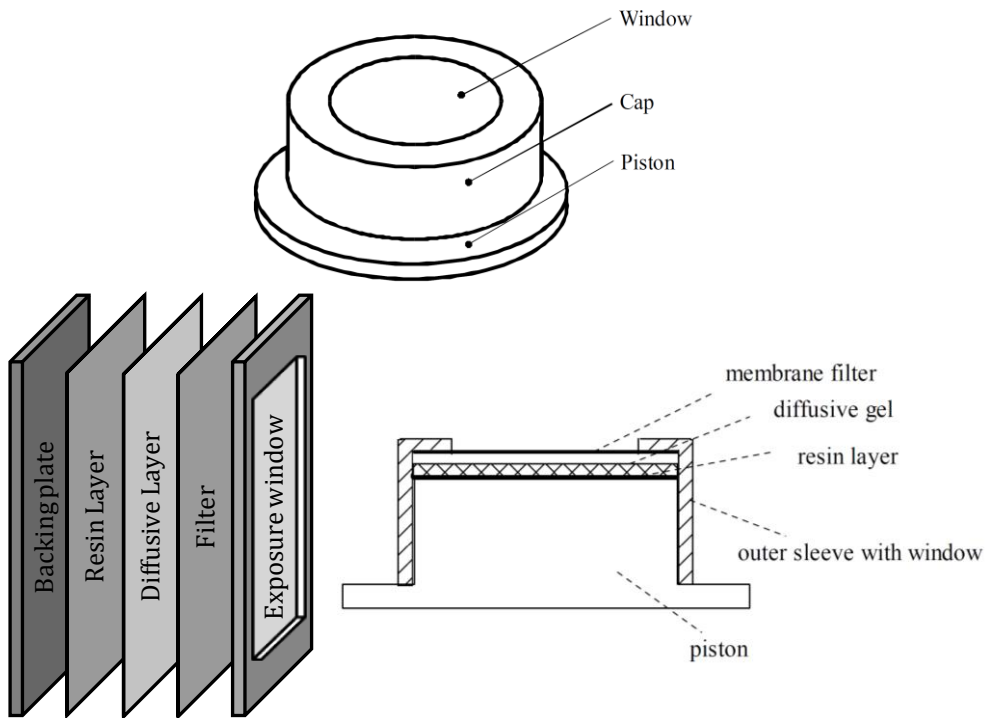


**Figure 5.1:** A schematic overview of the DGT assembly with the different layers. **Top:** the complete DGT probe, top view. **Bottom:** (left) the different layers with the base of the casing, the gel with binding resin (Resin layer), the diffusion gel (Diffusive layer), the filter membrane and the cap of the casing with exposure window; (right) side view of DGT probe. Adapted from reference 4.

A window in the cap allows diffusion into the gel layers. The gel assembly contains two different gel layers. The one closest to the base normally consists of a cation exchange binding resin which is embedded in a polyacrylamide hydrogel (resin layer). Usually the ion exchange resin consists of Chelex-100. On top of that layer

another gel is positioned. A polyacrylamide diffusive gel with a standard uniform pore size and thickness (diffusive layer). To protect the gel assembly a cellulose nitrate membrane filter (usually 0.45  $\mu\text{m}$ ) is placed on top of the assembly and exclude any particulates that are present in the water and can damage the gel assembly.

When the probe is placed in solution, water with metal species can enter the layers *via* the exposure window. The metals can diffuse through the diffusive layer into the layer containing the resin where they can interact with the Chelex-100 and be immobilized. The free metal concentration throughout the whole DGT probe and bulk solution are shown in Figure 5.2. At the boundary between the resin and the diffusive layer, the concentration of the metals is zero, assuming that the immobilizing takes place very quickly and efficiently.

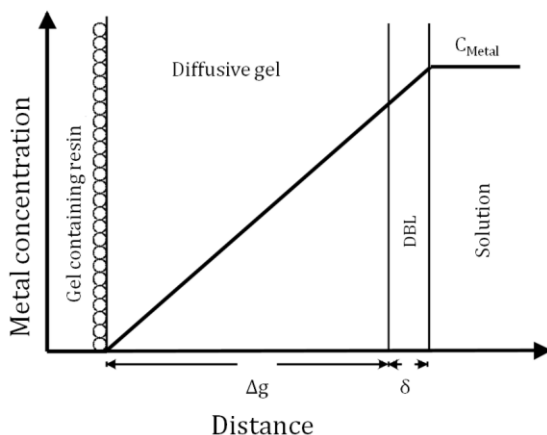


**Figure 5.2: Representation of the metal concentration gradient in the different layers of the DGT probe as well as the bulk solution. Figure adapted from reference 5. DBL = diffusive boundary layer.**

The capacity of the probe is dependent upon the maximum capacity of the resin and is therefore determined by the total amount of resin embedded in the layer. The transport of the metals on the other hand is controlled by the diffusive gel layer and the rate is represented by their diffusion coefficients ( $D$ ).  $D$  is dependent upon the size of the metal compared to the pore size of the gel which is typically 2-5 nm. A not exhaustive list of diffusion coefficients is described by Zhang and Davison.<sup>6</sup>

### 5.1.2 Advantages of the DGT method

Using the DGT method implies having a few advantages over the current ways of monitoring the water quality and of course sampling methods. The DGT probe only takes up free metal ions and labile metal complexes, therefore giving an idea of the bioavailability of the metal. This is a huge advantage over the techniques that determine the total amount of metals present in the environment. Furthermore, the DGT probe also performs an *in-situ* speciation in contrast to other methods. The metals bound to the resin are unaffected by changing physical parameters when retracting the probe from the aqueous environment and it can be used to monitor the metal up-take over longer periods of time and therefore it averages out natural variations in metal concentration.<sup>3, 5, 7, 8</sup>

### 5.1.3 Parameters affecting the DGT measurement

It is known that several parameters affect the measurements with the DGT technique: temperature,<sup>3,4</sup> flow rate,<sup>9</sup> pH<sup>5,9</sup> and ionic strength<sup>10-12</sup> of the solution. Of course when measuring in a laboratory controlled environment, these parameters can be changed so that the DGT can operate under ideal conditions. In a real set-up under field conditions, it is naturally impossible to alter these parameters.

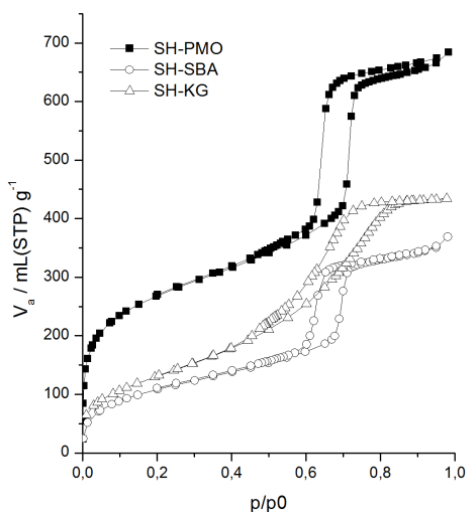
## 5.2 Synthesis and characteristics of the resins used in the DGT probe

The 3-mercaptopropyl functionalised ethenylene-bridged Periodic Mesoporous Organosilica, herein abbreviated as SH-PMO and a 3-mercaptopropyl functionalised SBA-15 material (SH-SBA) are included in a *Diffusive Gradients in Thin* film (DGT) probe. The functionalised SBA-15 is prepared in the same manner as described in Chapter 4, where a grafting procedure with triethylamine is employed. The modification procedure to obtain SH-PMO can be found in the same chapter.

The adsorbents SH-PMO and SH-SBA are compared to similar commercially available resins which also contain thiol groups, such as Sumichelate Q10R (SQR) and 3-mercaptopropyl functionalised silica gel (SH-KG), but also to the Chelex-100 resin

for the determination of labile Hg concentrations. In this research, an agarose gel was used as the diffusive gel because the classic polyacrylamide gel shows more than 20% of Hg adsorption.<sup>13</sup> In the following discussion, the adsorbents will be referred to as *resins*.

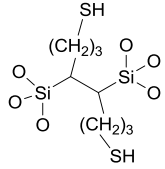
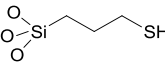
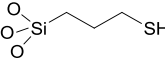
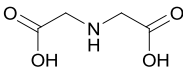
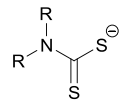
The three mesoporous functionalised silicon based materials (SH-KG, SH-SBA and SH-PMO) are first characterised with nitrogen sorption measurements to check their mesoporosity (Figure 5.3).



**Figure 5.3: Nitrogen sorption isotherms of SH-PMO, SH-SBA and SH-KG.**

The adsorbents showed specific surface areas between 450 and 822 m<sup>2</sup> g<sup>-1</sup> and their pore volumes and pore diameters are presented in Table 5.1. The functionalised PMO resin exhibited the highest surface area and pore volume. The SH-KG material showed a very broad pore size distribution in comparison with the very narrow distribution of SH-SBA and SH-PMO.

**Table 5.1: Overview of the characteristics of the resins.**

	Matrix	Functionality	Porosity	Morphology		$S_{\text{BET}}^{\text{a}}$ $\text{m}^2 \text{g}^{-1}$	$V_{\text{p}}^{\text{b}}$ $\text{mL g}^{-1}$	$d_{\text{p}}^{\text{c}}$ $\text{nm}$	Functionality <sup>d</sup> $\text{mmol g}^{-1}$	Capacity <sup>e</sup> $\text{mg g}^{-1}$
SH-PMO <sup>f</sup>	$\text{O}_3\text{Si-CH=CH-SiO}_3$		Ordered Mesoporous	Powder Irregular particles	Hydrophobic	822	0.9	5.47	0.30 (thiol)	75
SH-SBA <sup>f</sup>	$\text{SiO}_2$		Ordered Mesoporous	Powder Irregular rods	Hydrophilic	750	0.7	5.47	1.40 (thiol)	69
SH-KG <sup>g</sup>	$\text{SiO}_2$		Ordered Mesoporous	Powder Irregular particles	Hydrophilic	450	0.6	6.19	1.18 (thiol)	66
Chelex-100 <sup>g</sup>	Styrene-divinylbenzene		Not ordered Macroporous	Small particles	Hydrophobic	Macro	-	-	0.57 (iminodiacetic)	18
SQR <sup>g</sup>	Polyethylene polyamine		Not ordered Macroporous	Small beads	Hydrophobic	Macro	-	-	1.20 (dithiocarbamate)	80

<sup>a</sup> Specific surface area determined *via* the BET theory.

<sup>b</sup> Total pore volume at  $P/P_0 = 0.98$ .

<sup>c</sup> Pore diameter calculated from the desorption branch with the BJH method.

<sup>d</sup> Total amount of functionalities determined *via* a thiol titration.

<sup>e</sup> Mercury capacity of the various resins.

<sup>f</sup> Synthesized in this research.

<sup>g</sup> Commercially available.

X-ray diffraction measurement confirmed the molecular ordering of the SBA-15 and PMO based resins whereas the SH-KG was not ordered on a molecular level. Both diffractograms of SH-SBA and SH-PMO exhibited three clearly visible diffraction peaks indicating the (100), (110) and (200) reflections (Figure 5.4). This XRD pattern is very typical for materials with a 2D hexagonal structure with a  $P6mm$  space group.

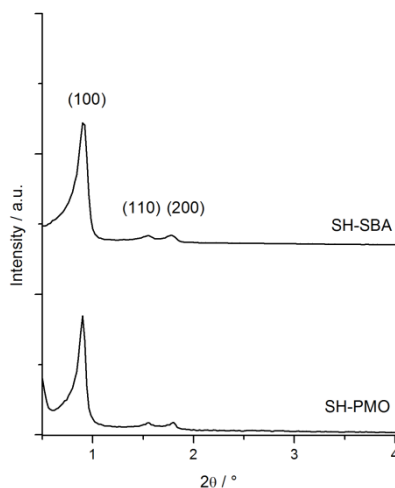


**Figure 5.4: X-ray diffraction patterns of the resins SH-SBA and SH-PMO.**

The total amount of reachable functionalities for the thiol containing materials was determined via a silver titration and is also presented in Table 5.1. The functionalised PMO material contained less thiol groups than the two silica materials. The interaction between the thiol group and the mercury atoms was for all the thiol containing materials a 1:1 ratio with the mercury. The mercury capacities of the various resins are presented in Table 5.1: the highest capacity was observed for SQR followed by SH-PMO, SH-SBA, SH-KG and Chelex-100. All thiol containing resins showed a mercury capacity above  $66 \text{ mg Hg g}^{-1}$  resin whereas Chelex-100 had a capacity of  $18 \text{ mg Hg g}^{-1}$  resin. The Chelex-100 and Sumichelate Q10R adsorbents are both macroporous polymers with a typically very low specific surface area and did not possess any ordering. Chelex-100 is a styrenedivinyln benzene polymer and contains iminodiacetate groups. This group can interact via its nitrogen and oxygen atoms with the mercury according to a tridentate interaction. The Sumichelate Q10R on the other



hand possesses a dithiocarbamate group which has a 1:2 ratio towards the mercury atoms.

### **5.3 Mercury DGT experiments with the resins**

The five resins are incorporated in the DGT probes. Therefore they are each included in a gel, *i.e.*, the resin gel. The procedures to prepare the gels and probe are described in the experimental section. Before performing the mercury speciation experiment in the field, laboratory controlled experiments are conducted with a prepared mercury solution. First the mercury in the bulk solution is determined. Afterwards, the experiments are conducted with the commonly used Chelex-100 and the other resins: SQR, SH-KG, SH-SBA and more importantly SH-PMO.

#### **5.3.1 Mercury concentrations in the bulk solution**

Mercury concentrations in the 10 L bulk solution were monitored each hour by sampling 5 mL of solution and appropriate dilution. The mercury concentration decreased by about 30% during the first 4 hours, most likely due to adsorption on the wall of the recipient, but after 4 hours it remained steady until the end of the experiment at a concentration of approximately 60 g L<sup>-1</sup>.

#### **5.3.2 Mercury accumulation on the Chelex-100 resin gel in a DGT**

Chelex-100 with iminodiacetic acid groups (see Table 5.1) competes efficiently with natural ligands for divalent and trivalent metal ions. It is reported<sup>4</sup> that in a DGT assembly, Chelex-100 is trapping at a continuous rate Ag, Al, Cd, Co, Cr, Cu, Fe, Mn, Ni, Pb and Zn from the aquatic system. In most natural aquatic systems, the capacity of the resin for these metals is high enough to avoid a decrease in the trapping rate. The adsorption efficiency of the Chelex-100 resin with regard to mercury is, however, controversial. Docekalova and Divis<sup>13</sup> compared the Hg pre-concentration of a DGT containing a Chelex-100 resin with one containing a Spheron-Thiol resin.<sup>14</sup> They concluded that they were able to assess ionic mercury, and labile mercury complexes with both resins, but apparently the Chelex-100 resin had less affinity for mercury

than the Spheron-Thiol one. Conversely, Cattani *et al.* reported only 50–58% recovery of the Hg from their solution using Chelex-100 as resin gel in the DGT, whereas 83–97% of recovery was obtained with the Spheron-Thiol resin.<sup>15</sup>

In our study, the Chelex-100 resin presents during the first 2 hours a fast accumulation of Hg, similar to the 4 other resins but after 4 hours the adsorption rate slows down (Figure 5.5), while this is not the case for the other resins.

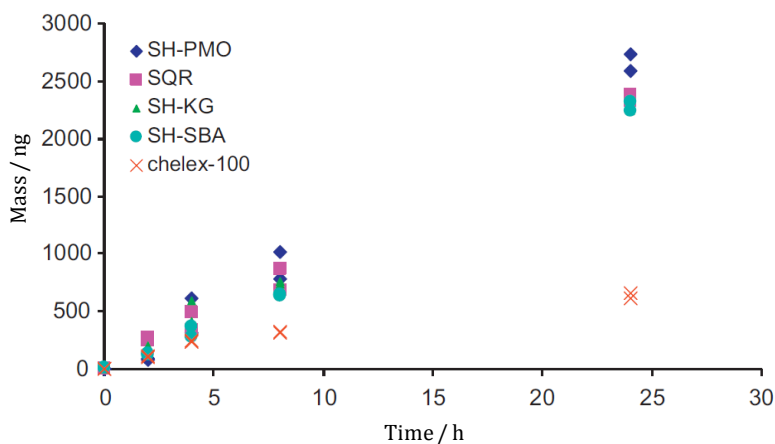


**Figure 5.5: Mercury uptake rate of different resin gels: SH-PMO, SH-SBA, SH-KG, SQR and Chelex-100.**

This phenomenon shows that the Chelex-100 resin has a lower affinity and capacity for Hg than the thiol based ones. It is possible that the iminodiacetate functionality causes this observed affinity. The Hard and Soft Acids and Bases theory of Pearson<sup>16</sup> clearly states that mercury atoms have more affinity for sulfur atoms than nitrogen or oxygen atoms which are present in the iminodiacetate functionality. The non-linear accumulation profile of Hg with time for the Chelex-100 resin makes it in this case impossible to use Fick's law for estimating the diffusion coefficient of Hg. This result is opposite to the one obtained by Docekalova and Divis<sup>13</sup>, but similar to the observations of Cattani *et al.*<sup>15</sup>

### 5.3.3 Mercury accumulation on SH-PMO, SH-SBA, SQR and SH-KG resin gels in a DGT

The 4 other resins all show a linear accumulation profile of mercury with time (Figure 5.5). Despite the fact that SH-PMO has the lowest amount of thiol groups per mass unit of material, it shows a similar accumulation efficiency with Hg. The diffusion coefficient in the agarose gel can be calculated with following formula:

$$\frac{M}{C_{Hg}} = \frac{DA t}{\Delta g}$$

with  $M$  is the accumulated mass of mercury;  $C_{Hg}$  is the mercury concentration in the bulk solution;  $D$  is the diffusion coefficient of Hg in agarose gel;  $A$  is the exposure area of the gel to the bulk solution;  $t$  is the deployment time;  $\Delta g$  is the thickness of the diffusive layer. When the accumulated mass of mercury ( $M$ ) is plotted as a function of time ( $t$ ), the angular coefficient of the curve equals:

$$k = \frac{DA t}{\Delta g}$$

This angular coefficient is calculated with a least squares linear regression (Excel software) through the data points. The diffusion coefficients for each thiol containing resin can then be calculated as:

$$D = \frac{k \Delta g}{A t}$$

Since for all the thiol containing resins the diffusion coefficients are quite similar, an average value is calculated together with its standard deviation. This average Hg diffusion coefficient in agarose at 20°C equals  $8.44 \pm 0.33 \times 10^{-6} \text{ cm}^2 \text{ s}^{-1}$ . The diffusion coefficient of Hg in water column is  $9.13 \times 10^{-6} \text{ cm}^2 \text{ s}^{-1}$  while a value of  $9.08 \pm 0.13 \times 10^{-6} \text{ cm}^2 \text{ s}^{-1}$  in agarose gel was reported by Docekalova and Divis.<sup>13</sup>

### 5.3.4 Field work results

DGT assemblies with the various resin gels tested in this study, were deployed in a water pond at the campus of Vrije Universiteit Brussel, for *in-situ* mercury

measurements in March 2011. Water samples and 12 eluted gel solutions obtained from the field work were analyzed by PSA 10.035 Millennium Merlin in Galahad mode, which means the cold vapor method was selected for low level Hg analysis (ppt level). The concentration of dissolved Hg in the water sample was  $0.0232 \pm 0.0093 \text{ g L}^{-1}$  and the DGT measured concentration was  $0.0176 \pm 0.0036 \text{ g L}^{-1}$ , which indicates that about 75% of mercury is present as labile species in this water pond. This labile Hg fraction is more dangerous for the micro-organisms, such as phytoplankton and microzooplankton living in this pond since the small size of that labile fraction (<10 nm) can easily pass the cell wall of those organisms. It will finally accumulate along the food chain and furthermore influence all organisms living in this small aquatic system.

## 5.4 Conclusions

Two laboratory synthesized mercaptopropyl nanoporous resins SH-PMO and SH-SBA together with three commercial available resins SQR, SH-KG and Chelex-100 were tested as the binding layer in the DGT technique for assessing labile Hg concentrations in this study. SH-PMO, SH-SBA, SQR and SH-KG resins showed high affinity with labile Hg due to high specific surface for binding Hg and the efficient functional thiol or dithiocarbamate groups, whereas Chelex-100 presented poor binding ability with Hg due to low specific surface and less efficient functional iminodiacetate groups. With these 4 efficient Hg binding resins, a slightly higher accumulation rate is observed for SH-PMO followed by SQR, SH-KG and SH-SBA. The Hg diffusion coefficient in agarose at 20°C was obtained by using these 4 resins as the binding layer in the DGT technique and the value of  $8.44 \pm 0.33 \times 10^{-6} \text{ cm}^2 \text{ s}^{-1}$  is comparable to the literature value of  $9.08 \pm 0.13 \times 10^{-6} \text{ cm}^2 \text{ s}^{-1}$ . DGT assemblies with these 4 resin gels determined the labile Hg concentration in the water pond of the campus and the result of  $0.0176 \pm 0.0036 \text{ g L}^{-1}$  is 75% of total Hg concentration in the same pond indicating the major part of Hg in this pond is labile and bioavailable species.

## 5.5 Experimental section

**Reagents and Materials.** Acrylamide solution (40%; pro analysi), N,N,N,N-tetraethylenediamine (99%; pro analysi), NaNO<sub>3</sub> (Suprapur) and thiourea were obtained from Merck. Agarose powder and Chelex-100 (200–400 mesh) were purchased at Biorad. Furthermore ammoniumpersulfate (10%, 0.1 g in 1 g of water), DGT cross-linker (DGT Research Ltd), durapore membrane filter (Millipore), hydrochloric acid (37%; Roth), 3-mercaptopropyl functionalised silica gel (200–400 mesh, Aldrich), mercury stock solution 1000 ppm (Alfa Aesar), MilliQ water (Millipore, >18 MΩ cm), 15 L PFA bucket (Nalgene), pH indicator paper (VWR), Sumichelate Q10R (Sumitomo, Osaka) were obtained. All reagents were used as received. Other reagents and solvents necessary are described in Chapter 4.

**Synthesis of 3-mercaptopropyl functionalised SBA-15 material.** The SBA-15 support and the anchoring of (3-mercaptopropyl)triethoxysilane was performed according to the procedures described in Chapter 4.

**Preparation of the thiol modified ethenylene-bridged PMO material.** The *trans* ethenylene-bridged precursor was synthesized prior to the preparation of the PMO material. The synthetic procedures are described in Chapter 3. Afterwards, the bromination and functionalisation with mercaptopropyl was executed by following the recipe explained earlier in Chapter 4.

**Preparation of the Diffusive Gradients in Thin films.** The DGT probes have been prepared by dr. Yue Gao (VUB) as described in the following sections.

**Diffusive gel.** An amount of 0.3 g agarose powder is diluted in 20 mL MilliQ water and the mixture is placed in a boiling water bath, covered and gently stirred until all the agarose is dissolved and the solution is immediately pipetted into two glass plates with a spacer separating the plates. After 1 hour of cooling down, the agarose gels are cut into 2.5 cm circles with a plexi-glass cutter.

**Resin gels.** Before including the different resins in the agarose gel, Sumichelate Q10R beads are grinded into a fine powder of about 200-400 mesh, washed in 5% thiourea

and rinsed three times with MilliQ water. The water is removed by filtration and the cleaned resin is ready to be included in a gel, which results in a resin gel. All other resins, Chelex-100, SH-KG, SH-SBA and SH-PMO were also cleaned in the same way. For the Sumichelate Q10R, a total amount of 3 g of resin is added to 10 mL gel solution (15% acrylamide, 0.3% DGT cross-linker) and this solution is mixed well. For the other resins, the optimal amount has to be determined to obtain a uniform distribution of the resin in the gel. Then 50  $\mu\text{L}$  10% ammoniumpersulfate solution and 15  $\mu\text{L}$  N,N,N,N-tetraethylenediamine (TEMED) are added. The solution is mixed well and poured between two glass plates with a spacer separating the plates. The assembly is placed in an oven at 45°C for 1 hour, and then hydrated in Milli Q water for at least one day until use.

**Assembling DGT units for solution deployment.** Resin gels are cut into 2.5 cm circles with a plexi-glass gel cutter. The resin gel is mounted on the moulding base with the resin side face up. Then the diffusive gel is placed on top of the resin gel and covered by a Millipore Durapore membrane filter (HVLP). The cap is then placed on the moulding base and pressed down to the bottom of the base.

**DGT performance test experiment.** Performance tests with the various DGT assembly types were carried out in a 10 L mercury solution of 100  $\mu\text{g L}^{-1}$  containing 0.01 M  $\text{NaNO}_3$ . During the experiment, the accurate Hg concentration in the solution was monitored and changes were taken into account for the comparison with the DGT derived mercury concentration. The pH of the solution was adjusted to around 5. Eight DGT assemblies all facing down to the solution were plugged into the holes of a round Teflon plate. For each type of resin used in the DGTs, a Teflon plate was inserted in 100  $\mu\text{g L}^{-1}$  Hg solution, which was continuously stirred. After 2, 4, and 8 up to 24 hours, 2 of the DGT assemblies were removed of the solution. The resin gels were extracted with 2 mL of 5% thiourea. Since thiourea has a strong affinity with mercury, the Hg extraction with thiourea was made in a 30% KOH solution.

**Field deployment of DGT units in a local water pond.** A total of 12 DGT assemblies with four various resin gels were deployed in a local water pond inside the university campus for 2 days. Simultaneously, several water samples were taken from the pond

and after filtration stored in a 150 mL acid washed Teflon bottle with 0.5% HCl. DGT assemblies were removed from the pond after two days deployment. The resin gels were extracted with 2 mL of 5% thiourea.

**Mercury analysis.** All mercury solutions (standards, test solutions, resin gel extracted solutions and water samples) were analyzed by a PSA 10.035 Millennium Merlin AA instrument and using the EPA cold vapor method. The Millennium Merlin AA system was developed to be compliant with EPA Cold Vapor methods stipulating the use of atomic absorption for the determination of mercury at low levels.

**Determination of thiol functionalities.** The amount of reachable thiol functionalities was determined by silver titration.<sup>17,18</sup> The procedure is described in Chapter 4.

**Characterisation of the solids.** The nitrogen sorption isotherms were recorded on Belsorp Mini II equipment at -196°C. The samples were pretreated at 120°C while degassing. CHNS elemental analysis was executed by the *Centre National de la Recherche Scientifique* (CNRS, France). X-ray diffraction was performed with an ARL X'tra X-ray diffractometer of Thermo Scientific equipped with a Cu K $\alpha$ 1 tube and a Peltier cooled lithium drifted silicon solid stage detector.

## 5.6 References

1. H. Emons, in *Handbook of Elemental Speciation: Techniques and Methodology*, eds. R. Cornelis, H. Crews, J. Caruso and K. Heumann, John Wiley & Sons, Ltd, West Sussex, England, 2003, pp. 7-22.
2. R. Cornelis, H. Crews, J. Caruso and K. Heumann, in *Handbook of Elemental Speciation: Techniques and Methodology*, eds. R. Cornelis, H. Crews, J. Caruso and K. Heumann, John Wiley & Sons, Ltd, West Sussex, England, 2003, pp. 1-5.
3. W. Davison and H. Zhang, *Nature*, 1994, **367**, 546-548.
4. DGT Research Ltd. (2003) DGT-for measurements in water, soils and sediments: Users guide for DGT technique. <http://www.dgtresearch.com>. June 2013.
5. H. Zhang and W. Davison, *Analytical Chemistry*, 1995, **67**, 3391-3400.
6. H. Zhang and W. Davison, *Analytica Chimica Acta*, 1999, **398**, 329-340.
7. C. D. Luidier, J. Crusius, R. C. Playle and P. J. Curtis, *Environmental Science & Technology*, 2004, **38**, 2865-2872.
8. S. Meylan, N. Odzak, R. Behra and L. Sigg, *Analytica Chimica Acta*, 2004, **510**, 91-100.
9. J. Gimpel, H. Zhang, W. Davison and A. C. Edwards, *Environmental Science & Technology*, 2003, **37**, 138-146.
10. M. C. Alfaro-De la Torre, P. Y. Beaulieu and A. Tessier, *Analytica Chimica Acta*, 2000, **418**, 53-68.
11. M. R. Sangi, M. J. Halstead and K. A. Hunter, *Analytica Chimica Acta*, 2002, **456**, 241-251.
12. A. J. Peters, H. Zhang and W. Davison, *Analytica Chimica Acta*, 2003, **478**, 237-244.
13. H. Docekalova and P. Divis, *Talanta*, 2005, **65**, 1174-1178.
14. Z. Slovak, M. Smrz, B. Docekal and S. Slovakova, *Analytica Chimica Acta*, 1979, **111**, 243-249.
15. I. Cattani, S. Spalla, G. M. Beone, A. A. M. Del Re, R. Boccelli and M. Trevisan, *Talanta*, 2008, **74**, 1520-1526.
16. R. G. Pearson, *Journal of the American Chemical Society*, 1963, **85**, 3533-3539.
17. A. I. Vogel, *A text-book of quantitative inorganic analysis including elementary instrumental analysis*, Harlow : Longman, London, 1961.
18. E. B. Sandell and I. M. Kolthoff, *Textbook of quantitative inorganic analysis*, Macmillan Company, New York, 1952.



## **6 The development of nitrogen containing PMO as adsorbent for CO<sub>2</sub>**

The adsorption of CO<sub>2</sub> on amine modified Periodic Mesoporous Organosilicas is investigated in this chapter of this dissertation. An ethylene-bridged PMO is used as starting material for the development of a carbon dioxide sequestration material and the PMO material is modified with a wide range of diamines and polyamines.

A variety of dangling N-containing functionalities, *i.e.*, diaminobutane, diaminohexane, diaminododecane, diethylenetriamine and tetraethylenepentamine as nucleophiles in a substitution reaction is used. The CO<sub>2</sub> adsorption capacity of these materials is probed and compared with amine functionalised SBA-15 material, in an effort to reach the maximal CO<sub>2</sub>/N ratio of 0.5 when using dry conditions in a chemisorption process. The materials showed good CO<sub>2</sub> adsorption behaviour and this maximum amine efficiency value has been approximated by the PMO material modified with diaminododecane.

Adsorption experiments were partially performed by drs. Isabelle Ascoop at Ottawa University in collaboration with Prof. dr. Abdelhamid Sayari.

The results presented in this chapter are published as  
Els De Canck, Isabelle Ascoop, Abdelhamid Sayari and Pascal Van Der Voort, *Physical Chemistry Chemical Physics*, **2013**, 15, 9792-9799.

## **6.1 Introduction**

The amount of reports published on the matter of carbon dioxide PMO-based adsorbents is rather limited<sup>1-5</sup> and moreover, no reports were published on CO<sub>2</sub> adsorption by the use of post-modified PMO materials. The major advantage of using a post-synthesis modification step to introduce nitrogen functionalities is the retention of the mesoporous structure of the pristine PMO material with high specific surface area. Furthermore it is known that hydrophobic groups, such as ethenylene bonds, on the surface of the adsorbent improve the adsorption of CO<sub>2</sub> considerably.<sup>6</sup>

In this research, ethenylene-bridged PMO materials were modified to obtain amine functionalities grafted on the C-C backbone of the PMO material. The anchorage of functional groups on the organic bridge of the PMO drastically improves the chemical and structural stability of the material.<sup>7</sup>

Therefore substituents with different amounts of amines (both primary and secondary) and varying length of carbon chains are used in this post-synthesis modification procedure and are used as adsorbents for CO<sub>2</sub>. The synthesis and characterisation of these materials is discussed first, followed by an investigation of the CO<sub>2</sub> chemisorption properties under dry conditions. The focus is placed upon the carbon dioxide sorption at low pressures up to atmospheric pressure and a comparison with an amino functionalised silica material SBA-15, commonly used in the literature, is presented.

## **6.2 Modification of the PMO materials with amine functionality**

The ethenylene-bridged PMO materials (abbreviated as PMO) are modified with a series of amines to obtain dangling -NH<sub>2</sub> and -NH- functionalities which are anchored with a stable C-C bond to the PMO framework. It has been observed that the anchoring to the organic bridges of PMO materials results in an increase in stability compared to the usual grafting procedure *via* the silanol groups.<sup>7</sup> A bromination step<sup>7,8</sup> in gaseous phase on the ethene bond is performed first. This material, denoted as Br-PMO, is

subsequently used as a substrate for a nucleophilic substitution reaction as shown schematically in Figure 6.1.

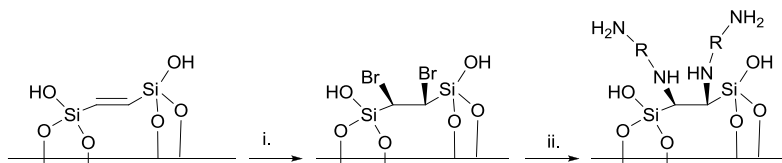


**Figure 6.1: Schematic overview of the modification performed on the ethenylene-bridged PMO material: i. bromination of double bond; ii. substitution with  $\text{NH}_2\text{-R-NH}_2$  where R represents an aliphatic carbon chain without or with additional secondary amines.**

Several nucleophiles are used in this reaction such as diaminobutane (DAB), diaminoethane (DAH), diaminododecane (DADD), diethylenetriamine (DETA) and tetraethylenepentamine (TEPA) to obtain dangling functionalities with different properties, *i.e.*, a variation in chain length, total nitrogen amount, primary and secondary amines. An overview of the obtained materials is presented in Figure 6.2 together with the abbreviations which will be used throughout the chapter. The  $\text{S}_{\text{N}}2$  reaction with DAH as nucleophile is used as an example and is discussed in depth.

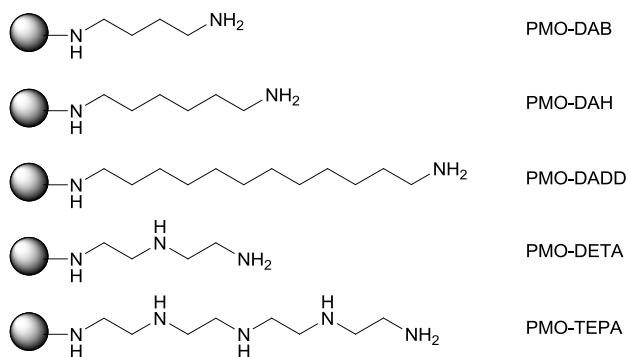


**Figure 6.2: Summary of the modified PMO materials with abbreviations.**

An optimization of the synthetic conditions for the substitution reaction with DAH is performed using different reaction temperatures (room temperature, 50 and 150 °C) and several reaction times (1, 3, 6, 20 hours). The total amount of amine functionalities and thus the success of functionalisation is probed *via* the nitrogen content obtained with elemental analysis. The data are presented in Table 6.1. The

materials are denoted as PMO-*nucleophile-x-y* where *nucleophile* represents the reagent used in the substitution, *x* the reaction temperature (°C) and *y* the reaction time (hours).

**Table 6.1: Overview of the nitrogen content of the PMO materials modified with the diamines: diaminohexane (DAH), diaminobutane (DAB) and diaminododecane (DADD) when using different synthetic conditions.**

	N w% <sup>a</sup>	N mmol g <sup>-1</sup> <sup>b</sup>
PMO-DAH-rt-1	1.34	0.96
PMO-DAH-rt-3	2.02	1.44
PMO-DAH-rt-6	1.36	0.97
PMO-DAH-rt-20	1.98	1.41
PMO-DAH-50-1	1.36	0.97
PMO-DAH-50-3	2.02	1.44
PMO-DAH-50-6	2.05	1.46
PMO-DAH-50-20	1.96	1.40
PMO-DAH-150-1	1.65	1.18
PMO-DAH-150-3	1.95	1.39
PMO-DAH-150-6	1.69	1.21
PMO-DAH-150-20	1.64	1.17
PMO-DAB-rt-3	2.54	1.81
PMO-DADD-rt-3	0.46	0.33

<sup>a</sup> Determined *via* elemental analysis. <sup>b</sup> Calculated from the N w%.

It can be inferred from Table 6.1 that the optimal synthesis conditions to maximize the grafting of the diamine are *3 hours* reaction time at *room temperature*. These conditions are also applied for the grafting of the reagents DAB and DADD. Their loading is shown in Table 6.1. The substitution reaction with a nucleophile containing a short carbon chain, *i.e.*, 4 carbons of diaminobutane clearly results in a higher N-content than the nucleophile with the dodecane chain. Probably the diffusion of DADD with its long carbon chain in the pores of the PMO is limited during the functionalisation reaction. The long alkyl chains of course also add to the weight of the adsorbent resulting in a lower relative N content. Also polyamines are used as

nucleophile in addition to the three diamines described above. Table 6.2 summarizes the nitrogen content of the different materials obtained when using diethylenetriamine and tetraethylenepentamine as reagents.

**Table 6.2: Overview of the nitrogen content of the PMO materials modified with diethylenetriamine (DETA) and tetraethylenepentamine (TEPA) when using different synthetic conditions.**

	N w% <sup>a</sup>	N mmol g <sup>-1</sup> <sup>b</sup>
PMO-DETA-rt-3	2.71	1.93
PMO-DETA-rt-5	3.47	2.48
PMO-DETA-rt-24	2.42	1.73
PMO-DETA-100-3	2.46	1.75
PMO-DETA-100-5	4.00	2.86
PMO-DETA-100-24	1.14	0.81
PMO-TEPA-rt-3	2.20	1.57
PMO-TEPA-rt-5	4.25	3.03
PMO-TEPA-rt-24	5.41	3.86
PMO-TEPA-100-3	4.25	3.03
PMO-TEPA-100-5	4.60	3.29
PMO-TEPA-100-24	3.52	2.51

<sup>a</sup> Determined *via* elemental analysis. <sup>b</sup> Calculated from the N w%.

**Table 6.3: Br content, N content and substitution yield of PMO-DAB-rt-3, PMO-DAH-rt-3, PMO-DADD-rt-3, PMO-DETA-rt-5 and PMO-TEPA-rt-5.**

	Br mmol g <sup>-1</sup> <sup>a</sup>	N mmol g <sup>-1</sup> <sup>b</sup>	Substitution yield %
PMO-DAB-rt-3	4.11	1.81	44
PMO-DAH-rt-3	2.01	0.60	30
PMO-DADD-rt-3	4.11	0.33	8
PMO-DETA-rt-5	3.60	2.48	69
PMO-TEPA-rt-5	4.40	3.04	69

<sup>a</sup> Determined gravimetrically. <sup>b</sup> Determined *via* elemental analysis.

The same denotation is employed as for the diamine modified PMO materials. In case of the DETA and TEPA functionalisation, the optimal grafting conditions are 5

hours at 100 °C for both type of materials. A selection of five CO<sub>2</sub> sorbents is made for further characterisation and actual sorption experiments. An overview of the selected materials is presented in Table 6.3. Furthermore, a summary of the bromine and nitrogen content together with the substitution yield is also presented.

### 6.3 *Materials characterisation*

The pristine, brominated and amine modified PMO materials are analyzed with various characterisation techniques. Again, the material modified with DAH is used as an example throughout the discussion. Similar results are obtained for the samples PMO-DAB, PMO-DADD, PMO-DETA and PMO-TEPA but are not shown. Nitrogen sorption experiments are performed to evaluate the mesoporosity of the materials. Figure 6.3 shows the typical type IV isotherms for mesoporous materials according to the IUPAC classification and the sharp capillary condensation step that indicates the presence of uniform pores. This results in a narrow pore size distribution (Figure 6.3; right). The physical properties of the materials are presented in Table 6.4. As can be seen, materials with relatively large specific surface areas are obtained. A decrease in the  $S_{\text{BET}}$ ,  $V_p$  and  $d_p$  values indicate the presence of functionalities inside the pores. However, this decoration of the pore wall does not influence the mesoporosity of the materials and no pore blocking is observed for these materials. Furthermore, Table 6.4 also presents the pristine SBA-15 material and its modified variant. *Via* a covalent anchoring or grafting procedure, (3-aminopropyl)triethoxysilane is attached to the surface of an SBA-15 material, thus obtaining a silica material with amine functionalities. As can be noticed a large decrease of the specific surface area (813 to 294 m<sup>2</sup> g<sup>-1</sup>) is observed and also the pore volume and pore diameter of SBA-15-APTES are significantly smaller than the pristine SBA-15 material, suggesting a successful anchoring of the functionality. A functionalisation degree of 2.37 w% N *via* elemental analysis or 1.20 mmol N per gram material is obtained.

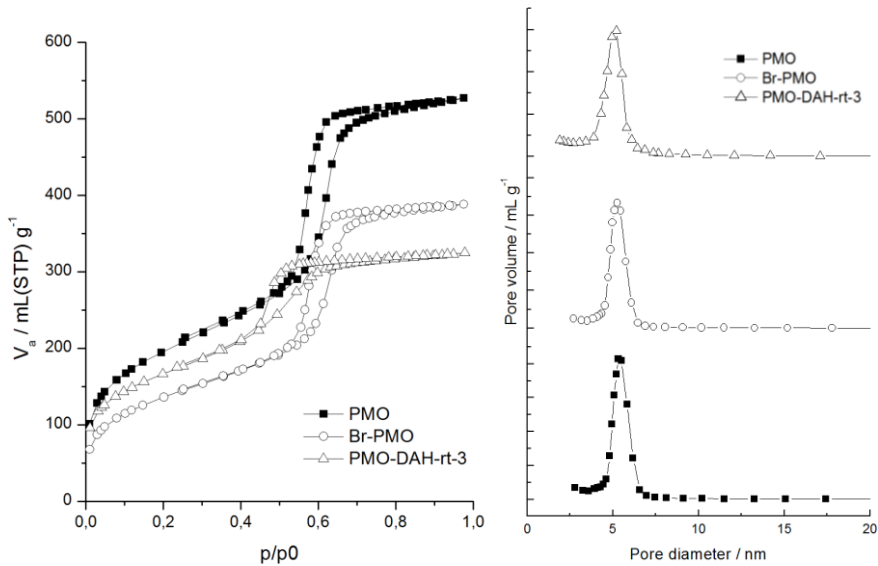


**Figure 6.3:** (left) Representative nitrogen sorption isotherms of the pristine (PMO), brominated (Br-PMO) and amine modified PMO (PMO-DAH-rt-3) materials. (right) Pore size distributions of PMO, Br-PMO and PMO-DAH-rt-3.

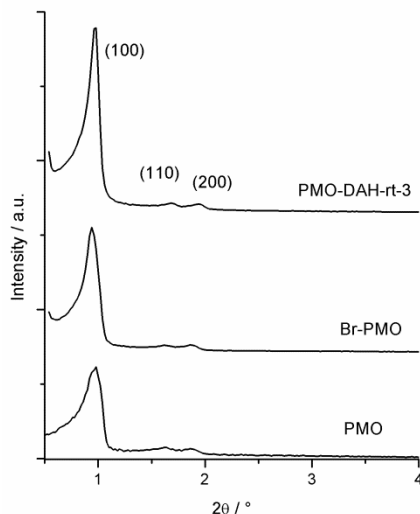
**Table 6.4:** Physical properties of the PMO and SBA-15 materials studied in this research.

	$S_{\text{BET}}^{\text{a}}$	$V_{\text{p}}^{\text{b}}$	$d_{\text{p}}^{\text{c}}$
	$\text{m}^2 \text{ g}^{-1}$	$\text{mL g}^{-1}$	nm
Pristine PMO	759	0.92	5.32
Br-PMO	578	0.73	5.25
PMO-DAB-rt-3	368	0.42	4.39
PMO-DAH-rt-3	449	0.56	5.10
PMO-DADD-rt-3	450	0.46	5.03
PMO-DETA-rt-5	379	0.47	4.14
PMO-TEPA-rt-5	530	0.56	4.54
SBA-15	813	0.89	6.44
SBA-15-APTES	294	0.41	5.24

<sup>a</sup> Determined *via* the BET equation. <sup>b</sup> Determined at  $P/P_0 = 0.98$ . <sup>c</sup> Calculated from the desorption branch using the BJH method.

Powder x-ray diffraction patterns (Figure 6.4) clearly show the (100) reflections as well as the second-order reflections (110) and (200) for the pristine PMO material.

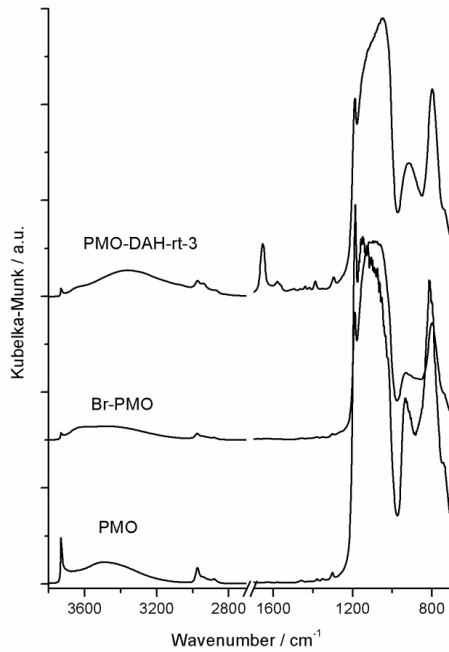
These well-resolved signals originate from the  $P6mm$  space group and this 2D-hexagonal ordering is maintained during the different functionalisation steps.



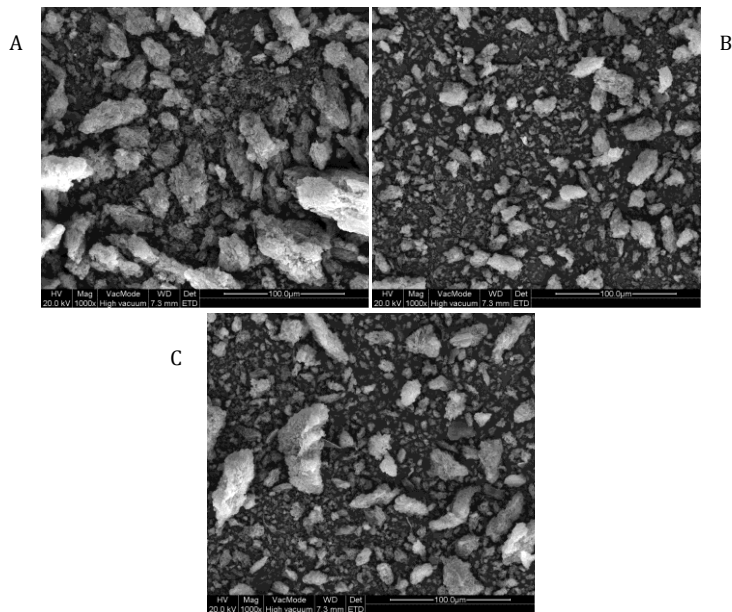
**Figure 6.4: X-ray diffraction patterns of PMO, Br-PMO, PMO-DAH-rt-3.**

Although the nitrogen contents obtained *via* elemental analysis already indicate a successful substitution reaction, further confirmation is obtained by infrared spectroscopy experiments (Figure 6.5). The DRIFT spectra of the pristine PMO and the brominated PMO clearly show the signals originating from the ethene bridges and the inorganic silica framework. Signals at 2974, 1628, 1602 and 934  $\text{cm}^{-1}$  indicate the trans C=C bond and large bands in the region of 1150-800  $\text{cm}^{-1}$  and the distinct narrow signal at 3731  $\text{cm}^{-1}$  originates from the siloxanes and silanols of the silica matrix, respectively. A few bands from the template P123 are still visible in the region 1600-1300 and at 2881  $\text{cm}^{-1}$  originating from the polyethylene oxide and polypropylene oxide moieties as the acetone extraction only removes ca. 95% of the template.<sup>9</sup> After functionalisation with DAH, an intense vibration at 1640  $\text{cm}^{-1}$  arises indicating the presence of primary amines. More intense signals in the region at 1400  $\text{cm}^{-1}$  are also observed due to the addition of extra -C-H and -C-C- stretches which are part of the dangling carbon chain of the anchored DAH. Furthermore, an enlargement of the signal at 3800-2700  $\text{cm}^{-1}$  towards 3350  $\text{cm}^{-1}$  can be explained by the presence of -NH<sub>2</sub> and -NH- moieties.





**Figure 6.5:** Infrared spectroscopy (DRIFT) of the pristine (PMO), brominated (Br-PMO) and amine modified PMO (PMO-DAH-rt-3) materials. For clarity, the region between 2750 and 1750 cm<sup>-1</sup> is not represented in the figure.



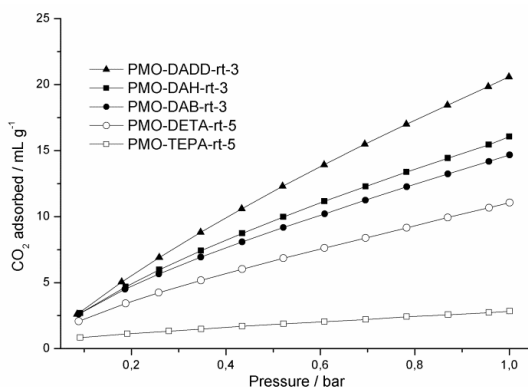
**Figure 6.6:** SEM images of (A) PMO; (B) Br-PMO; (C) PMO-DAH-rt-3.

Figure 6.6 shows the scanning electron microscope (SEM) images of the pristine PMO material and the solids obtained after bromination and further functionalisation with diaminoethane. The three images show irregularly shaped particles.

## 6.4 CO<sub>2</sub> adsorption experiments

The presence of amine functionalities enhances the carbon dioxide adsorption capacity. This has been demonstrated for the first time by Tsuda *et al.*<sup>10,11</sup> in 1992 for amorphous silica materials and later on for an amine functionalised mesoporous silica<sup>12</sup> in 1995. Thus an investigation of the CO<sub>2</sub> adsorption behavior of the materials functionalised with different amines is performed. CO<sub>2</sub> isotherms are recorded at 0 °C and the results are presented in Figure 6.7.

The isotherms clearly show a distinct trend. More CO<sub>2</sub> is adsorbed on the materials with a low nitrogen content. For the diamines, the following sequence can be noted: PMO-DADD > PMO-DAH > PMO-DAB which is the reverse of the functionalisation degree. The same phenomenon is observed for the materials modified with polyamines: PMO-DETA > PMO-TEPA. These isotherms show the low pressure affinity of the CO<sub>2</sub> molecules at 0°C and do not give the total capacity of the material.



**Figure 6.7:** CO<sub>2</sub> adsorption isotherms of the PMO materials modified with the diamines DAB, DAH, DADD and the polyamines DETA and TEPA. Adsorption experiments were performed at low pressure at 0°C.

The long chain diamine (DADD) adsorbs the most CO<sub>2</sub> at low pressures. Furthermore, these isotherms mainly reflect the physical adsorption of CO<sub>2</sub>. It is also interesting to know the chemical adsorption possibilities of these materials.

It is generally accepted for solutions that the acidic CO<sub>2</sub> molecules react chemically with the amine moieties (primary and secondary) *via* the formation of a zwitterion and subsequently an acid-base reaction with the ultimate formation of a carbamate ion when using dry CO<sub>2</sub> gas. This can be written down as equation 1 and 2 for primary and secondary amines, respectively:



The reaction mechanism was first introduced by Caplow<sup>13</sup> and prescribes that every molecule of the carbon dioxide stoichiometrically requires two amine functionalities in order to be chemically adsorbed to the solid.

**Table 6.5: CO<sub>2</sub> adsorption analysis results for the amine functionalised PMO and SBA-15 materials.**

	PMO-DAB-rt-3		PMO-DAH-rt-3		PMO-DADD-rt-3	
	w%	mmol g <sup>-1</sup>	w%	mmol g <sup>-1</sup>	w%	mmol g <sup>-1</sup>
N <sup>a</sup>	2.54	1.81	0.84	0.60	0.46	0.33
CO <sub>2</sub> <sup>b</sup>	0.70	0.16	0.58	0.13	0.60	0.14
CO <sub>2</sub> /N	0.09		0.22		<b>0.42</b>	

	PMO-DETA-rt-5		PMO-TEPA-rt-5		SBA-15-APTES	
	w%	mmol g <sup>-1</sup>	w%	mmol g <sup>-1</sup>	w%	mmol g <sup>-1</sup>
N <sup>a</sup>	3.47	2.48	4.25	3.04	2.37	1.20
CO <sub>2</sub> <sup>b</sup>	1.09	0.25	1.28	0.29	0.27	0.16
CO <sub>2</sub> /N	0.10		0.10		0.16	

<sup>a</sup> Determined *via* elemental analysis. <sup>b</sup> Determined *via* TGA analysis.

Therefore the maximum molar CO<sub>2</sub>/N ratio is 0.5. This ratio is also known as the amine efficiency of a material and it reflects how the material approximates its theoretical capacity. Furthermore it is a good measure to compare the uptake of CO<sub>2</sub> by materials functionalised with different amines.

Although the carbamate species has been observed by various authors,<sup>14-16</sup> some discussion is still on-going concerning the exact species on the surface during CO<sub>2</sub> adsorption, depending on the conditions used, such as carbonates and bicarbonates.<sup>17</sup> However in this discussion, we will only take into account equation 1-2 and the formation of carbamate species. Support for this assumption will be provided within this discussion (*vide infra*).

Further investigation of the CO<sub>2</sub> adsorption capacity and more importantly, amine efficiency is performed with CO<sub>2</sub> adsorption experiments *via* thermogravimetric analysis. First the materials were activated *via* a thermal pretreatment. Next, the amine modified PMO materials were exposed to a 5% CO<sub>2</sub> gas flow at atmospheric pressure at 25 °C. By using these conditions, only chemical adsorption of the CO<sub>2</sub> on the amine functions is possible and one can neglect physical adsorption.<sup>18</sup> Table 6.5 presents the obtained results for the SBA-15-APTES materials and the PMO materials functionalised with the diamines and polyamines. These results of the amine functionalised PMO materials confirm the trends observed in the CO<sub>2</sub> isotherms and the CO<sub>2</sub>/N ratio of the materials functionalised with DADD even approximates the maximum value of 0.50, reachable under dry conditions *via* chemisorption. For the other materials, lower values are obtained. PMO-DAH possesses a slightly higher amine efficiency than SBA-15-APTES (0.22 and 0.16 respectively) whereas PMO-DAB, PMO-DETA, PMO-TEPA exhibit more or less the same CO<sub>2</sub>/N ratio (0.09-0.10). Similar amine efficiency values were reported in the literature for SBA-15<sup>17, 19, 20</sup> materials functionalised *via* grafting of an amine functionality.

This rather low amine efficiency of the amine modified PMO materials can be explained by observations made by several authors.<sup>21-24</sup> As stated by equation 1 and 2, in order to chemically adsorb CO<sub>2</sub> using dry reaction conditions, two amine moieties per CO<sub>2</sub> are necessary, thus indicating that the amines must be close to each other so

that they are able to interact with the same CO<sub>2</sub> molecule. However, if a high amount of amines are too close, hydrogen bonding can occur with unreacted amines which deactivates these moieties for CO<sub>2</sub> adsorption (Figure 6.8) and therefore decreases the CO<sub>2</sub> adsorption capacity significantly.

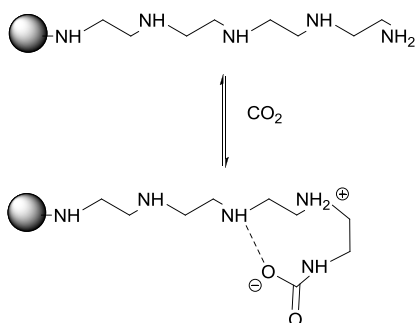


**Figure 6.8: Reaction mechanism: chemical adsorption of CO<sub>2</sub> on the PMO modified with TEPA. Scheme based on reference 21.**

Also hydrogen bonding between the amines and silanol groups of the PMO framework can occur, making the amines unavailable for CO<sub>2</sub> sorption.<sup>24</sup> This is more likely for the C<sub>4</sub> and C<sub>6</sub> alkyl chains than for the C<sub>12</sub> alkyl chain, in the latter case the hydrophobic interaction between the chains can prevent the chain from folding back to the surface. The ethenylene bridged PMO material used in this work contains a relatively large amount of silanol groups due to a lower condensation degree and the template removal with acetone.<sup>25</sup>

The hydrogen bonding and its direct influence on the CO<sub>2</sub>/N ratio is visible for the PMO materials modified with DAB, DETA and TEPA. The high nitrogen loading for the three samples results in the close proximity of the nitrogen atoms.

Furthermore the addition of secondary amines does not spectacularly increase the adsorption of CO<sub>2</sub>. It is reported that secondary amines possess a lower adsorption reactivity in comparison with primary amines.<sup>26</sup> Materials with a lower amount of nitrogen, *i.e.*, the samples functionalised with DAH and especially DADD, exhibit better CO<sub>2</sub>/N ratios which suggest that the hydrogen bonding phenomenon is less present with these amine modified PMO materials.

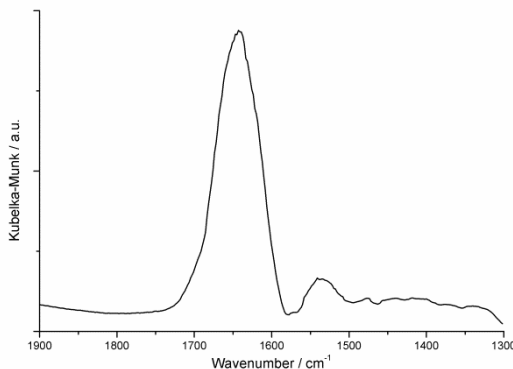


**Figure 6.9: Infrared spectroscopy (DRIFT) of the amine modified PMO (PMO-DAH-rt-3) material after equilibration with pure CO<sub>2</sub>. For clarity, only the region between 1900 and 1750 cm<sup>-1</sup> is represented in the figure.**

The CO<sub>2</sub> adsorption mechanism presented in equation (1) and (2) is confirmed by infrared measurements. The material PMO-DAH-rt-3 was allowed to come in contact with pure CO<sub>2</sub> gas inside the DRIFT cell. The spectrum of PMO-DAH-rt-3 was used as background in order to record only the changes attributed to the CO<sub>2</sub> adsorption. This method is described in literature.<sup>14</sup> The spectrum clearly shows vibrations concerning CO<sub>2</sub> adsorption. A strong vibration band at 1642 cm<sup>-1</sup> is present next to some weaker bands in the region of 1600-1400 cm<sup>-1</sup> probably originating from the -NH<sub>3</sub><sup>+</sup> and carbamate species, respectively.<sup>14, 15, 27</sup>

## 6.5 Conclusions

In this research several modified PMO materials are prepared. The pristine PMO materials possess an ethene bond which can be functionalised. This modification consists of two steps: (1) the bromination of the double bond, followed by (2) the substitution of the bromine with diamines or polyamines. Several amine reagents are used such as: diaminobutane, diaminohexane, diaminododecane, diethylenetriamine and tetraethylenepentamine and different reaction conditions are probed. This results in different types of amine modified mesoporous materials and the CO<sub>2</sub> adsorption capacity and CO<sub>2</sub>/N ratio is examined. It is observed that the modification with diaminododecane (DADD) results in almost the theoretical maximum adsorption efficiency (0.5) despite the relatively low amine loading of 0.33 mmol g<sup>-1</sup> and appears to be a good candidate for CO<sub>2</sub> chemisorption under dry conditions. For these amine functionalised PMO materials, grafting with nitrogen-rich chains, such as DETA and TEPA, does not result in an increased adsorption.

## 6.6 Experimental section

**Chemicals.** (3-aminopropyl)-triethoxysilane (APTES; 98%) was purchased from ABCR. Diaminobutane (DAB; 99%), diaminohexane (DAH; 98%), diaminododecane (DADD; 98%), diethylenetriamine (DETA; 99%) and tetraethylenepentamine (TEPA; technical grade) were acquired from Sigma-Aldrich. Toluene (Rotipuran, >99,5% p.a.) and dimethylformamide (DMF; >99.5%) were obtained from Carl Roth. Other used reagents are described in Chapter 4. All reagents and solvents were used as received.

**Synthesis and bromination of the ethenylene-bridged PMO material.** The synthesis of the ethenylene-bridged precursor, the ethenylene-bridged PMO material and surfactant extraction was performed according to the procedure described in Chapter 3. In Chapter 4, a description is given of the bromination of the double bonds.

**Modification of the brominated ethenylene-bridged PMO.** After bromination of the double bonds of the ethenylene-bridged PMO material, the bromine was substituted with one of the following reagents: diaminobutane (DAB), diaminohexane (DAH), diaminododecane (DADD), diethylenetriamine (DETA) and

tetraethylenepentamine (TEPA). In a typical synthesis a total amount of 0.1 g of brominated ethylene-bridged PMO material was mixed with the amine (5 mol equivalents with regard to the amount of bromine) and 50.0 mL of DMF under inert atmosphere. The reaction mixture was stirred for a certain amount of time at different reaction temperatures. The exact reaction conditions were specified in Table 6.1 and Table 6.2. Finally, the sample was washed thoroughly with DMF, distilled water and acetone and the solids were dried under vacuum at 90 °C. The materials were denoted as PMO-*nucleophile-x-y* where *nucleophile* represents the reagent used in the substitution, *x* the reaction temperature (°C) and *y* the reaction time (hours).

**Synthesis and amine functionalisation of SBA-15.** The well-known SBA-15 material was synthesized according to the procedure described in Chapter 4. The material was functionalised with the silane APTES. In a typical synthesis, an amount of 2 g SBA-15 and 60 mL of toluene was added to a flask. Next, 5.18 mL of APTES was added and the mixture was refluxed during 24 h. Afterwards the solids were filtered and washed thoroughly with toluene and acetone. Finally, the material, SBA-15-APTES, was vacuum dried at 90°C.

**Characterisation.** Nitrogen sorption experiments were performed on a Tristar 3000 (Micromeritics) at -196°C. Samples were pre-treated at 120°C for 16 hours while degassing. X-ray diffraction (XRD) patterns were recorded on an ARL X'TRA Diffractometer (Thermo Scientific) equipped with a Cu K $\alpha$  tube and a Peltier cooled lithium drifted silicon solid stage detector. Diffuse reflectance infrared fourier transform (DRIFT) spectroscopy was performed on a hybrid IR-Raman spectrophotometer, the Nicolet 6700 (Thermo Scientific) with a liquid nitrogen cooled MCT-A detector, using a Graseby Specac diffuse reflectant cell. Measurements were performed in vacuum at 120°C. DRIFT measurements were also used to investigate the species formed after the adsorption process. KBr together with the PMO material were used as background in order to record the changes due to the adsorption of the CO<sub>2</sub>. The material was allowed to come into contact with pure CO<sub>2</sub> gas inside the DRIFT cell until equilibrium was reached and subsequently a spectrum was recorded. Elemental analysis (CHN) was performed on a Thermo Flash 2000 elemental analyzer. During the measurement, a V<sub>2</sub>O<sub>5</sub> catalyst was used.



**CO<sub>2</sub> adsorption experiments.** CO<sub>2</sub> isotherms were obtained on a Tristar 3000 (Micromeritics) at 0°C. Samples were pre-treated at 140°C for 16 hours while degassing. The chemisorption experiments were performed on a TGA Q500 instrument, where a thermogravimetric analysis was used to record the CO<sub>2</sub> adsorption. First, a pretreatment step was required which involves 2 h heating at 120°C under inert atmosphere. This was followed by exposure of the sample for 2 h at 25°C to a gas flow containing 5% of CO<sub>2</sub> in N<sub>2</sub>.

## 6.7 References

1. A. Comotti, S. Bracco, P. Valsesia, L. Ferretti and P. Sozzani, *Journal of the American Chemical Society*, 2007, **129**, 8566-8576.
2. Y. D. Tang and K. Landskron, *Journal of Physical Chemistry C*, 2010, **114**, 2494-2498.
3. S. Y. Bai, J. Liu, J. S. Gao, Q. H. Yang and C. Li, *Microporous and Mesoporous Materials*, 2012, **151**, 474-480.
4. G. Qi, L. Fu, X. Duan, B. H. Choi, M. Abraham and E. P. Giannelis, *Greenhouse Gases: Science and Technology*, 2011, **1**, 278-284.
5. U. Martinez and G. Pacchioni, *Microporous and Mesoporous Materials*, 2010, **129**, 62-67.
6. A. Heydari-Gorji, Y. Belmabkhout and A. Sayari, *Langmuir*, 2011, **27**, 12411-12416.
7. E. De Canck, L. Lapeire, J. De Clercq, F. Verpoort and P. Van Der Voort, *Langmuir*, 2010, **26**, 10076-10083.
8. K. Nakai, Y. Oumi, H. Horie, T. Sano and H. Yoshitake, *Microporous and Mesoporous Materials*, 2007, **100**, 328-339.
9. C. Vercaemst, M. Ide, B. Allaert, N. Ledoux, F. Verpoort and P. Van Der Voort, *Chemical Communications*, 2007, 2261-2263.
10. T. Tsuda and T. Fujiwara, *J Chem Soc Chem Comm*, 1992, 1659-1661.
11. T. Tsuda, T. Fujiwara, Y. Taketani and T. Saegusa, *Chem Lett*, 1992, 2161-2164.
12. O. Leal, C. Bolivar, C. Ovalles, J. J. Garcia and Y. Espidel, *Inorg Chim Acta*, 1995, **240**, 183-189.
13. M. Caplow, *Journal of the American Chemical Society*, 1968, **90**, 6795-&.
14. B. Aziz, N. Hedin and Z. Bacsik, *Microporous and Mesoporous Materials*, 2012, **159**, 42-49.
15. Z. Bacsik, N. Ahlsten, A. Ziadi, G. Y. Zhao, A. E. Garcia-Bennett, B. Martin-Matute and N. Hedin, *Langmuir*, 2011, **27**, 11118-11128.
16. S. Y. Hao, H. Chang, Q. Xiao, Y. J. Zhong and W. D. Zhu, *Journal of Physical Chemistry C*, 2011, **115**, 12873-12882.
17. A. C. C. Chang, S. S. C. Chuang, M. Gray and Y. Soong, *Energy Fuel*, 2003, **17**, 468-473.
18. R. Serna-Guerrero, E. Da'na and A. Sayari, *Industrial & Engineering Chemistry Research*, 2008, **47**, 9406-9412.
19. N. Hiyoshi, K. Yogo and T. Yashima, *Chem Lett*, 2004, **33**, 510-511.

20. N. Hiyoshi, K. Yogo and T. Yashima, *Microporous and Mesoporous Materials*, 2005, **84**, 357-365.
21. R. Serna-Guerrero, Y. Belmabkhout and A. Sayari, *Chemical Engineering Journal*, 2010, **158**, 513-519.
22. E. F. da Silva and H. F. Svendsen, *Industrial & Engineering Chemistry Research*, 2006, **45**, 2497-2504.
23. I. Kim and H. F. Svendsen, *Industrial & Engineering Chemistry Research*, 2007, **46**, 5803-5809.
24. P. J. E. Harlick and A. Sayari, *Industrial & Engineering Chemistry Research*, 2007, **46**, 446-458.
25. M. Ide, M. El-Roz, E. De Canck, A. Vicente, T. Planckaert, T. Bogaerts, I. Van Driessche, F. Lynen, V. Van Speybroeck, F. Thybault-Starzyk and P. Van Der Voort, *Physical Chemistry Chemical Physics*, 2013, **15**, 642-650.
26. A. Sayari, Y. Belmabkhout and E. Da'na, *Langmuir*, 2012, **28**, 4241-4247.
27. A. Danon, P. C. Stair and E. Weitz, *The Journal of Physical Chemistry C*, 2011, **115**, 11540-11549.

## **7 The modification of an ethenylene-bridged PMO material towards sulfonic acid groups**

Sulfonic acid containing ethenylene-bridged PMO materials are developed *via* the direct sulfonation of the double bond. Two different sulfonation reagents are employed such as chlorosulfonic acid and fuming sulfuric acid (65% SO<sub>3</sub>; oleum). These sulfonated materials are characterised and their catalytic activity is studied for the esterification of acetic acid with 1-propanol.

The resulting catalysts, synthesized with chlorosulfonic acid and fuming sulfuric acid, appear to be good catalysts in the first catalytic run for this esterification reaction. The TOF and TON values are higher than values obtained for the commercially available Amberlyst-16. Furthermore, the TOF and TON are comparable to the zeolite ZSM-5. However, the acid solids lose their acidity after the first catalytic run and elemental analysis proves the complete loss of the –SO<sub>3</sub>H functionality.

Therefore, a different route is utilized in order to obtain a sulfonic acid functionality attached to a PMO material. An ethenylene-bridged PMO functionalised with sulfonic acid groups is successfully synthesized *via* a sequence of post-synthetic modification steps. The double bond is functionalised *via* a bromination and subsequent substitution obtaining a thiol functionality. This is followed by an oxidation towards a sulfonic acid group. After full characterisation, the solid acid catalyst is used in the acetylation of glycerol.

The catalytic reactivity and reusability of the sulfonic acid modified PMO material is investigated. The catalyst showed a catalytic activity and kinetics that are comparable with the commercially available resin, Amberlyst-15, and furthermore our catalyst can be recycled for several subsequent catalytic runs and retains its catalytic activity.

Catalytic experiments were partially performed by dr. Inmaculada Dosuna-Rodríguez at *Université catholique de Louvain* in collaboration with Prof. dr. Eric M. Gaigneaux.

Partial results presented in this chapter are published as

Els De Canck, Carl Vercaemst, Francis Verpoort and Pascal Van Der Voort, *Studies in Surface Science and Catalysis*, **2010**, 175, 365-368.

Els De Canck, Inmaculada Dosuna-Rodríguez, Eric M. Gaigneaux and Pascal Van Der Voort, *Materials*, **2013**, 6, 8, 3556-3570.

## 7.1 PART 1: Sulfonation of the double bond of the ethenylene-bridged PMO material

### 7.1.1 Introduction

In this chapter the introduction of acid groups on PMO materials and their applicability as a solid acid catalyst is researched. The most commonly introduced functionalisation is the sulfonic acid group. Several diverse methods have been applied to prepare sulfonic acid containing PMO materials. These strategies include the direct sulfonation of the phenylene bridge,<sup>1-3</sup> as first attempted by Inagaki *et al.*<sup>4</sup>, and furthermore the co-condensation of an organo bis-silane (*e.g.* BTEB, BTME, ...) with (3-mercaptopropyl)trimethoxysilane<sup>5-8</sup> followed by an oxidation of the thiol functionality.

Herein, the direct sulfonation of the double bonds of the ethenylene-bridged PMO material is explored, similar to the direct sulfonation of the aromatic bridge of the phenylene-bridged PMO material. This functionalisation reaction can occur with different sulfonation reagents under diverse conditions. The materials are probed as acid catalysts in the esterification of acetic acid with 1-propanol. Furthermore, the reusability of these sulfonic acid containing PMO materials is studied.

### 7.1.2 Sulfonation of the double bond

The sulfonic acid groups are anchored to the double bond *via* the addition of chlorosulfonic acid or the reaction between the double bonds of the material with SO<sub>3</sub> fumes originating from fuming sulfuric acid (Figure 7.1). The protons of the –SO<sub>3</sub>H groups will act as acid catalyst in the catalytic reaction.

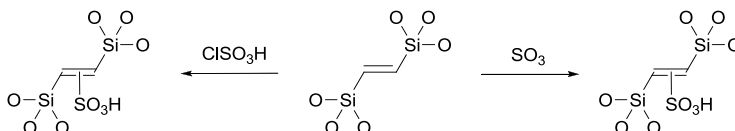
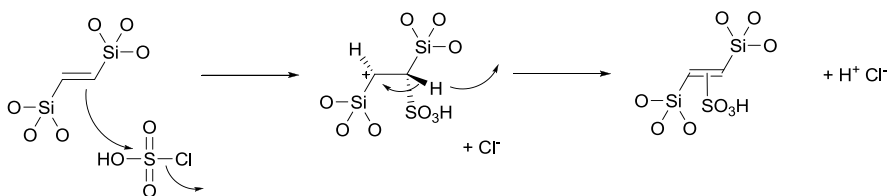


Figure 7.1: Introduction of –SO<sub>3</sub>H functionalities *via* two different procedures.

### 7.1.2.1 Chlorosulfonic acid as sulfonating reagent

The sulfonation with chlorosulfonic acid is based upon the recipe described by Li *et al.*<sup>9</sup> The authors have performed this sulfonation on phenylene-bridged PMO materials. The recipe is slightly adapted for the ethenylene-bridged PMO material.<sup>10</sup> Figure 7.2 represents the presumable reaction mechanism similar to the sulfonation of the phenylene moiety.<sup>9,11</sup> The double bond will act as nucleophile towards ClSO<sub>3</sub>H and dichloromethane is used as solvent. A light orange material is obtained which is denoted as PMO-SO<sub>3</sub>H-c.



**Figure 7.2:** Presumable reaction mechanism of the sulfonation of the double bond of the ethenylene-bridged PMO material with chlorosulfonic acid. Scheme based upon references 9 and 11.

### 7.1.2.2 Fuming sulfuric acid as sulfonating reagent

Another procedure is reported next to the method using chlorosulfonic acid. This method employs fuming sulfuric acid where the SO<sub>3</sub> gasses (oleum with 65% SO<sub>3</sub>) will act as reagent and this procedure is applied in literature on phenylene bridges.<sup>11, 12</sup> The presumable reaction scheme is shown Figure 7.3.

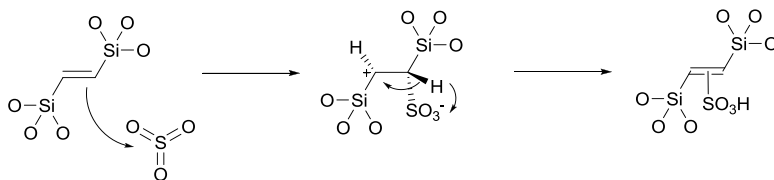


**Figure 7.3:** Presumable reaction mechanism of the sulfonation of the double bond of the ethenylene-bridged PMO material with SO<sub>3</sub> gasses originating from fuming sulfuric acid.

The sulfonation procedure involves the use of a home-made set-up with Schlenk techniques where the ethenylene-bridged PMO material is allowed to come in contact

with the sulfur trioxide gasses. Figure 7.4 shows the laboratory set-up employed for the sulfonation. The resulting material is denoted as PMO-SO<sub>3</sub>H-f.

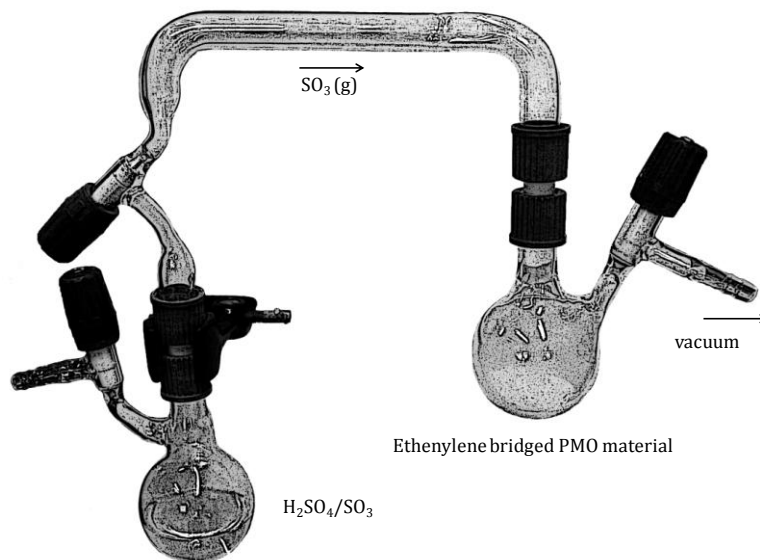


**Figure 7.4:** Laboratory set-up for the sulfonation using fuming sulfuric acid.

### 7.1.3 Characterisation of the sulfonated solids

The influence of the sulfonation process on the ethylene-bridged PMO materials is evaluated for the two different sulfonation procedures. As both chlorosulfonic acid and oleum are corrosive chemicals, it is of great importance to check the structure of the material after sulfonation. Table 7.1 provides an overview of the physicochemical characteristics of the materials. As can be seen, the material treated with chlorosulfonic acid mostly retains the structural characteristics of the parent PMO material. Only a small decrease in pore volume and pore diameter is observed due to the functionalisation of the pore walls. The difference in  $S_{BET}$  is within the experimental error of the nitrogen sorption measurement. The treatments with fuming sulfuric acid have a more pronounced effect on the porosity. Lower values for especially the pore volume are observed, either due to a successful functionalisation or partial destruction of the mesostructure. This is especially valid for the material PMO(2)-SO<sub>3</sub>H-f3, which is treated for 3 hours with the SO<sub>3</sub> gasses.

**Table 7.1: Details of the synthetic procedures to obtain sulfonated PMO materials and a comparison of the structural and chemical properties of the materials modified *via* the different procedures.**

	Synthesis	Reaction Time	$S_{\text{BET}}^{\text{a}}$ $\text{m}^2 \text{g}^{-1}$	$V_{\text{p}}^{\text{b}}$ $\text{mL g}^{-1}$	$d_{\text{p}}^{\text{c}}$ nm	Acidity <sup>d</sup> mmol $\text{H}^+ \text{g}^{-1}$
PMO(1)	-	-	937	1.07	5.47	-
PMO(1)-SO <sub>3</sub> H-c	ClSO <sub>3</sub> H	6 h	949	1.04	5.47	0.84
PMO(1)-SO <sub>3</sub> H-f1	oleum	1 h	800	0.89	5.47	1.16
PMO(2)	-	-	963	1.04	4.82	-
PMO(2)-SO <sub>3</sub> H-f3	oleum	3 h	788	0.84	4.82	1.58

<sup>a</sup> Specific surface area determined *via* the BET equation. <sup>b</sup> Pore volume determined at  $P/P_0 = 0.98$ . <sup>c</sup> Pore diameter calculated from the desorption branch of the isotherm with the BJH method. <sup>d</sup> Determined *via* acid-base titration.

Nonetheless, the material PMO(2)-SO<sub>3</sub>H-f3 still exhibits a high specific surface area, pore volume and pore diameter. Typical type IV isotherms are noticed in Figure 7.5 (left) indicating a good retainment of the mesoporosity of all the sulfonated samples.

Furthermore, the examination of the XRD patterns reveals that the sulfonation procedures have no effect on the ordering of the materials, prepared *via* both methods (Figure 7.5; right). The three characteristic reflections, (100), (110) and (200), of the  $P6mm$  space group can be seen after sulfonation, indicating the presence of 2D-hexagonal ordering. This confirms that the structure did not undergo any destruction.



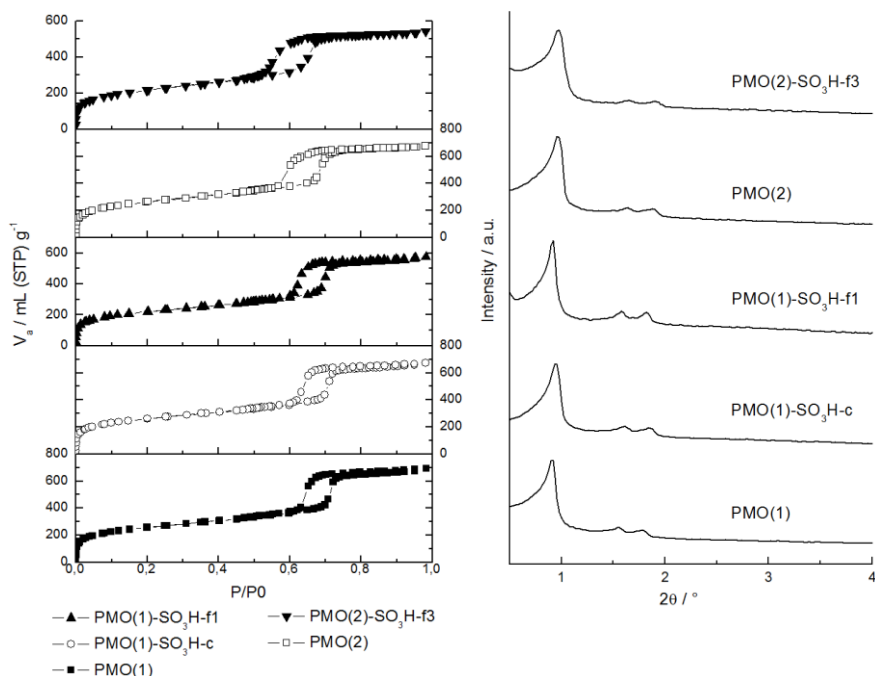


**Figure 7.5: Nitrogen sorption isotherms of the materials before and after sulfonation. (left) X-ray diffraction patterns before and after sulfonation. (right)**

The acidity of the catalysts is determined *via* acid-base titration and the values are summarized in Table 7.1. The procedure with SO<sub>3</sub> fumes gives rise to materials with a higher amount of acidity. Also, prolonging of the sulfonation procedure from 1 hour to 3 hours increases the amount of protons. However, this increase is rather limited when PMO(1)-SO<sub>3</sub>H-f1 and PMO(2)-SO<sub>3</sub>H-f3 are compared. Only a difference of 0.42 mmol H<sup>+</sup> g<sup>-1</sup> is noticeable. Although this method delivers materials with a relative high acidity up to 1.58 mmol H<sup>+</sup> g<sup>-1</sup>, it is extremely difficult to control the sulfonation process with oleum. Even when the contact time is kept constant, variation on the concentration of the SO<sub>3</sub> fumes exists. This of course influences the reproducibility of the sulfonation process. Values between 1.2 mmol H<sup>+</sup> g<sup>-1</sup> to 1.6 mmol H<sup>+</sup> g<sup>-1</sup> are obtained. The acidity of the materials prepared with ClSO<sub>3</sub>H can be more controlled as the reaction appears to be reproducible. Values of approximately 0.7-0.8 mmol H<sup>+</sup> g<sup>-1</sup> are obtained.

## 7.2 Catalysis: the esterification of acetic acid with 1-propanol

The catalytic activity of the sulfonated ethylene-bridged PMO materials will be examined by evaluating their performance in a Fisher esterification. A relatively easy esterification reaction is chosen as proof of concept, *i.e.*, the reaction between acetic acid and 1-propanol. The reaction mechanism is presented below, showing the role of acidic protons originating from the sulfonic acid group of the PMO material. (Figure 7.6) The ester propyl acetate is obtained as end product.

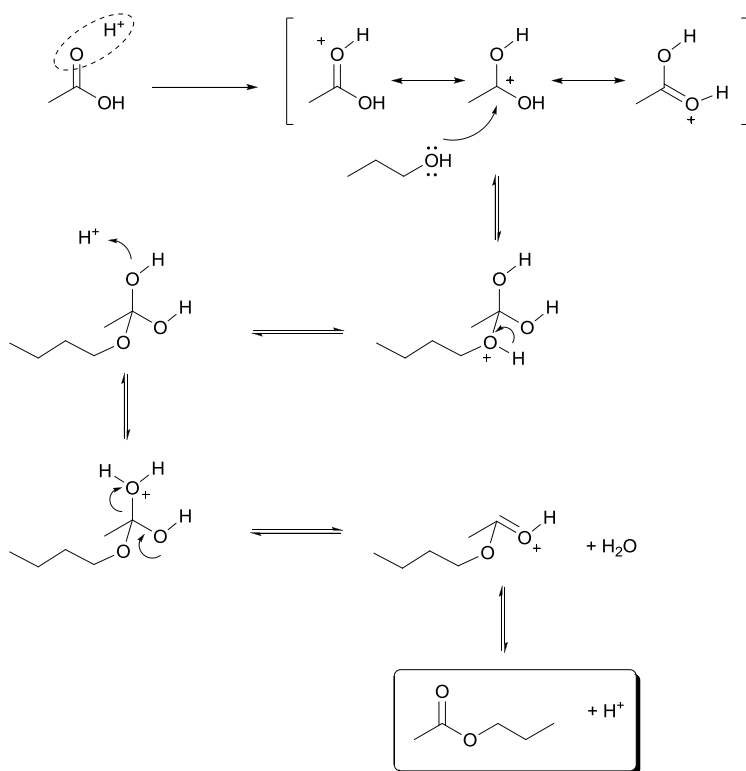


**Figure 7.6:** Reaction scheme of a Fischer esterification reaction, using acetic acid and 1-propanol as reagents, a proton originating from the heterogenized sulfonic acid group as catalyst and propyl acetate as product.

In the catalytic experiments, acetic acid will be used as solvent of the catalytic reaction and thus the alcohol will be the limiting reagent. Furthermore, the use of a Dean Stark apparatus is avoided as the constant removal of water influences the

equilibrium of the esterification which is clearly visible in the last reaction step of Figure 7.6 with the escape of water. The reaction mixture that consists of 1-propanol, acetic acid and the catalyst are stirred at 90°C. The conversion of 1-propanol is followed with gas chromatography. Therefore, an internal standard is used throughout the catalytic experiments.<sup>10, 13</sup>

### 7.2.1 Catalytic experiments with sulfonated PMO materials

First, the material PMO-SO<sub>3</sub>H-f1 (1.20 mmol H<sup>+</sup> g<sup>-1</sup>) is compared to a homogenous catalyst, the acid *p*-toluene sulfonic acid. The catalytic reaction with the heterogeneous and the homogeneous catalyst is monitored during 3 successive hours, to situate the activity of the sulfonated PMO material with respect to the homogenous variant. The conversion of 1-propanol is shown in Figure 7.7 for the two catalysts.

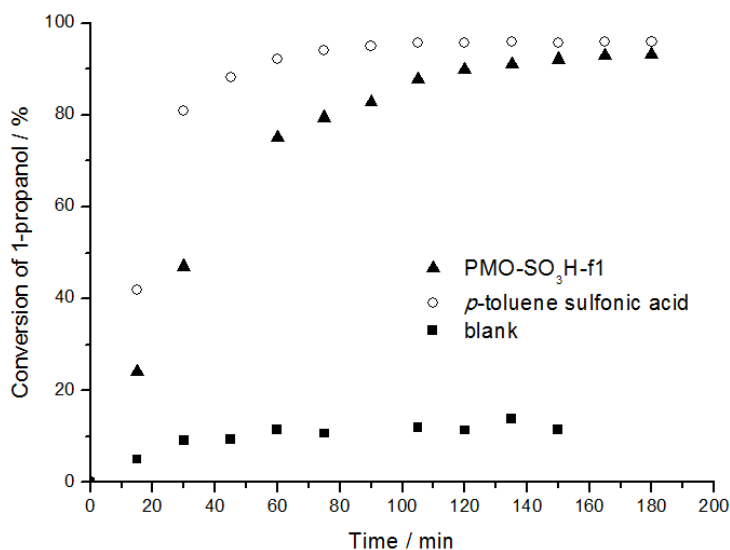


**Figure 7.7:** Conversion of 1-propanol as a function of time for PMO-SO<sub>3</sub>H-f1 (1.20 mmol H<sup>+</sup> g<sup>-1</sup>) and *p*-toluene sulfonic acid. The reaction mixture consists of 30 mmol 1-propanol, 100 mmol acetic acid and 30 mmol internal standard. An amount of 0.2 g of catalyst is added or a molar equivalent of the total acidity of *p*-toluene sulfonic acid.

The material PMO-SO<sub>3</sub>H-f1 exhibits a catalytic activity which is comparable to the activity of *p*-toluene sulfonic acid. The heterogeneous catalyst reaches the equilibrium with a total conversion of 93% after approximately 3 hours of reaction, whereas the

homogeneous acid catalysts reaches the equilibrium slightly sooner with a conversion of  $\sim 96\%$  after almost one hour of reaction time. The graph shows that the initial reaction speed of PMO-SO<sub>3</sub>H-f1 is slightly slower than the homogeneous catalyst. This is expected as heterogeneous catalysts normally possess a slower initial reaction speed.

Nevertheless, one can conclude that the material PMO-SO<sub>3</sub>H-f1 is a catalyst which provides apparently a good alternative for the homogeneous catalyst. In addition, Figure 7.7 also shows the blank reaction, *i.e.*, the auto-catalysis as acetic acid possesses acidic protons which can also induce the esterification. However, during the first 3 hours of the reaction, this process appears to be slow as only a conversion of 11-12% is observed. This clearly shows the necessity of adding a catalyst to perform the esterification reaction when no other techniques or methods are used to influence the equilibrium, such as the already mentioned Dean Stark set-up.

Next to the comparison between the homogeneous and the heterogeneous acid catalysts, it is also interesting to compare the sulfonic acid ethenylene-bridged PMO materials with commercially available catalysts. In this study, ZSM-5 and Amberlyst-16 are selected as comparison. The catalyst ZSM-5 (*Zeolite Socony Mobil-5*) is a microporous aluminosilicate zeolite with an acidity of 0.66 mmol H<sup>+</sup> g<sup>-1</sup>. The resin Amberlyst-16 on the other hand is a sulfonic acid ion exchange resin ( $S_{\text{BET}} = 30 \text{ m}^2 \text{ g}^{-1}$ ,  $V_p = 0.20 \text{ mL g}^{-1}$ ,  $d_p = 25 \text{ nm}$ ). This polymer consists of a sulfonated polystyrene polymer cross-linked with 20% divinylbenzene and the determination of the acidity reveals an extremely high amount of acid protons. A total of 4.42 mmol H<sup>+</sup> g<sup>-1</sup> is observed.

In this catalytic experiment a PMO material sulfonated with fuming sulfuric acid during 1 hour is used. Acid-base titration on this material results in 1.16 mmol H<sup>+</sup> g<sup>-1</sup>. The obtained catalytic data are presented in Table 7.2, together with the apparent TON and TOF values for the catalysts PMO-SO<sub>3</sub>H-f1, ZSM-5 and Amberlyst-16. It is clear that from the data that the TON and TOF values of the zeolite and PMO are similar within the experimental error. Amberlyst-16 on the other hand appears to be the least efficient catalyst regardless of its high acidity.

**Table 7.2: Comparison between the sulfonated ethenylene-bridged PMO material (PMO-SO<sub>3</sub>H-f1) and the commercially available catalysts, ZSM-5 and Amberlyst-16.**

	Acidity <sup>a</sup>	Yield <sup>b</sup>	Yield <sup>c</sup>	TON <sup>d</sup>	TOF <sup>e</sup>
	mmol H <sup>+</sup> g <sup>-1</sup>	%	%		min <sup>-1</sup>
PMO-SO <sub>3</sub> H-f1 <sup>f</sup>	1.16	94.60	98.86	187.9	10.3
ZSM-5	0.66	79.85	84.73	194.2	11.5
Amberlyst-16	4.42	95.17	99.02	34.3	1.9

The reaction mixture consists of 30 mmol 1-propanol, 100 mmol acetic acid and 30 mmol internal standard. This is vigorously refluxed at 90°C and subsequently an amount of 0.19 g of PMO-SO<sub>3</sub>H-f, 0.19 g ZSM-5 or 0.14 g Amberlyst-16 is added to the reaction mixture. <sup>a</sup> Determined *via* acid-base titration. <sup>b</sup> Determined *via* GC after 1 hour. <sup>c</sup> Determined *via* GC after 3 hours. <sup>d</sup> Turnover number calculated after 180 minutes of reaction. <sup>e</sup> Turnover frequency calculated after 15 minutes of reaction. <sup>f</sup> The PMO material is sulfonated using fuming sulfuric acid during 1 hour.

An important factor concerning the use of heterogeneous catalysts is the possibility of reusing the material in several catalytic cycles. This implies that the catalysts are stable during the catalytic run and filtration process, which does not only involve the structural stability but also the chemical stability of the functional groups. Therefore experiments are performed to evaluate the reusability of the materials. For this purpose, two acid solids are selected, each prepared *via* a different sulfonation method.

### 7.2.2 Reusability of the sulfonated PMO materials

When the catalyst (PMO-SO<sub>3</sub>H-c) is reused, no acidic solution or regeneration reagents are employed to evaluate the actual reusability of the catalyst. The catalytic activity approximates the blank reaction of the esterification. Thus the catalyst appears not to be reusable. Determination of the acidity of the pristine and spent catalyst shows values of 0.74 and 0.19 mmol H<sup>+</sup> g<sup>-1</sup>. This loss of ~ 74% of the total amount of protons causes the inactivity during the second run. This result can be explained in two ways: the protons are lost in the catalytic mixture or the complete sulfonic acid group is detached from the PMO material.

The complete destruction and/or detachment of the sulfonic groups can be evaluated by determining the sulphur content *via* elemental analysis. An overview of the amount of sulfur is provided in Figure 7.8 for the pristine and sulfonated PMO materials but also for the solids after the first and even second catalytic run. It is immediately noticeable that the amount of protons on the sulfonated PMO material is much higher than the sulfur content, *i.e.*, 1.37 and 0.72 mmol H<sup>+</sup> g<sup>-1</sup>. Although the pristine (not sulfonated) PMO material also contributes to the total acidity with the acidic silanol groups, the discrepancy between the acidity and sulfur content is too high to be explained merely by silanol acidity.

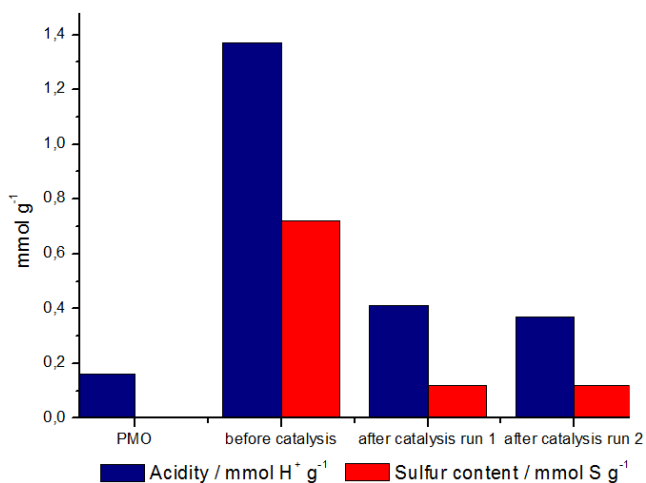


**Figure 7.8:** Acidity (blue) and sulfur (red) content of the catalyst PMO-SO<sub>3</sub>H-f (1.37 mmol H<sup>+</sup> g<sup>-1</sup>) before and after the first and second catalytic run. The acidity of the pristine PMO material is also presented for clarity.

This probably indicates that the sulfonated PMO material contains not chemically bonded protons which are not removed by the thorough washing step immediately after synthesis. This can partially explain the loss of acidity after the first catalytic run. Nevertheless by examining further Figure 7.8, it is also clear that the amount of sulfur after the first catalytic run is lower than the initial amount. A decrease of 0.72 to 0.12 mmol S g<sup>-1</sup> is observed. A loss of 83% of sulfur can only mean that a large part of the sulfonic acid groups is split off due to a cleavage of the C-S bond (*vide infra*). This can also be explained if instead of a C-S bond an C-O-SO<sub>3</sub>H bond was formed or if a reaction between the silanol group and the sulfonating reagent occurred (*vide infra*).

Additionally, the H<sup>+</sup> and S contents remain relatively constant after the first and second catalytic run. However, the resulting amounts are low.

It is obvious that a large part of the sulfonic acid groups are either not strongly chemically bonded to the PMO material and does not resist hydrolysis or that the functional groups are attached *via* strong physical interaction. Only a very small amount of the sulfonic acid groups can survive two catalytic reactions (0.12 mmol sulfur g<sup>-1</sup>). Both cases mentioned above can explain the observed behaviour during the catalytic experiments and the low amount of sulfur (or acidic protons) that is detected.

These results raise questions concerning the nature of the bond or interaction between the PMO material and the sulfonic acid group. It is generally known that the sulfonation of an aromatic ring with sulphuric acid or oleum is reversible.<sup>11</sup> It is in fact an equilibrium reaction. In contrast, the sulfonation of an unsaturated aliphatic and especially solid substrate is less described and appears more complicated. When using chlorosulfonic acid as sulfonating reagent, the type of reaction will strongly depend on the added solvent and synthetic conditions. When the reaction occurs in a polar solvent, for example diethyl ether, the chlorosulfonic acid will first form a complex with the solvent. To form the complex, it should be added first to the solvent at 0°C before adding the alkene. In this step, the temperature control is of crucial importance, if not a number of complex reactions can occur. Nevertheless, when performed correctly, the following reactions can occur:<sup>11</sup>

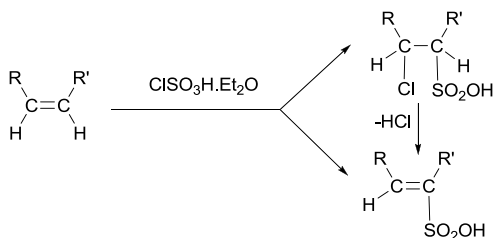


**Figure 7.9: The sulfonation of an alkene with ClSO<sub>3</sub>H.Et<sub>2</sub>O as sulfonating reagent. Adapted from reference 11.**

The use of a non-polar solvent, such as chloroform, gives rise to a different type of reaction, where for example a sulfonyl chloride can be formed.<sup>11</sup>

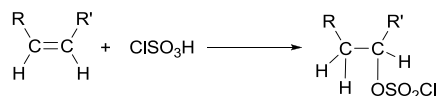


**Figure 7.10: The sulfonation of an alkene with ClSO<sub>3</sub>H as sulfonating reagent in a non-polar solvent. Adapted from reference 11.**

The presence of silanol groups on the PMO material can also interfere with the sulfonation of C=C bridge, similar to the reaction of ClSO<sub>3</sub>H and silica with the release of hydrochloric acid. This reaction is described by Zolfigol.<sup>15</sup>

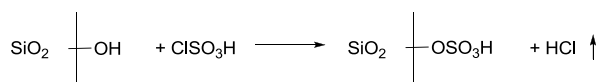


**Figure 7.11: The reaction between a surface silanol group with ClSO<sub>3</sub>H. Adapted from reference 15.**

This possible side reaction is however not mentioned by Li *et al.*<sup>9</sup> when describing the sulfonation of a phenylene-bridged PMO with ClSO<sub>3</sub>H in dichloromethane. As the ethenylene-bridged PMO materials contains a small amount of surface silanols<sup>16</sup> the possibility exist that Si-O-S bonds are formed. However, as this bond is highly sensitive for hydrolysis, the several washing steps after the sulfonation process have removed any species attached *via* the silanol groups.

Although it is stated that unsaturated substrates can be easily sulfonated, a variety of products can be formed. Sulfonation with SO<sub>3</sub> can result in the products shown below (Figure 7.12). The scheme represents the reactions that can occur for a SO<sub>3</sub>-dioxane system. First a β-sultone (A) or its adduct with dioxane (A') is formed. This sultone can also be formed in absence of solvent. Depending on the substituents (R<sub>1</sub>, R<sub>2</sub> and R<sub>3</sub>) and nature of the substrate, this sultone can be unstable and thus very reactive. This leads to many other products (B-G). The reaction conditions and substrate will play a key role in which kind of product will be mainly formed. Factors that influence the reaction are: reaction temperature, reaction time, nature of reagents (and solvent), substituents on the double bond, ratio of reagents, method of product



workup, water content in  $\text{SO}_3$  and even the degree of polymerization of the  $\text{SO}_3$ .<sup>11</sup> As can be seen from the figure, different routes can lead to the desired sulfonic acid group.

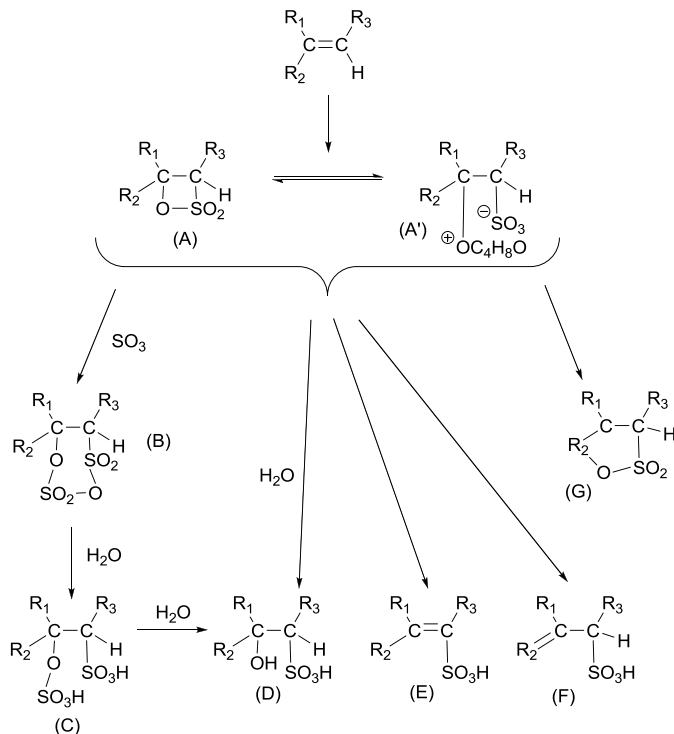


**Figure 7.12: The sulfonation of an alkene with the formation of different products by using  $\text{SO}_3$  gas as sulfonating reagent. Adapted from reference 11.**

The performed sulfonation reactions, described in Figure 7.2 and Figure 7.3, maybe did not occur as first expected. Perhaps a different reaction mechanism takes place and this can include the formation of C-O-S bonds instead of C-S bonds. Unfortunately, characterisation of the sulfonated solids with different techniques did not provide any proof of either the correct attachment of the sulfonic acid groups or the occurrence of sulfonyl chloride groups. Furthermore, also no other products shown in Figure 7.12 are observed. Most likely, the strongly chemically bonded amount of the functionality, in which form it may be, is too low ( $\sim 0.12 \text{ mmol g}^{-1}$ ) to detect and characterise properly.

## **7.3 PART 2: The modification of the thiol containing PMO material towards a sulfonic acid group**

Another strategy is used to introduce sulfonic acid groups. Clearly this route should not involve the attachment of -SO<sub>3</sub>H functionalities on double bonds as the nature between the support and acid group is still questionable.

Thus, a sulfonic acid group attached to aliphatic chains is preferred, keeping in mind the examples reported in literature concerning the solids functionalised with MPTMS and further oxidized.<sup>5-8</sup> This in combination with our successful synthesis of the thiolpropyl functionalised ethenylene-bridged PMO,<sup>17</sup> has led to the use of this material as basis for a solid acid catalyst. An oxidation of the thiol functionality results in the intended functionalisation. In this chapter of this dissertation, the synthesis and thorough characterisation is described. Moreover, this solid acid catalyst is tested in an esterification reaction. However, a different catalytic reaction than in previous chapter is probed with this catalyst, which is more industrially interesting: the acetylation of glycerol. Furthermore, the reusability of this catalyst was investigated.

### **7.3.1 Synthesis of the PMO based acid catalyst**

Starting from the *trans* ethenylene-bridged PMO (EP), a sulfonic acid modified PMO material is prepared and characterised. A general overview of the preparation method, including the starting material, is presented in Figure 7.13. The synthesis of the ethene containing precursor,<sup>7</sup> the ethenylene-bridged PMO,<sup>8</sup> subsequent bromination (BEP) and thiol functionalisation reaction (EP-(CH<sub>2</sub>)<sub>3</sub>-SH)<sup>17, 18</sup> are discussed in detail elsewhere (Figure 7.13, pathway A-C; Chapter 3 and 4).

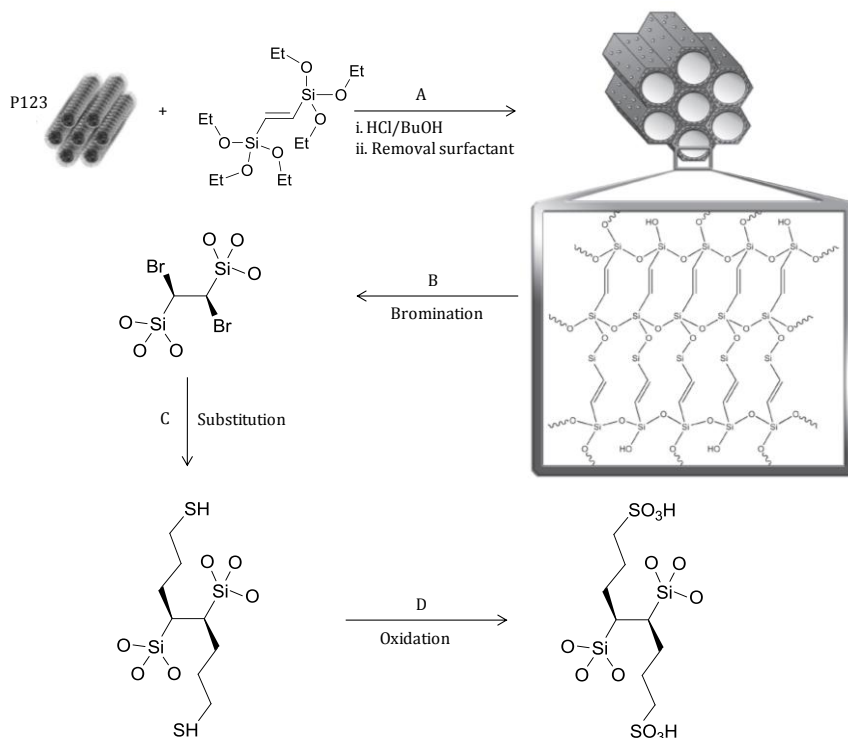


**Figure 7.13: Summary of the synthetic pathways followed to prepare the solid acid catalyst. (A) Synthesis of *trans* ethylene-bridged Periodic Mesoporous Organosilica [EP]; (B) Bromination of EP [BEP]; (C) Substitution of the bromine with Grignard reagent of 3-chloro-1-propanethiol [EP-(CH<sub>2</sub>)<sub>3</sub>-SH] and (D) Oxidation with sulfuric acid [EP-(CH<sub>2</sub>)<sub>3</sub>-SO<sub>3</sub>H].**

Oxidizing the thiol moiety is performed with H<sub>2</sub>SO<sub>4</sub> or other oxidizing agents such as HNO<sub>3</sub><sup>5-8</sup> or H<sub>2</sub>O<sub>2</sub><sup>2,19,20</sup>. In this study a treatment of EP-(CH<sub>2</sub>)<sub>3</sub>-SH with sulfuric acid and a thorough washing step was selected by which it converted the -SH into a -SO<sub>3</sub>H group (Figure 7.13, pathway D). This route resulted in the material EP-(CH<sub>2</sub>)<sub>3</sub>-SO<sub>3</sub>H.

### 7.3.2 Characterisation of the solids

Nitrogen sorption measurements were performed to examine the porosity of the different materials obtained by the reaction pathway shown in Figure 7.13 (EP, BEP, EP-(CH<sub>2</sub>)<sub>3</sub>-SH and EP-(CH<sub>2</sub>)<sub>3</sub>-SO<sub>3</sub>H). The nitrogen adsorption and desorption isotherms are shown in Figure 7.14. The type IV isotherms with the condensation step at relative pressures between 0.55-0.75 and the H1 hysteresis of the solids clearly

indicate that the materials are mesoporous and possess cylindrical pores with a narrow pore size distribution.

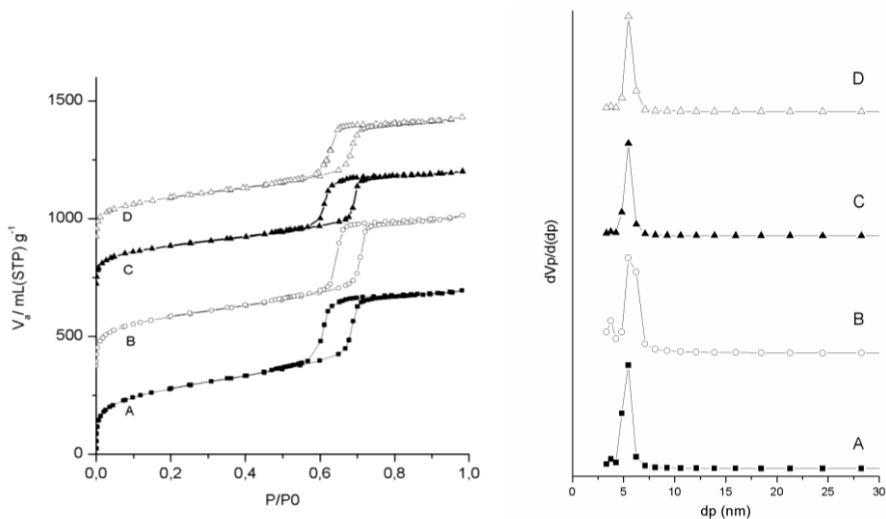


**Figure 7.14:** The nitrogen adsorption and desorption isotherms (left) and pore size distributions (right; calculated from the desorption branch) of (A) EP; (B) BEP; (C) EP-(CH<sub>2</sub>)<sub>3</sub>-SH and (D) EP-(CH<sub>2</sub>)<sub>3</sub>-SO<sub>3</sub>H. The isotherms of BEP, EP-(CH<sub>2</sub>)<sub>3</sub>-SH and EP-(CH<sub>2</sub>)<sub>3</sub>-SO<sub>3</sub>H are vertically offset for clarity by 350, 700 and 900 mL (STP) g<sup>-1</sup>, respectively.

A summary of the properties of these materials is shown in Table 7.3. The materials exhibit high specific surface areas ( $S_{\text{BET}}$ ) ranging from 850 to 523 m<sup>2</sup> g<sup>-1</sup> and large total pore volumes around 0.84 mL g<sup>-1</sup>. The  $S_{\text{BET}}$  decreases when the material is functionalised due to the decoration of the pore walls with the bromine and later on with the propylthiol functionality but also due to the overall weight gain of the functionalised materials. The pore diameter of all the materials lies in the range of 6 to 5 nm. Only a minor shift to smaller pore diameters and a slight broadening of the pore size distribution is observed (Figure 7.14 and Table 7.3). The structural characteristics of the commercially available resin Amberlyst 15 are also presented in Table 7.3 for comparison. This ethenylbenzenesulfonic acid polymer is a strong acid ion exchange resin with unordered macropores. Furthermore, the material is also prone to swelling.

**Table 7.3: Overview of the structural characteristics of the materials compared in this study.**

	Path	$S_{\text{BET}}^{\text{a}} / \text{m}^2 \text{g}^{-1}$	$V_{\text{p}}^{\text{b}} / \text{mL g}^{-1}$	$d_{\text{p}}^{\text{c}} / \text{nm}$
EP	A	850	1.03	5.8
BEP	B	663	0.84	5.6
EP-(CH <sub>2</sub> ) <sub>3</sub> -SH	C	523	0.59	5.3
EP-(CH <sub>2</sub> ) <sub>3</sub> -SO <sub>3</sub> H	D	688	0.72	5.4
Amberlyst 15	-	50	-	300

<sup>a</sup> Surface area calculated *via* the BET model; <sup>b</sup> Total pore volume at  $P/P_0 = 0.98$ ; <sup>c</sup> Pore diameter calculated *via* the BJH plot from the desorption branch.

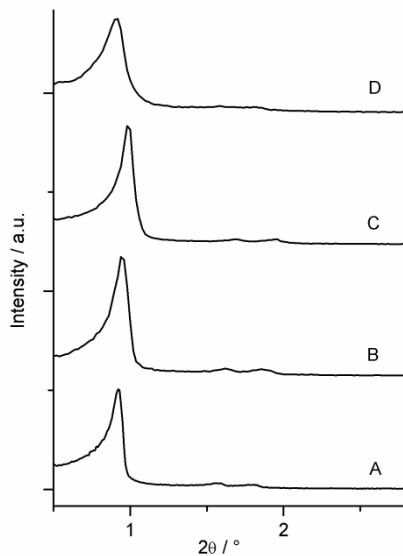


**Figure 7.15: The powder X-ray diffraction patterns of (A) EP; (B) BEP; (C) EP-(CH<sub>2</sub>)<sub>3</sub>-SH and (D) EP-(CH<sub>2</sub>)<sub>3</sub>-SO<sub>3</sub>H.**

The XRD patterns of the materials in Figure 7.15 reveal three well-resolved signals originating from the low angle (100) and second-order (110) and (200) reflections. This evidently indicates that the materials possess a 2D-hexagonal ordered structure and thus retain their  $P6mm$  space group ordering throughout the

syntheses. Only a slight broadening can be observed at the patterns of sample BEP, EP-(CH<sub>2</sub>)<sub>3</sub>-SH and EP-(CH<sub>2</sub>)<sub>3</sub>-SO<sub>3</sub>H.

It is quite remarkable that all the materials discussed in this study, show outstanding structural stability. The materials retain porosity and ordering after 3 consecutive reactions as can be seen from the nitrogen sorption and XRD data. These results also confirm the reported stability of periodic mesoporous organosilicas.<sup>21, 22</sup>

Table 7.4 presents an overview of the chemical characterisation of the solids after the different synthetic procedures.

**Table 7.4: Overview of the chemical characteristics of the materials compared in this study.**

	Functionality	mmol g <sup>-1</sup>
BEP	-Br <sup>a</sup>	2.39
EP-(CH <sub>2</sub> ) <sub>3</sub> -SH	-SH <sup>b</sup>	0.40
EP-(CH <sub>2</sub> ) <sub>3</sub> -SO <sub>3</sub> H	-SO <sub>3</sub> H <sup>c</sup>	0.60 <sup>d</sup>

<sup>a</sup> Determined gravimetrically. <sup>b</sup> Determined *via* silver titration. <sup>c</sup> Determined *via* acid base titration. <sup>d</sup> The deviation between the amount of thiols and total acidity is due to the acidity of the surface silanols.

After oxidation of the thiol groups using sulfuric acid and a thorough washing step, a total amount of 0.60 mmol H<sup>+</sup> per gram of material has been observed. This also includes the intrinsic acidity of the PMO material originating from the surface silanols (~ 0.15 mmol g<sup>-1</sup>), as we described earlier.<sup>16</sup>

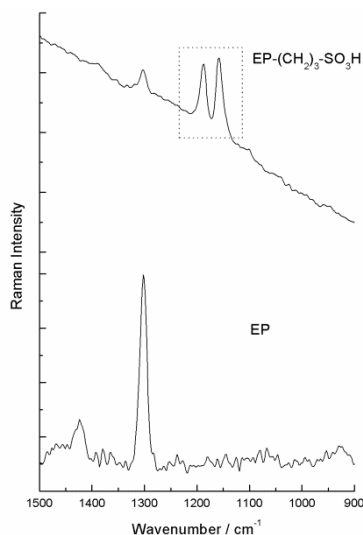


**Figure 7.16: Raman spectrum of EP and EP-(CH<sub>2</sub>)<sub>3</sub>-SO<sub>3</sub>H. The highlighted area shows the signals of the sulfonic acid group.**

It is clear that the conversion of the thiol containing PMO into the sulfonic acid containing-material has occurred *via* the oxidation process. This is also confirmed by Raman spectroscopy by the appearance of two new signals in the region between 1160 and 1190 cm<sup>-1</sup> originating from the -SO<sub>3</sub>H moiety (See Figure 7.16). The signal at 1300 cm<sup>-1</sup> represents the in-plane C-H deformation of the *trans* double bonds of the PMO material. The smaller signal at 1425 cm<sup>-1</sup> originates from a small amount of *cis* double bonds (in-plane C-H deformation) present in the material. Also the thiol titration after oxidation showed a zero concentration of remaining thiol groups. Amberlyst-15 exhibits a high acidity of 4.7 mmol H<sup>+</sup> g<sup>-1</sup>.

## 7.4 Catalytic experiments and recyclability

The catalytic ability of the sulfonic acid functionalised PMO material has been explored for an esterification reaction, *i.e.*, the glycerol acetylation reaction (Figure 7.17). The activity of EP-(CH<sub>2</sub>)<sub>3</sub>-SO<sub>3</sub>H is compared with a commercially available catalyst Amberlyst-15 and moreover the catalysts' reusability is explored.

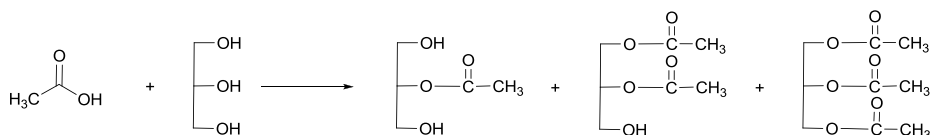


**Figure 7.17: The esterification reaction: the acetylation of glycerol with the formation of glycerol monoacetate (MAG), glycerol diacetate (DAG) and glycerol triacetate (TAG).**

In this study the esterification of glycerol is probed due to its economic importance. Glycerol is an important by-product of first generation biodiesel and is produced in a relative large quantity.<sup>23</sup> This overproduction of glycerol can be used in order to develop second generation biodiesel which uses glycerol as a raw product. As carboxylic acid, acetic acid is probed as shown in the general reaction (Figure 7.17). Three products may in principle be obtained from this reaction: glycerol monoacetate (MAG), glycerol diacetate (DAG) and glycerol triacetate (TAG). However, experimentally, only MAG (~94%) and DAG (~6%) are formed using the specific catalytic conditions described in the experimental part.<sup>24</sup>

The catalytic activity of EP-(CH<sub>2</sub>)<sub>3</sub>SO<sub>3</sub>H for the esterification of acetic acid with glycerol is presented in Figure 7.18 where the total acetylation yield is shown as a function of time. The total acetylation yield is defined according to the equation below:

$$Yield_t (\%) = \frac{[P]_t}{[HAc]_0} \frac{v_{HAc}}{v_P} \times 100$$

where [P]<sub>t</sub> and [HAc]<sub>0</sub> represent the product and acetic acid concentration at a certain reaction time (t) and at t=0, respectively. Furthermore, v<sub>HAc</sub> and v<sub>P</sub> represent the stoichiometric coefficients of the acetic acid and the ester formed, *i.e.*, 1 for mono-substituted, 2 for di-substituted and 3 for fully substituted products, respectively. Also, as acetic acid contains acid protons which can induce a self-catalyzed process,



the reaction in absence of any solid catalyst was monitored. Corresponding data are shown in Figure 7.18. It is clear that the sulfonated PMO possesses a significant catalytic activity with a yield of almost 80% for this reaction after ~300 min; whereas the blank test (without any solid catalyst involved) yielded only ~50% of esters after ~300 min. The conversion of Amberlyst-15 is shown in the same figure. Comparing the two materials clearly shows that EP-(CH<sub>2</sub>)<sub>3</sub>SO<sub>3</sub>H exhibits a similar catalytic activity as Amberlyst-15, which is known as a well-performing catalyst in this type of reaction.

Furthermore, the recyclability of the sulfonic acid containing PMO material is studied for three consecutive runs. First, the initial rate of the catalytic reaction is studied for each run by focusing on the first hour of the acetylation (Figure 7.19). These experiments are all performed in the same catalytic set-up as the standard catalytic experiment. The solid is filtered after 1 hour and re-used without any further treatment in the subsequent run with a fresh reaction medium (run 2); this being performed again for 2 additional consecutive runs (runs 3 and 4). As one can see from the figure, the material still possesses catalytic activity for the acetylation after 4 runs. However recycling of the material in the consecutive runs results in a slight decrease of the initial reaction rate.

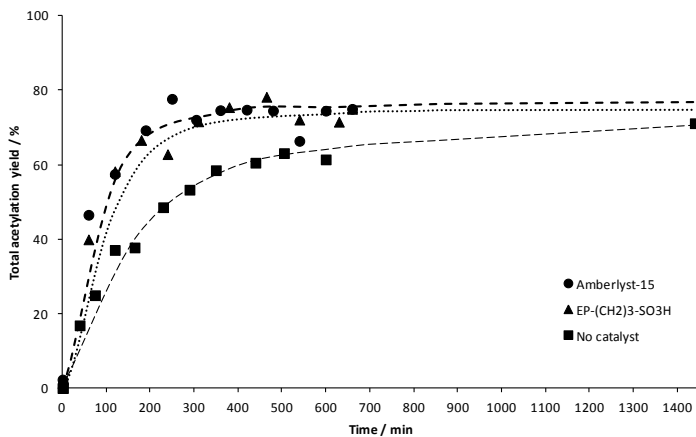


**Figure 7.18:** The total acetylation yield for the catalytic reaction with EP-(CH<sub>2</sub>)<sub>3</sub>-SO<sub>3</sub>H and Amberlyst-15. Also the blank reaction is represented for clarity. A catalyst loading of 0.25g per 40 mL glycerol was used. The lines are intended as visual aids only.

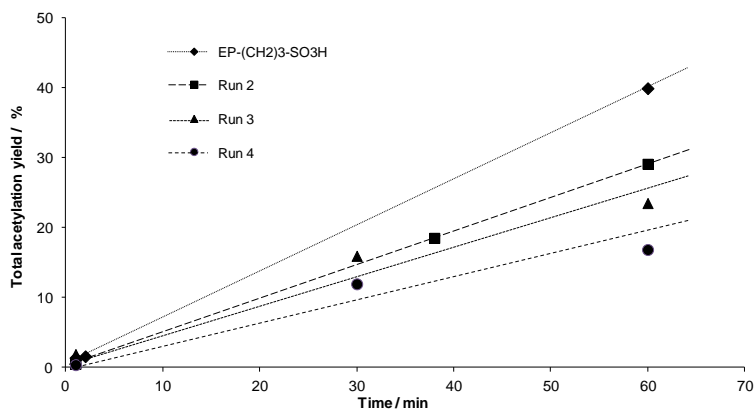


**Figure 7.19:** Recyclability experiments for EP-(CH<sub>2</sub>)<sub>3</sub>-SO<sub>3</sub>H with several runs during the first hour of the reaction. The lines are intended as visual aids only.

After the last catalytic run, *i.e.*, run 4, the total acetylation yield is monitored for approximately 10 hours in order to compare it with the acetylation yield of the pristine sulfonated PMO material, EP-(CH<sub>2</sub>)<sub>3</sub>-SO<sub>3</sub>H (Figure 7.20). Although a decrease in the initial reaction rate was observed as already mentioned, at the third consecutive run, the material still reaches the equilibrium after approximately 5 hours and finally results in the same acetylation level as the fresh pristine material.

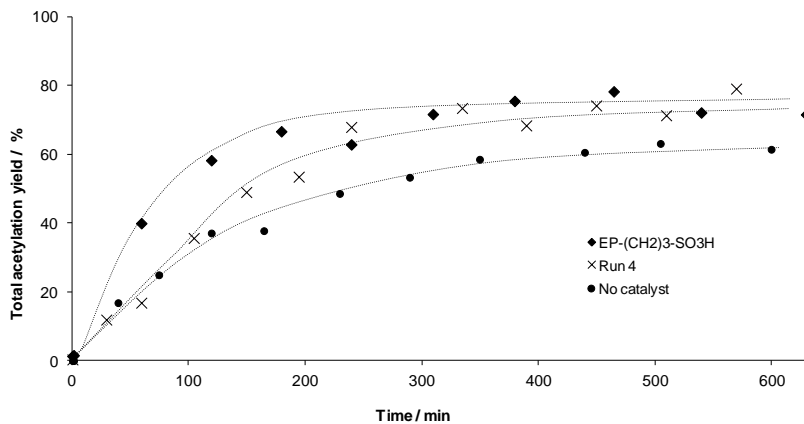


**Figure 7.20:** Recyclability experiment for EP-(CH<sub>2</sub>)<sub>3</sub>-SO<sub>3</sub>H: a comparison between the catalytic activity of the pristine material and the fourth catalytic run. The blank reaction is presented for clarity. The lines are intended as visual aids only.

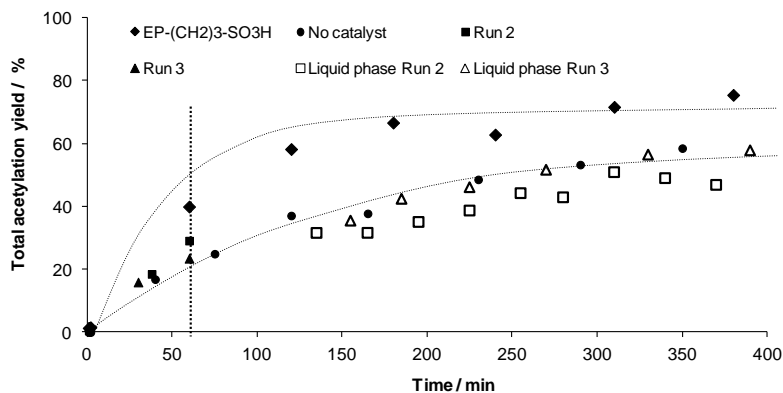


**Figure 7.21:** The total acetylation yield for the EP-(CH<sub>2</sub>)<sub>3</sub>-SO<sub>3</sub>H, the first and second run. After 60 minutes (represented by the vertical line) the liquid is separated from the catalyst and the catalytic activity of the liquid phase of run 2 and 3 is further followed in function of time (open square and triangle). The blank reaction is presented for clarity. The dotted lines are intended as visual aids only.

Moreover, additional tests are performed to evaluate the actual heterogeneous character of the observed catalytic activity. Therefore, the solids are removed from the liquid after 1 hour along the second and third runs, and the corresponding recovered solutions are kept under the catalytic conditions to follow the occurrence of a further evolution of the total acetylation yield without solid catalyst in the system anymore. As can be seen from Figure 7.21, it is clear that the acetylation occurs much slower, *i.e.*, in the range of the blank, when the catalysts are removed of the reaction media, than when the catalyst is maintained in the reactor for the whole test duration.

## 7.5 Conclusions

Periodic Mesoporous Organosilica functionalised with sulfonic acid groups is successfully synthesized and characterised. An ethenylene-bridged PMO material was chosen as starting material and this was further post-modified in several steps. A bromination and subsequent substitution reaction was used followed by an oxidation turning the material into a solid acid catalyst. This material has been investigated for the acetylation of glycerol. The material showed an equal activity as Amberlyst-15; the latter being usually considered as the reference most-efficient catalyst material for such kind of reactions. Recyclability experiments showed that the sulfonated Periodic Mesoporous Organosilica is reusable and showed the same total acetylation yield after

three runs. Homogeneous tests showed that the acetylation of glycerol indeed occurs heterogeneously, suggesting the absence of leaching, *e.g.* of sulfonate species, in the medium, and thus the high stability of our material under working conditions.

## 7.6 Experimental section

### Chemicals.

**PART 1.** Dichloromethane (Rotidry,  $\geq 99.8\%$ ), sodium chloride (99%), sodium hydroxide ( $\geq 98\%$ ), butyl acetate (Chromasolv Plus, HPLC, 99.7%), 1-propanol (Chromasolv, HPLC), acetic acid (p.a.), acetonitrile (Chromasolv, HPLC), concentrated sulfuric acid (95-97%) and chlorosulfonic acid (99%) were obtained from Sigma Aldrich. Fuming sulfuric acid (65%  $\text{SO}_3$ ) was required from Merck.

**PART 2.** Acetic acid (puriss. p.a., ACS reagens,  $\geq 99.8\%$ , GC/T), glycerol (puriss. p.a., ACS reagens, anhydrous, dist.,  $\geq 99.5\%$ ) were purchased from Fluka. Sulfuric acid, 1-propanol, 1-heptanol (98%) and o-xylene (98%) were obtained from Sigma Aldrich. Other used reagents are described in Chapter 4. All reagents and solvents were used as received.

**Synthesis of the ethenylene-bridged PMO material.** The synthesis of the ethenylene-bridged precursor, the ethenylene-bridged PMO material and surfactant extraction is performed according to the procedure described in Chapter 3.

### Sulfonation of the ethenylene-bridged PMO.

**With chlorosulfonic acid.** An amount of 0.3 g dry ethenylene-bridged PMO material is added to a Schlenk flask under inert atmosphere. The flask is placed in an ice-bath and 15 mL of dry dichloromethane is added to the solids. Under vigorous stirring, 5 mL chlorosulfonic acid is slowly added. *Remark: chlorosulfonic acid is very corrosive and reactive.* This mixture is stirred for 6 hours at  $0^\circ\text{C}$  while retaining the inert atmosphere. Afterwards, the mixture is poured out in a large amount of water, destroying the excess of chlorosulfonic acid. The solids are thoroughly washed with copious amounts of water to remove physisorbed chlorosulfonic acid groups. At the

end, the material is washed three times with acetone and dried under vacuum at 110°C. The resulting solid is denoted as PMO-SO<sub>3</sub>H-c.

**With fuming sulfuric acid.** The sulfonation is carried out with the specially designed set-up using Schlenk techniques that is shown in Figure 7.4. One Schlenk flask is charged with dry ethenylene-bridged PMO material (typically 0.5 g). This flask is attached to the set-up and the pressure is lowered until vacuum is reached. Subsequently, a certain amount (~ 30-40 mL) of fuming sulfuric acid (65% SO<sub>3</sub>) is poured into a second Schlenk flask. *Remark: fuming sulfuric acid with such a high amount of SO<sub>3</sub> gasses is very reactive and dangerous. Extreme care should be taken when working with this chemical and safety precautions should be taken in advance.* This flask is attached to the Schlenk set-up. The connection between both flasks is opened and due to the lower pressure, SO<sub>3</sub> gas escapes from the sulfuric acid and reacts with the PMO material in a highly exothermic reaction. This contact is maintained during a certain amount of time (1 or 3 hours). Afterwards, the sulfonated material is poured out in a large amount of water (at least 0.5 L) to remove any physisorbed reagent. *Remark: remaining reagent react extremely violently with water.* The solids are filtrated and washed with copious amount of water. Finally, the material is washed with acetone and dried at 110°C. The sulfonated PMO material is denoted as PMO-SO<sub>3</sub>H-f.

**Bromination of the ethenylene-bridged PMO material (Figure 7.13; pathway B).** Chapter 4 gives a description the bromination of the double bonds. The material is denoted as BEP.

**Modification of the brominated ethenylene-bridged PMO with a propylthiol functionality (Figure 7.13; pathway C).** The brominated PMO material is modified according to the procedure described in Chapter 4. The resulting material is denoted as EP-(CH<sub>2</sub>)<sub>3</sub>-SH.

**Oxidation of the thiol group (Figure 7.13; pathway D).** A volume of 25 mL H<sub>2</sub>SO<sub>4</sub> (2.5 M) was added to 0.50 g of EP-(CH<sub>2</sub>)<sub>3</sub>-SH and stirred at room temperature. After 1 h, the solids were filtered and washed thoroughly with water and acetone.

Finally, the material was dried at 90°C for 16 h under vacuum and referred to as EP-(CH<sub>2</sub>)<sub>3</sub>-SO<sub>3</sub>H.

**Characterisation.** The nitrogen sorption isotherms are recorded on Belsorp Mini II equipment at -196°C. Samples are pre-treated at 90°C or 110°C for 16 hours while degassing. The specific surface area ( $S_{\text{BET}}$ ) was determined by the BET equation ( $p/p_0=0.05-0.15$ ). The pore size distribution was determined from the desorption branch of the isotherm using the BJH theory. X-ray diffraction (XRD) patterns are recorded on an ARL X'TRA Diffractometer (Thermo Scientific) equipped with a Cu K $\alpha$  tube and a Peltier cooled lithium drifted silicon solid stage detector. The gas chromatography analysis was performed with a Finnigan Trace Ultra GC equipped with a standard FID detector. CHNS elemental analysis (S determination) was executed by the *Centre National de la Recherche Scientifique* (CNRS, France). Raman spectra are recorded using a Raman type FRA106/S spectrometer of Bruker, equipped with a Nd-YAG laser ( $\lambda = 1064$  nm).

**Titration of the total acidity.** An acid-base titration is performed to determine the total acidity.<sup>25</sup> A total amount of 0.05 g material is weighed and added to 20 g of a 2M NaCl solution. The mixture is stirred for 24 hours. This mixture is titrated with a known amount of NaOH with phenolphthalein as indicator.

**Determination of the amount of reachable thiols.** A titration is performed as described in literature.<sup>17</sup> A solution of silver nitrate with a known concentration is added to 0.050 g of material and left to stir until the equilibrium is reached. The excess of silver is titrated with potassium thiocyanate and FeNH<sub>4</sub>(SO<sub>4</sub>)<sub>2</sub>·12H<sub>2</sub>O in 0.3 M HNO<sub>3</sub> as indicator.

### Catalysis.

**Esterification of acetic acid and 1-propanol.** In a typical catalytic experiment, the reaction mixture consists of 30 mmol 1-propanol, 100 mmol acetic acid (excess, solvent), 30 mmol internal standard (toluene) and an amount of 0.2 g of catalyst (unless stated otherwise) which are added together under inert atmosphere using

Schlenk techniques. The mixture is refluxed at 90°C and the conversion of 1-propanol is followed using gas chromatography. Every 15 minutes, during 3 hours, a sample is taken, diluted with acetonitrile and injected in the GC. Afterwards, the solids are filtered and washed briefly with acetone (unless stated otherwise). Finally, the catalyst is dried under vacuum at 90°C overnight.

**Esterification of acetic acid with glycerol.** The catalytic reaction was carried out at 105°C and at atmospheric pressure in a round bottom flask reactor equipped with a magnetic stirrer. The sulfonic acid containing material was dried prior to use at 105°C under vacuum for 18 hours. The following concentrations of the reagents were used: 100 g acetic acid per liter of glycerol and the catalyst concentration was 6.25 g per liter of glycerol. First, the catalyst and glycerol are added together to the flask and are brought to reaction temperature. When the temperature is reached, the acetic acid is injected. Before analysis the samples are extracted with 1-heptanol and using o-xylene as an internal standard. The total yield of the esters was determined with gas chromatography. After one minute a sample of the reaction mixture is taken and analyzed with gas chromatography. This sample represents the starting point of the catalytic experiment. The recyclability experiments were carried out under identical conditions as the catalytic tests. Therefore, the catalyst was separated from the liquid phase after 1 hour and reused in a consecutive run without further treatment. The liquid phase was kept under reaction conditions and further followed as a function of time. Gas chromatography was performed with a Varian CP-3800 using a Cp-Sil 8CD column (Varian) with a FID detector.

## 7.7 References

1. D. Esquivel, C. Jimenez-Sanchidrian and F. J. Romero-Salguero, *Journal of Materials Chemistry*, 2011, **21**, 724-733.
2. B. Rac, P. Hegyes, P. Forgo and A. Molnar, *Applied Catalysis a-General*, 2006, **299**, 193-201.
3. M. P. Kapoor, Y. Kasama, M. Yanagi, T. Yokoyama, S. Inagaki, T. Shimada, H. Nanbu and L. R. Juneja, *Microporous and Mesoporous Materials*, 2007, **101**, 231-239.
4. S. Inagaki, S. Guan, T. Ohsuna and O. Terasaki, *Nature*, 2002, **416**, 304-307.
5. Q. H. Yang, M. P. Kapoor, N. Shirokura, M. Ohashi, S. Inagaki, J. N. Kondo and K. Domen, *Journal of Materials Chemistry*, 2005, **15**, 666-673.

6. Q. H. Yang, M. P. Kapoor, S. Inagaki, N. Shirokura, J. N. Kondo and K. Domen, *Journal of Molecular Catalysis a-Chemical*, 2005, **230**, 85-89.
7. Q. H. Yang, J. Liu, J. Yang, M. P. Kapoor, S. Inagaki and C. Li, *Journal of Catalysis*, 2004, **228**, 265-272.
8. Q. H. Yang, M. P. Kapoor and S. Inagaki, *Journal of the American Chemical Society*, 2002, **124**, 9694-9695.
9. C. Li, J. Yang, X. Shi, J. Liu and Q. Yang, *Microporous and Mesoporous Materials*, 2007, **98**, 220-226.
10. C. Vercaemst, Ghent University, Ph.D. thesis, 2009.
11. E. E. Gilbert, *Sulfonation and related reactions*, Interscience, New York, 1965.
12. J. Yang, Q. Yang, G. Wang, Z. Feng and J. Liu, *Journal of Molecular Catalysis A: Chemical*, 2006, **256**, 122-129.
13. E. De Canck, C. Vercaemst, F. Verpoort and P. Van der Voort, in *Scientific Bases for the Preparation of Heterogeneous Catalysts: Proceedings of the 10th International Symposium*, eds. E. M. Gaigneaux, M. Devillers, S. Hermans, P. A. Jacobs, J. A. Martens and P. Ruiz, Elsevier Science Bv, Amsterdam, 2010, pp. 365-368.
14. P. L. Dhepe, M. Ohashi, S. Inagaki, M. Ichikawa and A. Fukuoka, *Catal Lett*, 2005, **102**, 163-169.
15. M. A. Zolfigol, *Tetrahedron*, 2001, **57**, 9509-9511.
16. M. Ide, M. El-Roz, E. De Canck, A. Vicente, T. Planckaert, T. Bogaerts, I. Van Driessche, F. Lynen, V. Van Speybroeck, F. Thybault-Starzyk and P. Van Der Voort, *Physical Chemistry Chemical Physics*, 2013, **15**, 642-650.
17. E. De Canck, L. Lapeire, J. De Clercq, F. Verpoort and P. Van Der Voort, *Langmuir*, 2010, **26**, 10076-10083.
18. Y. Gao, E. De Canck, M. Leermakers, W. Baeyens and P. Van Der Voort, *Talanta*, 2011, **87**, 262-267.
19. S. Hamoudi and S. Kaliaguine, *Microporous and Mesoporous Materials*, 2003, **59**, 195-204.
20. S. Hamoudi, S. Royer and S. Kaliaguine, *Microporous and Mesoporous Materials*, 2004, **71**, 17-25.
21. M. C. Burleigh, M. A. Markowitz, S. Jayasundera, M. S. Spector, C. W. Thomas and B. P. Gaber, *Journal of Physical Chemistry B*, 2003, **107**, 12628-12634.
22. F. Goethals, C. Vercaemst, V. Cloet, S. Hoste, P. Van Der Voort and I. Van Driessche, *Microporous and Mesoporous Materials*, 2010, **131**, 68-74.
23. P. S. Nigam and A. Singh, *Prog Energ Combust*, 2011, **37**, 52-68.
24. I. Dosuna-Rodriguez and E. M. Gaigneaux, *Catal Today*, 2012, **195**, 14-21.
25. D. Margolese, J. A. Melero, S. C. Christiansen, B. F. Chmelka and G. D. Stucky, *Chemistry of Materials*, 2000, **12**, 2448-2459.



## **8 Anchoring a manganese complex on PMOs for oxidation catalysis**

A manganese complex,  $\text{Mn}(\text{acac})_2$ , is heterogenized on a Periodic Mesoporous Organosilica. First, the ethenylene-bridged PMO is chosen as support and it is attempted to anchor the manganese complex *via* three subsequent steps: an epoxidation of the double bond, a ring opening with ammonia which results in a primary amine and the attachment of the complex  $\text{Mn}(\text{acac})_2$  *via* a reaction between the amine and an acac ligand. It appeared not to be possible to perform the epoxidation on this type of material and therefore, a different type of PMO is selected.

In contrast to the ethenylene-bridged PMO, a multi-organic bridged PMO material with interconnected  $[\text{Si}(\text{CH}_2)]_3$  rings and an allyl moiety is successfully modified with the three functionalisation steps. The catalyst is characterised with different techniques which confirmed the attachment of the complex. It resulted in a material bearing  $0.6 \text{ mmol Mn g}^{-1}$ .

This catalyst is evaluated for the liquid phase oxidation of cyclohexene and moreover, the reusability of the catalyst is examined. It is observed that the manganese containing PMO material is reusable and can be applied in three consecutive catalytic runs. However further elucidation of the catalytic behaviour is necessary.

The allyl ring precursor and spray dried allyl ring-PMO were provided by dr. Matthias Ide of our research group.

## 8.1 Introduction

This chapter describes the anchoring of a manganese complex on a Periodic Mesoporous Organosilica material. Homogenous manganese Schiff-base complexes are well-known and important catalysts for olefin epoxidation reactions. The immobilization of these catalysts on a solid support combines the inherent advantages of heterogeneous catalysis and the high activity of the manganese.<sup>1,2</sup>

The following strategy, based upon the work of Inagaki and Sasidharan,<sup>3,4</sup> is pursued to heterogenize  $\text{Mn}(\text{acac})_2$  on an ethylene-bridged PMO. An overview of the pathway is presented in Figure 8.1. The double bond is first epoxidized and afterwards the resulting oxirane ring is opened with ammonia. The amine functionality acts as anchoring point for the manganese complex where a reaction between one of the acetylacetonate ligands and the amine results in an imine bond.<sup>5</sup>

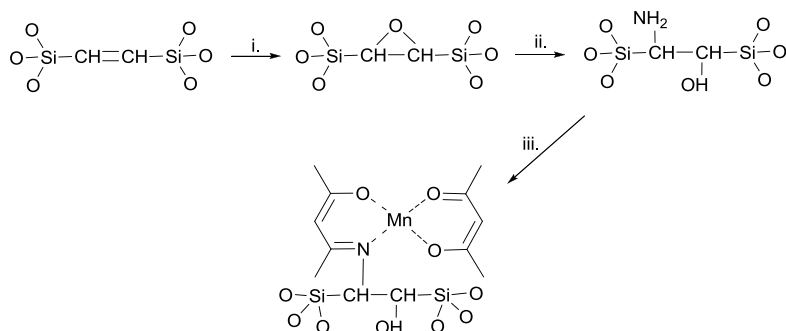


**Figure 8.1: Overview of the pathway followed to heterogenize the  $\text{Mn}(\text{acac})_2$  catalyst: i. Epoxidation of double bond; ii. Oxirane opening via ammonia treatment; iii. Heterogenization of  $\text{Mn}(\text{acac})_2$  complex.**

Inagaki *et al.*<sup>3</sup> already described the epoxidation and subsequent ammonia treatment and further optimized the synthetic procedures. This research was subsequently more expanded in a recent follow-up publication.<sup>4</sup> In an attempt to use these functionalisation reactions as basis for our modification, several epoxidation experiments on the *trans* ethylene-bridged PMO materials were performed to obtain the oxirane ring. The described procedure did not work, even when several synthetic parameters were altered such as the concentrations of *tert*-butyl

hydroperoxide (TBHP), base, reaction time and temperature, *etc.* A completely different recipe is employed based upon the Prilezhaev epoxidation<sup>6</sup> with 3-chloroperoxybenzoic acid (mCPBA) in dichloromethane. But this also did not lead to a successful epoxide.

It is possible that remaining fractions of the surfactant P123 interfere with the epoxidation. The procedure used for template extraction, does not completely remove the template as ~6 mol% is still left in the PMO material.<sup>7</sup> Furthermore, as the report of Inagaki *et al.* described the epoxidation of a PMO with a mixture of *cis* and *trans* ethene bonds,<sup>3</sup> another possibility is that sterical factors restrict the epoxidation of the *trans* ethene bonds. Therefore an extra set of ethene PMOs were prepared with the commercially available 1,2-bis(triethoxysilyl)ethenylene (80% *trans* – 20% *cis*) and Brij-76 or OTAC as surfactants, based upon the recipes of Esquivel<sup>8</sup> and Goto *et al.*,<sup>9</sup> respectively. Although the first surfactant resembles P123, it contains less ether bonds which can negatively influence the oxidation reaction. A PMO material with a specific surface area of 1060 m<sup>2</sup> g<sup>-1</sup>, a pore volume of 1.05 mL g<sup>-1</sup> and a pore size 3.5 nm was obtained. CTAB on the other hand is a cationic surfactant with a completely different chemical structure. The synthesis resulted in a material with the following structural properties:  $S_{\text{BET}} = 1071 \text{ m}^2 \text{ g}^{-1}$ ,  $V_p = 0.8 \text{ mL g}^{-1}$  and  $d_{p(\text{KJS})} = 2.8 \text{ nm}$ . It was attempted to epoxidize the double bond of the resulting PMO materials with both recipes described above. However, no epoxide was observed for the performed functionalisations.

These attempts clearly indicate that the epoxidation of the ethene bond is not as straightforward as shown by Inagaki *et al.* and this highly questions the reactivity of the double bond between two silicon atoms. A PMO material where the ethene bond is not directly enclosed by two silicon atoms can offer the solution and therefore a butenylene PMO is chosen. The precursor 1,4-bis(trimethoxysilyl)butene is prepared *via* olefin metathesis, in an analogous manner to the synthesis of 1,2-bis(triethoxysilyl)ethenylene.<sup>10</sup> The resulting PMO material possesses a specific surface area of 635 m<sup>2</sup> g<sup>-1</sup>, a pore volume of 0.76 mL g<sup>-1</sup> and a pore diameter of 4.4 nm and is utilized in the epoxidation reaction. Both procedures, with TBHP and mCPBA, did not show any epoxide formation.

From the results above, one can conclude that the epoxidation of an ethene bond embedded in a PMO, either a Si-CH=CH-Si or Si-CH<sub>2</sub>-CH=CH-CH<sub>2</sub>-Si moiety, cannot be achieved. Factors such as sterical hindrance by the PMO surface and low reactivity of the double bond because of the influence of the silicon atom can prevent a successful functionalisation.

The incorporation of an allylic function seems more promising as the reactivity of a terminal double bond is higher and sterical hindrance is less an issue. A different PMO material is selected which allows incorporation of an allyl function. This material is a multi-organic bridged PMO material based upon interconnected [Si(CH<sub>2</sub>)<sub>3</sub>] moieties where one of the methylene groups can be modified with an allyl function. Afterwards, the unsaturated bond can be adapted according to the prescribed functionalisation pathways, *i.e.*, an epoxidation and subsequent ammonia treatment.

## 8.2 Synthesis of a multi-organic bridged PMO material

This type of PMO was first reported by Ozin *et al.*<sup>11</sup> and later more studied in detail and applied as low-*k* insulator by Goethals *et al.*<sup>12,13</sup> The PMOs are based upon the precursor 1,1,3,3,5,5-hexaethoxy-1,3,5-trisilacyclohexane which is commercially available and can be synthesized according to the reaction scheme presented below (Figure 8.2).

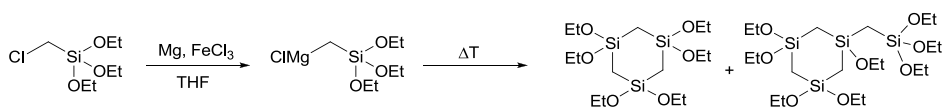


**Figure 8.2: Schematic overview of the synthesis of the precursor 1,1,3,3,5,5-hexaethoxy-1,3,5-trisilacyclohexane. Based upon references 11-13.**

The PMO synthesis with the resulting silicon oil and the surfactant Brij-76 in acidic conditions produced highly ordered materials with specific surface areas and pore volumes of 1000-1120 m<sup>2</sup> g<sup>-1</sup> and 0.83-1.02 mL g<sup>-1</sup>, respectively.<sup>12</sup> During the synthesis KCl was added to improve the quality of the multi-organic bridged PMO material, also denoted as ring-PMO. Moreover, a higher hydrothermal, mechanical and chemical stability was observed in comparison with ordered mesoporous silicas.<sup>12</sup>

However, before the actual PMO material synthesis, the allylic function must be introduced first. This occurs *via* the reaction presented in Figure 8.3 where the commercially available 1,1,3,3,5,5-hexaethoxy-1,3,5-trisilacyclohexane is converted into an allyl containing silane. The successful functionalisation is confirmed by NMR spectroscopy.

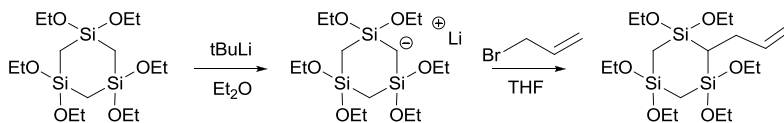


**Figure 8.3: Overview of the synthesis of the allyl containing ring precursor.**

Instead of using this allyl ring precursor in a hydrothermal synthesis procedure, a different approach is exploited similar to the synthesis of a pure ring-PMO which is described by our group.<sup>14</sup> In this work, it was attempted by means of spray drying to produce PMO spheres that are highly hydrophobic for chromatographic applications.

CTAB is used as surfactant in an acidic environment with the addition of butanol. A mixture between the allyl functionalised ring (50 v%) and unfunctionalised ring precursor is used (50 v%) and added to the dissolved surfactant and subsequently spray dried. The template was removed afterwards and the solids are characterised (*vide infra*).

### 8.3 Anchoring of manganese (acac)<sub>2</sub> on the allyl ring-PMO

The heterogenization of the manganese (acetylacetonate)<sub>2</sub> complex on the allyl ring-PMO occurs by following the pathways presented in Figure 8.4. This figure also shows the abbreviations that will be used throughout this chapter. As discussed earlier, the allyl bond is first epoxidized with mCPBA as oxidant in dichloromethane. Afterwards, an ammonia treatment at room temperature results in the formation of a primary amine and alcohol function. The reaction between the -NH<sub>2</sub> moiety and Mn(acac)<sub>2</sub> leads to a N=C bond which covalently anchors the manganese complex to the support.

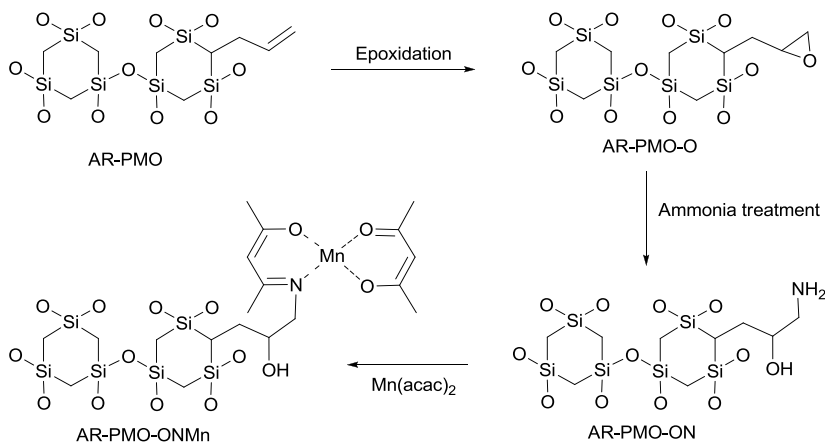


**Figure 8.4: Anchoring of Mn(acac)<sub>2</sub> on the modified allyl ring-PMO.**

## 8.4 Characterisation of the different modified allyl ring-PMOs

The modified allyl ring-PMOs are characterised by a variety of characterisation techniques to assess their structural and chemical properties.

Bromination of the double bonds is performed to determine the amount of reachable  $-\text{CH}=\text{CH}_2$  moieties. The same procedure as for the bromination of the ethylene-bridged PMO material was utilized. After gravimetric determination of the amount of bromine, it is established that 0.73 mmol double bonds per gram AR-PMO are present.

Raman spectroscopy was first used to evaluate the epoxidation procedure (Figure 8.5). The Si-CH<sub>2</sub>-Si moieties and allyl function can be found in the region between 2800 and 3100 cm<sup>-1</sup> with several characteristic bands of the C-H stretch vibrations. Moreover, the asymmetric C-H stretch vibration of the end-standing double bond can be found at 3080 cm<sup>-1</sup>. In the lower Raman shift region of the spectrum, the C=C bond also gives an intense signal at 1637 cm<sup>-1</sup>. Smaller signals can be found at 1448, 1416, 1353 and 1294 cm<sup>-1</sup> originating from the remaining surfactant, unhydrolyzed ethoxy groups and double bond. After epoxidation, the characteristic signals of the double bond at 3080 and 1637 cm<sup>-1</sup> decrease and a new signal at 1260 cm<sup>-1</sup> appears. The

latter originates from the oxirane ring formed after epoxidation and represents a ring breathing vibration. This proves that the epoxidation occurred successfully. The signals of the double bond does not completely disappear as a part of the double bonds are embedded inside the pore walls and therefore not reachable for chemical modification.

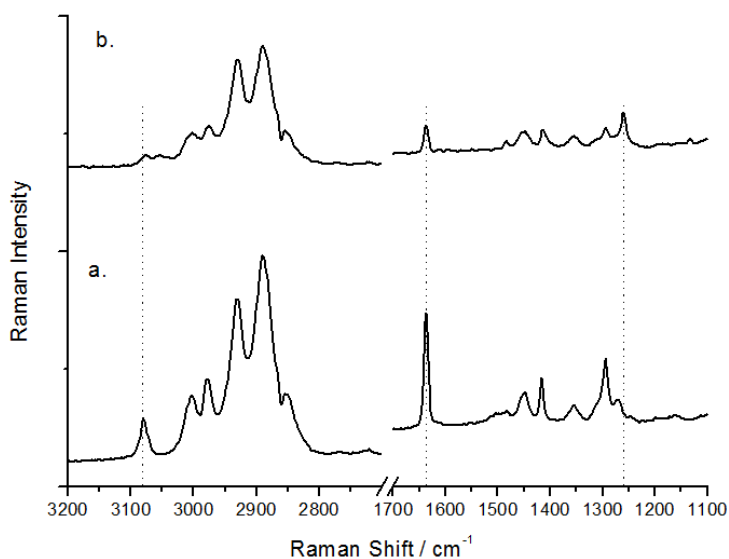


**Figure 8.5: Raman spectra of the allyl ring-PMO before and after epoxidation: (a.) AR-PMO and (b.) AR-PMO-O. The spectrum shows the areas of importance: 3200-2700 and 1700-1100 cm<sup>-1</sup>.**

The subsequent ammonia treatment and anchoring of the manganese complex is studied by DRIFT measurements (Figure 8.6). By comparison of the spectra of AR-PMO-O and AR-PMO-ON, a small shoulder at 1663 cm<sup>-1</sup> emerges. This signal represents a weak N-H bending vibration of the newly introduced amine functionality. After the reaction with the Mn(acac)<sub>2</sub>, this band and shoulder disappear again. Furthermore, new signals in the region between 1600 and 1500 cm<sup>-1</sup> appear. The signals originate from the new acetyl acetonate ligands. At 1565 and 1519 cm<sup>-1</sup>, the vibrations of the acetyl acetonate ring that reacted with the amine and the acetyl acetonate anion can be found, respectively. The signal at 1609 cm<sup>-1</sup> represents the C=O bond vibration of the acetylacetonate moiety without a manganese ion.<sup>5, 15, 16</sup> A broadening in the region around 1390 cm<sup>-1</sup> can be seen due to the CH<sub>3</sub> moieties. The

C=N bond could not be clearly distinguished in the infrared spectrum. This bond can be confirmed *via* a very weak signal in the region 1640-1690  $\text{cm}^{-1}$ , however due to possible overlap with vibrations of C=C and the acetylacetonate species, it is difficult to confirm.<sup>5,17</sup>

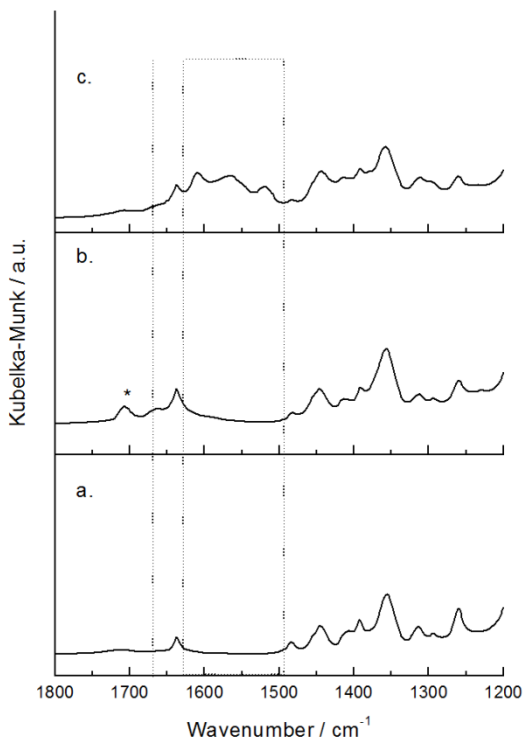


**Figure 8.6: DRIFT spectrum of (a.) AR-PMO-O; (b.) AR-PMO-ON and (c.) AR-PMO-ONMn. The spectrum shows the important area between 1800-1200  $\text{cm}^{-1}$ . The asterisk indicates acetone from the washing treatment.**

$^{13}\text{C}$  CP/MAS NMR spectroscopy measurements confirm the successful functionalisation of the allyl ring-PMO material with the eventual manganese complex. Figure 8.7 shows the results for AR-PMO, AR-PMO-ON and AR-PMO-ONMn together with the assignments. In the  $^{13}\text{C}$  CP/MAS NMR spectrum of the allyl ring-PMO, the signals arising from the ring and allyl structure are clearly visible, with the Si-CH<sub>2</sub>-Si (8 ppm) and the double bond at 142 and 113 ppm. Furthermore it corroborates with the Raman and DRIFT spectra because it shows some remains of the surfactant CTAB<sup>18</sup> (54 and 30 ppm) but also a small amount of 1-butanol is still present (67 ppm). The result of the epoxidation and subsequent ammonia treatment can be seen 8.8



by the appearance of additional signals. The oxirane ring can be opened in two different manners with two different structures as result (Species 1 and 2; Figure 8.7). Probably a mixture of the two species exists. The chemical shifts at 76 and 48 ppm can be attributed to species 1, *i.e.*, the carbons close to the alcohol and amine function, respectively. Also signals at 67 and 57 ppm could be found indicating the formation of species 2 as they originate from the carbons of the alcohol and amine functionality, respectively. Furthermore, it is also possible that some epoxide did not react. It is difficult to distinguish these signals as they would appear at  $\sim 58$  and  $\sim 48$  ppm.

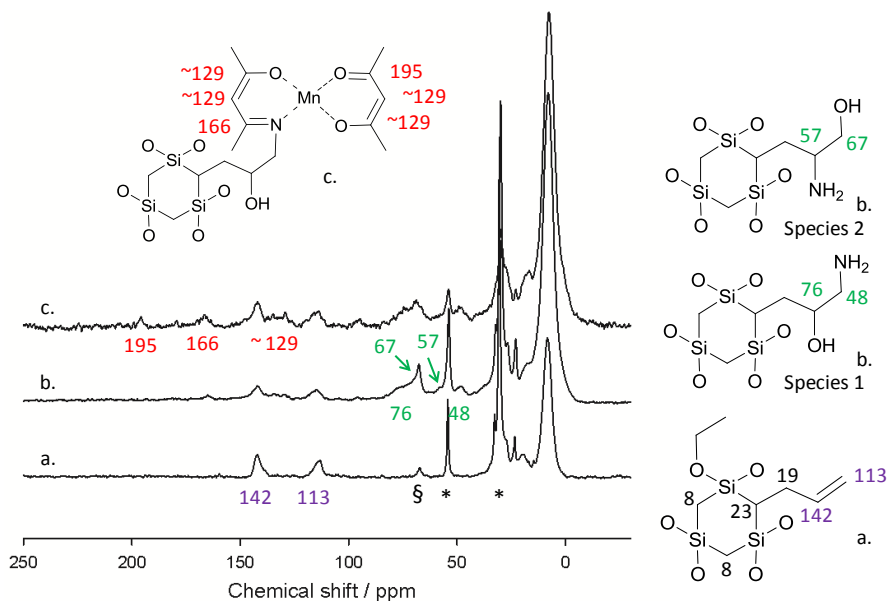


**Figure 8.7:**  $^{13}\text{C}$  CP/MAS NMR spectrum of (a.) AR-PMO; (b.) AR-PMO-ON and (c.) AR-PMO-ONMn and the assignment. The symbols \* and § indicate leftovers of the surfactant and 1-butanol from the synthesis.

Additional signals are observed in the  $^{13}\text{C}$  CP/MAS NMR spectrum after the reaction with the manganese complex. The signals at 195, 166 and a broad band at  $\sim 129$  ppm indicates the presence of the acetylacetonate species and the C=N bond.

Nitrogen sorption experiments were performed on the allyl ring-PMO and the PMO material containing the manganese complex. The isotherms can be seen in the figure below. The AR-PMO originally possesses a specific surface area of  $896 \text{ m}^2 \text{ g}^{-1}$ , a pore volume of  $0.53 \text{ mL g}^{-1}$  and a pore diameter  $d_{p(KJS)}$  of 2.8 nm. After the three

functionalisation steps, a general decrease in porosity is observed for AR-PMO-ONMn ( $S_{\text{BET}} = 709 \text{ m}^2 \text{ g}^{-1}$ ;  $V_p = 0.37 \text{ mL g}^{-1}$ ;  $d_{p(\text{KJS})} = 2.6 \text{ nm}$ ). This originates from the introduction of a metal complex where the two acac ligands occupy space within the pores.

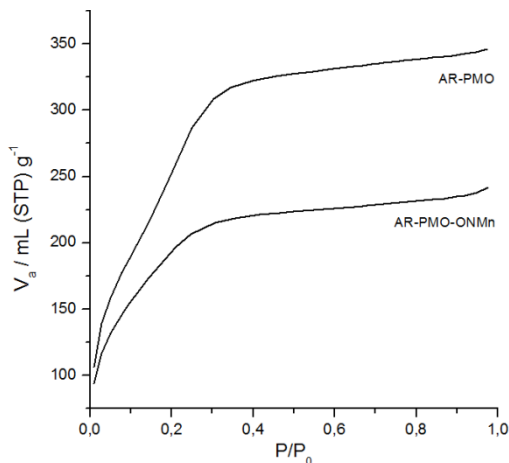


**Figure 8.8: Nitrogen adsorption isotherms of AR-PMO and AR-PMO-ONMn.**

Elemental analysis by means of X-ray fluorescence spectroscopy showed that  $0.60 \text{ mmol Mn g}^{-1}$  is present on AR-PMO-ONMn. Taking into account the amount of reachable double bonds on AR-PMO ( $0.73 \text{ mmol g}^{-1}$ ) and the amount of nitrogen determined by CHNS analysis on AR-PMO-ON ( $0.575 \text{ mmol g}^{-1}$ ), one can conclude that the functionalisation of the ally ring-PMO occurred with an overall yield of  $\sim 82\%$ .

## 8.5 Oxidation Catalysis

The catalyst AR-PMO-ONMn is evaluated for the epoxidation of the olefin cyclohexene. This epoxide is an important intermediate in the synthesis of adipic acid which can be converted in the polymer nylon-6,6.<sup>19</sup>

Different catalytic systems exist for the aerobic epoxidation of an olefin. Herein, the Mukaiyama epoxidation is chosen which is a mild procedure that operates at low temperatures.<sup>20</sup> As oxidant, molecular  $\text{O}_2$  is selected and furthermore a co-oxidant is added to assist in the reaction mechanism. Different aldehydes can act as co-oxidant but isobutyraldehyde is frequently used and rather inexpensive. Besides the desired

product cyclohexene oxide (**2**) (Figure 8.9), several other products can be formed. The epoxide ring can be opened in the presence of water and cyclohexane-1,2-diol (**3**) can be produced. The 2-chlorocyclohexanol (**4**) can be observed when an undesired side-reaction with the solvent chloroform occurs (*vide infra*). Furthermore an allylic oxidation can take place creating 2-cyclohexene-1-one (**5**) and 2-cyclohexene-1-ol (**6**). Especially cyclohexene is very sensitive for this allylic oxidation and therefore it can provide more information on catalytic pathways that take place.<sup>20</sup>

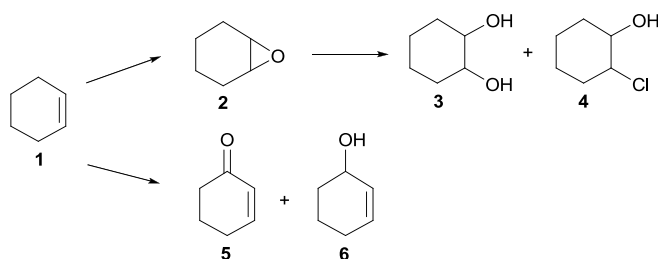


**Figure 8.9: Overview of the epoxidation of cyclohexene (1) with molecular  $O_2$ . The following products can be formed: the desired product cyclohexene oxide (2) and consecutive ring opening to cyclohexane-1,2-diol (3) or 2-chlorocyclohexanol (4). The allylic oxidation of (1) gives rise to 2-cyclohexene-1-one (5) and 2-cyclohexene-1-ol (6).<sup>20</sup>**

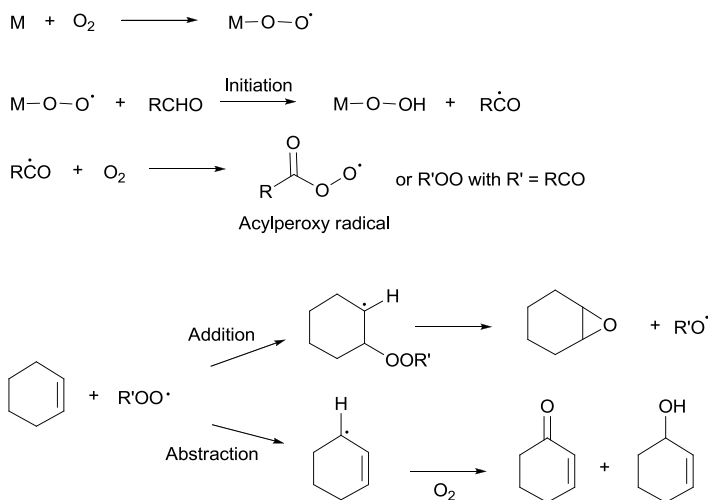


**Figure 8.10: General mechanism for the epoxidation of cyclohexene using  $O_2$  as oxidant and an aldehyde as co-oxidant.<sup>20</sup>**

Figure 8.10 provides the general catalytic reaction mechanism for the epoxidation of cyclohexene which is related to the aldehyde autoxidation. The formation of an

acylperoxy radical as oxidizing species is an important step in the reaction mechanism. They are known to react with double bonds which result into epoxides. Hydroxyl and alkylperoxy radicals favour the abstraction of allylic hydrogens with the formation of allylic oxidation products.

**Table 8.1: Conversion of the cyclohexene, formation of epoxide and the distribution of by-products formed together with the TON and TOF values. The leaching of the manganese complex is also presented.**

	<b>(1)</b>	<b>(2)</b>	<b>(3)</b>	<b>(4)</b>	<b>(5)</b>	<b>(6)</b>	TON <sup>a</sup>	TOF <sup>b</sup>	Leaching <sup>c</sup>
	%	%	%	%	%	%		h <sup>-1</sup>	%
AR-PMO-ONMn									
Run 1 <sup>d</sup>	31.8	20.1	1.5	11.8	2.0	1.9	122.33	24.43	0
Run 2 <sup>d</sup>	20.9	15.4	0.8	5.2	1.3	1.2	97.31	24.40	6
Run 3 <sup>d</sup>	43.6	24.0	0.8	9.2	1.7	1.6	148.32	37.76	0

<sup>a</sup> Turnover number calculated after 7 hours of reaction. <sup>b</sup> Turnover Frequency calculated after 30 minutes of reaction. <sup>c</sup> Determined by XRF measurements. <sup>d</sup> The blank reaction: 24.9% conversion of cyclohexene **(1)** and the formation of 11.8% of **(2)**; 0.7% of **(3)**; 5.4% of **(4)**; 3.0% of **(5)**; and 1.3% of **(6)**.

The catalyst is reused in three catalytic runs and the leaching of the manganese is determined between every catalytic run by examination of the filtrate obtained after catalysis. The obtained conversion and formation percentages are presented in Figure 8.1 together with the calculated TON and TOF values. Analysis of the data shows that during the first run almost ~32% of the cyclohexene is converted and that the epoxide is the main product (~20%). A small amount of 2-chlorocyclohexanol **(4)** is observed by ring opening of the epoxide. It is believed that this unwanted reaction can occur when the solvent chloroform degrades and the degradation products react with cyclohexene oxide.<sup>21,22</sup> Product **(4)** is also formed in absence of the catalyst (~5.4%). The other by-products **(3)**, **(5)** and **(6)** only consist of ≤2% each and these percentages are at the same level as the blank reaction. After the first catalytic run, no leaching was observed indicating a strong covalent attachment of the complex *via* the imine bond. After a short washing treatment and drying of the catalyst at room temperature, a second catalytic run is performed. It is immediately clear that the conversion is much lower in comparison with the first run and is similar to the blank reaction. These peculiar results are difficult to explain when the initial catalytic results

and especially the lack of leaching during the first run are quite promising. One possible explanation could be that the treatment between the first and second run did not sufficiently remove any remaining reagents and products. As the Mukaiyama epoxidation occurs *via* a radical pathway,<sup>20</sup> it is possible that the radicals continued to react. This could negatively affect the catalyst and cause a partial destruction which results in leaching of manganese (6%). Furthermore, remaining products and reagents in the pores of AR-PMO-ONMn can hinder the catalysis or can occupy and deactivate the catalytic site.

After the second run, the catalyst is carefully filtered, washed and almost immediately reused in the third catalytic run. As can be seen from Table 8.1, the catalyst again reaches and even exceeds the cyclohexene conversion of the first run. A conversion of ~44% is observed with the formation of 24% of cyclohexene oxide. The by-product distribution remains the same with a relatively large contribution of **(4)**. After the catalytic run, no leaching of the manganese is observed. These remarkable results corroborate the proposed explanation for the performance of the catalyst during the second run. Probably, the second run and after treatment removed any remaining reagents and activates the catalytic site again. It clearly indicates that more care should be taken during the washing and drying treatment of the catalyst between two runs.

Furthermore, when the product distribution of the first and third run is examined, it is clear that the catalyst mainly forms the epoxide **(2)** and the derived by-products **(3)** and **(4)**. Hence, only a very small amount of the cyclohexene is converted following the allylic oxidation pathways, although the cyclohexene is sensitive for this type of reaction. Especially metals with high oxidation states tend to induce this pathway. As our catalytic site is Mn(II), it will not favour this reaction.

The oxidation state before and after catalysis was determined by X-ray photoelectron spectroscopy measurements (Figure 8.11). The spectrum of AR-PMO-ONMn (before catalysis) shows a peak of Mn  $2p^{3/2}$  at 641.48 eV with a typical shake-up satellite that can be found at higher binding energies.<sup>23</sup>

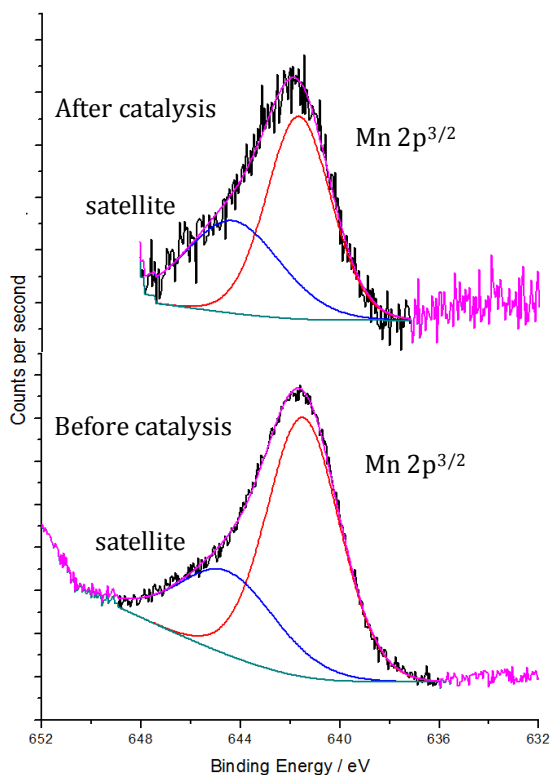


**Figure 8.11:** X-ray photoelectron spectroscopy measurements in the Mn 2p region of AR-PMO-ONMn before and after catalysis. The green line represents the base line, the red and blue lines are the deconvolution of the Mn 2p<sup>3/2</sup> and its shake-up satellite, respectively.

The peak of Mn<sup>2+</sup>, present in the complex Mn(acac)<sub>2</sub>, is normally found at 642.31 eV (not shown in the figure). By the heterogenization of the complex, the coordination of the manganese changes and the Mn 2p<sup>3/2</sup> peak shifts to lower binding energies. This occurs as one oxygen coordinated to Mn is replaced by a nitrogen atom which increases the electron density in Mn and thus, the binding energy decreases.<sup>16</sup> To conclude, the spectrum indicates that the oxidation state is +II. After catalysis, the Mn 2p<sup>3/2</sup> peak is found at 641.70 eV, again with the typical shake-up satellite. This means that no change in oxidation state occurred after three catalytic runs and this corroborates with the observed product distribution.

The nitrogen adsorption isotherm were also recorded after catalysis. Figure 8.11 gives a comparison between the AR-PMO-ONMn catalyst before and after epoxidation

catalysis. Only a small decrease in specific surface area could be observed as  $S_{\text{BET}}$  decreased from 709 to 562  $\text{m}^2 \text{g}^{-1}$ , showing the structural stability of the material.

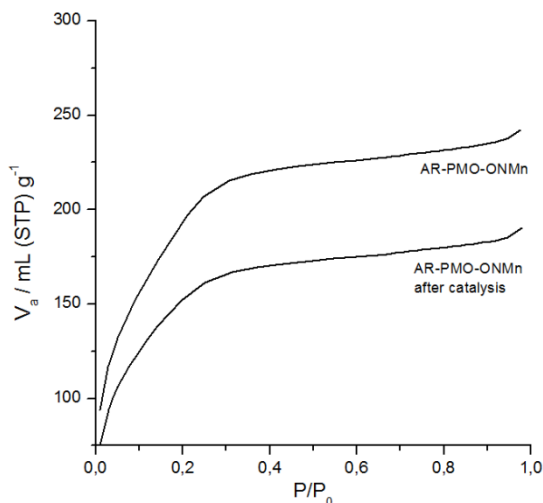


**Figure 8.12: Nitrogen adsorption isotherms of AR-PMO-ONMn, before and after catalysis.**

Although some promising results are obtained during the catalytic evaluation of AR-PMO-ONMn, it is clear that more research needs to be performed to elucidate the observed catalytic behaviour. And several issues need to be addressed, *i.e.*, (1) a more in-depth investigation on the treatment between two catalytic runs so that the effect of remaining reagents, products and radicals in the materials is clear; and (2) the formation of the by-product 2-chlorocyclohexanol (**4**) should be studied more in detail.

## 8.6 Conclusions

A multi-organic bridged PMO material based upon interconnected  $[\text{Si}(\text{CH}_2)]_3$  rings and modified with an allyl moiety is successfully used as a support for a  $\text{Mn}(\text{acac})_2$  catalyst. This metal complex is heterogenized *via* three subsequent steps: the epoxidation of the allyl functionality, the ring-opening of the oxirane to obtain an amine and a reaction between the amine and acac ligand of the metal complex. The materials are characterised with various techniques proving the different modifications. A PMO material with  $0.6 \text{ mmol Mn g}^{-1}$  is acquired.

This catalyst is probed in the epoxidation of cyclohexene using the Mukaiyama mechanism. The catalyst performed well in the first catalytic run with a preference for epoxide formation. Although the results were less for the second catalytic run, the third run reached the same level as the first run again. It is believed that the performance of the catalyst was hindered by remaining reagents, products and radicals. This leads to a lower catalytic activity but also a small amount of leaching of the manganese. Nevertheless, in the first and third run, no leaching was observed.

Further research should be performed on this matter to elucidate the behaviour of the catalyst. The excellent catalytic activity and zero leaching in the first and third run are already promising.



## 8.7 Experimental section

### Chemicals.

**For the allyl ring-precursor (ATDSCH).** 3-Bromo-1-propene (allyl bromide; 99%), diethylether (Et<sub>2</sub>O, contains 1 ppm BHT as stabilizer); tetrahydrofuran (THF, anhydrous) and t-butyl lithium (1.7 M solution in pentane) were obtained at Sigma Aldrich. 1,1,3,3,5,5-hexaethoxy-1,3,5-trisilacyclohexane (1,3,5[tris(diethoxy)sila]cyclohexane, TDSCH; 95%) was acquired at ABCR. NaHCO<sub>3</sub> (p.a.) was obtained at Acros Organics.

**For the allyl ring-PMO (AR-PMO).** Hexadecyl-trimethyl-ammonium bromide (CTAB, purum, 96.0%) was obtained from Fluka. Hydrochloric acid (37%; p.a.), 1-butanol were acquired from Sigma-Aldrich. Ethanol (denatured, ≥96%) was obtained from Carl Roth.

**For the modifications of AR-PMO.** 3-Chloroperoxybenzoic acid (mCPBA), Mn(acac)<sub>2</sub> and toluene (anhydrous, 99.8%) were acquired from Sigma Aldrich. Ammonia (rotipuran, 25% aqueous solution), dichloromethane (DCM, rotidry, ≥99.8%) and dimethylformamide (DMF, rotipuran, ≥99.8%) were obtained from Roth.

**For the oxidation catalysis.** Chloroform (anhydrous, 99.0%), cyclohexene (≥99.0%), ethyl acetate (LC-MS chromasolv) and 1,2,4-trichlorobenzene (reagent plus) were acquired from Sigma Aldrich. Isobutyraldehyde was obtained from TCI Europe.

All reagents and solvents were used as received except for the solvent dichloromethane which is first distilled on CaH<sub>2</sub> and stored on molecular sieves.

**Synthesis of 2-allyl-1,3,5[Tris(diethoxy)sila]cyclohexane (ATDSCH; allyl ring precursor).** A volume of 50 mL commercially available 1,1,3,3,5,5-hexaethoxy-1,3,5-trisilacyclohexane (TDSCH) is dissolved in 150 mL Et<sub>2</sub>O under inert atmosphere. Afterwards, t-butyl lithium (100 mL) is added drop wise to this solution. The mixture is stirred at -78.5°C for 30 minutes. Next, 11 mL of 3-bromo-1-propene in 200 mL THF is added drop wise and stirred for 15 h where the temperature is gradually raised to

room temperature. The allyl ring precursor (ATDSCH) is washed and purified with 200 mL Et<sub>2</sub>O and 1 w% NaHCO<sub>3</sub> in a separation funnel. The organic phase is recuperated and solvents are evaporated until a yellow oil is obtained. The product is characterised with NMR measurements. <sup>1</sup>H NMR (CDCl<sub>3</sub>): δ = 5.9 (m, 1H, CH=CH<sub>2</sub>); δ = 4.8 (dd, 2H, CH=CH<sub>2</sub>); δ = 3.65 (m, 12H, -CH<sub>2</sub>CH<sub>3</sub>); δ = 2.25 (t, 2H, CH<sub>2</sub>-CH=CH<sub>2</sub>); δ = 1.1 (t, 18H, -CH<sub>2</sub>CH<sub>3</sub>); δ = 0.29 (t, 1H, (Si)<sub>2</sub>-CH-CH<sub>2</sub>); δ = ~ 0 ppm (s, 4H, Si-CH<sub>2</sub>-Si).

**Synthesis of the allyl ring-PMO (AR-PMO).** A total amount of 1.745 g CTAB is dissolved in 850 mL distilled water, 16.25 mL butanol and 8.75 mL hydrochloric acid. The mixture is vigorously stirred at room temperature until CTAB is completely dissolved. A volume of 3 mL ring precursor (TDSCH) and 3 mL allyl containing ring precursor (ATDSCH) are added together to this mixture. After stirring for 30 minutes, the mixture is spray dried. The spray drying was performed on a Buchi B290 apparatus with a two-fluid nebulizer connected to pressurized air. The spray drier was utilized with the following settings, *i.e.*, an inlet temperature of 220°C, an outlet temperature of 110°C, the aspirator velocity was set on 40 m<sup>3</sup> h<sup>-1</sup>, a solution feed of 2.8 mL min<sup>-1</sup> and a nozzle gas flow of 8 L min<sup>-1</sup>. The template is removed by an extraction procedure using acidified ethanol. The resulting material, denoted as allyl ring-PMO or AR-PMO, is dried at 120°C under vacuum.

**Epoxidation of AR-PMO.** An amount of 0.9511 g of dried AR-PMO is added to 50 mL dry dichloromethane under inert atmosphere. The flask is placed in an ice bath. Separately, 0.5136 g of mCPBA is very slowly added under inert atmosphere to 10 mL of dry dichloromethane, also cooled at 0°C. The mCPBA solution is slowly added to the PMO while maintaining the inert atmosphere. This mixture is stirred for 24 hours at 0°C. The solids are filtered under inert atmosphere and thoroughly washed with dry dichloromethane. The solids are vacuum dried on the filter for two hours. Afterwards, the solids are transferred under inert atmosphere to a vial where they are further dried at 50°C under vacuum. The resulting material is denoted as AR-PMO-O.

**Ammonia treatment on AR-PMO-O.** A certain amount of dried AR-PMO-O is added to a flask and covered completely with an aqueous solution of ammonia. The mixture is vigorously stirred for 4.5 hours at room temperature. Afterwards, the solids

are washed with copious amounts of water to remove any physisorbed ammonia and finally the solids are washed with acetone and dried at 50°C under vacuum. The material is denoted as AR-PMO-ON.

**Anchoring of the manganese complex on AR-PMO-ON.** Dried AR-PMO-ON (0.80 g) is added to 70 mL of dry toluene under inert atmosphere. Subsequently, 1 g of  $\text{Mn}(\text{acac})_2$  is added to the PMO and the mixture is stirred for 20 h at 55°C. The solids are filtered and washed with DMF to remove the excess of  $\text{Mn}(\text{acac})_2$ . Afterwards, the material is stirred in toluene for 3 hours at 55°C and then filtered and washed with toluene and acetone. The solid, denoted as AR-PMO-ONMn, is dried at 50°C under vacuum.

**Oxidation catalysis.** In a typical catalytic set-up, a Schlenk flask was charged with 7.0 mL of cyclohexene, 12.88 mL of isobutyraldehyde (co-oxidant), 9.0 mL of 1,2,4-trichlorobenzene (internal GC standard) and 40 mL of chloroform. Molecular oxygen (99.9% pure) was bubbled through the liquid phase with a constant oxygen flow of 7.3 mL min<sup>-1</sup> by means of a mass flow controller. The Schlenk flask was equipped with a liquid condenser coupled with recirculating cooling liquid at -4°C to prevent evaporation of the reaction mixture. The catalytic mixture was stabilized at 40°C before a certain amount of catalyst was added (0.3 g of AR-PMO-ONMn or 0.2 mmol of Mn). Aliquots were taken out of the reaction mixture and were analyzed with gas chromatography.

**Characterisation.** Nitrogen sorption experiments are performed on a Tristar 3000 (Micromeritics) at -196°C. Samples are pre-treated at 120°C for 16 hours while degassing. Diffuse Reflectance Infrared Fourier Transform (DRIFT) and Raman spectroscopy are performed on a hybrid apparatus of Thermo Scientific containing a Nicolet 6700 IR and NXR FT-Raman spectrometer with a nitrogen cooled MCT-A detector and InGaAs detector, respectively. The DRIFT spectra are obtained using a Graseby Specac diffuse reactant cell, operating under vacuum. Elemental analysis (CHN) is performed on a Thermo Flash 2000 elemental analyzer. During the measurement, a  $\text{V}_2\text{O}_5$  catalyst is used. X-ray Fluorescence (XRF) measurements were performed on a NEX CG from Rigaku using a Mo X-ray source. The cross polarization

magic angle spinning nuclear magnetic resonance ( $^{13}\text{C}$  CP MAS NMR) spectra were recorded at 100.6 MHz on a Bruker AVANCE-400 WB spectrometer at RT. The samples were spun at 13 kHz. An overall 10 000 free induction decays were accumulated with 4 s of recycle time. Chemical shifts were measured relative to a tetramethylsilane (TMS) standard. Ultra-fast gas chromatography (GC) was performed on a Finnigan Trace Ultra GC with flame ionization detector (FID) and a 5% diphenyl/95% polydimethylsiloxane column with 10 m length and 0.1 mm internal diameter. X-ray photoelectron spectroscopy measurements were recorded on a S-Probe XPS spectrometer with monochromated Al (1486 eV) exciting radiation from Surface Science Instruments (VG). The sample was positioned onto a conducting carbon tape. In order to compensate for charging of the sample a nickel grid was used, placed 2 mm above the sample. A low energy electron flood gun 6 eV was used as a neutralizer. All measurements were calibrated towards a value for the C 1s peak of adventitious carbon at 284.6 eV. Calculation of the atomic concentrations and peak fittings were performed using Tougaard background subtraction and Scofield sensitivity factors within Casa XPS software.

## 8.8 References

1. S. Shylesh, M. J. Jia and W. R. Thiel, *European Journal of Inorganic Chemistry*, 2010, 4395-4410.
2. K. C. Gupta, A. K. Sutar and C.-C. Lin, *Coordination Chemistry Reviews*, 2009, **253**, 1926-1946.
3. M. Sasidharan, S. Fujita, M. Ohashi, Y. Goto, K. Nakashima and S. Inagaki, *Chemical Communications*, 2011, **47**, 10422-10424.
4. M. Sasidharan and A. Bhaumik, *Acs Applied Materials & Interfaces*, 2013, **5**, 2618-2625.
5. P. Oliveira, A. Machado, A. M. Ramos, I. M. Fonseca, F. M. B. Fernandes, A. M. B. Do Rego and J. Vital, *Catalysis Communications*, 2007, **8**, 1366-1372.
6. R. S. Porto, M. Vasconcellos, E. Ventura and F. Coelho, *Synthesis-Stuttgart*, 2005, 2297-2306.
7. C. Vercaemst, M. Ide, B. Allaert, N. Ledoux, F. Verpoort and P. Van Der Voort, *Chemical Communications*, 2007, 2261-2263.
8. D. Esquivel, Universidad de Córdoba, Ph.D. thesis, 2011.
9. Y. Goto and S. Inagaki, *Microporous and Mesoporous Materials*, 2006, **89**, 103-108.
10. C. Vercaemst, Ghent University, Ph.D. thesis, 2009.
11. K. Landskron, B. D. Hatton, D. D. Perovic and G. A. Ozin, *Science*, 2003, **302**, 266-269.
12. F. Goethals, B. Meeus, A. Verberckmoes, P. Van der Voort and I. Van Driessche, *Journal of Materials Chemistry*, 2010, **20**, 1709-1716.
13. F. Goethals, I. Ciofi, O. Madia, K. Vanstreels, M. R. Baklanov, C. Detavernier, P. Van der Voort and I. Van Driessche, *Journal of Materials Chemistry*, 2012, **22**, 8281-8286.
14. M. Ide, Ghent University, Ph.D. thesis, 2012.
15. V. Parvulescu, M. Mureseanu, A. Reiss, R. Ene and S.-H. Suh, *Revue Roumaine De Chimie*, 2010, **55**, 1001-1008.
16. S. Bhattacharjee, D.-A. Yang and W.-S. Ahn, *Chemical Communications*, 2011, **47**, 3637-3639.
17. D. H. Williams and I. Fleming, *Spectroscopic Methods In Organic Chemistry*, McGraw-Hill Publishing Company, Birkshire, 1995.
18. B. K. Lavine, W. T. Cooper, Y. F. He, S. Hendayana, J. H. Han and J. Tetreault, *Journal of Colloid and Interface Science*, 1994, **165**, 497-504.
19. P. Jin, Z. Zhao, Z. Dai, D. Wei, M. Tang and X. Wang, *Catal Today*, 2011, **175**, 619-624.
20. B. B. Wentzel, P. L. Alsters, M. C. Feiters and R. J. M. Nolte, *The Journal of Organic Chemistry*, 2004, **69**, 3453-3464.
21. E. A. Ibrahim, R. L. Lippincott, L. Brenner, I. H. Suffet and R. E. Hannah, *Journal of Chromatography A*, 1987, **393**, 237-253.
22. A. M. Dietrich, R. F. Christman and G. S. Durell, *Biological Mass Spectrometry*, 1988, **15**, 453-458.
23. H. W. Nesbitt and D. Banerjee, *American Mineralogist*, 1998, **83**, 305-315.



## 9 Concluding remarks

In this dissertation several modification procedures for Periodic Mesoporous Organosilicas were developed to obtain materials which are suitable as mercury or CO<sub>2</sub> adsorbent or as acid or oxidation catalyst.

Chapter 4 described the modification of the double bond of the ethylene-bridged PMO *via* two subsequent functionalisation steps. First a bromination was applied, then a substitution of the bromine with a propyl thiol group was performed. The latter occurred *via* the *in-situ* generation of the Grignard reagent of 3-chloro-1-propane thiol. The modification was successful and the thiol-containing PMO material was utilized as mercury(II) adsorbent in a batch-type adsorption reaction. The adsorption experiments showed that the thiol-containing PMO material adsorbed the mercury in a 1:1 ratio. The reusability of the functionalised PMO was compared with thiol-containing silica adsorbents. The PMO retained its structural and chemical characteristics upon reuse of the adsorbent.

This application was further explored for this modified PMO material by its incorporation in *Diffusive Gradients in Thin* film probes (Chapter 5). With these probes, the amount of labile mercury can be determined. The thiol containing PMO material showed the highest accumulation rate in comparison with commercially available resins (Chelex-100 and Sumichelate Q10R) and two thiol functionalised silica materials. Furthermore, the DGT probe was placed in a water pond. The results demonstrated that the PMO could be used outside the laboratory environment.

The results above clearly indicate that these PMO materials are proper candidates for metal adsorption. The chemical and structural stability of the PMO material is a huge advantage over ordered mesoporous silicas which are generally functionalised *via* grafting or co-condensation processes. Probably, these advanced PMO materials have a bright future in advanced *high-end* metal adsorption applications where reusability is a real asset. Or where precious metals need to be recovered.

The introduction of amine functionalities in Chapter 6 turned the ethylene-bridged PMO in a CO<sub>2</sub> adsorbent. Different amines were employed, varying the chain length and the amount of primary and secondary amines. The incorporation occurred successfully and the PMO materials functionalised with diaminododecane (DADD) exhibited an amine efficiency or CO<sub>2</sub>/N ratio of 0.42. This value approximated the maximum theoretical value of 0.5, which can be achieved under dry conditions for CO<sub>2</sub> chemisorption processes. Furthermore, proof was found with infrared spectroscopy that the chemisorption on the PMO material occurs *via* the formation of a carbamate species. Although the PMO material functionalised with DADD performed well in the sequestration of CO<sub>2</sub>, it will be very difficult for this type of mesoporous materials to compete with zeolites and MOF materials. The loading of the PMO should be increased and the deactivation of amines due to close proximity of carbamate species should be diminished as this significantly decreases the amine efficiency.

Besides the incorporation of thiol and amine functionalities, also sulfonic acid functions were incorporated to obtain a solid acid catalyst. First, the direct sulfonation of the ethylene-bridged PMO material was attempted as described in Chapter 7. However, it was not possible to strongly anchor sulfonic acid groups. A loss of acid groups occurred when used in the straightforward esterification of acetic acid with 1-propanol. It was not possible to elucidate the exact nature of the bond between the –SO<sub>3</sub>H functionality and the ethene bridge. Therefore, another strategy was executed: the thiol containing PMO material, first developed to acquire a mercury adsorbent, was oxidized. The catalytic ability of this sulfonic acid containing PMO was evaluated for the acetylation of glycerol. A similar catalytic activity was observed for this catalyst when it was compared with the commercially available catalyst Amberlyst-15. The PMO with –SO<sub>3</sub>H could be reused for several catalytic runs.

The obtained catalytic results of this sulfonic acid group containing PMO are promising as the catalyst can be reused and it can compete with a commercial catalyst. The attachment of the sulfonic acid function *via* propyl groups instead of directly to the ethene bridge solved the leaching problem which was first observed. Most importantly, this evidently shows the enormous versatility of the developed PMO materials as an mercury adsorbent can be relatively easy transformed into an acid



catalyst. And additionally both modified PMO materials (-SH and -SO<sub>3</sub>H) performed well for their own specific application.

Chapter 8 expanded the use of PMOs in the field of catalysis by the development of a manganese(II) containing material. Efforts were done to anchor Mn(acac)<sub>2</sub> on an ethenylene-bridged PMO *via* several subsequent modification pathways. The first step consisted of an epoxidation of the double bond. This appeared to be the actual bottleneck of the entire manganese functionalisation. It was not possible to epoxidize the organic bridge of the ethene PMO. Therefore, a different type of PMO material was selected: a multi-organic bridged PMO, namely the ring-PMO. After the incorporation of an allyl functionality on the precursor and spray-drying of the allyl ring-PMO, the subsequent modification procedures could be successfully performed. A manganese(acac)<sub>2</sub> complex was anchored and 0.6 mmol g<sup>-1</sup> of manganese sites were obtained. The catalyst was evaluated for the epoxidation of cyclohexene and the Mn containing PMO performed well in the first catalytic run. A cyclohexene conversion of ~32% was obtained with ~20% of epoxide formation. Although, the catalyst appeared not reusable in the second run, it performed well in the third run with ~44% cyclohexene conversion. Some issues concerning the second catalytic run should be elucidated, but nevertheless this catalyst is a promising candidate for oxidation catalysis. The ring-PMO is a support that exhibits a high chemical and structural stability and moreover, the introduction of the allyl group creates an excellent function available for further chemical modifications.

Overall, the modification of the allyl ring-PMO with the Mn(acac)<sub>2</sub> is a success story. Nonetheless, questions remain such as why the ethene bond of the ethenylene-bridged PMO material could not be epoxidized. The nature of this double bond is of course very different as it is part of an solid framework and it is directly surrounded by two silicon atoms. Probably this not only influenced the reactivity in the epoxidation reaction but also during the direct sulfonation. The terminal ethene bond of the allyl is therefore a better candidate for further modifications as it is a dangling functionality and the influence of the silicon atoms is limited.

The research performed in this dissertation together with the literature overview in Chapter 1 and 2, show that great potential lies within these hybrid mesoporous materials. However, many challenges still remain to improve their overall properties and I believe the future of these hybrids can be found in fine-tuning the material for a very specific *high-end* application.

Especially in the field of low-*k* materials, the PMO seems to be suitable as the real strength of the PMO comes from its intrinsic properties such as their hydrophobicity, better hydrothermal stability and incorporated chemical functions. By using the PMO as a low-*k* film, one can take advantage of these properties together with its porosity. Several studies already proved their potential. Although this type of research is extremely challenging because it is a combination of material science, chemistry and micro-electronics, this application is probably more evolved than any other. However, research still is necessary to further improve the stability of the films.

The intrinsic properties are also beneficial for chromatography. Further investigation is definitely needed to obtain the wanted spherical morphology and at the same time the right particle size and uniformity. Without these requirements, it will be difficult to apply PMOs as stationary phase. Spray-drying of PMOs could provide a solution for this and in the mean time scale up the synthesis. The latter is an issue most often forgotten, but it strongly limits the applicability of PMOs in almost every field.

Other applications such as catalysis, adsorption and biomedical purposes require more research and still need to find their “special niche” where they can outperform commercial or benchmark materials. Their reusability, hydrophobicity and chemical and structural stability will be key factors.

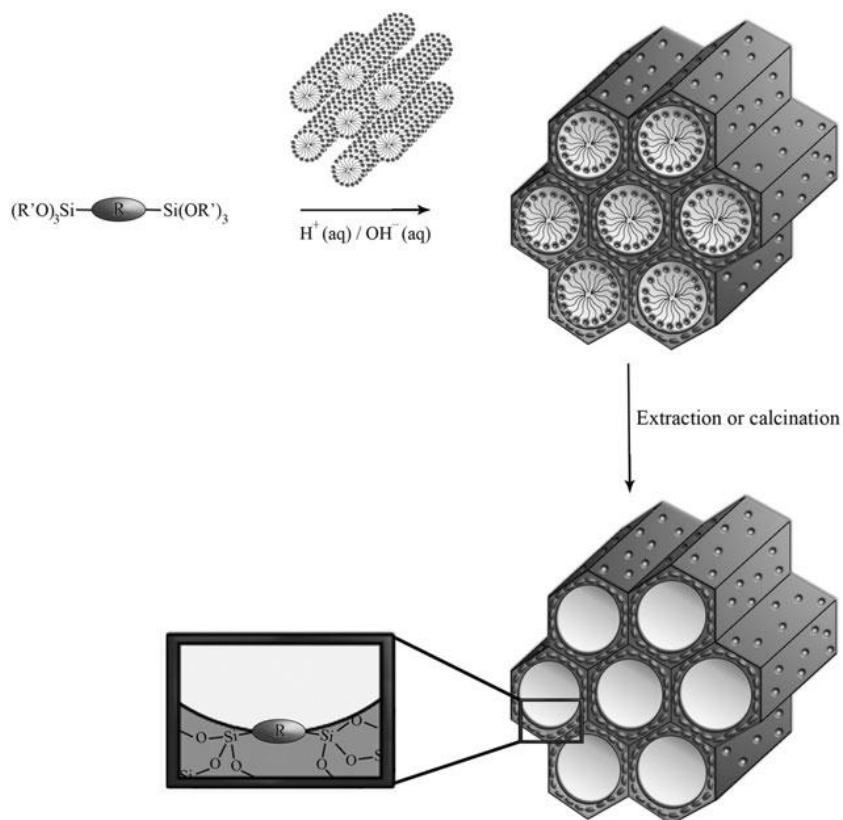
## **10 Nederlandse samenvatting**

### **10.1 Periodieke Mesoporeuze Organosilica's**

Periodieke Mesoporeuze Organosilica's of PMO's zijn geordende poreuze silica materialen met ingebouwde organische bruggen (Figuur 10.1). PMO's worden gesynthetiseerd door de hydrolyse en daaropvolgende polycondensatie van een polysilsesquioxaan, of meestal een bis-silaan, rondom een surfactant. Dit surfactant vormt namelijk micellen in een waterige oplossing en zal als mal dienst doen. Wanneer het netwerk gevormd is, wordt het surfactant verwijderd door middel van een extractie of milde thermische behandeling onder inerte atmosfeer. Het resultaat is een poreus materiaal met hoog specifiek oppervlak, groot porievolume, uniforme poriegroottedistributie en mesoporiën. De uiteindelijke eigenschappen van PMO's worden sterk beïnvloed door de synthesecondities, zoals de pH, temperatuur, synthese- en roertijd, surfactant en het toevoegen van additieven. Het type bis-silaan is eveneens van groot belang. De organische brug tussen de twee silicium atomen kan vrij eenvoudig zijn zoals bv. methaan, ethaan, etheen en benzeen functionaliteiten. Daarnaast bestaan er ook vrij complexe en geavanceerde bruggen waar bv. chirale bruggen met metalen ingebouwd zijn in PMO-materialen.

Deze materialen vertonen grote gelijkenissen met de synthese van MCM- en SBA-type materialen alhoewel enkele grote verschillen bestaan. De functionele groepen in PMO's zijn homogeen verdeeld doorheen de poriewanden. Dit betekent dat een groot deel van de functionaliteiten niet beschikbaar zijn voor enige chemische modificatie. Deze groepen dragen wel bij tot de algemene karakteristieken van de PMO zoals rigiditeit en flexibiliteit. De organische bruggen aanwezig aan het oppervak daarentegen zijn wel bereikbaar en kunnen chemisch gemodificeerd worden.

PMO's kunnen gebruikt worden in een brede waaier aan toepassingsgebieden. Onderzoek wordt verricht naar het aanwenden van deze materialen in chromatografie, katalyse, adsorptie, sensoren en biomedische applicaties.



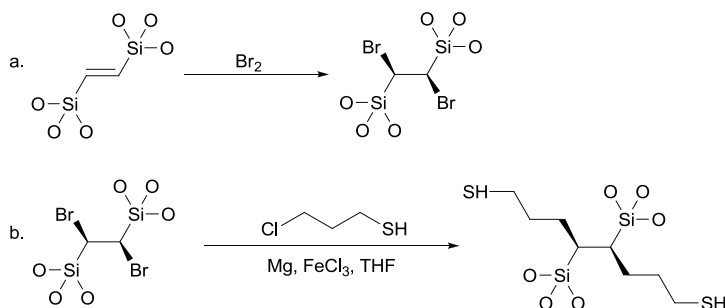
**Figuur 10.1:** Schematische voorstelling van de synthese van een Periodieke Mesoporeuze Organosilica: een bis-silaan met de organische groep R en een alkoxy groep R' hydrolyseert en polycondenseert rond de micellen van het surfactant. Na verwijdering via extractie of calcinatie wordt een poreus materiaal verkregen.

Deze doctoraatsthesis handelt over de ontwikkeling van adsorbentia en heterogene katalysatoren op basis van PMO-materialen voor respectievelijk de verwijdering van kwik, de adsorptie van koolstofdioxide en het katalyseren van esterificaties en epoxidaties.

## 10.2 Thiol-gefunctionaliseerde PMO's als kwik adsorbens

Een thiol-gefunctionaliseerd PMO-materiaal werd bekomen door de post-modificatie van de etheenbruggen aanwezig in de etheenleen-gebrugde PMO. Door middel van een bromering van de etheenfunctionaliteit en vervolgens een substitutie

met het Grignard reagens van 3-chloro-1-propaanthiol wordt het PMO-materiaal omgevormd tot een adsorbens (Figuur 10.2).



**Figuur 10.2: Modificatie van het ethenyleen-gebrugde PMO-materiaal: a. Bromering van de dubbele binding en b. Substitutie van het broomatoom met het Grignard reagens van 3-chloro-1-propanethiol.**

Na optimalisatie van de modificatiereacties, werd een materiaal vervaardigd met  $0.44 \text{ mmol SH g}^{-1}$ . De structurele eigenschappen, bepaald met stikstofsorptie metingen, worden samengevat in Tabel 10.1.

**Tabel 10.1: De structurele eigenschappen van de Periodieke Mesoporeuze Organosilicas: het ethenyleen-gebrugde, gebromeerde en thiol gefunctionaliseerde materiaal worden weergegeven.**

	$S_{\text{BET}}^{\text{a}}$ $\text{m}^2 \text{g}^{-1}$	$V_{\text{p}}^{\text{b}}$ $\text{cm}^3 \text{g}^{-1}$	$d_{\text{p}}^{\text{c}}$ nm	mmol SH $\text{g}^{-1}$ <sup>d</sup>	aantal SH $\text{nm}^{-2}$
ePMO	1182	1.08	6.23	-	-
Br-ePMO	558	0.55	5.47	-	-
SH-ePMO	636	0.55	6.23	0.44	0.22

<sup>a</sup> Het specifieke oppervlak berekend met de BET-vergelijking. <sup>b</sup> Totale porievolume bij  $P/P_0 = 0.98$ . <sup>c</sup> Poriediameter berekend van de desorptie isotherm met de BJH-methode. <sup>d</sup> Bepaald via de thioltitratie.

De kwikadsorptie eigenschappen van dit materiaal werden onderzocht en vergeleken met een aantal referentiematerialen. Zo werden twee SBA-15 materialen op verschillende wijze gefunctionaliseerd met MPTES: (1) aan de hand van een preactivatie stap met  $\text{NEt}_3$  waardoor een monolaag aan mercaptopropyl functionaliteiten wordt verkregen en (2) met behulp van  $\text{HCl}$  waardoor een zelfcondensatie van MPTES op het oppervlak van de SBA plaatsvindt. Daarnaast werd

eveneens een thiolhoudende silica gesynthetiseerd door MPTES en TEOS te co-condenseren via een één-pot-synthese. Een overzicht van de drie gesynthetiseerde adsorbentia is te vinden in Tabel 10.2.

**Tabel 10.2: Overzicht van de structurele en chemische eigenschappen van de geselecteerde adsorbentia.**

	$S_{\text{BET}}^{\text{a}}$	$V_{\text{p}}^{\text{b}}$	$d_{\text{p}}^{\text{c}}$	mmol SH $\text{g}^{-1}$ $^{\text{d}}$	# SH $\text{nm}^{-2}$
	$\text{m}^2 \text{g}^{-1}$	$\text{mL g}^{-1}$	nm		
SBA-NEt <sub>3</sub> (10x)-/-2u-65°C	587	0.61	4.82	1.60	1.10
SBA-5%HCl-90-96u-50°C	286	0.29	4.25	10.00	7.02
co-cond-10	704	0.78	4.82	1.10	0.75

<sup>a</sup> Het specifieke oppervlak berekend met de BET-vergelijking. <sup>b</sup> Totale porievolume bij  $P/P_0 = 0.98$ . <sup>c</sup> Poriediameter berekend van de desorptie isotherm met de BJH-methode. <sup>d</sup> Bepaald via de thioltitratie.

De kwikadsorptie eigenschappen en regeneratiemogelijkheden van bovenstaande adsorbentia werden geëvalueerd in een aantal adsorptie-experimenten. Daaruit bleek dat bij de silica-gebaseerde adsorbentia ofwel een groot verlies van functionele groepen plaatsvond, ofwel dat de structurele eigenschappen van het materiaal aangetast werden. Het thiol-gefunctionaliseerde PMO materiaal toonde echter geen verlies van thiolgroepen en behield zijn porositeit. Het was duidelijk dat dit PMO adsorbens zowel chemisch als structureel stabiel was. Een maximale adsorptiecapaciteit van  $64 \text{ mg g}^{-1}$  werd waargenomen en er werd eveneens vastgesteld dat één thiolgroep reageert met één kwikatoom.

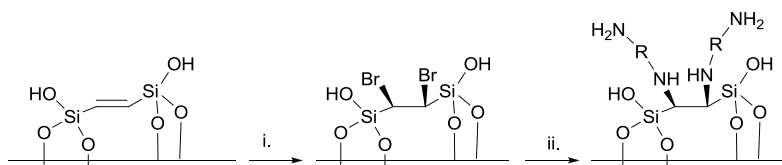
De toepassing van dit thiol-gefunctionaliseerde PMO materiaal werd verder uitgebreid door het te implementeren in de *Diffusive Gradients in Thin (DGT) film* techniek. Dit laat toe om labiel kwik te bepalen in meren of rivieren zonder dat het transport en opslag van het staal beïnvloed kan worden door externe factoren.

De thiol-gefunctionaliseerde PMO werd vergeleken met twee commercieel beschikbare adsorbentia (Chelex-100 en Sumichelate Q10R). Daarnaast werden ook twee thiol-gefunctionaliseerde silica materialen getest: een commerciële thiol-bevattende silica en een SBA-15 waarop MPTES is verankerd. Een enigszins hogere accumulatiesnelheid werd geobserveerd voor het PMO materiaal in vergelijking met

de andere silica-materialen en Sumichelate Q10R. Chelex -100 daarentegen vertoonde een relatief lagere accumulatiesnelheid. De toepassing werd nog verder uitgebreid door het gebruiken van de thiol-gefunctionaliseerde PMO-materiaal voor het adsorberen van kwik in een vijver. Deze experimenten toonden aan dat ongeveer 75% van het kwik aanwezig was in een labiele vorm.

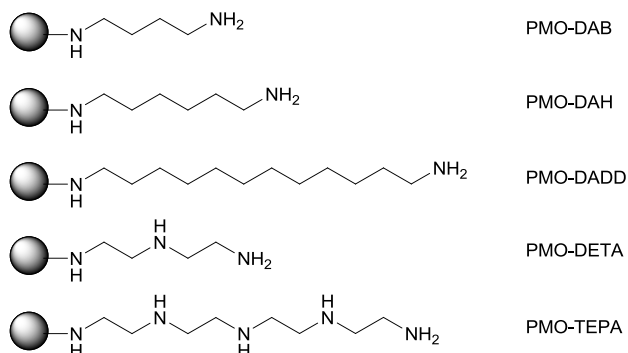
### 10.3 Amine-gefunctionaliseerde PMO's als CO<sub>2</sub> adsorbens

Koolstofdioxide adsorbentia werden ontwikkeld door de incorporatie van stikstofhoudende groepen (primaire en secundaire amines) in ethenyleen-gebrugde PMO-materialen. Dit werd bewerkstelligd door een bromering van de dubbele binding waarbij het broom vervolgens werd gesubstitueerd door een amine (Figuur 10.3). Hierbij werden verschillende amines gebruikt waardoor de ketenlengte en het soort functionaliteit (primair of secundair), maar ook de hoeveelheid aan amines werd gevarieerd. Zo werden diaminobutaan (DAB), diaminohexaan (DAH), diaminododecaan (DADD), diethyleentriamine (DETA) en tetraethyleenpentamine (TEPA) uitgekozen als reagens, waarbij de functionalisatie eerst werd geoptimaliseerd vooraleer CO<sub>2</sub> adsorptie experimenten plaatsvonden. De resulterende materialen worden schematisch weergegeven in Figuur 10.4.



**Figuur 10.3: Schematisch overzicht van de modificatie van de ethenyleen-gebrugde PMO: i. bromering van de dubbele binding; ii. Substitutie van het broomatoom met het reagens NH<sub>2</sub>-R-NH<sub>2</sub> waarbij R een alifatische koolstofketen voorstelt met of zonder extra secundaire amines.**

Na karakterisatie werd de CO<sub>2</sub> adsorptiecapaciteit en de amine-efficiëntie bepaald van de stikstof-gefunctionaliseerde materialen en vergeleken met een SBA-15 materiaal gefunctionaliseerd met APTES. De maximale amine-efficiëntie of de CO<sub>2</sub>/N ratio is theoretisch 0.5 voor processen waarbij chemische adsorptie optreedt onder droge condities door middel van carbamaatvorming.



**Figuur 10.4:** Overzicht van de gemodificeerde PMO-materialen waarbij de gebruikte benamingen eveneens worden weergegeven.

**Tabel 10.3:** CO<sub>2</sub> adsorptie resultaten voor de amine-gefunctionaliseerde PMO's en SBA-15 gefunctionaliseerd met APTES.

	PMO-DAB-kt-3		PMO-DAH-kt-3		PMO-DADD-kt-3	
	w%	mmol g <sup>-1</sup>	w%	mmol g <sup>-1</sup>	w%	mmol g <sup>-1</sup>
N <sup>a</sup>	2.54	1.81	0.84	0.60	0.46	0.33
CO <sub>2</sub> <sup>b</sup>	0.70	0.16	0.58	0.13	0.60	0.14
CO <sub>2</sub> /N	0.09		0.22		<b>0.42</b>	

	PMO-DETA-kt-5		PMO-TEPA-kt-5		SBA-15-APTES	
	w%	mmol g <sup>-1</sup>	w%	mmol g <sup>-1</sup>	w%	mmol g <sup>-1</sup>
N <sup>a</sup>	3.47	2.48	4.25	3.04	2.37	1.20
CO <sub>2</sub> <sup>b</sup>	1.09	0.25	1.28	0.29	0.27	0.16
CO <sub>2</sub> /N	0.10		0.10		0.16	

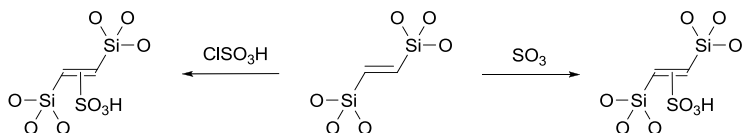
<sup>a</sup> Bepaald via elementaire analyse. <sup>b</sup> Bepaald via TGA analyse.

De amine-efficiëntie van PMO-DADD-kt-3 (0.42) benaderde de maximale theoretische waarde van 0.5. De relatieve lage waarden van de andere adsorbentia kunnen enerzijds verklaard worden door de relatief lage functionalisatiegraad. Anderzijds, bij de materialen met een hoge hoeveelheid amine, zoals PMO-DETA-kt-5 en PMO-TEPA-kt-5, kan een deactivatie van de amines optreden door waterstofbrugvorming tussen een gevormd carbamaat en een vrij amine van dezelfde of een andere keten. Deze deactivatie zorgt voor een drastische vermindering van de adsorptiecapaciteit.



## 10.4 PMOs gemodificeerd met sulfonzure groepen als katalysator voor esterificatie reacties

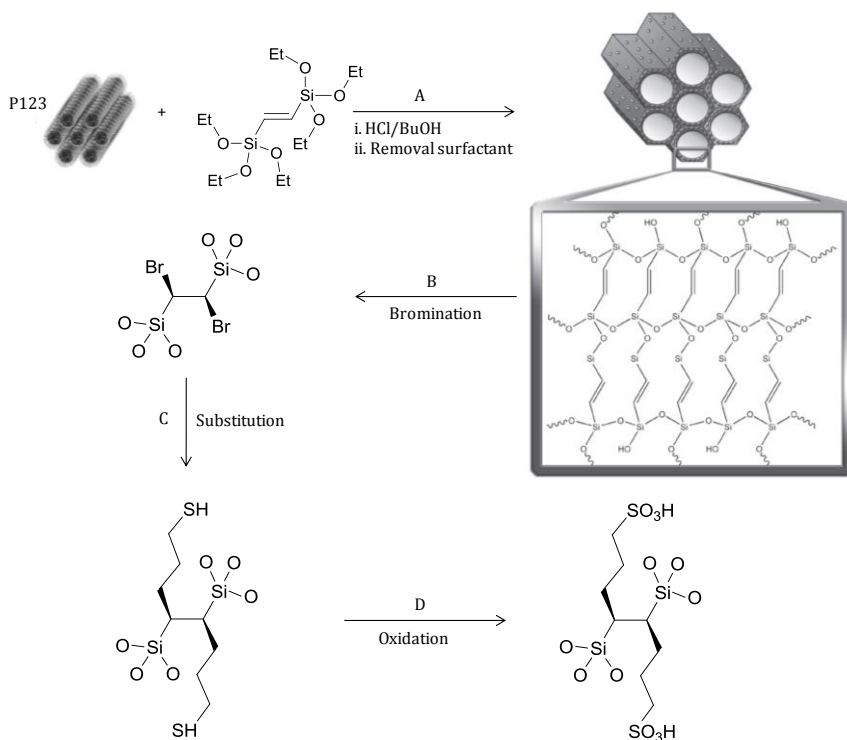
Esterificatie reacties kunnen gekatalyseerd worden door zure groepen zoals bijvoorbeeld sulfonzure functionaliteiten. Deze groepen werden geïncorporeerd door middel van de directe sulfonering van de etheenverbindingen van de ethenyleen-gebrugde PMO. De sulfonering vond plaats met chloorsulfonzuur of met rokend zwavelzuur (Figuur 10.5). Alhoewel eerst een goed werkende katalysator voor de esterificatie van azijnzuur met 1-propanol werd bekomen, bleek dat deze materialen hun functionele groepen verliezen.



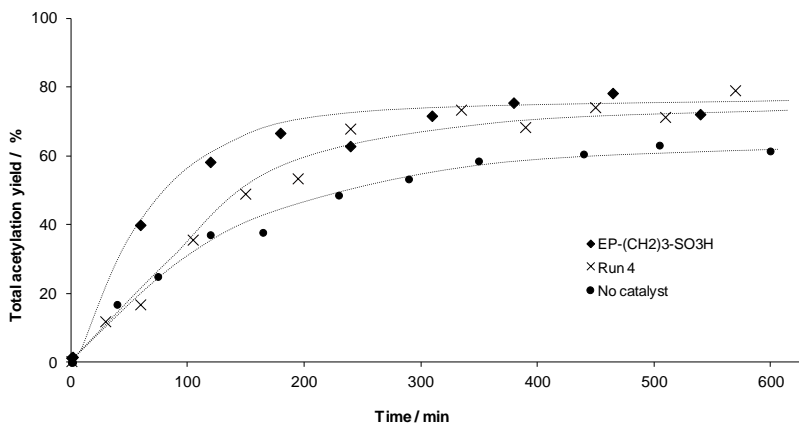
**Figuur 10.5: Functionalisatie van de dubbele binding met chloorsulfonzuur of met rokend zwavelzuur.**

Daarom werd voor een andere methode geopteerd om een sulfonzuurhoudend PMO-materiaal te verkrijgen. De synthesemethode wordt weergegeven in Figuur 10.6 en hield in dat de  $-SH$  groep van de thiol-gefunctionaliseerde PMO werd doorgeoxideerd waardoor een  $-SO_3H$  groep werd verworven, verankerd aan de PMO via een propylketen. Een zure katalysator werd bekomen met een aciditeit van  $0.60 \text{ mmol H}^+ \text{ g}^{-1}$ . Dit materiaal werd onderzocht als katalysator voor de glycerol acetylatie en zijn katalytische activiteit werd eveneens vergeleken met het commercieel verkrijgbare hars Amberlyst-15. Het materiaal bleek een gelijkaardige activiteit te bezitten met een opbrengst van 80% na 300 minuten. De zure PMO is dus evenwaardig aan Amberlyst-15 wat een gekende goed werkende katalysator is voor dit type van reacties.

Daarnaast werd eveneens de herbruikbaarheid van de katalysator bestudeerd. Hiervoor werd de katalysator een aantal keer opnieuw gebruikt zonder een speciale behandeling om het materiaal te regenereren.



**Figuur 10.6:** Overzicht van de gevolgde synthesesweg om een etheen-PMO met sulfonzure groepen te bekommen. (A) Synthese van het PMO-materiaal; (B) Bromering van de etheenverbinding; (C) Substitutie van het broomatoom met het Grignard reagens van 3-chloro-1-propanethiol en (D) Oxidatie van het thiol tot een sulfonzure groep.

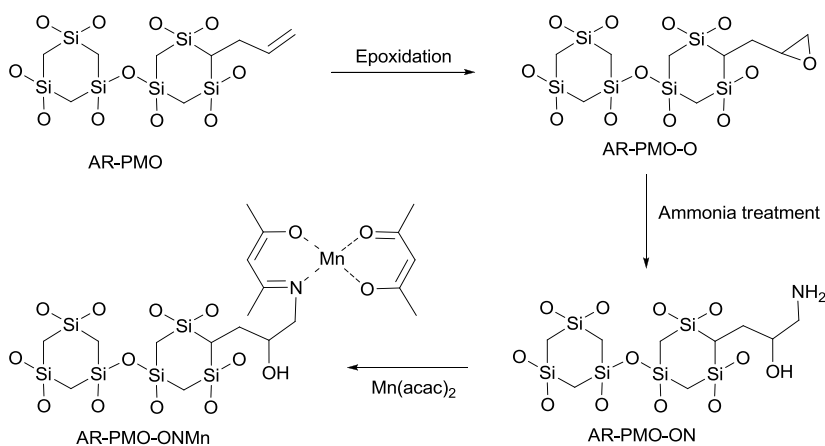


**Figuur 10.7:** Herbruikbaarheid van de zure PMO: een vergelijking tussen de katalytische activiteit van de eerste en vierde run wordt weergegeven. De blanco reactie wordt eveneens weergegeven voor de duidelijkheid. De verbindinglijnen dienen enkel als visuele hulp.

Een lichte daling in initiële reactiesnelheid kon opgemerkt worden, maar uiteindelijk bereikte de zure PMO hetzelfde niveau als in de eerste katalytische test. Extra experimenten toonden daarenboven aan dat de katalyse heterogeen verliep en er geen sprake was van uitloging van de sulfonzure groepen.

## 10.5 PMOs gemodificeerd met een mangaancomplex als katalysator voor epoxidatie reacties

Een  $\text{Mn}(\text{acac})_2$  complex werd verankerd op een PMO-materiaal om toe te passen als heterogene katalysator voor de epoxidatie van cyclohexeen. Om het mangaancomplex covalent vast te hechten aan het oppervlak van de PMO werd ervoor geopteerd eerst de dubbele binding van de etheen PMO te epoxideren, de epoxide ring te openen met ammoniak en vervolgens de bekomen amine functie te laten reageren met het acac-ligand van het complex. De vorming van een C=N verbinding zorgt voor een stevige covalente verankering.

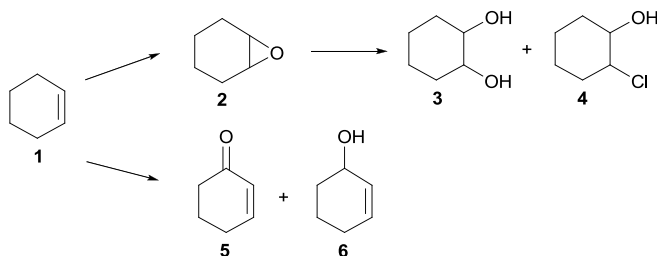


**Figuur 10.8:** Verankering van het  $\text{Mn}(\text{acac})_2$  complex op de allyl ring-PMO.

De epoxidatie van de etheenverbinding van de ethenyleen-gebrugde PMO bleek echter niet mogelijk te zijn waardoor gebruik gemaakt moest worden van een ander type PMO, namelijk een PMO-materiaal met geconnecteerde  $[\text{Si}(\text{CH}_2)]_3$ -eenheden, ook wel ring-PMO genoemd. Deze organosilica werd verder modificeerd met een allylfunctionaliteit. De epoxidatie op dit materiaal bleek wel vlot te verlopen waarna

een geslaagd Mn-verankering plaatsvond. Een functionalisatiegraad van ongeveer 0.60 mmol Mn g<sup>-1</sup> werd bekomen.

De katalytische activiteit van deze PMO werd bestudeerd aan de hand van de epoxidatie van cyclohexeen. Verschillende reactieproducten kunnen gevormd worden en zijn weergegeven in Figuur 10.9.



**Figuur 10.9:** Overzicht van de epoxidatie van cyclohexeen (1) met moleculaire O<sub>2</sub>. De volgende producten worden gevormd: het gewenste product cyclohexeen oxide (2) en de producten cyclohexaan-1,2-diol (3) en 2-chlorocyclohexanol gevormd door een ringopening reactie. De allylische oxidatie van (1) geeft aanleiding tot de producten 2-cyclohexeen-1-on (5) en 2-cyclohexeen-1-ol (6).

**Tabel 10.4:** Conversie van cyclohexeen, de vorming van het epoxide en de bij-productendistributie samen met de TON- en TOF-waarden. De uitloging van het mangaancomplex is eveneens weergegeven.

	(1)	(2)	(3)	(4)	(5)	(6)	TON <sup>a</sup>	TOF <sup>b</sup>	Uitloging <sup>c</sup>
	%	%	%	%	%	%		h <sup>-1</sup>	%
AR-PMO-ONMn									
Test 1 <sup>d</sup>	31.8	20.1	1.5	11.8	2.0	1.9	122.33	24.43	0
Test 2 <sup>d</sup>	20.9	15.4	0.8	5.2	1.3	1.2	97.31	24.40	6
Test 3 <sup>d</sup>	43.6	24.0	0.8	9.2	1.7	1.6	148.32	37.76	0

<sup>a</sup> Turnover Number berekend na 7 uur reactie. <sup>b</sup> Turnover Frequency berekend na 30 minuten reactie. <sup>c</sup> Bepaald met behulp van XRF-metingen. <sup>d</sup> De blanco reactie: 24.9% conversie van cyclohexeen (1) en de vorming van 11.8% van (2); 0.7% van (3); 5.4% van (4); 3.0% van (5); en 1.3% van (6).

De verkregen katalytische resultaten wordt weergegeven in Tabel 10.4. Uit de eerste katalytische test bleek dat de katalysator een cyclohexeenconversie van ~32% vertoonde. Bovendien vond er geen uitloging van de katalysator plaats. Bij hergebruik van de katalysator, daalde de katalytische activiteit echter tot op het niveau van de blanco reactie. Een kleine hoeveelheid Mn werd uitgeloozd (6%). Dit was waarschijnlijk te wijten aan de behandeling van de katalysator tussen de katalytische

testen. Daarom werd, na de 2<sup>de</sup> katalytische test, voorzichtiger omgesprongen met de katalysator. Tijdens de derde katalytische test bevond de katalytische activiteit zich echter weer op hetzelfde niveau als tijdens de eerste test en is de conversie zelfs iets hoger. Opnieuw werd er geen mangaanuitloging vastgesteld.

## **10.6 Concluisies**

Men kan besluiten dat in dit doctoraatswerk aangetoond werd dat Periodieke Mesoporeuze Organosilica's veelzijdige en veelbelovende materialen zijn. Ze kunnen succesvol omgevormd worden tot adsorbens voor toxische kwikatomen door de incorporatie van zwavelhoudende functionaliteiten, maar ze kunnen eveneens gebruikt worden als adsorbens voor het broeikasgas koolstofdioxide wanneer stikstofbevattende groepen aanwezig zijn. Naast de ontwikkeling van adsorbentia, kunnen PMO's ook dienst doen als heterogene katalysator, namelijk als zure katalysator met  $-SO_3H$  groepen en als dragermateriaal voor het mangaancomplex  $Mn(acac)_2$  in katalytische reacties zoals respectievelijk esterificaties en epoxidaties.